SYNTHESIS AND REACTIVITY OF UNUSUAL PALLADIUM (II) COMPLEXES SUPPORTED BY A DIARYLAMIDO/BIS(PHOSPHINE) PNP PINCER LIGAND

A Dissertation

by

RAFAEL HUACUJA

Submitted to the Office of Graduate and Professional Studies of
Texas A&M University
in partial fulfillment of the requirements for the degree of

DOCTOR OF PHILOSOPHY

Chair of Committee,	Oleg V. Ozerov
Committee Members,	Donald J. Darensbourg
	John A. Gladysz
	Mark T. Holtzapple
Head of Department,	David H. Russell

May 2014

Major Subject: Chemistry

ABSTRACT

This dissertation discusses the synthesis and reactivity of divalent palladium complexes supported by diarylamido bis-phosphine pincer ligands (PNP). The PNP is a tridentate pincer type ligand which typically adopts meridional type coordination. The rigidity and tight coordination of the PNP ligand provides the unique opportunity to study the coordination of ligands such as O_2 and C_2H_4 to a single coordination site on palladium, or the reactivity of a single empty coordination site *trans* to a weak *trans*-influencing ligand such as diarylamido.

Irradiation of $[(^{F}PNP^{iPr})Pd\text{-}]_2$ under an atmosphere of dioxygen irreversibly produces a mixture of a monohapto palladium(II) superoxide ($(^{F}PNP^{iPr})PdO_2$) and a palladium μ-peroxide ($[(^{F}PNP^{iPr})PdO\text{-}]_2$). Under photolytic conditions these two complexes are in equilibrium with each other. $(^{F}PNP^{iPr})PdO_2$, an open-shell paramagnetic species, was characterized by a combination of single-crystal X-ray crystallography, EPR, and ^{19}F NMR spectroscopies. In addition, irradiation of $[(PNP)Pd\text{-}]_2$ under an atmosphere of C_2H_4 produces a mixture of $[(PNP)Pd\text{-}]_2$ and a ethylene-bridged dinuclear palladium complex ($[(PNP)Pd\text{-}CH_2\text{-}]_2$). If the ethylene headspace is removed, and $[(PNP)Pd\text{-}CH_2\text{-}]_2$ is irradiated it is completely converted to $[(PNP)Pd\text{-}]_2$. This suggests that in the presence of ethylene these two complexes are in photolytic equilibrium with each other.

In addition, this dissertation will also discuss the synthesis and reactivity of $[(PNP^{R})Pd]^{+}$ (R = ^{i}Pr, ^{t}Bu) cations. $[(^{F}PNP^{iPr})Pd]^{+}$ cations are highly electrophilic

complexes that are able to coordinate Lewis bases such as THF, H_2O, and even extremely poor Lewis bases such as toluene and benzene. In addition, irradiation of $[(^{F}PNP^{iPr})Pd]^{+}$ cations in bromobenzene induces the abstraction of a bromine atom from bromobenzene, consistent with a metalloradical species. Addition of dioxygen to $[(^{F}PNP^{iPr})Pd]^{+}$ cations generates a paramagnetic, cationic η^1 superoxide.

In non-halogenated arene solvents $[(^{F}PNP^{iPr})Pd]^{+}$ cations undergo a highly unusual photo-induced isomerization of the isopropyl groups on the supporting phosphines to *n*-propyl. This unprecedented isomerization is believed to occur via C-P bond cleavage and is driven by the decrease in sterics around the metal, which allows for the facilitated coordination of the arene solvent.

DEDICATION

To my family whom I love very much

ACKNOWLEDGEMENTS

First of all I want to thank my advisor Oleg V. Ozerov for his guidance, encouragement and patience throughout my graduate tenure in his group. Working for him has been an incredible experience, and I am very grateful for the education I have received from him. His willingness to always share his vast knowledge of chemistry with our group has been a key factor in my success. I am thankful to him for always taking the time to listen to my ideas, and for helping me sort out the best ones. Without his help and guidance my projects would not have been as fruitful.

I would like to thank Chun-I Lee and Dr. Yanjun Zhu for their friendship and great advice in chemistry. The endless number of discussions we had throughout my graduate studies has undoubtedly made me a much better chemist. I would also like to thank Chan Park, a very talented undergraduate student whom I had the privilege to mentor. Having him as a student helped me learn how to effectively convey the knowledge that I have accumulated in graduate school to another. Working with him has been a great teaching experience that will help me throughout my career.

I would also like to thank Billy McCulloch, a brilliant chemist whom I have had the pleasure to work with. From him I have learned skills beyond chemistry that will certainly help me throughout my professional career. During my graduate career I have worked with many great colleagues who have inspired me to become a better chemist: Dr. Dan Smith, Samantha Yruegas, Dr. Morgan MacInnis, Chelsea Mandell, Wei-Chun Shih, Dr. Weixing Gu, Jessica DeMott, Chrissy Brammell, Chandra Palit, Dr. David

Herbert, Dr. Justin Walensky, Chris Pell, Jill Davidson, Sam Timpa, and Rodrigo Ramirez. I would also like to thank the X-ray diffractometry staff at Texas A&M University, Drs. Bhuvanesh Nattamai and Joseph H. Reibenspies for their help in solving many a structure and for putting up with the endless number of questions about crystallography. With their help I have learned a great deal about crystallography.

On a more personal note, I would like to thank my girlfriend Jenny Pirela for her love, comfort and support throughout my graduate career, especially while writing this dissertation. Most of all I would like to thank my family for all their love and support. My two sisters (Isabel and Laura Huacuja), my mom (Isabel Alonso de Florida) and my dad (Rafael Huacuja Sr.) have always been a source of inspiration. My parents have made me everything I am today. Their encouragement and unwavering faith in me and my abilities has propelled me much farther than I ever could have imagined. Thank you mom and dad!

TABLE OF CONTENTS

Page

LIST OF FIGURES

Page

LIST OF SCHEMES

Page

LIST OF TABLES

Page

CHAPTER I

INTRODUCTION AND OVERVIEW

1.1 General Introduction to Pincer Complexes and Their Reactivity

Since the development of the first example by Shaw and co-workers[1] in the mid 1970s, the use of pincer ligands in organometallic chemistry has become quite ubiquitous.[2-4] A pincer, in common English, is a hand tool used for grasping objects, and as the name suggests, a pincer ligand is able to clasp onto the metal tightly and "hold" on to it.

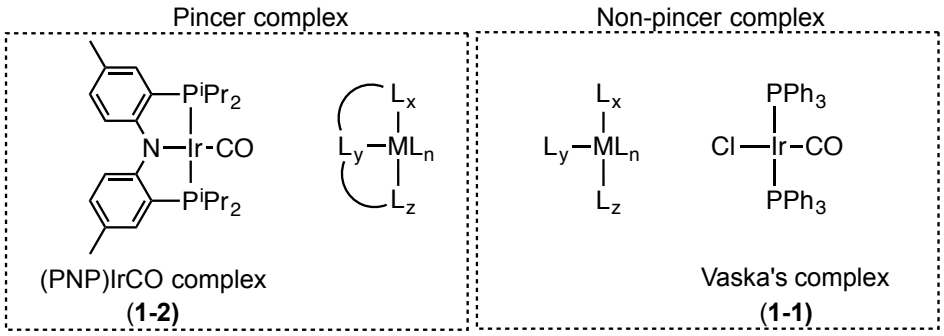

Figure 1.1 Examples of pincer type ligand (left) and non-pincer complex (right).

As **Figure 1.1** illustrates, a pincer ligand is essentially three monodentate ligands (L_x L_y, L_z) that are covalently tethered to each other and typically bind in a meridional fashion. In contrast, in non-pincer compounds such as Vaska's complex (**1-1**),[5,6] the ligands are independent of each other. In addition, in pincer ligands, L_x, L_y and L_z can be

composed of a combination of X-type and L-type ligands such as (^{Me}PNP^{iPr})IrCO (**1-2**). Because in pincer complexes the ligands are linked to each other, dissociation of the X and L type ligands is considerably less favorable than in non-pincer complexes, hence the tight coordination of pincer ligands.

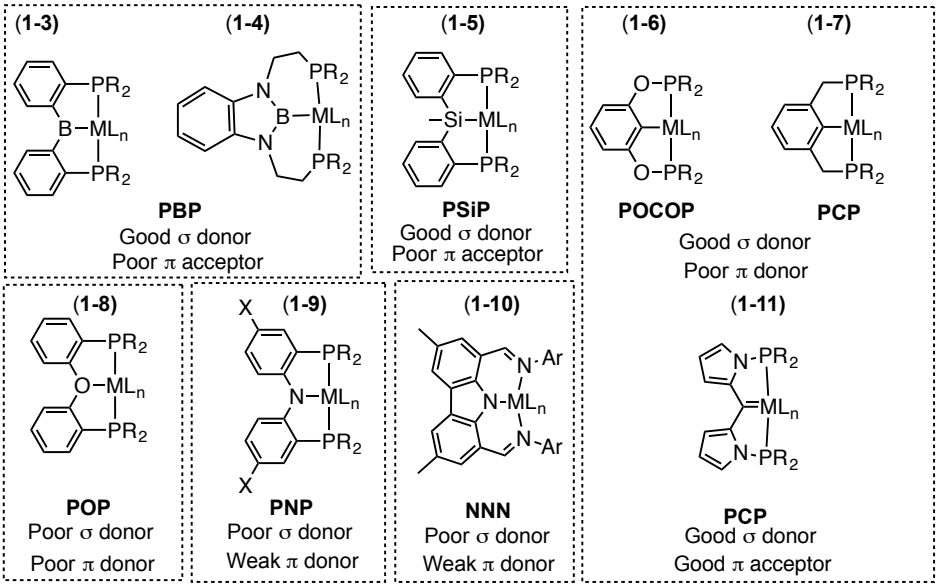

Figure 1.2 Electronic properties of PL_xP (L_x = B, Si, C, O) and PNN pincer type ligands.

This fact is especially true for cases where the pincer ligand is composed of at least one X-type ligand; the electrostatic forces between M^+ and X^- make dissociation more difficult. In recent years the number of different types of pincer ligands has increased dramatically, and many of these complexes are discussed in reviews and books.[3,4] However, this chapter will focus on only a handful of pincer complexes and their reactivity. **Figure 1.2** illustrates a few examples of different types of pincer

complexes that in recent years have shown remarkable reactivity. By convention, pincer ligands are named by the atoms that are directly bound to the metal center. For example, the PCP ligand (**1-3**, **1-4**, **1-5; Figure 1.2**) consists of a phosphine, an aryl, and a second phosphine, hence the name PCP. In POCOP (**1-3**), a type of PCP ligand, the O represents the oxygen linker between the phosphite and the aryl ligands. Pincer ligands have been made in virtually every combination of L_x L_y, L_z. **Figure 1.2** shows only a few examples of pincer complexes were both L_x and L_y are neutral ligands such as phosphorus or nitrogen, and the central ligand L_y is varied between neutral and anionic. Some examples of the central ligand include: silyl (R_3Si^-) (**1-6**), boryl (R_2B^-) (**1-7**, **1-8**), aryl (Ar^-)(**1-4**, **1-5**), carbene (R_2C=) (**1-5**), diarylamido (R_2N^-) (**1-9**, **1-10**) and diarylether (R_2O) (**1-11**).[7-13] Each of these ligands imposes different properties onto the metal and as a result very different reactivity is observed between these complexes. For example, silyl, boryl, and aryl ligands are good σ-donors and strong *trans*-influence ligands, but poor π acceptors. The carbene based PCP ligand (**1-5**) is a good sigma donor and a good π donor. However, the diarylamido (**1-9**) and diarylether (**1-8**) are poor π and σ donors and weak *trans*-influence ligands. These ligand properties can have a profound effect on the structure and reactivity of the complex. For example, a strong *trans*-influence ligand can help stabilize unsaturated, low coordinate complexes. However, the use of pincer ligands to force a weak *trans*-influence ligand to be *trans* to an empty coordination site can lead to highly electrophilic complexes with unusual reactivity (see Chapter V).

Pincer complexes have been shown to be highly robust and therefore capable of functioning as catalysts even under harsh conditions.[7] Other pincer ligands have been

shown to be non-innocent and easily undergo reversible reactions such as deprotonation and protonation.[2] The first example discussed will be Goldman's and Brookhart's (PCP)Ir(L) metal complexes (**1-12**, **1-13**). These complexes represent a class of pincer catalysts that are known to be highly robust and capable of functioning as effective catalysis even at elevated temperatures.[7] This will then be followed by a discussion of metal complexes supported by nitrogen based (PNP) and (PNN) ligands. This will include a very recent example of a novel PNP type ligand developed by Gandelman and coworkers.[14] Following this will be the analysis of some notable examples of non-innocent, pyridine based ^{Pyr}PNP and PNN metal complexes, developed by Milstein and coworkers, and their application towards catalysis.[15,16] These systems are a prime example of how non-innocent pincer ligands can work cooperatively with the metal center to achieve catalysis. In addition, the chemistry of both diarylamido PNP and the Fryzuk PNP metal complexes and their application towards the synthesis of low coordinate unsaturated metal complexes.[17-22] Finally, this chapter will conclude with a discussion of the synthesis and properties of three-coordinate Pd and Pt complexes supported by non-pincer type ligands.[18,23-28]

1.1.1 The chemistry of (PCP)Ir(L) and (POCOP)Ir(L) complexes

One of the most noteworthy examples of extraordinary organometallic chemistry using pincer metal complexes is the catalytic dehydrogenation of alkanes using (PCP)Ir(L) complexes (**1-13**). These complexes have shown remarkable stability under the high temperature conditions needed to catalyze dehydrogenation of alkanes.[29] In

addition, (POCOP)Ir(L) (**1-12**) and (PCP)Ir(L) (**1-13**) have been used in tandem with alkene metathesis catalysts, in a process that has become known as alkane metathesis (**Scheme 1.1a**).[30]

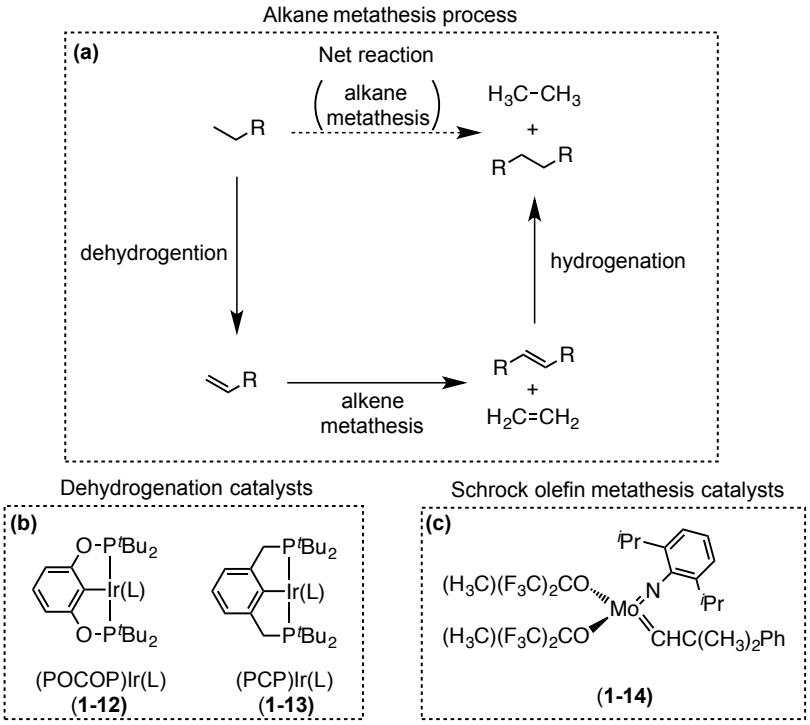

Scheme 1.1 Alkane metathesis catalysis pathway (a); dehydrogenation catalysts (b); Schrock olefin metathesis catalyst (c).

The first step of alkane metathesis involves the dehydrogenation of an unactivated alkane to generate a terminal alkene. The resulting alkene is then intercepted by an olefin metathesis catalyst (e.g. **1-14**) and undergoes alkene metathesis, producing a longer chain internal alkene and ethylene. The resulting internal alkene is then hydrogenated by (PCP)Ir(L) to generate an alkane with higher molecular weight

(**Scheme 1.1a**). The overall process generates a mixture of lower molecular weight alkanes and higher molecular weight alkanes. This process is highly coveted because of its potential application towards the production of fuels such as diesel, which is predominantly composed heavier alkanes ranging from C_9 to C_{20} in length.

1.1.2 Transition metal PNP complexes and their reactivity

Even within just the subcategory of PNP pincer ligands there is a large volume of pincer ligand architectures (see **Figure 1.3**) and new ligand architectures are being developed even now.[4] The PNP ligand motif consists of two *trans* phosphines and a central nitrogen donor. The central nitrogen can either be anionic (**1-10**, **15**, **16**), neutral (**1-17**, **18**), or cationic (**1-19**). Several examples of PNP metal complexes will be discussed in the following sections. One of the most recent examples of a PNP is the nitrenium based ^{Nit}PNP pincer ligand reported by Gandelman and coworkers.[14] The triazolium cation is isoelectronic and isostructural to the Arduengo type NHC carbenes (**Figure 1.3 c** and **d)**,[31] which have become common ligands for virtually every transition metal.[31-38] Despite this fact, previously reported examples of 1,2,3 triazolium cations have been shown to be poor ligands to transition metals.[39-41] However, in the Gandelman example the pincer nature of ^{Nit}PNP ligand allows the central nitrogen of the triazolium cation to approach the metal, and ligate to make both Rh(I) (**1-20**) and Ru(II) (**1-21**) complexes (**Figure 1.3b**).

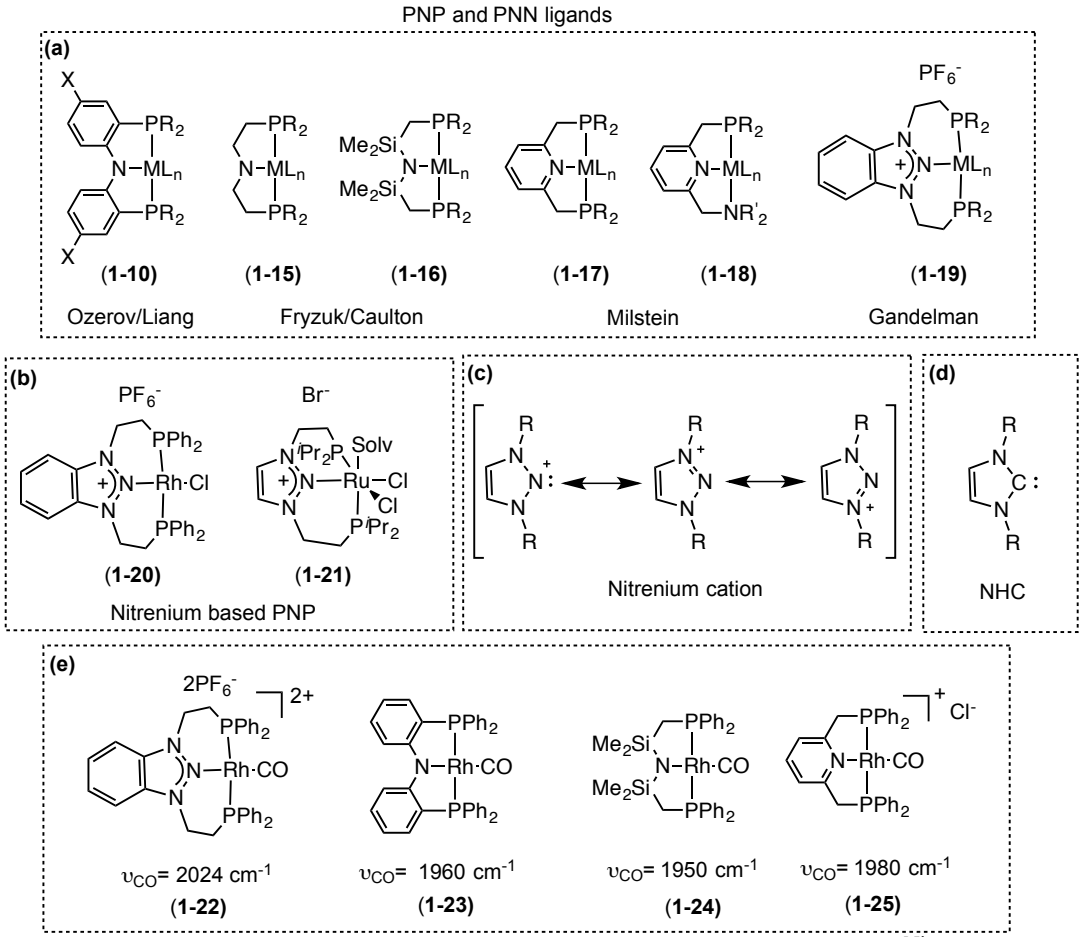

Figure 1.3 Examples of PNP and PNN type ligands (a); nitrenium based ^{Nit}PNP metal complexes (b); resonance structures of nitrenium cation (c); NHC carbene (d); CO stretching frequencies of (PNP)RhCO complexes (e).

The higher CO stretching frequency of the nitrenium based PNP in $[(^{Nit}PNP)RhCO]^{2+}[BF_4]^{2-}$ (2024 cm^{-1}; **1-22**) compared to the diarylamido $(PNP^{Ph})RhCO$ (1960 cm^{-1}; **1-23**),[42] the Fryzuk $(^{Fr}PNP^{Ph})RhCO$ (1950 cm^{-1}; **1-24**),[43] and the pyridine-based $[(^{Pyr}PNP)RhCO]^{+}Cl^{-}$ (1980 cm^{-1}; **1-25**)[44] suggests that the nitrogen in the nitrenium fragment is poorer σ-donor. In addition, DFT calculations (vide infra) determined that the nitrenium based PNP was a reasonable π-acceptor. Although this

ligand is the first of its kind, and little is know about its coordinating ability with other metals, it is likely that in the near future the chemistry of this new class pincer ligand will be developed further.

1.1.3 Activation of N-H and O-H bonds with pyridine based (^{Pyr}PNP)Ru(H)CO complexes (application of non-innocent ligands)

Both the pyridine based ^{Pyr}PNP (**1-18**), and its close analog PNN developed by Milstein and coworkers have been shown to be acid/base non-innocent ligands. The transition metal complexes with the pyridine based ^{Pyr}PNP and PNN ligands have the unique ability to undergo cycles of dearomatization/aromatization without changing the metal oxidation state.[2] This can be viewed as a form of metal-ligand cooperation, were the ligand functions as an internal base and deprotonates substrates that are coordinated to the metal center. The PNP and PNN metal complexes have been applied, by Milstein and coworkers, towards small molecule activation. For example, Milstein and coworkers reported the activation of N-H bonds in ammonia and anilines using a dearomatized pyridine based (^{Pyr}PNP)RuH(CO) (**1-26**) complex (**Scheme 1.2**).[15] N-H bonds are typically considered difficult to activate and only a few examples of metal-based activation of ammonia have been reported in the literature.[13,45-55] Complex **1-26** is capable of quantitatively activating electron-poor anilines such as 4-nitroaniline and generate the aromatized (^{Pyr}PNP)Ru(H)(NHAr)(CO) (**1-28**). **1-28** has an octahedral geometry with the hydride *trans* to the resulting amide ligand. However, less acidic

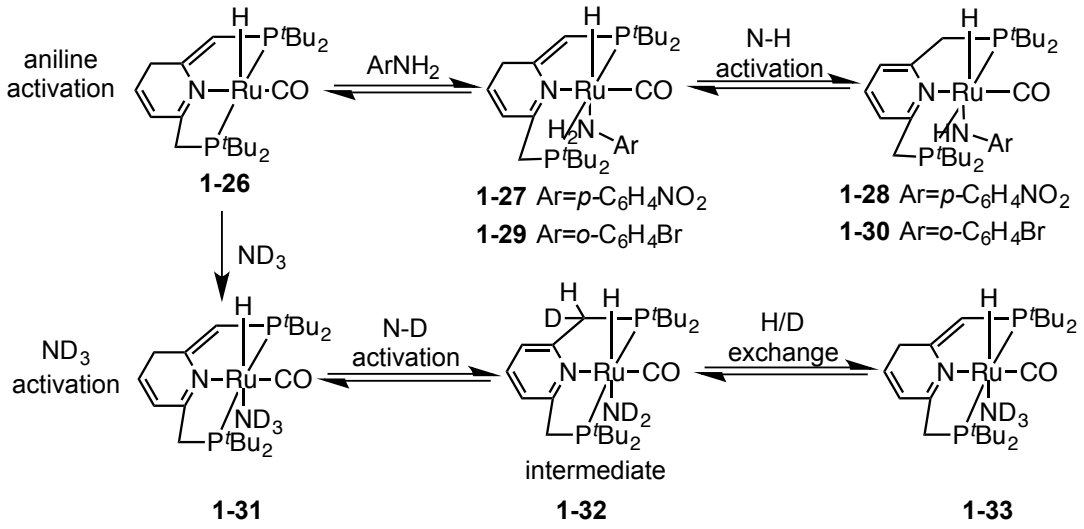

Scheme 1.2 Activation of anilines and ammonia with pyridine based (PNP)Ru(H)CO complexes.

anilines such as 2-bromoaniline are not fully activated and an equilibrium between the coordinated aniline **1-29** and the fully activated hydrido amide **1-30** was observed. In addition, using the same dearomatized starting complex **1-26** Milstein and coworkers were able to activate ammonia. However, unlike the aniline substrates the activated product of NH_3 is not directly observed. To prove that NH_3 was being activated, Khaskin and coworkers treated compound **1-26** with a large excess of ND_3 and observed the slow disappearance of pyridinylmethylenic protons on the ancillary ligand.[15] This suggests that N-D activation does occur, and that although the product of N-H activation (**1-33**) is not isolable it is kinetically accessible and reversible.

In addition to ammonia activation, in 2009 Milstein and coworkers reported the conversion of H_2O into H_2 and O_2.[16] This is a rare example of a complex that is capable

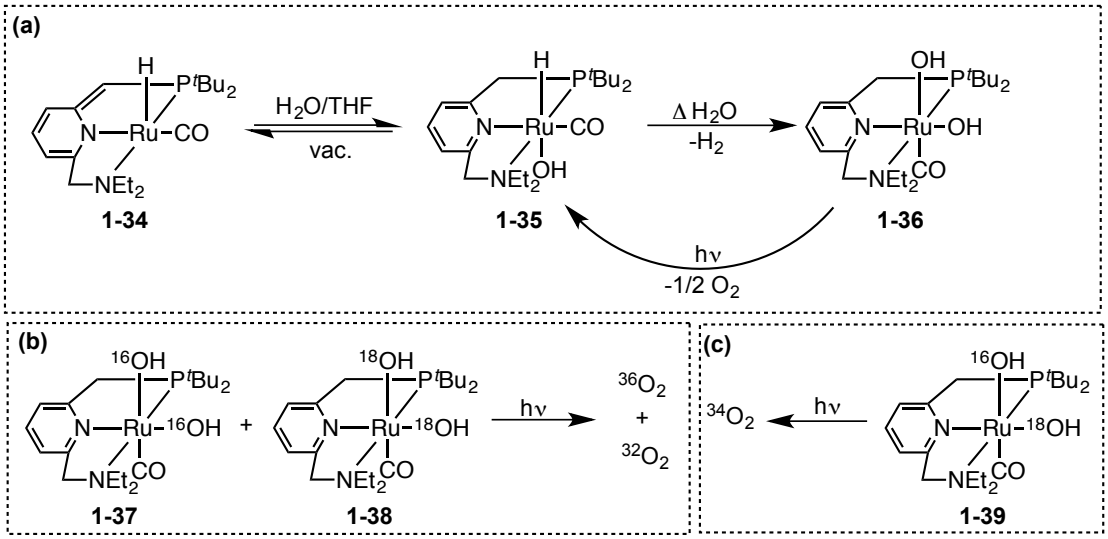

Scheme 1.3 Thermal and photochemical activation of H_2O using pyridine based (PNP)Ru(H)CO complexes (a); cross-over experiment between **1-37** and **1-38** (b); mixed isotope labeling experiment (c).

of mediating both water oxidation and reduction at a single metal site. The dearomatized pyridine based (PNN)Ru(H)CO complex (**1-34**), is able to convert water into dihydrogen thermally, and dioxygen photochemically (**Scheme 1.3**a) . In a manner analogous to N-H activation, **1-34** is able to cleave an H-O bond in H_2O to generate (PNN)Ru(H)(OH)CO (**1-35**). Thermolysis of this complex in H_2O generates (PNN)Ru$(OH)_2$CO (**1-36**) and induces the evolution of H_2. Under photolytic conditions **1-36** complex undergoes O-O reductive elimination and generates hydrogen peroxide, which subsequently decomposes into O_2 and H_2O. To determine if elimination of H_2O_2 occurs from **1-36** occurs via an inter or intra molecular process a crossover experiment between (PNN)Ru$(^{16}OH)_2$CO (**1-37**) and (PNN)Ru$(^{18}OH)_2$CO (**1-38**) was conducted. Photolysis of the above mixture, produces $^{36}O_2$ and $^{32}O_2$ almost exclusively, suggesting that reductive elimination from **1-37** and **1-38** is intramolecular process (**Scheme 1.3b**). In addition, photolysis of the

mixed isotope complex (PNN)Ru(^{18}OH)(^{16}OH)CO (**1-39**) produces almost exclusively $^{34}O_2$, giving further evidence that reductive elimination from **1-36** is an intramolecular process. There was also the concern that hydroxyl radicals could be responsible for O-O bond formation, however, the use of 5,5-dimethyl-1-pyrroline-1-oxide (DMPO), an $^{\bullet}$OH radical trap, indicated that only a small amount of hydroxyl radicals was formed in the reaction.

1.1.4 The chemistry of unsaturated diarylamido (^{X}PNP^{R})Rh(I) complexes

Since the development of the diarylamido ^{X}PNP^{R}, the Liang,[56,57] Mindiola[58-60] and Ozerov[8,54,61-75] and other groups[61,76,77] have done extensive research using the ^{X}PNP^{R} ligand as a platform for late transition metal complexes (see Chapter II for diarylamido ^{X}PNP^{R} nomenclature). Much of the work done in the Ozerov group has revolved around the topic of strong bonds activation such as C-H,[65,75] C-O[78] and its potential application towards catalysis. In many of these transformations, an unsaturated metal complex is generated prior to activating strong bonds. For example, in 2006 Ozerov and coworkers reported the synthesis of a (^{Me}PNP$^{i Pr}$)Rh(I) (**1-41**) by reductive elimination from (^{Me}PNP$^{i Pr}$)Rh(Me)(Ph) (**1-40**). **1-41** which is capable of undergoing oxidative addition of unactivated aryl chlorides, bromides and iodides (**Scheme 1.4**) to generate (^{Me}PNP$^{i Pr}$)Rh^{II}(Ar)X (**1-42**, **43** or **44)**.[79] After oxidative addition of the aryl halide, the resulting **1-42**, **43** or **44** can undergo transmetallation with PhLi, producing (^{Me}PNP$^{i Pr}$)Rh^{II}(Ar)(Ph) (**C**) (**Scheme 1.4b**). This complex rapidly undergoes reductive elimination, and in the presence of an aryl halide regenerates (^{Me}PNP$^{i Pr}$)Rh(Ar)X (**B**).

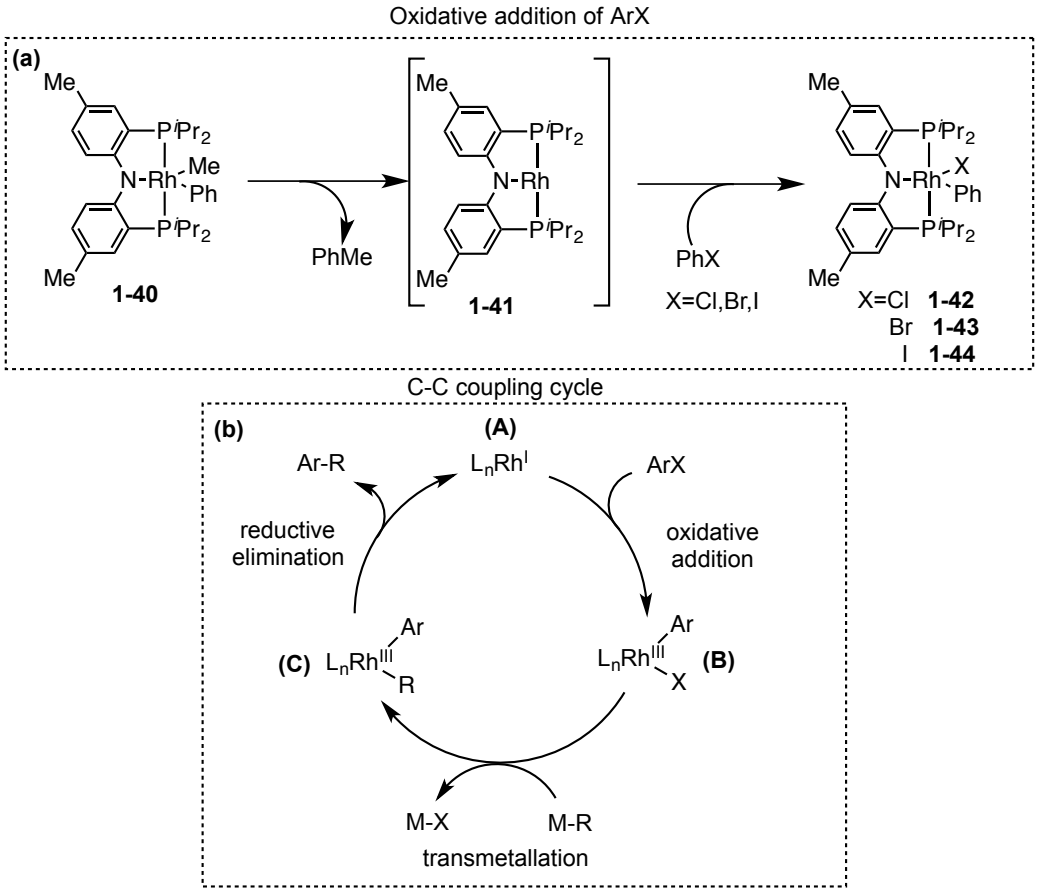

Scheme 1.4 Reductive elimination of C-C bonds and oxidative addition of aryl halides (a); mechanism of rhodium catalyzed C-C coupling (b).

Although not isolable, **1-41** can be generated in situ via reductive elimination of C-C bonds. Typically these unsaturated, three-coordinate Rh complexes are proposed intermediates,[61,62,80-82] however there are examples in the literature of isolable three-coordinate Rh complexes,[27,83,84] albeit stabilized by agostic interactions. Although **1-40** is not a catalyst for C-C coupling, it is capable of undergoing all the fundamental steps in the C-C coupling catalytic cycle. This concept was later applied by Ozerov and coworkers towards catalytic C-C coupling reactions using (POCOP)Rh(H)(Cl) as a catalyst precursor.[62]

1.1.5 Synthesis of three-coordinate metal complexes supported by the Fryzuk based ^{Fr}PNP ligand

Since the development of the amido-^{Fr}PNP ligand by Fryzuk and coworkers[85-87] the ^{Fr}PNP ligand **1-16** has been used to investigate fundamental organometallic transformations. The Fryzuk ^{Fr}PNP ligand differs from the diarylamido ^{X}PNP^{R} in that it is a better π donor ligand (see **Figure 1.3e**) and that the silyl based backbone is less rigid than the diarylamido ^{X}PNP^{R}. In additon, the diarylamido ^{X}PNP^{R} is more robust and less susceptible to decomposition than the Fryzuk ^{Fr}PNP. This section will discuss a the synthesis and reactivity of a series of unsaturated (^{Fr}PNP^{tBu})M (M = Co, Ni) complexes and the comparison to analogous complexes synthesized using the diarylamido ^{X}PNP^{R} ligand. Many of these unsaturated complexes are stable at room temperature and have shown remarkable reactivity.

Reduction of (^{Fr}PNP^{tBu})CoCl (**1-45**) with magnesium powder generates a paramagnetic, three-coordinate (^{Fr}PNP^{tBu})Co(I) complex (**1-46**). As expected, the product shows a paramagnetically shifted ^{1}H NMR spectrum and is silent by ^{31}P NMR spectroscopy. In addition, Evans method magnetic susceptibility measurements of **1-46** gave a μ_B = 3.2, consistent with a high-spin, triplet species. The d^8, high-spin configuration is consistent with analogous Co(I) complexes reported by Holland and coworkers.[88] In contrast to other Co(I) complexes, such as Mindiola's (^{Me}PNP^{iPr})Co(I) dimer,[89] single-crystal X-ray crystallography confirmed that **1-46** does not form dimers, solvent adducts, or agostic interactions. It is believed that the high-spin, triplet character protects the metal center from formation of dimers, solvent adducts or agostic interactions.

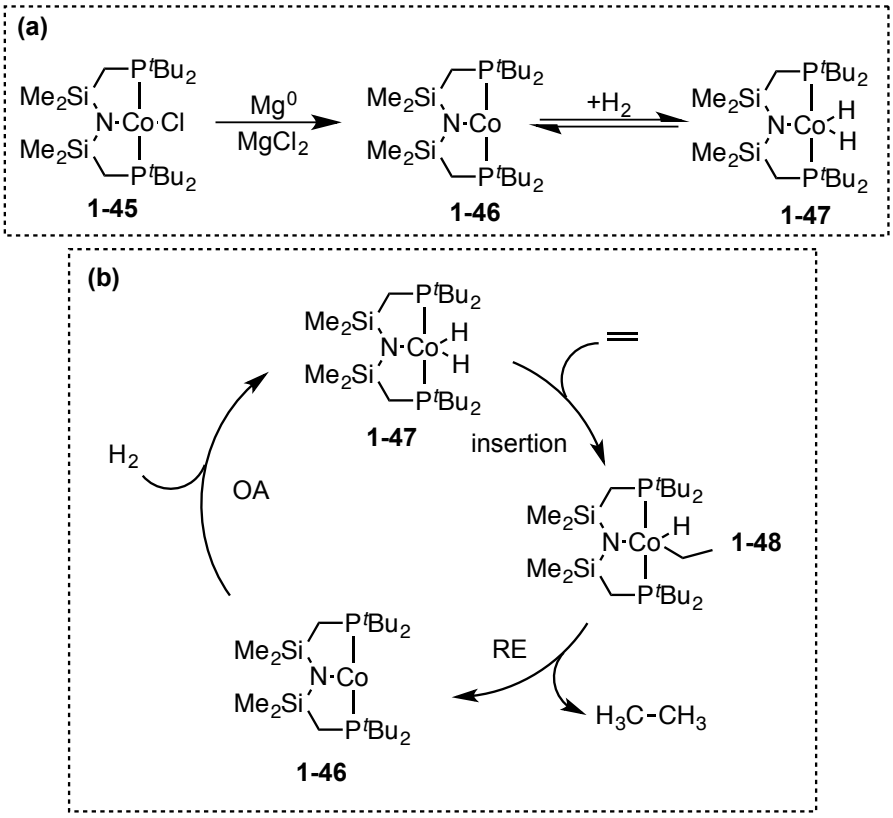

Scheme 1.5 Synthesis and reactivity of **1-46** (a); mechanism of cobalt catalyzed C_2H_4 hydrogenation (b).

In addition, if **1-46** is placed under an atmosphere of dihydrogen, a diamagnetic dihydride complex ($^{Fr}PNP^{tBu}$)CoH_2 (**1-47**) is formed via oxidative addition. However, removal of the volatiles by vacuum regenerates **1-46**, indicative that **1-47** and **1-46** are in equilibrium with each other under an atmosphere of dihydrogen. Addition of an equivalent of ethene to **1-47** rapidly converts it back to **1-46** with concomitant formation of ethane. This process presumably occurs, via coordination of ethene, followed by insertion into the Co-H producing **1-48**, followed by reductive elimination of ethane and regeneration of **1-46** (**Scheme 1.5**). This type of reactivity is quite unusual for Co complexes, which are typically known to undergo one-electron transformations.[90] In this

system **1-46** is in essence mimicking the two-electron chemistry that is traditionally observed for second and third row transition metals such as Pd and Rh. In the previous section we discussed how **1-41** is capable of undergoing oxidative addition of substrates such as aryl halides.

Like in the case of **1-45**, reduction of (^{Fr}PNP^{tBu})NiCl (**1-49**) with magnesium powder produces (^{Fr}PNP^{tBu})Ni(I) (**1-50**) (**Scheme 1.6**) .[19,91] **1-50**, a paramagnetic species, is silent by ^{31}P NMR spectroscopy, but does exhibit a paramagnetically shifted ^{1}H NMR spectrum corresponding to the ligand framework. The X-band EPR spectrum of this complex reveals a broad signal with no hyperfine coupling to the phosphines or nitrogen. Single-crystal X-ray crystallography determined that (^{Fr}PNP^{tBu})Ni(I) is three-coordinate and T-shaped, with no agostic interactions. It is also important to point out that this compound does not dimerize as in the case of the diarylamido (^{Me}PNP^{iPr})M (M = Pd, Ni) complexes reported by the Mindiola[59] and Ozerov[54,92] groups. **1-50** is believed to be stabilized by π-donation from the nitrogen lone pair of the amido to the metal center. Surprisingly, **1-50** does not form a THF adduct, but when treated with an atmosphere of CO does produce (^{Fr}PNP^{tBu})NiCO (**1-51)**. Compound **1-51**, which is also paramagnetic, shows a sharp triplet by X-band EPR spectroscopy as a result of the symmetrical phosphines. However, removal of the dissolved CO under vacuum regenerates **1-50**, suggesting that CO binding is weak. In contrast, if the analogous compound (^{Fr}PNP^{tBu})Fe(I) (**1-52**) is treated with an atmosphere of CO, (^{Fr}PNP^{tBu})Fe(CO)$_2$ (**1-53**) is formed irreversibly.[91] The deviation from planarity in the crystal structure of **1-51** (relative to **1-50**) is a result of hy bridization of the d(x^2-y^2) with 4s and 4p.

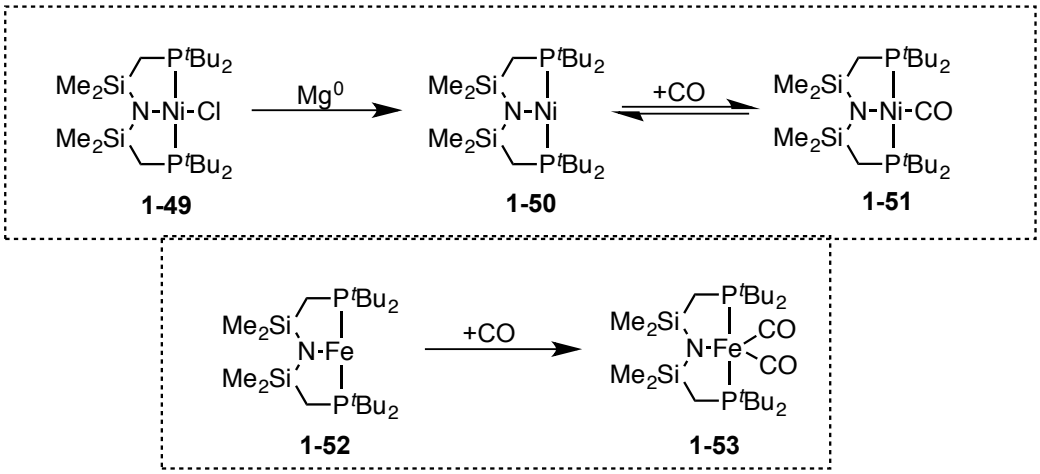

Scheme 1.6 Synthesis and reactivity of **1-50** and **1-52** with CO.

This gives access an empty metal orbital for the coordination CO and form of a new SOMO. In the previous section we discussed the results of reducing **1-49** with magnesium powder. However, if instead **1-49** is treated with $Na[BArF_{24}]$ in CH_2Cl_2, the chloride is abstracted, producing ($^{Fr}PNP^{tBu}$)Ni[$BArF_{24}$] (**1-54**) with concomitant formation of NaCl. Normally three-cooordinate unsaturated species are stabilized by solvent coordination or C-H agostic interactions.[27,93-99] However, ($^{Fr}PNP^{tBu}$)Ni[$BArF_{24}$] instead adopts a transannular interaction, were the C-Si bond donates its electrons to the metal in a σ bonding fashion, and the phosphine is pushed closer towards the orbital *trans* to the amido (see **Scheme 1.7**). This can be viewed as a form of stabilization analogous to an agostic interaction, where the lone pair of the phosphine satiates the empty coordination site. In fact, the authors calculated the relative energy of **A** and **B** (**Scheme 1.7**) and determined B to be more stable by 7.5 kcal/mol. This relatively small energetic gap suggests that A can be thermally accessible, and Lewis acid/base adducts can be synthesized.

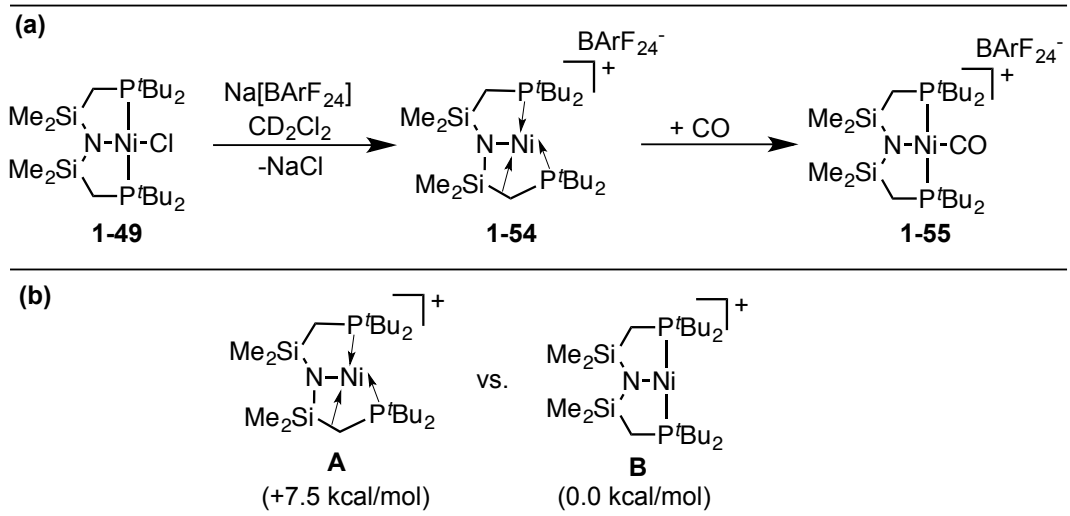

Scheme 1.7 Synthesis and reactivity of three-coordinate $[(PNP)Ni]^+$ cation (**1-54)** (a); and relative stability of **A** and **B** (b).

Consistent with these calculations, treating **1-54** with CO quantitatively produces $[(^{Fr}PNP^{tBu})Ni(CO)]^+[BArF_{24}]^-$ (**1-55**). The use of weakly-coordinating anions such as $[BArF_{24}]$ generates a highly electrophilic $[(^{Fr}PNP^{tBu})Ni]^+$ cation that is stabilized by a Si-C transannular σ bond interaction. However the stability of these complexes is highly dependent on the basicity of the WCA; the higher the basicity of the anion the less "gentle" the anion will be on the cation. For example, when **1-50** is treated with AgOTf, **1-50** is slowly converted (via intermediate **1-56)** into compound **1-57**. This unusual isomerization is believed to be the product of nucleophilic attack of the triflate onto the silicon of the ^{Fr}PNP ligand. Although such decomposition might be anticipated with more nucleophilic substrates it is surprising that triflate, a very poor base/nucleophile, is nucleophilic enough to attack the silicon center in $[(^{Fr}PNP^{tBu})Ni]^+$ cation.

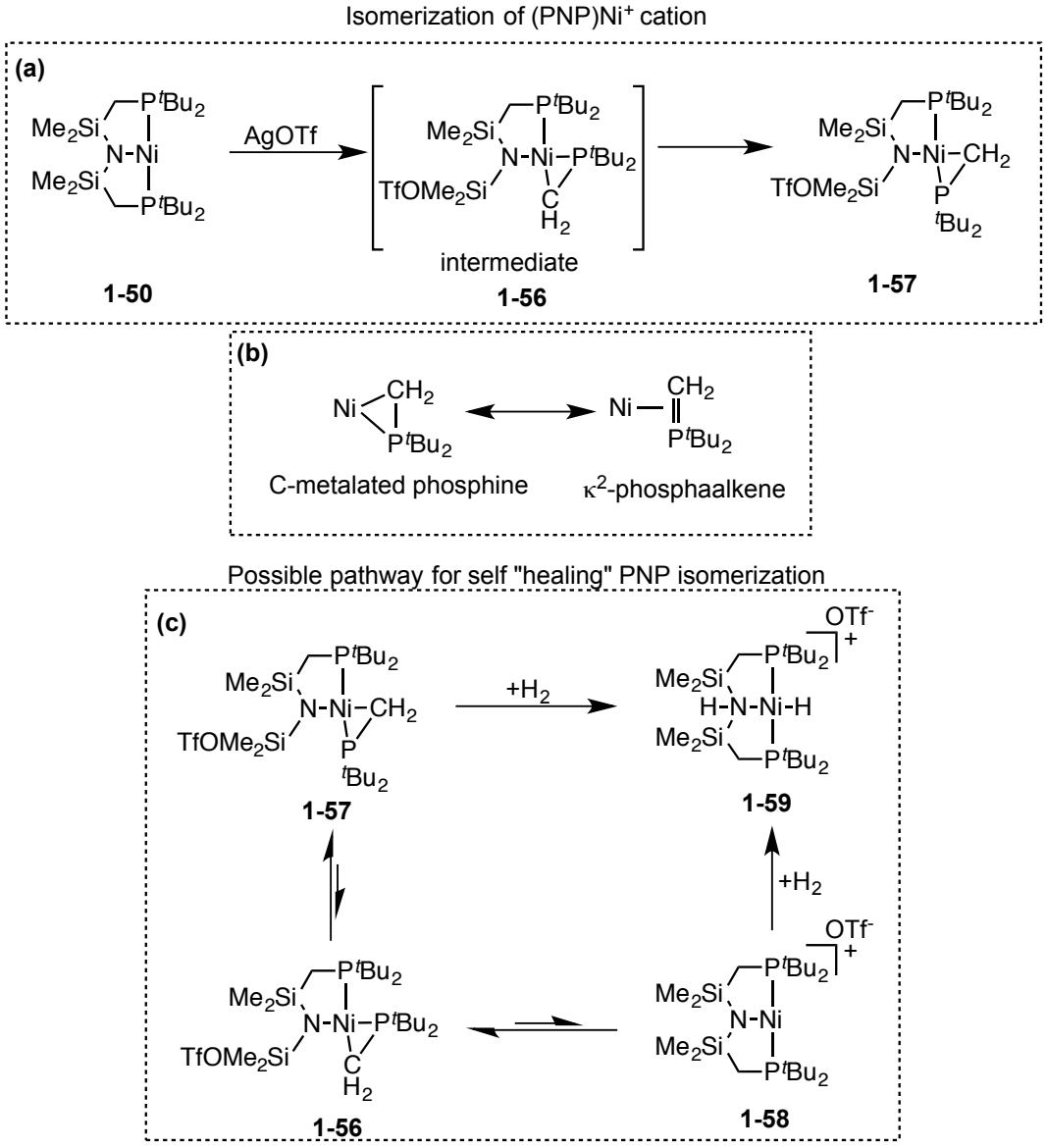

Scheme 1.8 Isomerization of $[(PNP)Ni]^+$ cation (a); possible binding modes of C-P fragment in **1-57** (b); possible pathway for self "healing" of (PNP) ligand framework (c).

Compound **1-57** contains a CH_2-P fragment as a ligand, which can be viewed as κ^2-phosphaalkene with donation from the C-P double bond to the metal center (**Scheme 1.8b**). Alternatively the fragment can be seen as a C-metalated phosphine, with an

anionic carbon and neutral phosphine. This example very clearly demonstrates the susceptibility of the Si-C bond in the Fryzuk $^{Fr}PNP^{tBu}$ ligand (**1-16**) to nucleophiles even as weak as triflate. In addition, in 2006 Caulton and coworkers reported an example detailing the susceptibility of the Fryzuk $^{Fr}PNP^{tBu}$ ligand towards hydrolysis.[100] In contrast, diarylamido $^{X}PNP^{R}$ (**1-10**), is significantly more robust towards decomposition by nucleophilic attack or hydrolysis. Surprisingly, when the authors investigated the reactivity of **1-57** with H_2, they determined that under an atmosphere of H_2, **1-57** is converted into $[(^{Fr}PN(H)P^{tBu})NiH]^+[OTf]^-$ (**1-59**) over a period of 7 days (**Scheme 1.8a-b**). This unusual result suggests that the isomerization is reversible, and that overtime **1-57** equilibrates to $[(^{Fr}PNP^{tBu})Ni]^+[OTf]^-$ (**1-58**), which subsequently reacts with H_2 to produce $[(^{Fr}PN(H)P^{tBu})NiH]^+[OTf]^-$ (**1-59**). This likely occurs because the carbon in the CH_2-$^{t}PBu_2$ fragment remains nucleophilic enough to attack the silicon center and displace the triflate anion, regenerating the ligand.

So far we have discussed the reactivity of a variety of different types of pincer complexes and their application to catalysis. In addition, we have also seen how the Fryzuk $^{Fr}PNP^{tBu}$ ligand (**1-16**) is able to stabilize three-coordinate Ni(I) and Co(I) complexes. Each of these unsaturated complexes are stabilized in a unique way. For example, the high-spin, triplet character of $(^{Fr}PNP^{tBu})Co(I)$ complex (**1-46**) is believed to protect the metal center from formation of dimers, agostic interactions or solvent adducts. In addition, the cationic complex, $[(^{Fr}PNP^{tBu})Ni]^+[BArF_{24}]^-$ (**1-54**), is stabilized by a *trans*-annular σ bond donation from the C-Si bond to the metal center (akin to a C-

H agostic interaction). The next section will discuss a variety of different Pd and Pt unsaturated complexes that are stabilized by non-pincer ligands.

1.2 Synthesis of Three-Coordinate Palladium (II) and Platinum (II) Complexes Supported by Non-Pincer Ligands

1.2.1 Three-coordinate palladium (II) complexes

Palladium phosphine complexes are well known for their ability to catalyze a vast number of cross-coupling reactions such as Stille, Suzuki, Heck, Hiyama, Sonogashira, Negishi coupling, and Buchwald-Hartwig amination.[101-103] The 2010 Nobel Prize awarded to Professor Richard F. Heck, Professor Ei-ichi Negishi and Professor Akira Suzuki for palladium catalyzed cross-coupling reactions highlights the importance of these reactions. **Scheme 1.9** shows a generic mechanism for these cross-coupling reactions.[103] The first step involves oxidative addition of an aryl halide on Pd(0) (**A**) to form a Pd(II) aryl halide (**B**) which then undergoes transmetallation to generate (**C**) followed by reductive elimination of ArR and regeneration of the Pd(0) catalyst (**A**). Intermediates with vacant coordination sites are typically invoked in many transition-metal catalyzed cross-coupling reactions.[103] For example, reductive elimination of Ar-R from intermediate (**B**) can be envisioned to occur from a four-coordinate or three-coordinate species (**Scheme 1.9b**). Many cross-coupling reactions have been proposed to go through monomeric, three-coordinate intermediates prior to reductive elimination.[104]

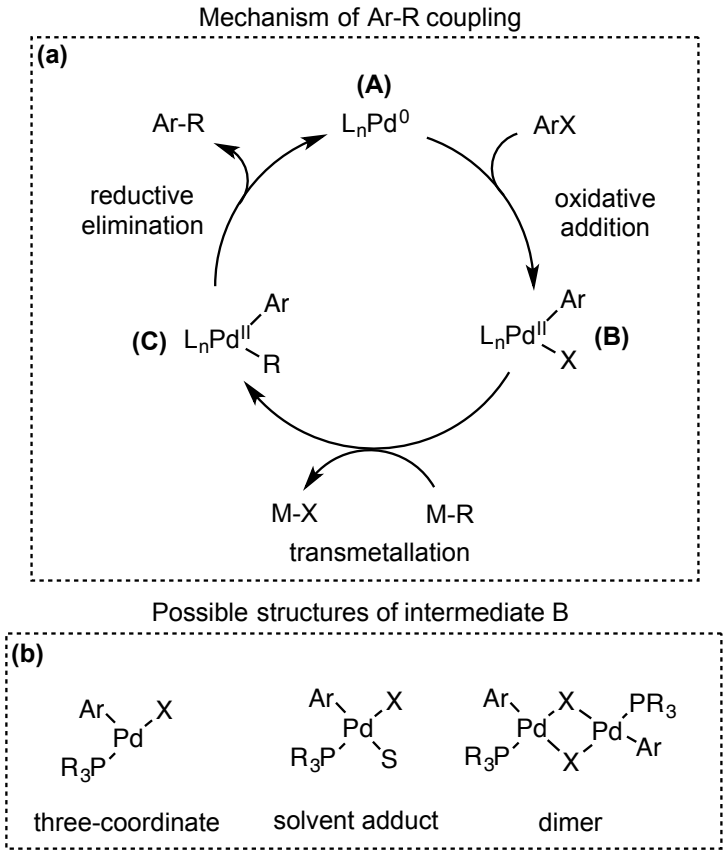

Scheme 1.9 Mechanism of palladium catalyzed Ar-R coupling reaction (a); possible structures of intermediate **B** (b).

A three-coordinate complex can be formed via direct oxidative addition with a bulky ligand or by dissociation from a four-coordinate palladium complex. However, despite the vast number of coupling reactions, there are only a few reports of isolated three-coordinate Pd(II) complexes. In 2004 Hartwig et al. reported the synthesis of a series of monomeric, T-shaped, neutral arylpalladium(II) halide complexes.[95,96] Complexes **1-60** and **1-61** can be easily made via direct oxidative addition of an ArX (X = Br, or I) from $Pd(P^tBu_3)_2$.

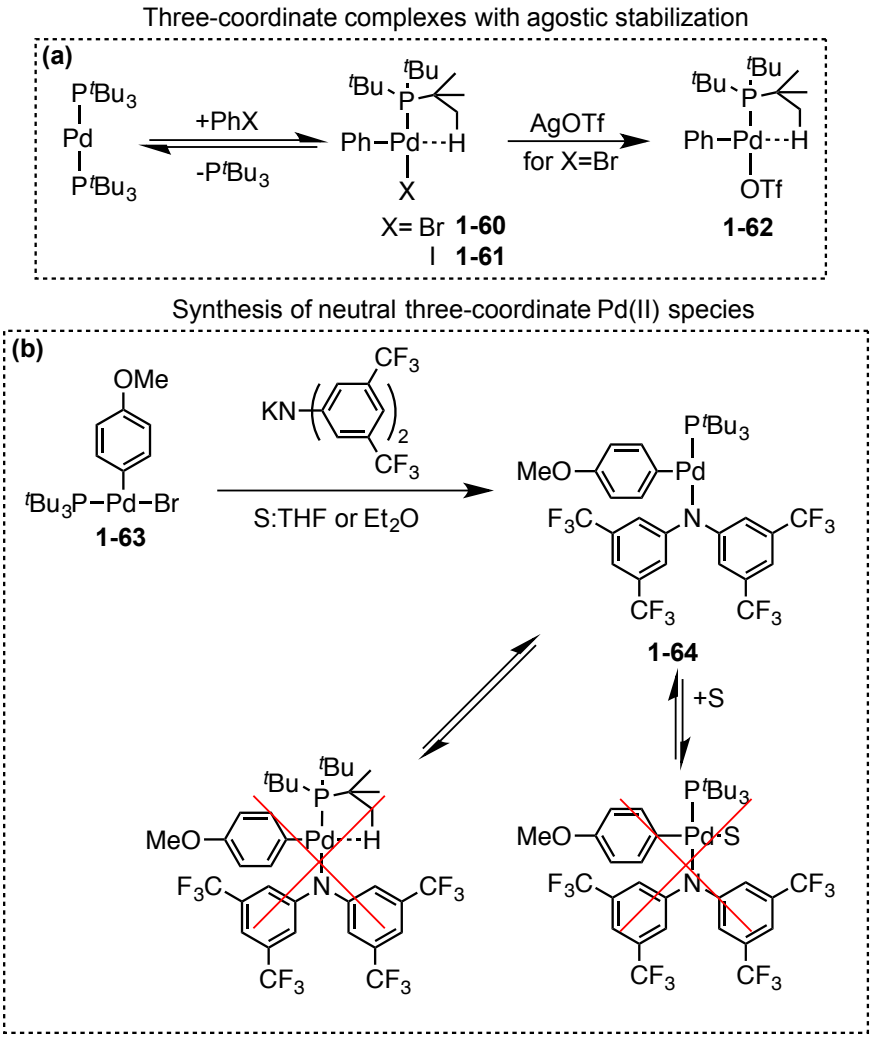

Scheme 1.10 Synthesis of three-coordinate palladium (II) supported by agostic interactions (a); and synthesis of truly three-coordinate palladium (II) species (b).

The triflate analog (**1-62**) can be made via salt metathesis of **1-60** with AgOTf. The bulky $^{t}Bu_3P$ ligand in these complexes prevents formation of dimers or solvent adducts. However, these complexes (**1-60**, **61**, **62**) are stabilized by a weak agostic interaction and therefore are not truly three-coordinate, 14-electron complexes. The empty site, which is stabilized by an agostic interaction, is *trans* to the phenyl ligand, the

ligand with the strongest *trans*-influence. In a separate communication, Hartwig et al. reported the synthesis of a truly three-coordinate, 14-electron complex (**1-64**; **Scheme 1.8**).[28] The three ligands of this complex, aryl, phosphine and amido form a T-shape structure. Complex **1-63** is made via oxidative addition of an electron rich aryl bromide such as 1-bromo-4-methoxy-benzene. Substitution of the bromide with [N(3,5-$(CF_3)_2C_6H_3)_2$], an electron poor diarylamide, produces **1-64**. This complex, unlike **1-61**, **1-62**, and **1-63** does not form an agostic interaction. The stability of these complexes with respect to formation of four-coordinate complexes was analyzed computationally by Espinet et al..[105,106] Formation of a four-coordinate square planar complex could involve coordination of solvent, dimerization or formation of an agostic interaction. The three factors analyzed were the substituents on the aryl, sterics on the phosphine and the relative effect of ligands such as -Br, -I, -OR and $-NR_2$. Each of these factors plays an important role in determining the stability of the three-coordinate complexes with respect to formation of a four-coordinate species. Among these factors, the most important is likely the *trans*-influence of the ligand *trans* to the empty site. Aryl, a strong *trans*-influence ligand, plays a significant role in stabilizing the three-coordinate, T-shape structure of compound **1-64**. A strong *trans*-influence ligand raises the energy of the orbital *trans* to it, thus weakening the bond strength of the ligand in the *trans* position. And of course the weaker the bond strength of the ligand in the *trans* position the more stable a three coordinate Pd(II) species will be. One would expect that addition electron-donating substituents on the para position of the aryl would further stabilize the

three-coordinate species; however, addition of a *p*-methoxy substituent to the aryl ligand was calculated to have only a minimal stabilization effect. [105]

The second factor analyzed was the role sterics on the stability of the three-coordinate species. As expected, bulkier phosphines such as P^tBu_3 and P^tBu_2Ad play a significant role in avoiding dimerization and coordination of solvent. However, bulkier phosphine ligands do not protect the metal center from formation of agostic interactions and may even facilitate their formation. Because of the larger cone angle, bulkier phosphines such as P^tBu_3, the C-H bonds are able to more easily reach the metal center. The final factor analyzed was the influence of the X-type ligand cis to the empty site. As shown in the previous section ligands such as -Br, -I, and -OTf in combination with bulky phosphines such as P^tBu_3 tend to form agostic interactions. However, as compound **1-64** illustrates, when X is a bulky amido ligand ($-NR_2$) no agostic interactions are observed. This is believed to be mostly an electronic effect. The amido, although a weak π donor, can donate electron density from the nitrogen lone pair to the metal. Calculations by Espinet et al. on the rotational barrier of the Pd-NR_2 bond, suggest that there is a "single-face π interaction" of the lone pair of the amido ligand with an unoccupied *d* orbital of the metal.[106] However, the calculations for this compound were done on a highly simplified version of **1-64** where the amido is $-NH_2$. The amide ($-NH_2$) ligand is a much better π donor than the electron deficient fluorinated diarylamido lingand used in **1-64**. The use of electron-donating diarylamines (i.e. N(*p*-tol)$_2$) as ligands in place of electron deficient N(3,5-$(CF_3)_2C_6H_3)_2$ could potentially stabilize the three-coordinate species even further; however, the use of N(*p*-tol)$_2$ as a

ligand dramatically accelerates the rate of $PhNAr_2$ reductive elimination thus preventing the isolation of the intermediate three-coordinate species even at low temperatures. Despite the use of an electron poor diarylamine, **1-64** still undergoes decomposition via reductive elimination of (anisyl)N(3,5-$(CF_3)_2C_6H_3)_2$. Based on the above discussion it is clear that the ability to access a Pd(II) three-coordinate species is reliant on a combination factors such as sterics, *trans*-influence ability, and the electron donating ability of the X-type ligand cis to the empty site.

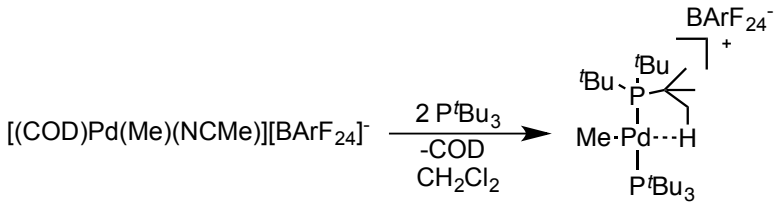

1-65 **1-66**

Scheme 1.11 Synthesis of agostic stabilized, three-coordinate palladium (II) complex (**1-66**).

In 2013 Brookhart and coworkers reported the synthesis of a bis(phosphine) complex, $[MePd(P^tBu_3)_2]^+[BArF_{24}]^-$ **(1-66)** from $[(COD)PdMe)(NCMe)]^+$ $[BArF_{24}]^-$ (**1-65**; **Scheme 1.11)**. Compound **1-66** is a T-shaped, Pd(II) complex, stabilized by an agostic interaction.[98] This example further illustrates how the combination of a strong *trans*-influence ligand such as methyl, and bulky ligands (i.e. P^tBu_3) is insufficient to prevent formation of an agostic interaction. Remarkably, the agostic interaction formed in this complex, is strong enough to impede coordination of even small ligands such as

H_2 and CO. From these few examples it is clear that stabilization of a three coordinate Pd(II) complex is dependent of a variety of factors. It is also important to point out that to this date there are no examples of cationic, three-coordinate Pd(II) complexes without C-H agostic bond stabilization or *trans* to an electronegative element (i.e. nitrogen). These complexes are likely more difficult to isolate because their cationic character makes them much more electrophilic, and as a result benefit more from agostic interactions. The next section will discuss the synthesis, characterization and reactivity of three-coordinate Pt(II) complexes.

1.2.2 Three-coordinate platinum (II) complexes

Since Shilov's initial discovery of Pt based C-H activation in the 1970's,[107-109] a significant effort has been devoted towards the development new Pt complexes that undergo C-H activation more effectively. Typically Pt based C-H activation is believed to occur via unsaturated, T-shaped Pt complexes. Because of their potential application towards C-H activation, and their fundamental importance, a significant amount of work has been dedicated towards isolating and characterizing unsaturated 14-electron, Pt(II) complexes.

In the previous section the synthesis and characterization of **1-66** was discussed. Prior to this publication, Weller and coworkers reported the synthesis of the Pt analog, $[MePt(P^iPr_3)_2]^+[CHB_{11}Me_{11}]^-$ (**1-67**).[94] This species can be synthesized via a one-electron oxidation of *cis*-$Me_2Pt(P^iPr_3)_2$ (**1-68**) with $[CHB_{11}Me_{11}]^\bullet$, generating CH_4 as the byproduct (**Scheme 1.12**).

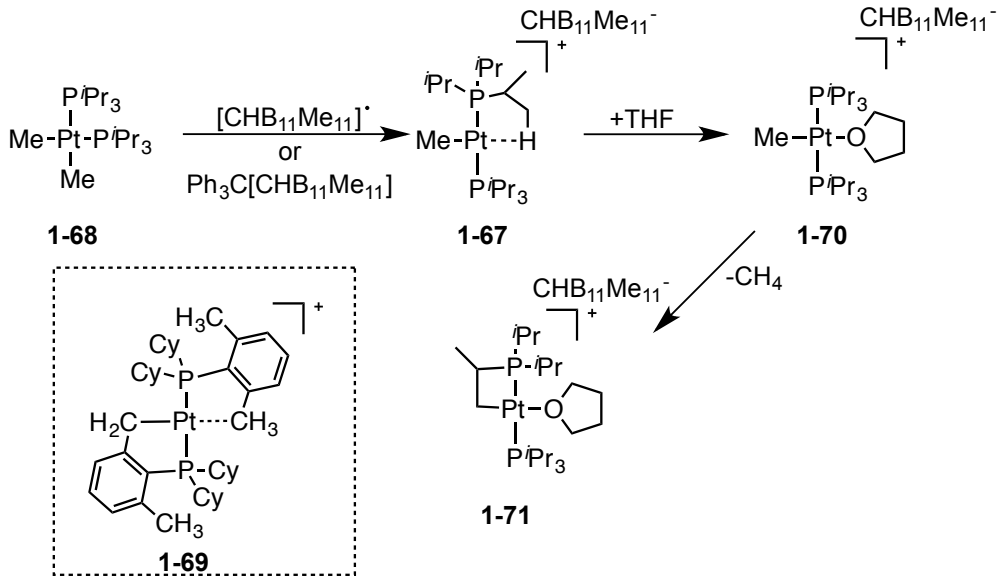

Scheme 1.12 Synthesis and reactivity of platinum three-coordinate cation stabilized by an agostic interaction (**1-67**).

Alternatively, addition of $Ph_3C[CHB_{11}Me_{11}]$ to **1-68** also produces the desired product with concomitant formation of Ph_3CMe. Although no agostic interactions were detected by NMR, single-crystal X-ray analysis of **1-67** revealed a relatively short Pt-C bond distance (2.859(7) Å), indicative of a C-H agostic interaction. This complex is also analogous to the cyclometalated Pt(II) species (**1-69**) reported by Baratta and coworkers in 2003 (**Scheme 1.12**).[93] These two cationic species are best described as 14-electron, T-shaped, Pt(II) complexes that are stabilized by a weak agostic interactions. Unlike its Pd analog (**1-66**) which does not coordinate solvent, complex (**1-67**) does coordinate THF and forms $[MePt(THF)(P^iPr_3)_2]^+$(**1-70**). This complex over time (10 d) undergoes acid catalyzed cyclometalation producing **1-71**. Although the methyl ligand is a strong

trans-influence ligand, it appears that it is not *trans* labilizing enough to stabilize an empty coordination site.

In 2005, Scheschkewitz and coworkers reported the synthesis of a cationic, three-coordinate, 14-electron Pt(II) complex supported by a boryl ligand.[110] Addition of $Na[BArF_{24}]$ to **1-72** produces **1-73** with concomitant formation of NaCl. Despite the use

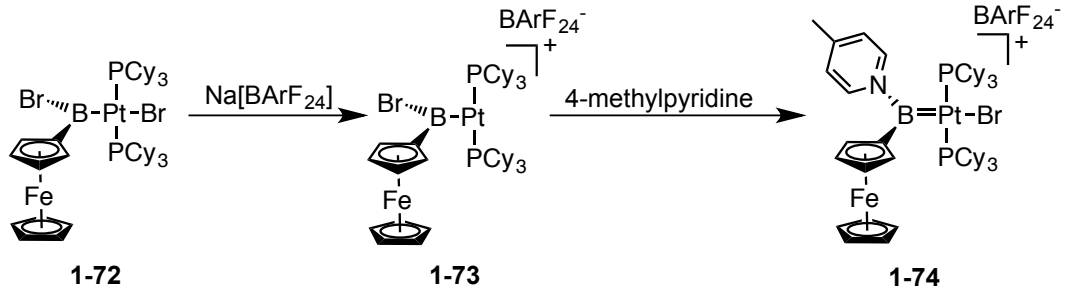

Scheme 1.13 Synthesis of three-coordinate, platinum (II) boryl complex (**1-73**) and borylene complex (**1-74**).

of PCy_3 as supporting ligands, which can easily cyclometalate or form agostic interactions, no such interactions were observed in **1-73** (**Scheme 1.13**). The authors attribute the absence of a fourth ligand to the boryl ligand's strong *trans*-influence.[110-112] The boryl ligand has been shown to be a stronger *trans*-influence ligand than σ-donors such as hydride, stannyl groups or CO.[110] It is interesting that even with the use of phosphines such as PCy_3, which is not as bulky as P^tBu_3, this complex remains three-coordinate even in solvents typically considered coordinating, such as CH_2Cl_2. In the presence of even stronger Lewis bases such as 4-methylpyridine, the expected Lewis acid/base adduct is not formed. Instead compound **1-73** is converted to a Pt(II) base-

stabilized borylene complex **1-74** via a 1,2 migration of the bromide from the boron to Pt center. Despite the seemingly unique stability of complex **1-73**, in 2008 Uttinger and coworkers synthesized a series of boryl complexes with the same three-coordinate, T-shaped architecture.[113,114] It is clear that the key stabilizing factor in these complexes is the strong *trans*-influence of the boryl ligand.

1.2.3 Three-coordinate platinum (II) complexes supported by NHC carbenes

Up to this point, all the unsaturated complexes that have been discussed in this chapter have involved the use of phosphines as supporting ligands. However, N-Heterocyclic carbenes have also been shown to be capable of supporting unsaturated Pt complexes. The following section will discuss the synthesis of two examples of unsaturated Pt(II) complexes supported by NHC carbenes. In 2012 Conejero and coworkers reported the synthesis of **1-75**, a three-coordinate, 14-electron Pt(II) complex without agostic bond stabilization (**Scheme 1.14**).[25] The synthesis of **1-75** starts by abstraction of iodide from Pt(I)Me(IMes*)$_2$ (**1-76**) with Na[BArF$_{24}$] which produces *trans*-[PtMe(IMes*)$_2$]$^+$[BArF$_{24}$]$^-$ (**1-77**). Thermolysis of **1-77** at 60 °C for 12 h generates the cyclometalated product (**1-78**). Compound **1-78** is capable of undergoing intermolecular C-H activation of a variety of arenes such as toluene, C_6H_6, $C_6H_2F_4$ and C_6F_5H. Compound **1-76,** the product of C-H activation of $C_6H_2F_4$, was characterized by single-crystal X-ray crystallography and was found to be a rare example of a three-coordinate, 14-electron complex without agostic stabilization.

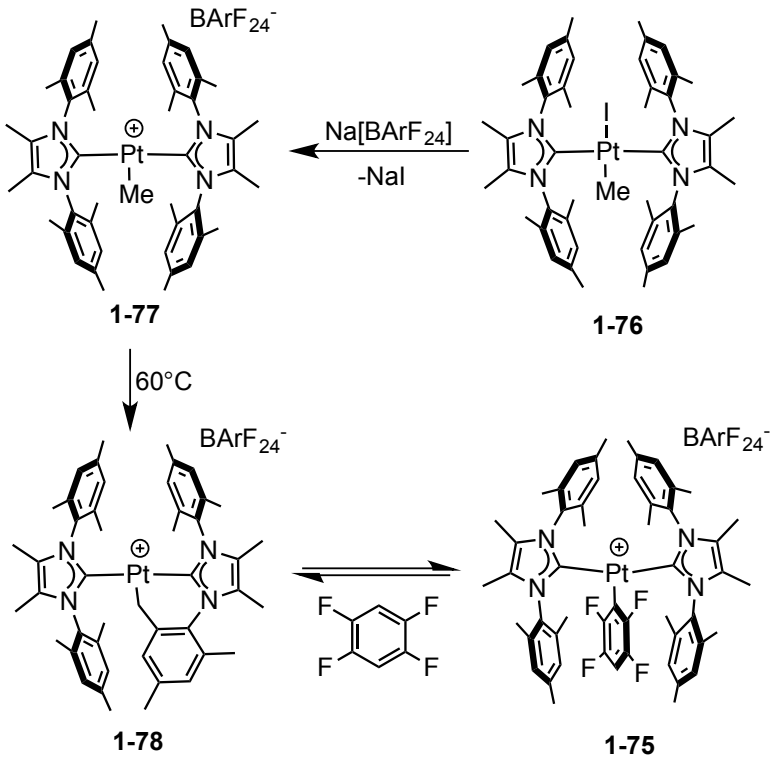

Scheme 1.14 Synthesis of NHC stabilized three-coordinate platinum (II) complex (**1-75**).

The nearest hydrogen to the Pt center is about 3.117 Å away, too far to be considered an agostic interaction. The stability of this complex towards formation of a Lewis adduct can be attributed to the strong *trans*-influence of aryl ligand, and the sterically imposing mesitylene substituents on the NHC carbene ligands. The fluorinated aryl ligand ($-C_6F_4H$) in **1-75** is likely a weaker *trans*-influence ligand than methyl in **1-67**. Despite this, compound **1-75** contains no agostic interactions, whereas compound **1-67** does. This suggests that the major difference lies on the supporting ligands (NHC versus $^{i}Pr_3P$). In terms of electronics, NHC carbenes are generally stronger σ-donors than trialkyl phosphines, and therefore donate greater electron density onto the metal

center.[115] This is important because it reduces electrophilicity of the metal center in cationic complexes such as **1-75**. In addition, the steric environment around tertiary phosphines is very different from that of NHC carbenes. Whereas the substituents in tertiary phosphines point away from the metal center (measured as cone angles), in NHC carbenes the substituents point towards the metal center (measured as percent buried volume).[115,116] In compound **1-75**, the fluorinated aryl ligand (C_6F_4H) pushes the mesityl groups closest to it away from each other, and at the same time brings the mesityl groups closer together. This is important because in compound **1-75**, the NHC carbenes are able to wrap around the empty site in such a way that blocks coordination of solvent or dimerization. However, the mesityl groups are far enough from the metal that agostic interactions are not formed.

Thus far, all the three-coordinate Pt and Pd complexes discussed in the previous sections have had a T-shape structure. However, in 2009 Markó et al. reported the synthesis of a rare example of a Y-shaped, three-coordinate Pt(II) complex (**1-79**). Compound **1-79** is synthesized by adding an excess of Me_2PhSiH to compound **1-80.** Upon addition of Me_2PhSiH the tetramethyldivinyl siloxane in complex **1-80** undergoes goes hydrosilation generating intermediate **1-81** (**Scheme 1.15**). It is suspected that compound **1-82** is an intermediate in the reaction that rapidly reacts with excess Me_2PhSiH to generate **1-79** and concomitant formation of dihydrogen. The angles around the Pt center in compound **1-79** are 141.7(2)° (for C-Pt-Si) and 80.9(1)° (for Si-Pt-Si), consistent with a Y-shape structure.

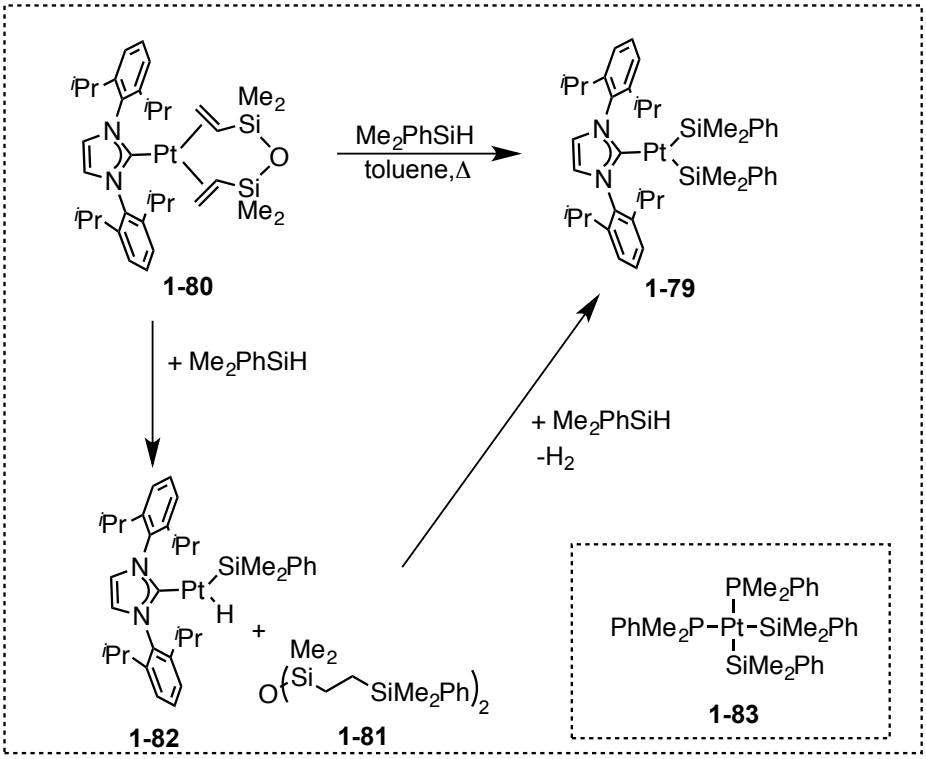

Scheme 1.15 Synthesis of a three-coordinate, Y-shape, d^8, and formally platinum (II) complex (**1-79**).

The Si-Si bond distance in compound **1-79** (2.980(5) Å) is significantly longer compared to what is observed for free disilanes such as $^{t}Bu_3Si\text{-}Si^{t}Bu_3$ (2.697(3) Å), $H_3Si\text{-}SiH_3$ (2.331(3) Å),[117] and the calculated for bond length of $Me_3Si\text{-}SiMe_3$ (2.364 Å).[26] However, the Si-Si bond length in **1-79** is significantly shorter than what is observed in square planar complexes such as *cis*-$[Pt(SiMe_2Ph)_2(PMe_2Ph)_2]$ (3.233(1) Å; **1-83**).[118] Certainly, the most intriguing aspect of complex **1-79** is the unusual Y-shape structure.

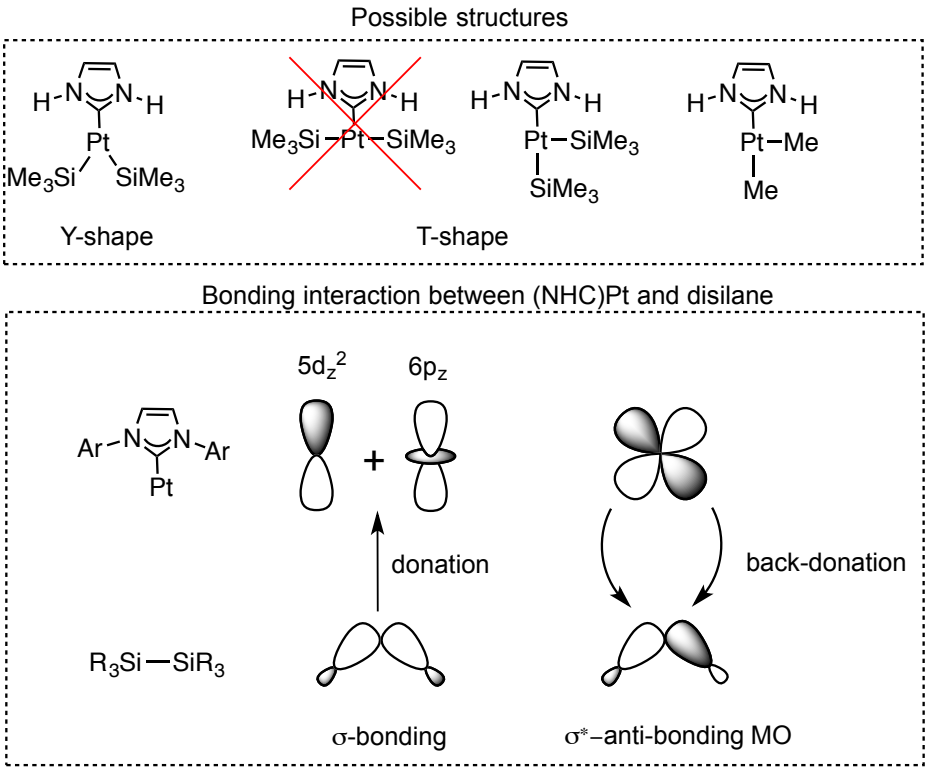

Figure 1.4 Y-shape versus T-shape platinum (II) complexes (top); bonding in **1-79** (bottom).

To address this phenomenon, the authors conducted DFT calculations on a simplified version of **1-79**, and determined the relative stability of both the T-shape, and Y-shape geometries (**Figure 1.4**). The results of their calculations determined that for purely σ donating ligands such as methyls the T-shape geometry is more favorable. This is consistent with the Pd(II), and Pt(II) structures discussed in previous sections. However, for silyl ligands, which are known to be both strongly σ donating and π accepting, the Y-shape is more favorable.[23]

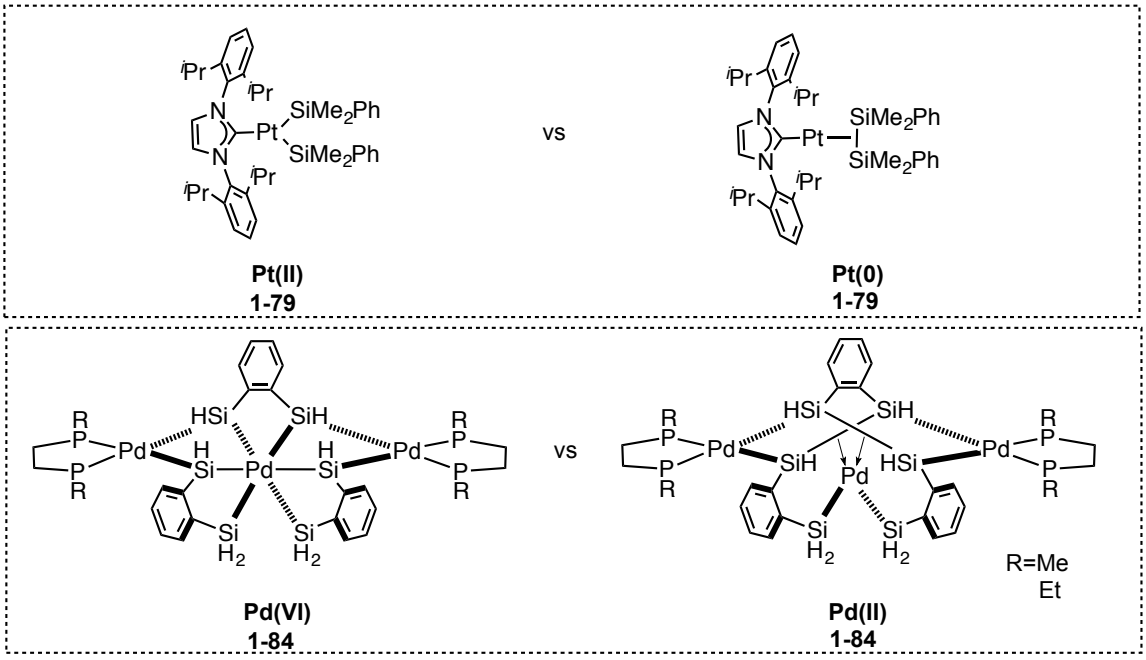

Figure 1.5 Possible oxidation states of disilane platinum (**1-79**) and palladium (**1-84**) complexes.

Compound **1-79** can essentially be viewed as a "snapshot" of reductive elimination (or oxidative addition) of disilane. In a more detailed DFT analysis of **1-79** undertaken by Sakaki and coworkers, it was found that complex **1-79** can best be described as a Pt(0) complex with two L type ligands, NHC and a disilane.[26] The bonding **1-79** is a combination of σ donation from $PhMe_2Si$-$SiMe_2Ph$ to Pt and backbonding from Pt to the disilane (**Figure 1.4**). This is consistent with the observed elongation Si-Si bond length in compound **1-79** relative to free disilane and the shortening relative to four-coordinate, square-planar *cis*-$[Pt(SiMe_2Ph)_2(PMe_2Ph)_2]$. In fact, **1-79** can more safely be considered to have an oxidation state of 0 or +2, hence the reason why it is considered a "snapshot of oxidative addition". In recent years several formally high valent complexes supported by silyl ligands have been reported. Most

notably, in 2002 Tanaka and coworkers published the synthesis of a formally hexavalent Pd complex (**1-84**; **Figure 1.5**).[119] In a 2002 Science Perspective Crabtree discussed the advent of new high valent Pd^{VI} complexes.[120]Crabtree makes the analogy to the hypothetical PdH_6 where Pd is in the +6 oxidation state. In his report he makes the argument that PdH_6 can instead be viewed as either $Pd^{IV}H_4(H_2)$, $Pd^{II}H_2(H_2)_2$ or $Pd^0(H_2)_3$. This analogy can be carried forward to complex **1-84**, where $Pd^{VI}(SiR_3)_6$ can really be either $Pd^{IV}(SiR_3)_4(R_3Si\text{-}SiR_3)$ or $Pd^{II}(SiR_3)_2(R_3Si\text{-}SiR_3)_2$ or $Pd^0(R_3Si\text{-}SiR_3)_3$. Based on Crabtree's analysis complex **1-84** is likely somewhere in between a Pd(II), and a Pd(VI) complex. In fact, computational work by Alvarez, and workers determined that **1-84** is indeed better described as being composed of two side-on Si-Si, L-type ligands, and two silyl, X-type ligands on Pd(II).[121]

1.3 Conclusion

This chapter discussed a handful of examples of the extraordinary reactivity exhibited by pincer metal complexes, such as (PCP)M, (PNN)M, and (PNP)M. These organometallic complexes have impacted key areas in chemistry such as the conversion of H_2O into H_2 and O_2, and alkane metathesis, which can be used to produce higher-grade fuels. In addition, utilizing the Fryzuk $^{Fr}PNP^{tBu}$ ligand as a platform, Caulton and coworkers isolated several unsaturated three-coordinate complexes that exhibited unusual reactivity. These unsaturated complexes are stabilized in a variety of ways. For example, the $[(^{Fr}PNP^{tBu})Ni]^+[BArF_{20}]^-$ complex is stabilized by an unusual *trans*-annular interaction. The $(^{Fr}PNP^{tBu})Co(I)$ complex is stabilized by accessing a triplet, high-spin

state that prevents formation of solvent adducts or agostic interactions. In addition, this chapter discussed the synthesis and characterization of several non-pincer ligand supported Pt and Pd unsaturated complexes. Based on Hartwig's example of a truly three-coordinate Pd(II) complex, it is clear that the stabilization of three-coordinate Pd(II) complexes is dependent on steric and electronic factors such as *trans*-influence and π donating ability. Analogously, the platinum(II) three-coordinate complexes reported in this review all have very strong *trans*-influencing ligands such as boryl or aryl. In addition, based on the example reported by Conejero, and coworkers it is clear that NHC carbenes are also capable of stabilizing three-coordinate unsaturated complexes. Finally, with the exception of the example reported by Markó and coworkers, all of the truly three-coordinate Pt(II) and Pd(II) complexes have had T-shape geometry around the metal. However, Markó's example of a Y-shaped Pt complex is best described as a Pt(0) complex with two L type ligands, NHC and a disilane. This complex can be viewed as a "snapshot" of reductive elimination of a Si-Si bond.

CHAPTER II

SYNTHESIS OF (^{F}PNP^{R})PdX (R = ^{i}Pr, ^{t}Bu, Ad) COMPLEXES AND THE USE OF FLUORINE AS AN NMR SPECTROSCOPIC PROBE*

2.1 Introduction

Pincer ligands have become an integral part in transition metal chemistry (see Chapter I).[3,122] The tridentate, meridional coordination allows for the synthesis of highly robust and structurally predictable metal complexes. Pincer metal complexes have been shown to have a remarkable balance between stability and reactivity allowing for the development highly effective catalysts.[3] In addition, pincer ligands can be easily tuned sterically and electronically, allowing for the development of improved catalysts.[123] Pincer ligands have found application in catalysis and strong bond activation. For example, (PCP)Ir(L) (**1-12**) and (POCOP)Ir(L) (**1-13**) complexes have been reported to be remarkable dehydrogenation catalysts (see Chapter I).[124-128] In addition these catalysts have been shown to be capable of undergoing catalytic alkane metathesis by working in tandem with olefin metathesis catalysts (see Chapter I).[30] In 2011, Goldman et al. reported the net oxidative addition of C(sp^3)-F bonds via an initial C-H bond activation using a (PCP)Ir complex.[129]

The Liang,[56,57] Mindiola,[58-60] Ozerov and other[61,76,77] groups have done extensive work with diarylamido PNP$^{i\text{Pr}}$ ligands, synthesizing both transition metals

* Sections 2.2.5-7 were reprinted with permission from "A terminal palladium fluoride complex supported by an anionic PNP pincer ligand" by Huacuja, R.; Herbert, D. E.; Fafard, C. M.; Ozerov, O. V., 2010. J. Fluorine Chem. 131, 1257-1261, Copyright [2010] by Elsevier Publisher

complexes,[54,56-58,60,130] and main group compounds[131,132] across the periodic table. The diarylamino framework in $^{X}PNP^{R}$ ligands makes this ligand significantly more rigid that the silyl based ^{Fr}PNP ligand developed by Fryzuk[85-87,133] and later employed by Caulton.[134] The use of the diarylamino $^{X}PNP^{R}$ ligand in with transition metals has led to the discovery of some unusual structures and remarkable reactivity.

The synthesis of diarylamido/bis(phosphine) $^{X}PNP^{Ra}$ ligands is modular and has been shown to be very adept to structural modifications.[8,70,135] For example, the substituents para to the amine functionality (X = Me, F, Br, Me_3Si-,[70] OMe[136]), and on the phosphorus atom (R = Ph, ^{i}Pr,[70] Et[137], pyrrolyl[138]) can be tuned to obtain the desired property such as sterics, electronic or even solubility (**Figure 2.1**). The $^{X}PNP^{R}$ ligand with a fluorine para to the amine functionality is particularly useful because of the extra convenience of the ^{19}F NMR spectroscopic handle.

[a] Note: The following describes the nomenclature of the bis(ortho-phosphinoaryl)amine based pincer ligand and the corresponding metal complexes: The abbreviation "($^{X}PN(Z)P^{R}$)" applies to the free ligand, and "($^{X}PNP^{R}$)MY" to metal complexes. In these abbreviations M is the metal, X represents the substituent para to the amine functionality. R represents the substituent on the phosphine and Z is simply the substituent on the nitrogen of the ligand. For example, "($^{X}PNP^{R}$)PdY" is an abbreviation for the compound shown in **Figure 2.1** . Whereas the abbreviation "(PNP)PdY" is more general and does not specify any particular substituents on the ligand.

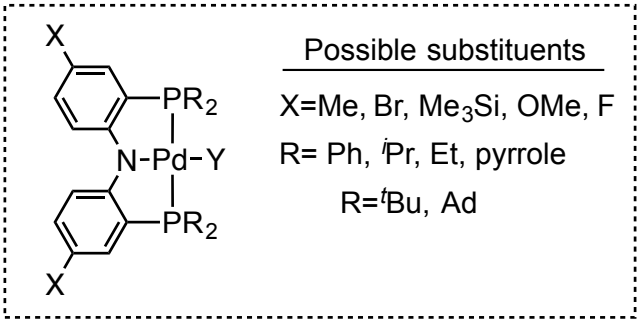

Figure 2.1 Illustrative depiction of square–planar palladium (II) complexes of the general type (^{X}PNP^{R})PdY and possible X and R substituents.

The first part of this chapter will consist of a general discussion of the synthesis of (^{X}PNP^{R})Pd-Y complexes. This will be followed by a description of the synthesis of bulky ^{F}PN(Me)P^{R} (R = ^{t}Bu and Ad) ligands and the corresponding (^{F}PNP^{R})PdY complexes. In addition, this chapter will discuss the correlation between the ^{19}F NMR chemical shifts of (^{F}PNP$^{i\text{Pr}}$)PdX complexes and the donicity of the ligand *trans* to the amido (X). Finally, this chapter will also discuss the synthesis, characterization, and reactivity of a palladium fluoride complex. Well-defined molecular transition-metal fluoride complexes have been attracting attention of synthetic chemists for a number of years.[139-142] The chemistry of Pd fluoride complexes has seen particular development over the last decade. Palladium fluoride complexes appear to be somewhat more synthetically challenging to access, and some are more prone to decomposition compared to the Pd complexes of heavier halides. This is especially true for complexes with phosphine ligands and for difluoride complexes. Only comparatively recently, the work of Grushin[143-145] and of Vigalok[139,146] has yielded isolable palladium fluoride complexes with phosphine donors and palladium difluoride complexes. The interest in

palladium fluoride complexes is partly guided by the quest for aryl-fluorine reductive elimination at Pd,[147,148] an essential step of the highly desirable catalytic C-F bond formation. Although many other aryl-heteroatom reductive eliminations from Pd(II) are well known,[103] unambiguous aryl-fluorine reductive elimination from Pd(II) in a catalytic cycle was first achieved only in 2009 by Buchwald et al.[149] At the same time, an alternative catalytic aryl-fluorine bond formation relying on reductive elimination from Pd(IV) complexes has been studied by the groups of Sanford and co-workers,[150] Yu and co-workers,[151] and Ritter and co-workers.[152-154]

The Ozerov group has studied complexes of the diarylamido/bis(phosphine) $^{X}PNP^{R}$ ligands,[4,130] versatile members of the pincer class.[4] Against the backdrop of interest in Pd fluoride complexes, we surmised that a square-planar Pd monofluoride complex supported by a $^{F}PNP^{i Pr}$ ligand should be accessible and robust. Sanford et al. reported a stable fluoropalladium complex supported by the NCN pincer ligand in 2010.[155] We also wanted to test whether our fluoride complex may prove to be a convenient precursor to other ($^{F}PNP^{i Pr}$)PdX complexes through F/X metathesis with silane reagents. We have chosen to use the fluoro-substituted ^{F}PNP ligand because of the extra convenience of the ^{19}F NMR spectroscopic handle built into the pincer ligand.

2.2 Results and Discussion

2.2.1 General overview of $^{F}PNP^{i Pr}$ ligands and metal complexes

The Ozerov group has extensively explored the synthesis of $^{X}PNP^{R}$ ligands and the corresponding palladium complexes.[8,54,63,66,67,69,70,135,156] **Scheme 2.1a** shows the

general protocol for the synthesis of ^{F}PN(Me)P$^{i\text{Pr}}$ (**2-1**) ligand. Addition of ^{n}BuLi to **2-2** produces **2-3**, via lithium/halogen exchange, which upon treatment with ClP^{i}Pr$_2$ produces **2-1**. The reaction between **2-1** and Pd(COD)Cl$_2$ or Pd(OAc)$_2$ (not cleanly), produces (^{F}PNP$^{i\text{Pr}}$)PdCl (**2-4**) or (^{F}PNP$^{i\text{Pr}}$)PdOAc (**2-5**), respectively.[70,135] These two complexes are starting complexes for the synthesis of most (^{F}PNP$^{i\text{Pr}}$)PdX complexes. **Scheme 2.1b** illustrates the synthesis of some (^{F}PNP$^{i\text{Pr}}$)PdX complexes that have been synthesized by the Ozerov group. The reactivity of several of these compounds will be discussed in Chapters III through VI. For example, (^{F}PNP$^{i\text{Pr}}$)PdOTf (**2-6**) which is used as a starting platform for the majority of the chemistry in Chapter IV and V, can be synthesized by treating **2-5** with Me$_3$SiOTf. An alternative route for the synthesis of **2-6** involves the conversion of **2-4** to (^{F}PNP$^{i\text{Pr}}$)PdH (**2-7**) with NaBH$_4$[70] followed by treatment of **2-7** with MeOTf.[157] (^{F}PNP$^{i\text{Pr}}$)PdOH (**2-8**) can be synthesized by treating **2-6** with excess KOH.[157] (^{F}PNP$^{i\text{Pr}}$)PdMe (**2-9**) can be made by treating **2-4** with alkylating reagents such as MeLi.[157] Irradiation or reduction of alkyl complexes such as **2-9** produces to [(^{F}PNP$^{i\text{Pr}}$)Pd-]$_2$ (**2-10**),[54] which will be used as a starting platform for most of the chemistry discussed in Chapter III.

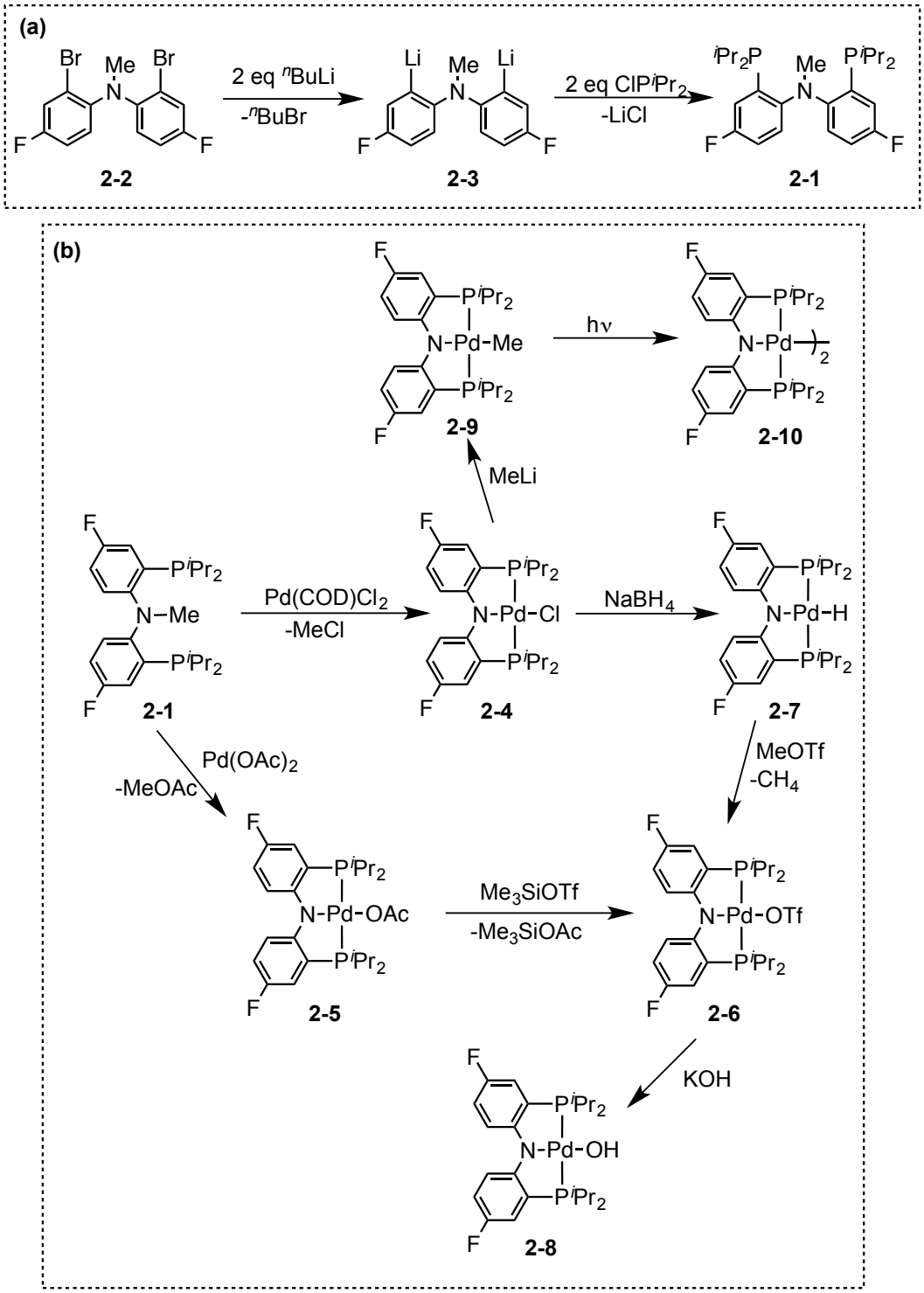

Scheme 2.1 Synthesis of **2-1** ligand (a); interconversion of ($^{F}PNP^{iPr}$)PdY complexes (b)

2.2.2 Synthesis of $^{F}PN(Me)P^{R}$ (R = ^{t}Bu and Ad) ligands

Although the substituents on the phosphorus can be varied (R = Ph, ^{i}Pr, Et,[137] pyrrolyl[138]) considerably in terms of sterics and electronics (**Figure 2.1**),[70,135,158] to date the bulkier *tert*-butyl and adamantyl ^{F}PNP ligands have not been synthesized. We were particularly interested in synthesizing bulky PNP ligands because of their potential application in isolating a three-coordinate $[(PNP)Pd]^{+}$ cation (see Chapter IV). The *tert*-butyl and adamantyl substituents are significantly bulkier than phenyl or isopropyl; the cone angle of tri-*tert*-butyl phosphine (182°) is considerably larger than triphenyl phosphine (145°), and triisopropyl phosphine (160°).[159]

As discussed in Chapter I, bulky ligands such as tri-*tert*-butyl phosphine have been used to isolate unsaturated, three-coordinate Pd(II) complexes.[28,95,96] In addition, pincer ligands such as POCOP with bulky di-*tert*-butyl substituted phosphines, have been shown by Brookhart and coworkers to be effective at stabilizing highly reactive species such rhodium methane complexes.[160] However, attempts to synthesize $^{F}PN(Me)P^{tBu}$ (**2-20**) using the traditional protocol used in the Ozerov group for R = ^{i}Pr, Ph, Et were unsuccessful (**Figure 2.1**). It is likely that the bulky *tert*-butyl groups in $ClP^{t}Bu_2$ dramatically decrease the P-electrophilicity, impeding nucleophilic attack by **2-3**. Even when iodide, a better leaving group, was used in place of chloride in $XP^{t}Bu_2$ no C-P bond formation is observed. In addition, attempts to synthesize **2-11** via **2-12** instead of **2-3** were unsuccessful.

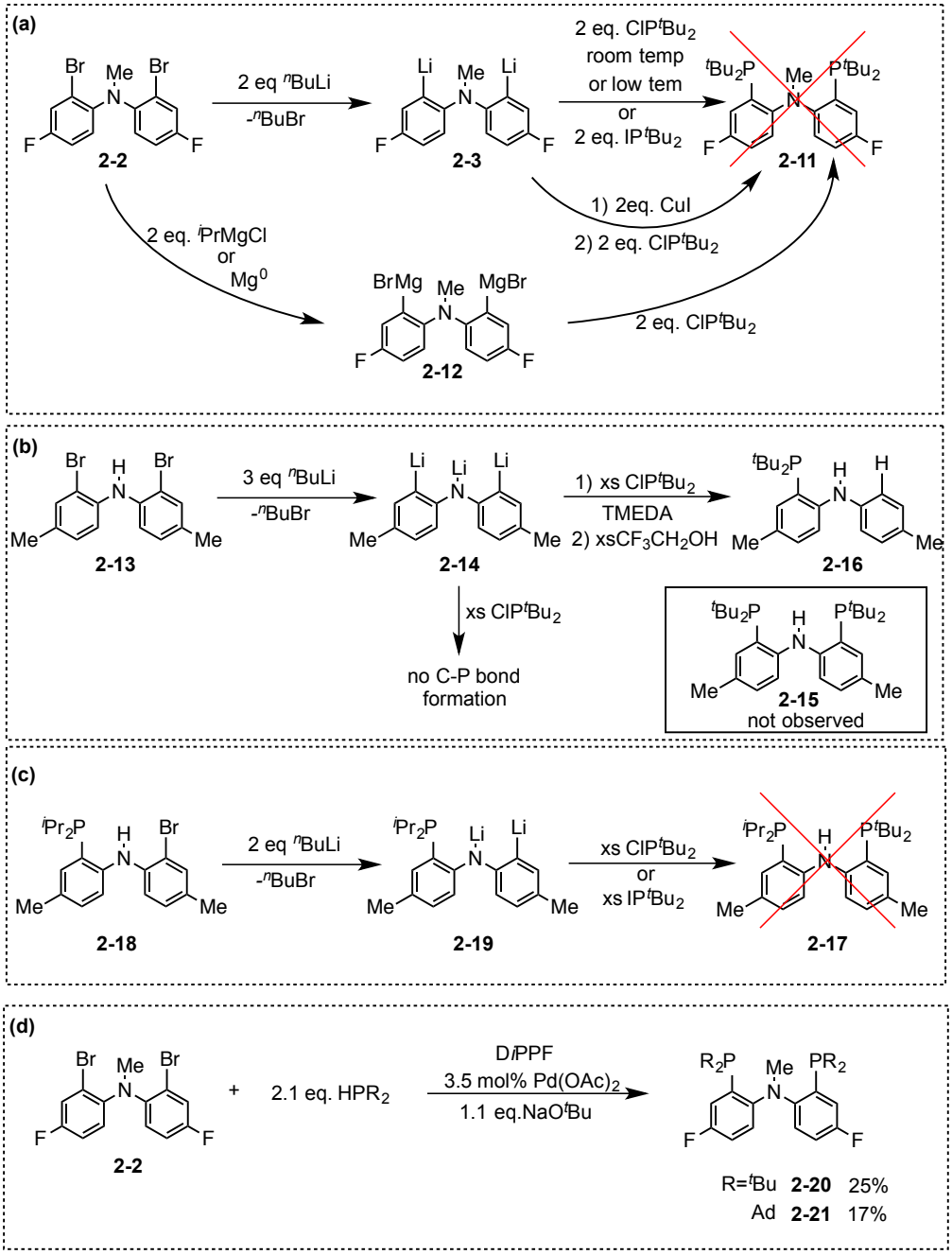

Scheme 2.2 Failed attempts of synthesis of **2-20** (a); Synthesis of **2-20** via Pd catalyzed C-P coupling (b).

This reaction was attempted via magnesium-halogen exchange with ^{i}PrMgCl; however, it is not clear if **2-12** formed in the reaction. In addition, attempts to synthesize **2-11** by treating **2-3** with CuI, and subsequent addition of Cl$P^{t}Bu_2$, were also unsuccessful (**Scheme 2.2a**). Presumably the reaction between **2-3** and CuI generates an organocuprate intermediate. The traditional protocol used by the Ozerov group were **2-13** is treated with ^{n}BuLi producing **2-14** followed by treatment with Cl$P^{t}Bu_2$ does not generate ^{Me}PN(H)P^{tBu} (**2-15**). However, addition of a few drops of TMEDA and quenching with CF_3CH_2OH generates a two products at 14.2 ppm and 3.62 ppm by ^{31}P NMR spectroscopy. Although more evidence is needed, it is possible that the final product is **2-16**. Attempts to synthesize ^{Me}PN(H)P^{iPrtBu} (**2-17**) by lithiation of ^{Me}PN(H)Br^{iPr} (**2-18**) with ^{n}BuLi generating **2-19** and addition of Cl$P^{t}Bu_2$ were also unsuccessful. However, a protocol developed by Buchwald and coworkers[161] gave access to the desired products ^{F}PN(Me)P^{tBu} (**2-20**) and ^{F}PN(Me)P^{Ad} (**2-21**). In his 2004 report, Buchwald reported the synthesis of aryl phosphines via a palladium catalyzed coupling of secondary phosphines with aryl halides. The reaction between **2-2**, two equivalents of HPR_2 (R = ^{t}Bu and Ad) and NaO^{t}Bu using $Pd(OAc)_2$ (3.5 mol%) and D*i*PPF as the catalyst produces **2-20** and **2-21** in 17% and 25% isolated yield, respectively. Because of the lipophilicity of the **2-20** ligand it is difficult to remove the impurities (unknown) by column chromatography (silica gel) without significant loss in yield. However, the ^{F}PN(Me)P^{Ad} ligand, which is less soluble than **2-20**, can be purified via a combination of silica gel and washings with pentane. The coupling of HPR_2 with **2-2** does seem to be a viable procedure to access **2-20** and **2-21**. However, the current

protocol is low-yielding, and requires relatively high Pd loading and is therefore not practical for large-scale synthesis. It is possible that other catalysts with different combinations of Pd precursors and ligands might lead to higher conversion and lower catalysts loading.

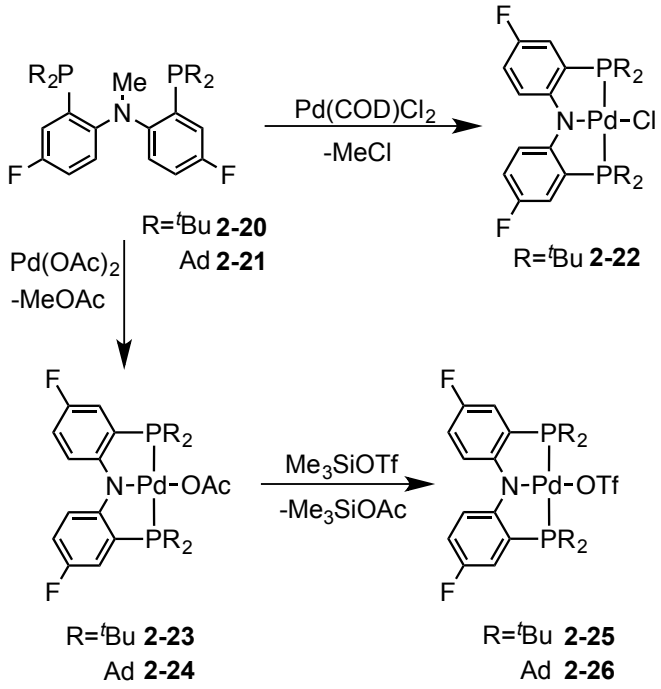

Scheme 2.3 Synthesis of (^{F}PNP^{R})PdY complexes (R = ^{t}Bu, Ad; **2-22**, **2-23**, **2-24**, **2-25** and **2-26**).

2.2.3 Synthesis of (^{F}PNP^{R})PdX (R = ^{t}Bu and Ad) complexes

Refluxing $Pd(COD)Cl_2$ with an equivalent of **2-20** in toluene overnight quantitatively produces (^{F}PNP^{tBu})PdCl (**2-22**; **Scheme 2.3**). Analogously, refluxing $Pd(OAc)_2$ with a slight excess of **2-20** and **2-21** in toluene produces (^{F}PNP^{tBu})PdOAc (**2-**

23) and (^{F}PNP^{Ad})PdOAc (**2-24**). Compounds **2-23** and **2-24** can be purified by column chromatography (see experimental for details). Even if the ligand contains organic impurities, **2-23** can be synthesized relatively pure (95%) by using a deficiency of $Pd(OAc)_2$ followed by washings with pentane and column chromatography. Treating **2-23** or **2-24** with a slight excess of Me_3SiOTf produces (^{F}PNP^{tBu})PdOTf (**2-25**; 40% isolated yield), and (^{F}PNP^{Ad})PdOTf (**2-26**) with concomitant formation of Me_3SiOAc.

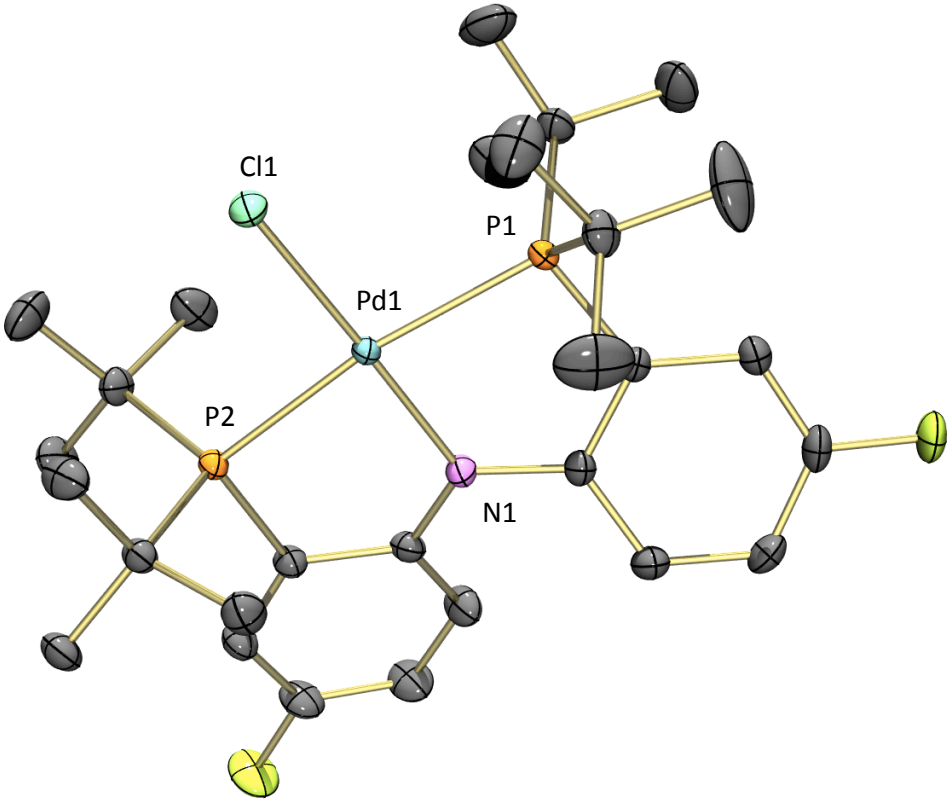

Figure 2.2 POV-Ray rendition of the ORTEP[162] drawing (50% thermal ellipsoids) of **2-22** showing selected atom labeling. Hydrogen atoms have been omitted for clarity. Selected bond distances (Å) and angles (deg): Pd1−P1, 2.3275(5); Pd1−P2, 2.3149(5); Pd1−Cl1, 2.3316(5); Pd1−N1, 2.0198(14); P1−Pd1−P2, 167.899(16); Cl1−Pd1−N1, 178.67(4).

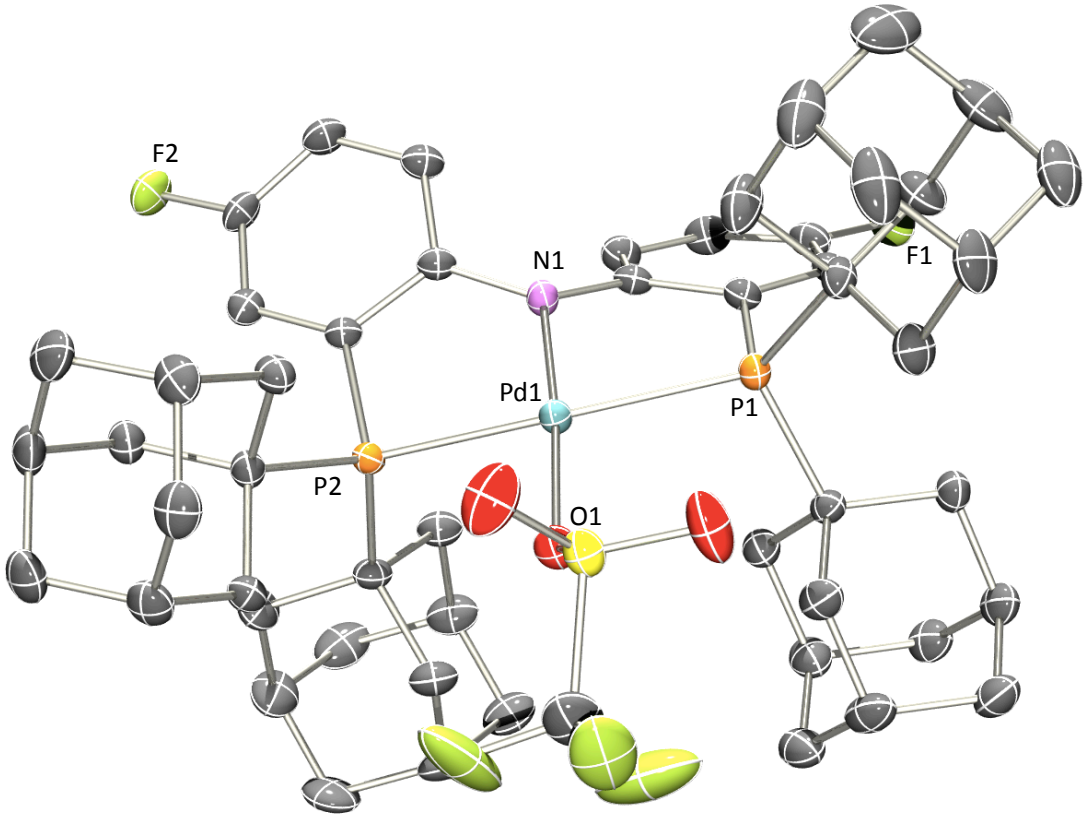

Figure 2.3 POV-Ray rendition of the ORTEP[162] drawing (50% thermal ellipsoids) of **2-26** showing selected atom labeling. Hydrogen atoms have been omitted for clarity. Selected bond distances (Å) and angles (deg): Pd1−P1, 2.3439(9); Pd1−P2, 2.3790(9); Pd1−O1, 2.1207(16); Pd1−N1, 1.9857(18); P1−Pd1−P2, 160.01(2); O1−Pd1−N1, 175.40(7).

2.2.4 Structural characterization of (^{F}PNP^{tBu})PdCl and (^{F}PNP^{Ad})PdOTf

Single-crystal X-ray diffraction of both **2-22** and **2-26** revealed a molecular structure that is closely related to other (PNP)PdX compounds (**Figure 2.2, 2.3**). The coordination environment about the Pd center in **2-22** and **2-26** is approximately square-planar. The largest deviation is the P1–Pd–P2 angle in **2-22** (167.899(16)°) and **2-26**

(160.01(2)°) which is likely a result of the constraint, imposed by the bulky Ad and ^{t}Bu groups on the phosphine ligands of ^{F}PNP. The P1–Pd–P2 angle in **2-22** is similar to what is observed in **2-5** (168.16(6)°) but somewhat than larger than (^{Me}PNP^{iPr})PdCl (**2-27**) (163.54(2)°).[70] However, the P1–Pd–P2 angle in **2-26** is significantly narrower than both of these compounds, presumably because of the large adamantyl groups and the steric pressure imposed by the triflate ligand. The Pd-P distances in **2-22** (2.3275(5) Å and 2.3149(5) Å) are marginally longer than what is observed for **2-5** and **2-27** which fall within the 2.27-2.29 Å range. The extended Pd-P bond distances are likely the result of the increased sterics of the ^{t}Bu groups. The Pd1−P1, bond distances in **2-26** (2.3439(9) Å and 2.3790(9) Å) are much longer than what is observed for **2-5**, **2-27** and **2-22**. This is likely due to a combination of steric pressure imposed by the triflate ligand and the bulky adamantyl phosphines. The Pd-N distance in **2-22** is 2.0198(14) Å, is similar to what is observed for **2-5**[135] (2.015(5) Å) and **2-27** (2.0258(19) Å),[70] but slightly longer than (^{F}PNP^{iPr})PdF (**2-28)** (1.996(5) Å).[156] However, the Pd-N bond distance in **2-26** (1.9857(18) Å) is shorter than what is observed in **2-27**,[156] consistent with poor *trans*-labilizing effect of the triflate ligand. The Pd-Cl distance in **2-22** is 2.3316(5) Å which is somewhat longer than what is observed in **2-27** (2.3157(7) Å).[70]

2.2.5 Synthesis of (^{F}PNP^{iPr})PdF and its reactivity with silicon based reagents

Treatment of the previously reported **2-6**[157] with CsF in toluene for 2 d with vigorous stirring resulted in the formation of **2-27**, which was isolated as a red crystalline powder in 64% yield upon workup (**Scheme 2.4)**. The NMR resonances

corresponding to the ^{F}PNP ligand in **2-27** are typical for (^{F}PNP)Pd-X complexes. C2v symmetry was observed on the NMR time scale. For example, two resonances for the inequivalent Me groups and a single CH resonance from the diisopropylphosphine arms were detected by ^{1}H and ^{13}C NMR spectroscopy. Consistent with this symmetry, only a single ^{19}F NMR and a single ^{31}P NMR resonance were detected for the ^{F}PNP ligand.

The Pd-bound fluoride resonated at −414.3 ppm in the ^{19}F NMR spectrum. This value of the chemical shift appears to be at the upfield end of the range of chemical shifts for metal fluorides.[139-142] There are but a few examples of the ^{19}F NMR chemical shifts upfield of −400 ppm,[163-168] and to the best of our knowledge, none with group 10 metals. For square-planar Pd(II) complexes, it appears there is some correlation between the ^{19}F NMR chemical shift and the nature of the ligand *trans* to the fluoride. The more negative chemical shifts are observed when fluoride is *trans* to a hard, weak *trans*-influence ligand. Grushin's *trans*-$(py)_2PdF_2$ (where py = pyridine or 4-t-butylpyridine) resonate at δ ca. −390 ppm (F *trans* to F)[143] and Sanford's (^{t}Bu-bpy)PdF_2 resonates at δ −354 ppm (F *trans* to N of bipyridine).[155] In contrast, when F is *trans* to an aryl ligand, the ^{19}F NMR chemical shift is considerably more downfield, as in $(Ph_3P)_2Pd(Ph)(F)$ (δ −274 ppm),[169] or (NCN)PdF (δ −244 ppm).[155] In $[(Et_3P)_3PdF]^{+}$, the fluoride resonated at δ −253 ppm when *trans* to a phosphine.[170] **2-27** reacted cleanly at ambient temperature in C_6D_6 with Me_3SiCl and with Et_3SiH to produce the known compounds **2-4** and **2-7**, respectively (**Scheme 2.1**). The reaction of **2-27** with $(MeO)_3SiPh$ under analogous conditions produced an 83:17 mixture of (^{F}PNP$^{i\text{Pr}}$)PdOMe (**2-29**) and (^{F}PNP$^{i\text{Pr}}$)PdPh (**2-30**).

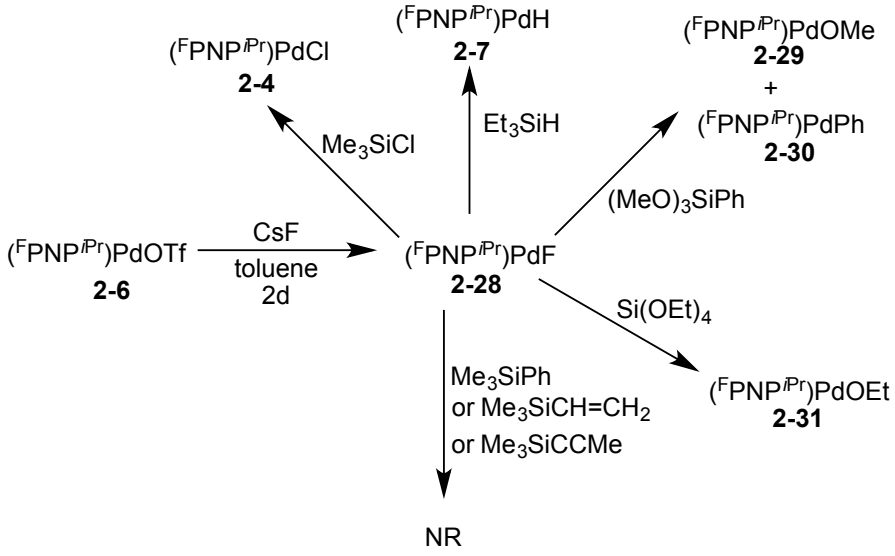

Scheme 2.4 Reactivity of **2-28** with silicon reagents.

The observation of the transfer of the phenyl group to Pd from Si is not surprising given the use of trialkoxyarylsilanes as aryl transfer agents in the Pd-catalyzed Hiyama coupling.[171] The reaction of **2-28** with $Si(OEt)_4$ in C_6D_6 resulted in the formation of 80% ($^{F}PNP^{iPr}$)PdOEt (**2-31**) in 1 hour, along with 20% of other, unidentified products. On the other hand, no reaction took place between **2-28** and Me_3SiPh or $Me_3SiCH{=}CH_2$ or $Me_3SiC{\equiv}CMe$ in C_6D_6. With the exception of Et_3SiH, the transfer of a substituent from Si to Pd appears to be facilitated by the presence of electronegative substituents on Si.

2.2.6 Structural characterization of ($^{F}PNP^{iPr}$)PdF

An X-ray diffraction study on a suitable single crystal of **2-28** revealed a molecular structure that is closely related to other (PNP)PdX compounds (**Figure 2.4**). The coordination environment about the Pd center is approximately square-planar. The

main deviation arises from the constraint of the ^{F}PNP ligand: the P1–Pd–P2 angle is 167.14(6)°. This value is similar to the P-Pd-Pd angles **2-5** (168.16(6)°)[70] and **2-27** (163.54(2)°).[70] The Pd-P distances in **2-28** are also unremarkable and fall within the 2.27-2.29 Å range for **2-5** and **2-27**. The Pd-N distance of 1.996(5) Å in **2-28** is among the shortest we have observed in any structurally analyzed (PNP)PdX complex; for comparison, the Pd-N distance is 2.015(5) Å in both **2-5** [70] and **2-27**.[70] The Pd-N distance is affected by the *trans*-influence of the ligand *trans* to it, as we discussed in a previous publication.[66] Fluoride is a weak *trans*-influence ligand and a short Pd-N distance *trans* to it is expected. The Pd-F distance in **2-28** is 1.981(4) Å. This is only slightly longer than the Pd-F distances of ca. 1.95 Å in *trans*-$(py)_2PdF_2$ reported by Grushin and Marshall in 2008 to be the shortest Pd-F distances for Pd(II).[143] The short Pd-F distances *trans* to either N_{PNP} or another fluoride are to be expected, from our point of view, given that both diarylamido N and F are weak *trans*-influence ligands. The Pd-F distance *trans* to N of a neutral donor in Sanford's [155] (^{t}Bu-bpy)PdF_2 of 1.999(4) is also comparable. Grushin and Marshall[143] paid significant attention to the π-effects on Pd-F bond distances, but considering that Pd(II) is a weak π-base, π-π repulsion with fluoride or N_{PNP} is likely insignificant. Notably, Ritter et al.[152] and Sanford et al.[172] reported two Pd(IV) complexes containing Pd-F bonds *trans* to N of sulfonamide ligands, and these Pd-F distances are quite short at 1.955(3) and 1.927(2) Å.

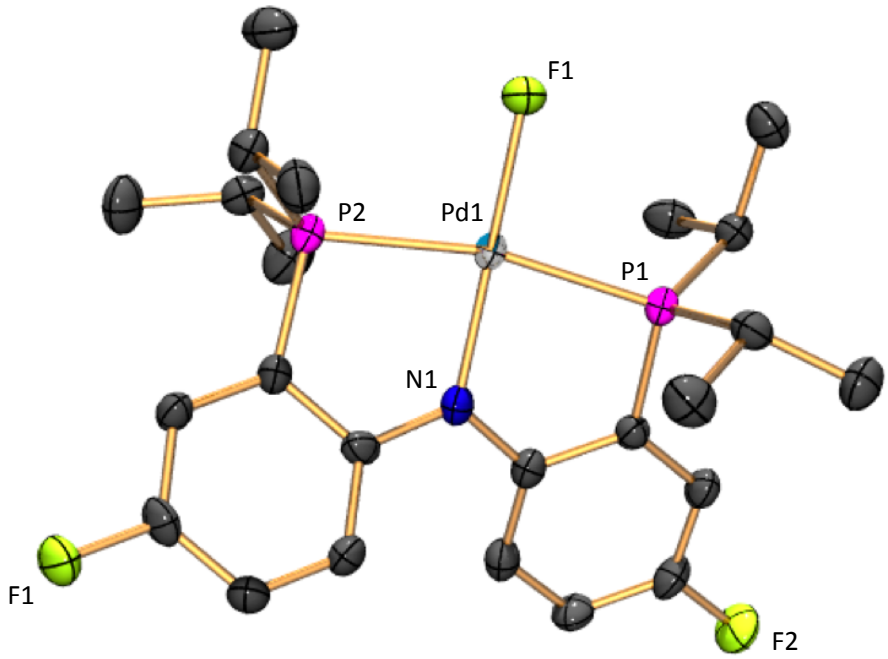

Figure 2.4 POV-Ray rendition of the ORTEP[162] drawing (50% thermal ellipsoids) of **2-28** showing selected atom labeling. Hydrogen atoms and the toluene solvent molecule are omitted for clarity. Selected bond distances (Å) and angles (deg) follow: Pd1–N1, 1.996(5); Pd1–F1, 1.981(4); Pd1–P1, 2.279(4); Pd1–P2, 2.288(4); F1–Pd1–N1, 179.12(15); F1–Pd1–P1, 96.77(10); N1–Pd1–P1, 83.47(13); F1–Pd1–P2, 96.04(12); N1–Pd1–P2, 83.74(14); P1–Pd1–P2, 167.14(6).

2.2.7 Analysis of the ^{19}F NMR chemical shifts in ^{F}PNP complexes[b,173]

The two equivalent fluorines of the ^{F}PNP ligand in **2-28** resonated at −128.4 ppm. While the ^{19}F NMR resonances of the Pd complexes of the ^{F}PNP ligand in its amido form fall within a fairly narrow chemical shift range, close examination reveals a dependence of the chemical shift on the identity of the fourth ligand (X) in (^{F}PNP)PdX. We do not endeavor to extract any quantitative relationship here, but there does exist a

[b] Some of the concepts discussed in this section are derived from [Fafard, C. M. PhD. Dissertation, Brandeis University, 2009].

correlation between the increasing donicity or *trans*-influence of X and the increasingly negative ^{19}F chemical shift (**Table 2.1**). The most downfield (least negative) chemical shift is found for **2-6** and triflate is certainly the least donating or *trans*-influencing X in **Table 2.1**. The most upfield chemical shifts are found for compounds where X is most strongly donating: a hydride or a metal or an alkyl. The chemical shift for X = F falls close to X = Cl and X = OAc, as may be expected. On the other hand, no correlation between the donicity of X and the ^{31}P chemical shifts can be discerned. The ^{19}F chemical shifts of the complexes of the $^{F}PNP^{iPr}$ ligand (amido-N) of other late transition metals (**Table 2.1**, entries 3-11) are generally within the −127 to −132 ppm range found in Pd complexes. In contrast, complexes of the N-methylated ^{F}PNP ligand (amine-N, entries 1 and 2 in **Table 2.1** and **Table 2.2**) display chemical shifts that are different enough to be clearly distinguishable from the amido-^{F}PNP complexes. The chemical shift of the ^{19}F nucleus attached to an aromatic ring can generally be correlated to how electron rich the aromatic ring is. This has been used for the analysis of substituent effects in organic chemistry. For the ^{F}PNP complexes, the increased donicity of the X ligand in (^{F}PNP)PdX increases the electron density on the diarylamido backbone and results in the upfield shift of the ^{19}F NMR resonance. N-methylation removes the lone pair of N from conjugation with the aromatic rings and thus causes a dramatic decrease in electron density and a consequent downfield shift of the ^{19}F NMR resonance (**Table 2.3**). All in all, the ^{19}F NMR resonance of the (^{F}PNP) ligand provides a spectroscopic handle that can be quite informative about the formal charge of the ligand and, to a useful degree, about the nature of the substituents on the metal.

Table 2.1 ^{31}P and ^{19}F NMR chemical shifts arising from the ^{F}PNP ligand in a series of ($^{F}PNP^{iPr}$)PdX compounds collected in C_6D_6 solutions. The chemical shifts should be considered with up to 0.1 ppm uncertainty in measurement.

#	X	δ, ^{31}P NMR	δ, ^{19}F NMR
1	OTf [157]	52.9	−126.5
2	NH_3^+ [64]	53.3[a]	−126.9
3	Cl[70]	47.4	−128.0
4	OAc [70]	38.0	−128.1
5	F[156]	43.1	−128.4
6	OEt [157]	38.6	−129.2
7	OPr^i [157]	38.7	−129.3
8	OH[157]	40.4	−129.3
9	NH_2	41.1	−129.8
10	Ph	39.2	−130.5
11	Me	40.9	−130.8
12	CH_2Ph	38.4	−130.9
13	Pd(^{F}PNP)[54]	46.5	−130.9
14	Et[157]	37.1	−131.0
15	$^{n}C_8H_{17}$	37.3	−131.0
16	^{n}Bu[157]	37.3	−131.1
17	H	59.1	−131.3
18	ZnPd(^{F}PNP)[63]	53.9	−131.9

However, as shown in **Table 2.2**, the ^{19}F NMR chemical shift in ($^{F}PNP^{R}$)Pd-X is highly insensitive to the substituents on the phosphines (R). For a given X ligand the difference ^{19}F NMR chemical shifts is <0.6 ppm. This is not surprising because the phosphines have little to no contribution to the π-system of the PNP ligand.

Table 2.2 ^{19}F NMR chemical shifts of (^{F}PNP^{R})PdX complexes (R = Ad, *t*Bu, ^{i}Pr).

#	X	δ, ^{19}F NMR of (^{F}PNP^{Ad})PdX	δ, ^{19}F NMR of (^{F}PNP^{tBu})PdX	δ, ^{19}F NMR of (^{F}PNP^{iPr})PdX
1	OTf	−126.6	−126.0	−126.5
2	Cl	n/a	−128.5	−128.0
3	OAc	−128.4	−128.3	−128.1

Table 2.3 ^{31}P and ^{19}F NMR chemical shifts arising from the ^{F}PNP ligand in a series of ^{F}PNP complexes collected in C_6D_6 solutions.

#	Compound	δ, ^{31}P NMR	δ, ^{19}F NMR
1	[(^{F}PN(Me)P^{iPr})PdCl]$^{+}$	43.6	−110.8
2	[(^{F}PN(H)P^{iPr})PtPh]$^{+}$	41.3	−111.7
3	(^{F}PN(Me)P^{iPr})RhCl	32.8	−116.3
4	(^{F}PNP^{iPr})PtCl	40.7	−127.8
5	(^{F}PNP^{iPr})NiCl	33.6	−128.1
6	(^{F}PNP^{iPr})Rh(Me)(Cl)	36.5	−128.3
7	(^{F}PNP^{iPr})Rh(CO)	61.5	−129.7
8	(^{F}PNP^{iPr})RhH$_2$	63.8	−130.1
9	(^{F}PNP^{iPr})PtH	58.8	−130.2
10	(^{F}PNP^{iPr})PtMe	40.9	−130.3
11	(^{F}PNP^{iPr})NiMe	35.4	−130.4
12	(^{F}PNP^{iPr})NiH	56	−130.5

In previous publications by the Ozerov group the ^{19}F NMR chemical shifts of (^{F}PNP^{iPr})PdX complexes have been referenced to 1 M CF_3COOH in $CDCl_3$. In this dissertation, we convert all the ^{19}F NMR chemical shifts to the scale that is referenced to 99% CF_3COOH at −78.5 ppm. This latter scale more properly corresponds to the

chemical shift of 0 ppm for $CFCl_3$. The difference between the ^{19}F chemical shifts of 1 M CF_3COOH in $CDCl_3$ and of 99% CF_3COOH is ca. 2.3 ppm.

2.3 Conclusion

In summary, new bulkier ligands (**2-20** and **2-21**) were synthesized using a Pd catalyzed C-P coupling protocol developed by Buchwald and coworkers. Unfortunately, the yields for **2-20** and **2-21** were relatively low and difficult to separate from the side products generated in the reaction. Additional catalyst combinations (i.e. Pd precursors, ligands) should be screened. In addition, the corresponding ($^{F}PNP^{R}$)PdX complexes of were synthesized using techniques analogous to those used for the synthesis of ($^{F}PNP^{iPr}$)PdX complexes. This new class of bulkier diarylamido PNP ligands can be applied towards the synthesis of coordinatively unsaturated complexes (see Chapter IV). In addition, we have also prepared and characterized a terminal palladium fluoride complex (**2-28)** supported by a diarylamido-based PNP pincer ligand. Compound **2-28** reacted with some silicon reagents by metathesis of the fluoride. With the exception of Et_3SiH, which is able to exchange a hydride for fluoride, the reaction appeared to proceed only in the case of silanes bearing electron-withdrawing groups on silicon. Finally, we have also analyzed the ^{19}F NMR chemical shifts arising from the fluorine substituents on the backbone of the ^{F}PNP ligand and demonstrated their relationship with the nature of ligand X in ($^{F}PNP^{iPr}$)PdX complexes.

2.4 Experimental

2.4.1 General considerations

All manipulations were performed under an argon atmosphere using standard Schlenk line or glovebox techniques. Toluene was dried over NaK/Ph_2CO/18-crown-6, distilled or vacuum transferred and stored over molecular sieves in an Ar-filled glovebox. Trimethoxyphenylsilane and trimethylethoxysilane were used as received from commercial vendors. Tetraethoxysilane, triethylsilane, trimethylsilyl chloride, tetraethoxysilane, trimethylphenylsilane, trimethyl(vinyl)silane and trimethylsilylpropyne were distilled under reduced pressure. All reactions between **2-28** and silicon reagents were run using a 0.050 M solution of **2-28** in C_6D_6. Compounds IP^{t}Bu$_2$,[174] HPAd$_2$,[175] HP^{t}Bu$_2$,[176] **2-6**,[157] **2-7**,[70] **2-4**,[70] **2-30**,[8] **2-29**,[157] **2-31**[157] have been previously synthesized according to literature procedures. NMR spectra were recorded on a NMRS 500 (^{1}H NMR, 499.703 MHz; ^{13}C NMR, 125.697 MHz; ^{31}P NMR, 202.289 MHz; ^{19}F NMR, 470.069 MHz) spectrometer. Chemical shifts are reported in δ (ppm). For ^{1}H and ^{13}C NMR spectra, the residual solvent peak was used as an internal reference. ^{31}P NMR spectra were referenced externally using 85% H_3PO_4 (δ, 0 ppm). ^{19}F NMR spectra were referenced externally using 99% CF_3CO_2H at −78.5 ppm. For the purpose of clarity, the following abbreviations are defined: apparent (app.), doublet of virtual triplet (dvt). Elemental analyses were performed by CALI Labs, Parsippany, NJ, USA.

Synthesis of ^{F}PN(Me)P$^{t\mathrm{Bu}}$ (2-20). An oven-dried, 25 mL polytetrafluoroethylene (PTFE)-valved flask was charged with Pd(OAc)$_2$ (50 mg, 0.22 mmol) and D*i*PPF (1,1'-

bis(diisopropylphosphino)ferrocene; 130 mg, 0.31 mmol) and toluene (2 mL) after which the solution was allowed to stir for 5 min. After this time, **2-2** (500 mg, 1.3 mmol) and NaO^tBu (320 mg, 3.3 mmol) were added as solids and the solution was allowed to stir for 5 min. After this time, HP^tBu_2 (410 mg, 0.52 mL, 2.8 mmol) was added and the vessel was placed (1/3 submerged) in a 110 °C oil bath and allowed to stir for 5 d. After this time, an aliquot was taken of the solution to determine if **2-2** had been completely consumed. The volatiles were then removed by short path distillation to remove any unreacted HP^tBu_2. The solid was redissolved in a mixture of Et_2O and pentane. The resulting solution was passed through a plug of Celite, and a second plug of silica gel. The volatiles were removed and the product was dissolved in a 1:20 mixture of Et_2O/pentane and passed through a column of silica gel. A different fraction was collected every 3 mL. Each fraction was analyzed by NMR spectroscopy to determine purity and the fractions were combined according to purity (165 mg, 0.32 mmol, 25%). ^1H NMR (C_6D_6): δ 7.50 (dd, J_{H-H} = 3 Hz, J_{H-F} = 9 Hz, 2H, Ar-H), 6.82 (m, 2H, Ar-H), 6.78 (m, 2H, Ar-H), 3.57 (s, 3H, N-CH_3), 1.10 (d, J = 11 Hz, 36H, CMe_3). $^{13}C\{^1H\}$ NMR (C_6D_6): δ 158.0 (d, J = 245 Hz, C-F), 155.1 (dd, J = 23, J = 2 Hz, C-N), 135.0 (dd, J = 4, J = 36 Hz), 128.1 (m, overlapping with solvent), 123.2 (d, J = 2 Hz), 116.3 (d, J = 22 Hz), 48.2 (t, J = 9 Hz), 32.9 (broad d, J = 23 Hz, $C(CH_3)_3$), 31.2 (d, J = 16 Hz, $C(CH_3)_3$); $^{31}P\{^1H\}$ NMR (C_6D_6): δ 15.9; ^{19}F NMR (C_6D_6): δ −121.5 (br s).

Synthesis of (^{F}PN(Me)P^{Ad}) (2-21). An oven-dried, 25 mL PTFE-valved flask was charged with $Pd(OAc)_2$ (71 mg, 0.27 mmol) and D*i*PPF (1,1'-

bis(diisopropylphosphino)ferrocene; 130 mg, 0.31 mmol) and toluene (2 mL). After stirring the solution for 5 min, **2-2** (1.0 g, 2.7 mmol) and NaO^{t}Bu (615 mg, 6.40 mmol) were added as solids and the solution was allowed to stir for an additional 5 min. $HPAd_2$ (1.6 g, 5.4 mmol) was added, and the solution was placed (1/3 submerged) in a 100 °C oil bath for 6 d. The solution was passed through a plug of silica gel, and the silica gel was rinsed with copious pentane. The volatiles were removed under vacuum and the solid was washed with pentane. The solid was dried under vacuum and weighed (376 mg, 0.46 mmol, 17%). ^{1}H NMR (C_6D_6): δ 7.60 (dd, J_{H-H} = 3 Hz, J_{H-F} = 9 Hz, 2H, Ar-H), 7.19 (m, 2H, Ar-H), 6.88 (m, 2H, Ar-H), 3.69 (s, 3H, N-CH_3), 2.17 (broad s, 12H), 1.87 (broad d, J = 60 Hz), 1.61 (broad s, 24H); ^{13}C{^{1}H} NMR (C_6D_6): δ 157.5 (d, J = 243 Hz, C-F), 155.3 (d, J = 24 Hz, C-N), 132.6 (dd, J = 4, J = 36 Hz), 130.2 (q, J = 6 Hz), 123.2 (d, J = 20 Hz), 115.6 (d, J = 22 Hz), 47.7 (t, J = 11 Hz), 42.1 (broad t, J = 13 Hz), 36.9 (broad s), 29.0 (d, J = 8 Hz); ^{31}P{^{1}H} NMR (C_6D_6): δ 20.0; ^{19}F NMR (C_6D_6): δ −121.8 (s).

Synthesis of (^{F}PNP^{tBu})PdCl (2-22). In a J. Young tube, the oily **2-20** (20 mg, 0.04 mmol) was dissolved in C_6D_6, and to the resulting solution $Pd(COD)Cl_2$ (5 mg, 0.02 mmol) was added as a solid. The sample was heated for a couple of minutes with a heat gun and the solution turned red. After determining the conversion by ^{19}F NMR spectroscopy, additional $Pd(COD)Cl_2$ (5 mg, 0.02 mmol) was added to drive the reaction to completion. The solution was passed through silica gel to remove excess $Pd(OAc)_2$. The volatiles were removed under vacuum. A small amount of hexamethyldisiloxane

was added and the solution was placed in the freezer overnight. Small crystals were formed at the bottom of the flask, and a single crystal was selected for single-crystal x-ray crystallography (see crystallographic data section for results). The remaining crystals were collected and dried under vacuum (13 mg, 0.018 mmol, 46%). ^{1}H NMR (C_6D_6): δ 7.35 (m, 2H, Ar-H), 7.16 (m, 2H, Ar-H), 6.60 (m, 2H, Ar-H), 1.38 (t, J = 7 Hz, 36H, CMe_3). $^{13}C\{^{1}H\}$ NMR (C_6D_6): δ 161.4 (t, J_{C-P} = 12 Hz, C-N), 154.2 (dvt, J_{C-F} = 237, J_{C-P} = 5 Hz, C-F), 120.2 (d, J_{C-F} = 22 Hz), 120.1 (app. q, J = 5 Hz, overlapping signals), 118.0 (d, J_{C-F} = 23 Hz), 117.0 (app. q, J = 7 Hz), 37.9 (t, J_{C-P} = 8 Hz, *C*Me_3), 29.9 (t, J_{C-P} = 3 Hz, C*Me*$_3$); $^{31}P\{^{1}H\}$ NMR (C_6D_6): δ 59.8; ^{19}F NMR (C_6D_6): δ −128.5 (app. q, 2F, J = 6 Hz).

Synthesis of (^{F}PNP^{tBu})PdOAc (2-23) with impure 2-20. An oven-dried PTFE-valved flask was charged with an impure mixture containing **2-20** (70%, 1.50 g, 2.16 mmol of **2-20**) and other non-phosphine impurities and dissolved in toluene (4 mL). To the resulting solution, $Pd(OAc)_2$ (250 mg, 1.1 mmol) was added as a solid. The solution was allowed to stir for a few minutes, after which the flask was placed (immersed 1/3 of flask; caution: take proper precautions as flask could overpressure) in a 100 °C oil bath overnight. The volatiles were removed and the solid was washed with pentane. The solid was dissolved in a minimum amount of toluene and then passed through a plug of silica gel. Most of the red solution remained on the silica gel. The silica gel was thoroughly washed with pentane to remove impurities. Once the rinses were colorless, the silica gel was washed (into a separate flask) with enough THF to allow the red elute to completely

pass through the silica gel. The volatiles were removed and the solid was dissolved in a minimum amount of toluene. The solution was layered with pentane and placed in the freezer at −35 °C. The solution was decanted and the solid was dried under vacuum (640 mg, 0.97 mmol, 45%, purity: 95%). ^{1}H NMR (C_6D_6): δ 7.21 (m, 2H, Ar-H), 7.14 (m, 2H, Ar-H), 6.58 (m, 2H, Ar-H), 2.11 (s, O_2C-CH_3), 1.34 (t, J = 7 Hz, 36H, CMe_3); $^{13}C\{^{1}H\}$ NMR (C_6D_6): δ 176.2 (s, O_2C-CH_3), 161.2 (t, J_{C-P} = 12 Hz, C-N), 154.3 (dvt, J_{C-F} = 234, 4 Hz, C-F), 121.2 (dvt, J_{C-P} = 17 Hz, J_{C-F} = 4 Hz), 119.6 (d, J_{C-F} = 22 Hz), 118.1 (d, J_{C-F} = 23 Hz), 117.4 (app. q, J = 7 Hz), 37.1 (t, J_{C-P} = 7 Hz, CMe_3), 29.5 (t, J_{C-P} = 3 Hz, CMe_3), 24.5 (s, O_2C-CH_3); $^{31}P\{^{1}H\}$ NMR (C_6D_6): δ 58.4; ^{19}F NMR (C_6D_6): δ −128.3 (app. q, 2F, J = 5 Hz).

Synthesis of (^{F}PNP^{Ad})PdOAc (2-24). An oven-dried, 25 mL PTFE-valved flask was charged with **2-21** (328 mg, 0.40 mmol) and dissolved in toluene (3 mL). To the resulting solution $Pd(OAc)_2$ (88 mg, 0.39 mmol) was added as a solid and the solution was immersed (1/3 of flask; take precautions as flask could overpressure) in an 100 °C oil bath overnight. The volatiles were removed, and the solid was washed with pentane. The solid was dissolved in a minimum quantity of toluene and then passed through a plug of silica gel. Most of the red solution remained on the silica gel. The silica gel was thoroughly washed with pentane to remove impurities. Once the rinses turned colorless, the silica gel was washed with enough THF to allow the red product to pass through the silica gel. The volatiles were removed and the solid was dissolved in a minimum amount of toluene. The resulting solution was layered with pentane and placed in the freezer at

−35 C. The solution was decanted, and the solid was dried under vacuum (120 mg, 0.12 mmol, 31%). ^{1}H NMR (C_6D_6): δ 7.34 (m, 4H, Ar-H), 6.61 (m, 2H, Ar-H), 2.58 (m, 12H, PCC*H*$_2$), 2.34 (m, 12H, PCC*H*$_2$), 2.15 (s, 3H, CO_2C*H*$_3$), 1.87 (m, 12H, $PCCH_2C$*H*), 1.71 (m, 12H, $PCCH_2CHC$*H*$_2$), 1.56 (m, 12H, $PCCH_2CHC$*H*$_2$); ^{13}C{^{1}H} NMR (C_6D_6): δ 175.7 (s, O_2*C*-CH_3), 162.2 (t, J_{C-P} = 11 Hz, C-N), 154.2 (dvt, J_{C-F} = 237, 4 Hz, C-F), 120.4 (d, J_{C-F} = 22 Hz), 118.9 (dvt, J_{C-P} = 11 Hz, J_{C-F} = 5 Hz), 117.9 (d, J_{C-F} = 23 Hz), 117.6 (app. q, J = 7 Hz), 42.7 (t, J_{C-P} = 6 Hz), 40.2 (s), 36.7 (s), 29.1 (t, J_{C-P} = 5 Hz), 24.9 (s, O_2C-*C*H_3); ^{31}P{^{1}H} NMR (C_6D_6): δ 54.7; ^{19}F NMR (C_6D_6): δ −128.4 (s).

Synthesis of (^{F}PNP^{tBu})PdOTf (2-25). In an oven-dried Schlenk flask, **2-5** (107 mg, 0.16 mmol) was dissolved in toluene (2 mL). While stirring, Me_3SiOTf (31 μL, 0.17 mmol) was added to the solution, and an immediate color change from red/orange to blue was observed. The solution was allowed to stir for 5 min, and the volatiles were removed under vacuum. The solid was washed with pentane, dissolved in a minimal amount of toluene, and carefully layered with pentane and placed in the freezer at −35 °C. Overnight a blue crystals precipitated. The solution was decanted, and the solid was dried under vacuum. A small impurity after recrystallization was observed. The solid was redissolved in a minimal amount of C_6H_5F, layered with pentane, and placed in the freezer at −35 °C. Overnight a mixture of purple and blue crystals was formed. The solution was decanted and dried under vacuum and the solid was collected. (48 mg, 0.064 mmol, 40%). ^{1}H NMR (C_6D_6): δ 7.05 (m, 2H, Ar-H), 6.97 (m, 2H, Ar-H), 6.47

(m, 2H, Ar-H), 1.30 (t, J = 8 Hz, 36H, CMe_3); $^{31}P\{^1H\}$ NMR (C_6D_6): δ 68.4; ^{19}F NMR (C_6D_6): δ −77.3 (s, 3F), −126.0 (s, 2F).

Reaction between ($^{F}PNP^{Ad}$)PdOAc (2-24) and Me_3SiOTf generating 2-26. An oven-dried J. Young tube was charged with a solution of **2-24** in C_6D_6 (concentration unknown). To the solution, Me_3SiOTf (10.0 μL, 0.055 mmol) was added, and allowed to mix. The volatiles were removed, and the solid was redissolved in C_6D_6 (NMR data below). The volatiles were removed, and the solid was dissolved in a small amount of pentane. After a few days, crystals formed at the bottom of the vial and a single crystal was selected for X-ray analysis (Yield: not isolated). ^1H NMR (C_6D_6): δ 7.21 (broad m, 4H, Ar-H), 6.53 (broad m, 2H, Ar-H), 2.50 (broad m, 12H), 2.34 (broad m, 12H), 1.90 (broad m, 12H), 1.69 (broad m, 12H), 1.53 (broad m, 12H); $^{31}P\{^1H\}$ NMR (C_6D_6): δ 63.8; ^{19}F NMR (C_6D_6): δ −77.1 (s, 3F), −126.6 (2F, s).

Attempted synthesis of $^{Me}PN(H)P^{tBu}$ (2-15) with $^{t}Bu_2PI$. In an oven-dried J. Young tube, **2-13** (50 mg, 0.14 mmol) was dissolved 0.5 mL of Et_2O. To the resulting solution 2.5 M ^{n}BuLi (186 μL, 0.47 mmol, 2.5 M in hexanes) was added, and the solution was mixed by vigorously shaking the J. Young tube. To the resulting solution, $^{t}Bu_2PI$ (88 mg, 0.32 mmol) was added and then thoroughly mixed and allowed to react overnight. The solution was then quenched with excess CF_3CH_2OH. Only (*p*-Me-$C_6H_4)_2NH$ (no **2-20)** was observed by ^{31}P NMR spectroscopy.

Attempted synthesis of (^{Me}PN(H)P^{iPrtBu}) (2-17) with ^{t}Bu$_2$PI. In an oven-dried flask, **2-18** (30 mg, 0.076 mmol) was dissolved 0.5 mL of Et_2O. The resulting solution was treated with ^{n}BuLi (66 μL, 0.17 mmol, 2.5 M) in hexanes, and allowed to stir for 5 min. To the resulting solution, $^{t}Bu_2PI$ (29 mg, 0.11 mmol) was added, and allowed to stir overnight. The solution was then quenched with excess H_2O. The only product observed by ^{31}P NMR spectroscopy was ^{Me}PN(H)H (no **2-17**).

Attempted synthesis of 2-20 at low temperature. In an oven-dried flask, **2-2** (50 mg, 0.13 mmol) was dissolved in 0.5 mL of Et_2O. While stirring, the resulting solution was treated with 2.5 M ^{n}BuLi (110 μL, 0.27 mmol, 2.5 M in hexanes). The solution was cooled to −78 °C, using a dry ice-acetone bath, and $^{t}Bu_2PCl$ (56 μL, 0.29 mmol) was added to the solution. The solution was allowed to slowly come to room temperature overnight. Only (p-Me-$C_6H_4)_2NH$ (no **2-20)** was observed by ^{31}P NMR spectroscopy.

Attempted synthesis of 2-20 via Grignard reagent. In an oven-dried flask, **2-2** (50 mg, 0.13 mmol) was dissolved in 1.0 mL of THF. While stirring, the solution was treated with ^{i}PrMgCl (130 μL, 0.27 mmol, 2.0 M) in THF, and allowed to react for a few minutes. Using a micro syringe, Cl$P^{t}Bu_2$ (46 μL, 0.29 mmol) was added, and allowed to stir overnight. Only (p-Me-$C_6H_4)_2NH$ (no **2-20)** was observed by ^{31}P NMR spectroscopy.

Attempted synthesis of 2-20 via organocopper reagent. In an oven-dried flask, **2-2** (50 mg, 0.13 mmol) was dissolved in 1.0 mL of Et_2O. While stirring, the resulting solution was treated with 2.5 M ^{n}BuLi (110 μL, 0.27 mmol, 2.5 M in hexanes). The solution was treated with solid CuI (52 mg, 0.27 mmol), and after stirring for 5 min Cl$P^{t}Bu_2$ (46 μL, 0.29 mmol) was added. The solution was allowed to stir overnight. Only (p-Me-$C_6H_4)_2$NH (no **2-20)** was observed by ^{31}P NMR spectroscopy.

Attempted synthesis of (^{Me}PN(H)P^{tBu}) using TMEDA. An oven-dried flask was charged with **2-13** (0.5 mL, 0.09 mmol, 0.2 M). While stirring, the resulting solution was treated with ^{n}BuLi (104 μL, 0.26 mmol, 2.5 M in hexanes). The resulting solution was treated with two drops of TMEDA (tetramethylethylenediamine) and allowed to stir overnight. The solution was quenched with two drops of water, passed through silica gel, and dried under vacuum. The solid was redissolved in C_6D_6, and subsequently analyzed by ^{31}P NMR spectroscopy, revealing two unknown products at 14.2 ppm (90%) and 3.62 ppm (10%).

Synthesis of (^{F}PNP^{iPr})PdF (2-28). **2-6** (145 mg, 0.210 mmol) was dissolved in 2.0 mL of toluene in a 10 mL Schlenk flask, and treated with CsF (90 mg, 0.59 mmol) at RT for 2 d. The mixture was then filtered through a pad of Celite, and the volatiles were removed from the filtrate under vacuum. The solid was redissolved in a minimum amount toluene, and layered with pentane. The solution was placed in a freezer overnight at −35 °C. The reaction yielded a red crystalline powder of **2-28** (75 mg, 0.13

mmol, 64%). ^{1}H NMR (C_6D_6): d 7.23 (m, 2H, Ar-H), 6.67 (m, 2H, Ar-H), 6.60 (td, 2H), 1.96 (m, 4H, C*H*Me$_2$), 1.33 (app. quartet (dvt), 12H, J = 9 Hz, PCH*Me$_2$*), 1.00 (app. quartet (dvt), 12H, J = 8 Hz, PCH*Me$_2$*); ^{13}C{^{1}H} NMR (C_6D_6): δ 161.4 (t, J_{C-P} = 11 Hz, C-N), 155.3 (dvt, J_{C-F} = 239 Hz, J_{C-P} = 5 Hz, C-F), 121.0 (dvt, J_{C-P} = 18 Hz, J_{C-F} = 5 Hz), 119.2 (d, J_{C-F} = 22 Hz), 119.1 (d, J_{C-F} = 21 Hz), 117.1 (app. q, J = 7 Hz), 25.0 (t, J_{C-P} = 13 Hz, *C*HMe$_2$), 19.0 (br s, CH*Me$_2$*), 18.4 (s, CH*Me$_2$*); ^{31}P{^{1}H} NMR (C_6D_6): δ 43.5; ^{19}F NMR (C_6D_6): δ −128.7 (m, C-F), −414.3 (br s, Pd-F). Anal. Calcd (Found) for $C_{24}H_{34}F_3NP_2Pd$, C, 51.30 (51.27); H, 6.10 (5.94).

Reaction of 2-28 with Et$_3$SiH. In an oven-dried J. Young tube, Et$_3$SiH (40 μL, 0.25 mmol) was added to a solution of **2-28** (0.50 mL of 0.050 M solution in C_6D_6, 0.025 mmol). After 20 h the reaction yielded an equimolar amount of **2-7** and Et$_3$SiF.

Reaction of 2-28 with Me$_3$SiCl. In an oven-dried J. Young tube, Me$_3$SiCl (32 μL, 0.25 mmol) was added to a solution of **2-28** (0.50 mL of 0.050 M solution in C_6D_6, 0.025 mmol). After 1 h the reaction yielded an equimolar amount of **2-4** and Me$_3$SiF.

Reaction of 2-28 with (MeO)$_3$SiPh. In an oven-dried J. Young tube, (MeO)$_3$SiPh (35 μL, 0.19 mmol) was added to a solution of **2-28** (0.50 mL of 0.050 M solution in C_6D_6, 0.025 mmol). After 1 h the reaction yielded a mixture of **2-29** (83%) and **2-30** (17%).

Reaction of 2-28 with $(EtO)_4Si$. In an oven-dried J. Young tube, $(EtO)_4Si$ (35 μL, 0.16 mmol) was added to a solution of **2-28** (0.50 mL of 0.050 M solution in C_6D_6, 0.025 mmol). The solution was allowed to react at RT for 1 h. The reaction yielded **2-31** (80%) and two unknown products (20%).

Attempted reactions of 2-28 with Me_3SiPh, $Me_3SiCH{=}CH_2$, Me_3SiOEt, and $Me_3SiC{\equiv}CMe$. Four oven-dried J. Young tubes were charged with a solution of **2-28** (0.50 mL of 0.050 M solution in C_6D_6, 0.025 mmol), and treated with 0.19 mmol of Me_3SiPh (25 μL), $Me_3SiCH{=}CH_2$ (28 μL), Me_3SiOEt (30 μL), $Me_3SiC{\equiv}CMe$ (35 μL). After 20 h there was no observable change by NMR spectroscopy. The reactions with $Me_3SiCH{=}CH_2$ and Me_3SiOEt were additionally placed into a 100 °C oil bath for 20 h, with no change by NMR spectroscopy after these thermolyses.

2.4.2 X-ray diffraction experiments

Data collection for 2-22 (solved by Dr. Bhuvanesh, N.). A small amount of **2-22** was dissolved in a minimum of hexamethyldisiloxane and the solution was placed in the freezer overnight. Small red crystals were formed at the bottom of the vial and a single crystal was selected for single-crystal X-ray crystallography. A Leica MZ 75 microscope was used to identify a suitable red block with very well defined faces with dimensions (max, intermediate, and min) 0.19 × 0.17 × 0.15 mm from a representative sample of crystals of the same habit. The crystal mounted on a nylon loop was then placed in a cold nitrogen stream (Oxford) maintained at 150 K.

A BRUKER APEX2 X-ray (three-circle) diffractometer was employed for crystal screening, unit cell determination, and data collection. The goniometer was controlled using the APEX2 software suite, v2008-6.0.[177] The sample was optically centered with the aid of a video camera such that no translations were observed as the crystal was rotated through all positions. The detector was set at 6.0 cm from the crystal sample (APEX2, 512x512 pixel). The X-ray radiation employed was generated from a Mo sealed X-ray tube (K_α = 0.70173 Å with a potential of 40 kV and a current of 40 mA) fitted with a graphite monochromator in the parallel mode (175 mm collimator with 0.5 mm pinholes).

Sixty data frames were taken at widths of 0.5°. These reflections were used in the auto-indexing procedure to determine the unit cell. A suitable cell was found and refined by nonlinear least squares and Bravais lattice procedures. The unit cell was verified by examination of the *h k l* overlays on several frames of data by comparing with both the orientation matrices. No super-cell or erroneous reflections were observed. After careful examination of the unit cell, a standard data collection procedure was initiated using omega and phi scans.

Data reduction, structure solution, and refinement. Integrated intensity information for each reflection was obtained by reduction of the data frames with the program APEX2.[177] The integration method employed a three dimensional profiling algorithm and all data were corrected for Lorentz and polarization factors, as well as for crystal decay effects. Finally the data was merged and scaled to produce a suitable data set. The absorption correction program SADABS[178] was employed to correct the data for absorption effects.

Systematic reflection conditions and statistical tests of the data suggested the space group *P21/c*. A solution was obtained readily using SHELXTL (XS).[179] Absence of additional symmetry or voids was confirmed using PLATON (ADDSYM).[180] Hydrogen atoms were placed in idealized positions and were set riding on the respective parent atoms. All non-hydrogen atoms were refined with anisotropic thermal parameters. The structure was refined (weighted least squares refinement on F^2) to convergence.[179,181] Olex2 was employed for the final data presentation and structure plots.[181]

Table 2.4 Crystal data and structure refinement for 2-22.

Empirical formula	$C_{28}H_{42}ClF_2NP_2Pd$	
Formula weight	634.42	
Temperature	150(2) K	
Wavelength	0.71073 Å	
Crystal system	Monoclinic	
Space group	*P2(1)/c*	
Unit cell dimensions	a = 12.1547(13) Å	α = 90°
	b = 12.1408(13) Å	β = 102.9080(10)°
	c = 20.184(2) Å	γ = 90°
Volume	2903.3(5) $Å^3$	
Z	4	
Density (calculated)	1.451 Mg/m^3	
Absorption coefficient	0.872 mm^{-1}	
F(000)	1312	
Crystal size	0.19 × 0.17 × 0.15 mm^3	
Theta range for data collection	2.38 to 27.22°	
Index ranges	$-15 \le h \le 15$, $-15 \le k \le 15$, $-25 \le l \le 25$	
Reflections collected	32241	
Independent reflections	6457 [R(int) = 0.0326]	
Completeness to theta = 27.22°	99.6%	
Absorption correction	Semi-empirical from equivalents	
Max. and min. transmission	0.8803 and 0.8518	
Refinement method	Full-matrix least-squares on F^2	
Data / restraints / parameters	6457 / 0 / 328	
Goodness-of-fit on F^2	1.057	
Final R indices [I>2σ(I)]	$R1$ = 0.0226, wR2 = 0.0533	
R indices (all data)	$R1$ = 0.0257, wR2 = 0.0547	
Largest diff. peak and hole	0.369 $eÅ^{-3}$ and −0.483 $eÅ^{-3}$	

Data collection for 2-26 (solved by Dr. Bhuvanesh, N.). In an oven-dried vial, a small quantity of **2-26** was dissolved in minimum amount of pentane. The resulting solution was allowed to slowly evaporate for 2 d. After this time, a few blue X-ray quality crystals were formed on the walls of the vial. A Leica MZ 75 microscope was used to identify a suitable blue block with very well defined faces with dimensions (max, intermediate, and min) 0.17 × 0.10 × 0.08 mm from a representative sample of crystals of the same habit. The crystal mounted on a nylon loop was then placed in a cold nitrogen stream (Oxford) maintained at 150 K.

A BRUKER APEX2 X-ray (three-circle) diffractometer was employed for crystal screening, unit cell determination, and data collection. The goniometer was controlled using the APEX2 software suite, v2008-6.0.[177] The sample was optically centered with the aid of a video camera such that no translations were observed as the crystal was rotated through all positions. The detector was set at 6.0 cm from the crystal sample (APEX2, 512 × 512 pixel). The X-ray radiation employed was generated from a Mo sealed X-ray tube (K_α = 0.70173 Å with a potential of 40 kV and a current of 40 mA) fitted with a graphite monochromator in the parallel mode (175 mm collimator with 0.5 mm pinholes).

Sixty data frames were taken at widths of 0.5°. These reflections were used in the auto-indexing procedure to determine the unit cell. A suitable cell was found and refined by nonlinear least squares and Bravais lattice procedures. The unit cell was verified by examination of the *h k l* overlays on several frames of data by comparing with both the orientation matrices. No super-cell or erroneous reflections were observed. After careful

examination of the unit cell, a standard data collection procedure was initiated using omega and phi scans.

Data reduction, structure solution, and refinement. Integrated intensity information for each reflection was obtained by reduction of the data frames with the program APEX2.[177] The integration method employed a three dimensional profiling algorithm and all data were corrected for Lorentz and polarization factors, as well as for crystal decay effects. Finally the data was merged and scaled to produce a suitable data set. The absorption correction program SADABS[178] was employed to correct the data for absorption effects.

Systematic reflection conditions and statistical tests of the data suggested the space group *P2(1)2(1)2(1)*. A solution was obtained readily using SHELXTL (XS).[179] Absence of additional symmetry or voids was confirmed using PLATON (ADDSYM).[180] Hydrogen atoms were placed in idealized positions and were set riding on the respective parent atoms. All non-hydrogen atoms were refined with anisotropic thermal parameters. The structure was refined (weighted least squares refinement on F^2) to convergence.[179,181] Olex2 was employed for the final data presentation and structure plots.[181]

Table 2.5 Crystal data and structure refinement for 2-26.

Empirical formula	$C_{53}H_{66}F_5NO_3P_2PdS$	
Formula weight	1060.47	
Temperature	150(2) K	
Wavelength	0.71073 Å	
Crystal system	Orthorhombic	
Space group	*P2(1)2(1)2(1)*	
Unit cell dimensions	a = 11.622(5) Å	α = 90°
	b = 18.538(8) Å	β = 90°
	c = 21.969(9) Å	γ = 90°
Volume	4733(3) $Å^3$	
Z	4	
Density (calculated)	1.488 Mg/m^3	
Absorption coefficient	0.569 mm^{-1}	
F(000)	2208	
Crystal size	0.17 × 0.10 × 0.08 mm^3	
Theta range for data collection	1.98 to 27.50°	
Index ranges	$-14 \le h \le 14$, $-24 \le k \le 24$, $-28 \le l \le 28$	
Reflections collected	54627	
Independent reflections	10823 [R(int) = 0.0518]	
Completeness to theta = 27.50°	99.6%	
Absorption correction	Semi-empirical from equivalents	
Max. and min. transmission	0.9559 and 0.9094	
Refinement method	Full-matrix least-squares on F^2	
Data / restraints / parameters	10823 / 0 / 595	
Goodness-of-fit on F^2	1.018	
Final R indices [I>2σ(I)]	$R1$ = 0.0261, wR2 = 0.0572	
R indices (all data)	$R1$ = 0.0304, wR2 = 0.0591	
Absolute structure parameter	−0.039(12)	
Largest diff. peak and hole	0.431 $eÅ^{-3}$ and −0.336 $eÅ^{-3}$	

X-ray data collection, solution, and refinement for 2-28 (solved by Dr. Herbert, D.). In an oven-dried flask, a small quantity of **2-28** was dissolved in a minimum amount toluene and layered with pentane. The solution was placed in a freezer overnight at –35 °C and produced several X-ray quality red crystals of **2-28**. A red, multi-faceted crystal of suitable size (0.2 × 0.1 × 0.1 mm) and quality was selected from a representative sample of crystals of the same habit using an optical microscope, mounted onto a nylon loop and placed in a cold stream of nitrogen (110 K). Low-temperature X-ray data were obtained on a Bruker APEXII CCD based diffractometer (Mo sealed X-ray tube, K_α = 0.71073 Å). All diffractometer manipulations, including data collection, integration and scaling were carried out using the Bruker Apex2 software.[177] An absorption correction was applied using SADABS.[178] The space group was determined on the basis of systematic absences and intensity statistics and the structure was solved by direct methods and refined by full-matrix least squares on F^2. No obvious missed symmetry was reported by PLATON.[180] The structure was solved in the triclinic *P-1* space group using XS[179] (incorporated in SHELXTL). All non-hydrogen atoms were refined with anisotropic thermal parameters. The hydrogen atoms were placed in idealized positions and refined using riding model. The structure was refined (weighted least squares refinement on F^2) to convergence.[179,181]

Table 2.6 Crystal data and structure refinement for 2-28.

Empirical formula	$C_{31}H_{42}F_3NP_2Pd$	
Formula weight	654.00	
Temperature	110(2) K	
Wavelength	0.71073 Å	
Crystal system	Triclinic	
Space group	*P-1*	
Unit cell dimensions	a = 9.332(17) Å	α = 93.66(2)°
	b = 12.35(2) Å	β = 99.63(2)°
	c = 13.66(2) Å	γ = 98.50(2)°
Volume	1529(4) $Å^3$	
Z	2	
Density (calculated)	1.421 Mg/m^3	
Absorption coefficient	0.751 mm^{-1}	
F(000)	676	
Crystal size	0.20 × 0.10 × 0.10 mm^3	
Theta range for data collection	2.16 to 27.50°	
Index ranges	$-12 \le h \le 12$, $-16 \le k \le 16$, $-17 \le l \le 17$	
Reflections collected	16859	
Independent reflections	6953 [R(int) = 0.0850]	
Completeness to theta = 27.50°	98.9%	
Absorption correction	Semi-empirical from equivalents	
Max. and min. transmission	0.9287 and 0.8644	
Refinement method	Full-matrix least-squares on F^2	
Data / restraints / parameters	6953 / 0 / 353	
Goodness-of-fit on F^2	0.996	
Final R indices [I>2σ(I)]	$R1$ = 0.0598, $wR2$ = 0.1230	
R indices (all data)	$R1$ = 0.0990, $wR2$ = 0.1477	
Extinction coefficient	0.0021(6)	
Largest diff. peak and hole	1.415 $eÅ^{-3}$ and −2.196 $eÅ^{-3}$	

CHAPTER III

REACTIVITY OF A Pd(I)-Pd(I) DIMER WITH O_2 AND C_2H_4*

3.1 Introduction

In 2007 Dr. Claudia M. Fafard, a former member of the Ozerov group, reported the synthesis of [(^{F}PNP$^{i\text{Pr}}$)Pd-]$_2$ (**2-10)** dimer and its reactivity towards small molecules such as ammonia (NH_3), water (H_2O) and dihydrogen (H_2).[54] Compound **2-10** is synthesized by irradiating a solution of (PNP)PdEt (**3-1**) in pentane with either sunlight or a UV light source. It was proposed that photolysis of **3-1** homolytically cleaves the Pd-C bond generating a monomeric (PNP)Pd(I) radical and a concomitant alkyl radical which subsequently dimerizes to form **2-10**.

Thermolysis of **2-10** with excess H_2O, NH_3 or H_2 homolytically cleaves the H-X (X = H, OH or NH_2) bond to yield (PNP)PdH (**2-7)** and the corresponding (PNP)PdX (X = H (**2-7)**, OH (**2-8)** or NH_2(**3-2**)) in a 1:1 ratio (**Scheme 3.1**).[54] These transformations can be best understood as a bimetallic oxidative addition,[173] were each metal oxidation state increases by +1. It was also reported that photolysis of **2-10** in the presence of Ph_3CCl generates **2-4** with concomitant formation of Gomberg's dimer. Although the mechanism of this reaction is not fully understood, these results may suggest that photolysis of **2-10** cleaves the Pd-Pd bond and generates a (PNP)Pd(I) radical.

---

*Some material in this chapter is reprinted with permission from "Reactivity of a Pd(I)-Pd(I) Dimer with O_2: Monohapto Pd Superoxide and Dipalladium Peroxide in Equilibrium" by Huacuja, R.; Graham, D. J., Fafard, C. M., Chen, C. H., Foxman, B. M., Herbert, D. E., Alliger, G., Thomas, C. M., Ozerov, O. V., 2011. *J. Am. Chem. Soc.*, 133, 3820-3823, Copyright [2011] by American Chemical Society. The majority of the chemistry in this article was done by Huacuja, R and Graham, D. J.

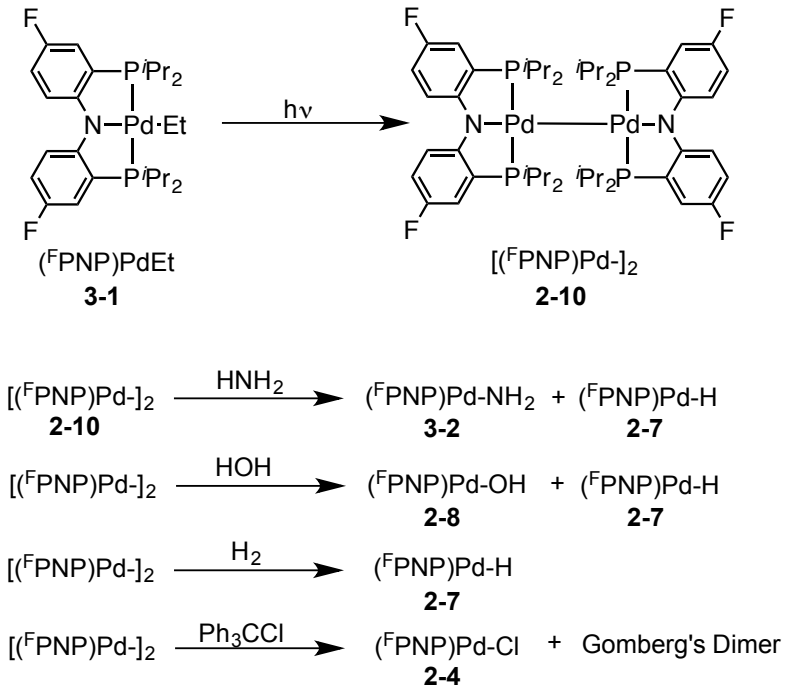

Scheme 3.1 Synthesis of **2-10** and homolytic cleavage of H-X bonds.

This radical then homolytically abstracts a chlorine atom from Ph_3CCl. However, analogous work reported by Wayland et al., using Rh(I) porphyrins, suggests that small substrates such as H_2 and H_2O first bind to the metal, and then undergo binuclear oxidative addition.[182] Given the above mentioned reactivity, we were curious to probe the reactivity of **2-10** towards molecular oxygen, a triplet ground state molecule.[183] In addition, the reactivity of **2-10** with ethylene, a singlet ground state molecule, will also be discussed. Despite the differences in electronic character between oxygen and ethylene, the reactivity between C_2H_4 and **2-10** is similar to that of O_2. In accordance with this observation, in 2010 Stahl and coworkers outlined the similarities in reactivity pathways between mononuclear Pd^0 complexes and alkenes and O_2.[184]

The use of dioxygen in transition metal chemistry has been a topic of intense research for over 50 years.[185-191] The potential to use dioxygen as a stoichiometric oxidant in catalytic reactions has fascinated chemists for decades.

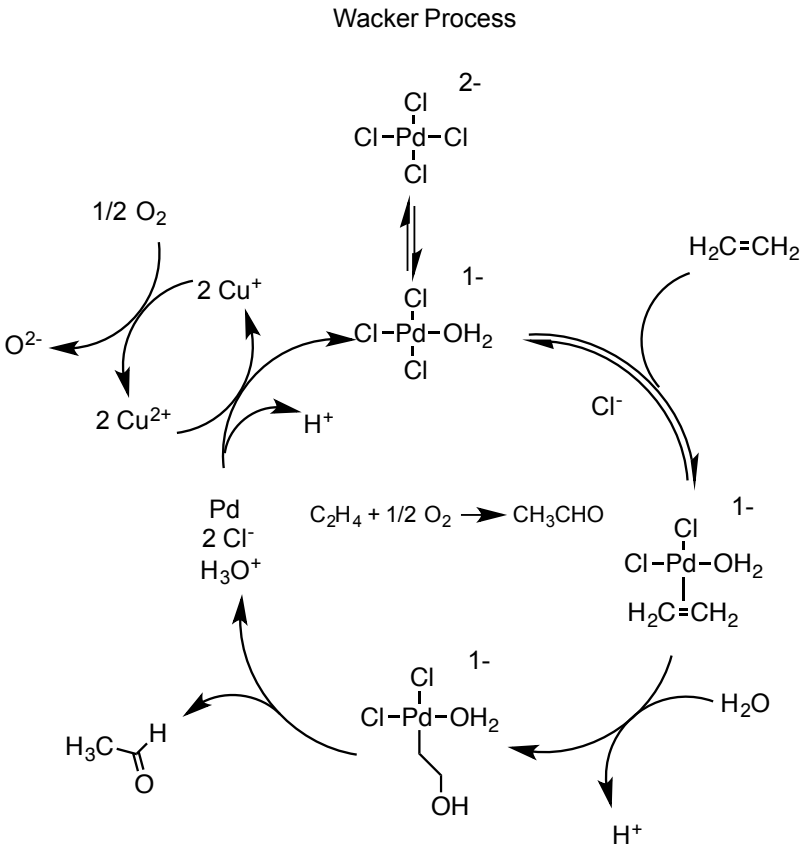

Scheme 3.2 Mechanism of Wacker process.

Using molecular oxygen as an oxidant is highly desirable because it is ubiquitous, cheap, and the byproducts produced are environmentally benign.[191-196] In the Wacker process (**Scheme 3.2**), oxygen is used as the stoichiometric oxidant in the conversion of ethylene into acetaldehyde with a palladium and copper catalyst system.[197]

In a more recent example, Stahl et al. reported the catalytic conversion of substituted cyclohexanones into phenols via a palladium catalyzed aerobic dehydrogenation. In this process, intermediate palladium hydrides produced by the dehydrogenation of cyclohexanones, are oxidized by molecular oxygen yielding water as the only side product in the reaction (**Scheme 3.3**).[195]

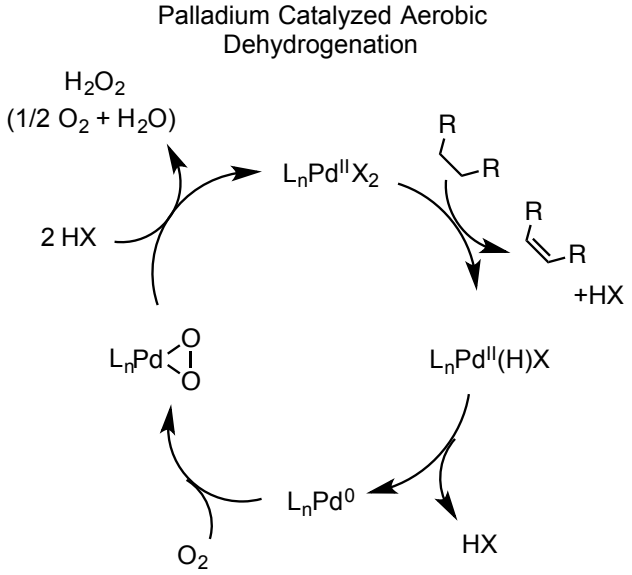

Scheme 3.3 Palladium catalyzed aerobic dehydrogenation of cyclohexanones.

In addition to the practical and applicable aspects of metal-oxygen chemistry, such as catalytic aerobic oxidation, it is also important to understand the fundamental chemistry between oxygen and metals. Understanding how dioxygen behaves as a ligand in transition metals is of great importance. Because of their relevance to biological systems such as hemoglobin and analogous metalloproteins, the reactivity of most metals with dioxygen has already been explored.[198] The binding between dioxygen and a

metal can be divided into three major categories: peroxides (O_2^{2-}), superoxides (O_2^{-}) and oxygen (O_2^{0}).[185] Superoxo and peroxo ligands bind to the metal in two main modes, η^1-O_2 and η^2-O_2 as shown in **Figure 3.1**. This chapter focuses on the binding of oxygen to palladium complexes supported by diarylamido/bis(phosphino) ligands.

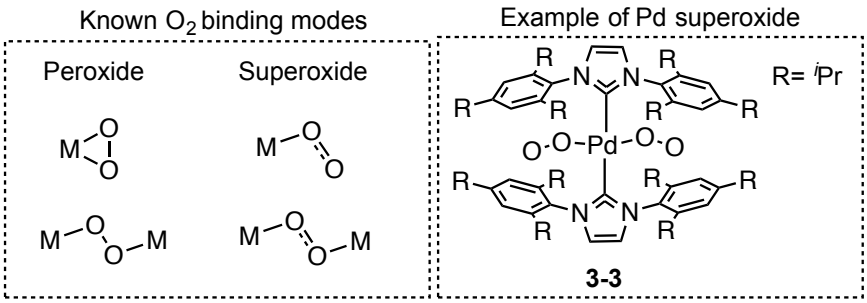

Figure 3.1 Known M-O_2 binding modes (left); $(NHC)_2Pd(\eta^1\text{-}O_2)_2$ (**3-3**), palladium bis-superoxide (right).

With the exception of $(NHC)_2Pd(\eta^1\text{-}O_2)_2$[199,c] (**Figure 3.1**; **3-3**), the reports of η^1 Pd-O_2 superoxide complexes are limited to in situ spectroscopic characterization of Pd(II) superoxides prepared by salt metathesis with KO_2.[191,200,201] A Pd(I) superoxide has also been proposed as an intermediate in the reaction between a Pd(0) complex and O_2.[184] While η^2-O_2 Pd complexes, cyclic peroxides,[194,202] (**Figure 3.1**) are well known in the literature, reports of bridging Pd peroxides (with a Pd-O-O-Pd substructure) are very rare. The only example of a μ-peroxide (**3-4**) reported, is synthesized via metathetic

[c] The chemistry reported in Ozerov, O. et. al. *J. Am. Chem. Soc.* **2011**, 133, 3820 was completed prior to the publication of Hoff, C. D. et al. *J. Am. Chem. Soc*. **2011**, 133, 1290 and was therefore not inspired by the work of Hoff, C. D. el al..

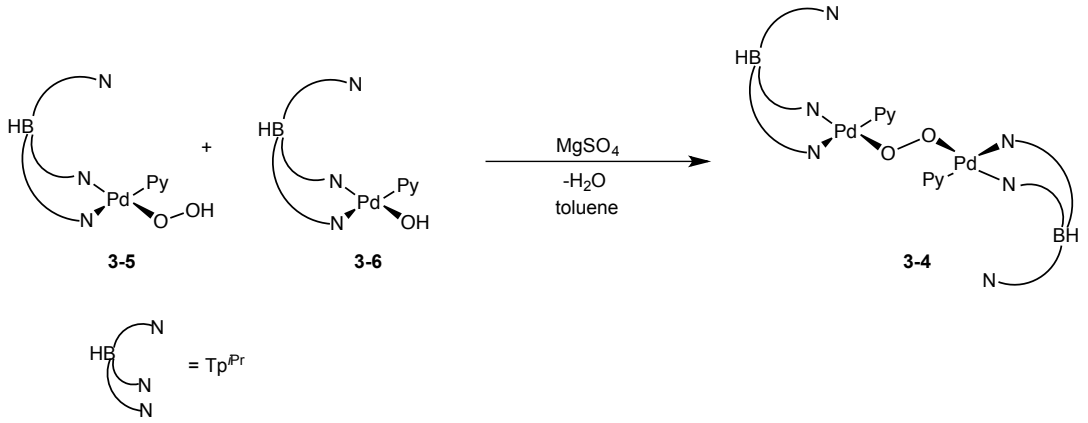

Scheme 3.4 Synthesis of palladium μ-peroxide via metathetic reactions with hydroperoxides.

reactions with organic hydroperoxides (**3-5**) and hydroxides (**3-6**) (**Scheme 3.4**).[203,204] This chapter will predominantly discuss the results of the reaction between **2-10** and O_2.

3.2 Results and Discussion

3.2.1 Reaction of [(^{F}PNP^{iPr})Pd-]$_2$ with molecular oxygen

Exposure of a solution of **2-10** in C_6D_6 (or THF) to excess O_2 (1 atm; >10 equiv), followed by irradiation with a halogen lamp, led to an immediate color change from green to orange. ^{19}F NMR spectroscopy confirmed complete disappearance of **2-10**, and emergence of two different products, a major (>95%) and a minor (<5%) (**Scheme 3.5**). These two products were determined to be rare examples of a palladium superoxide (**3-7**) and a bimetallic palladium peroxide (**3-8**), respectively. Systematic variation of the number of equivalents of O_2 introduced led to a change in the observed ratio of the palladium superoxo and peroxo products. **Figure 3.2** shows that if substochiometric

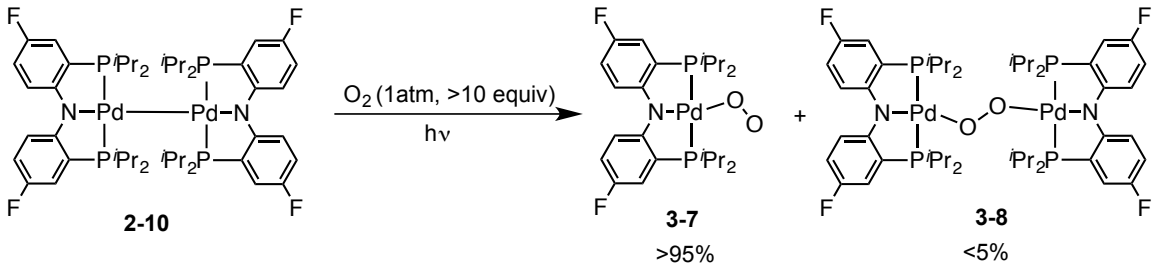

Scheme 3.5 Irradiation of **2-10** under 1 atm of O_2 yields **3-7** (95%) and **3-8** (<5%).

quantities of oxygen were introduced, partial conversion into palladium peroxide **3-8** occured, leaving some unreacted **2-10** and no palladium superoxide (**3-7**). However, as the number of O_2 equivalents increased from 1 eq. to 1.4 eq. we observed complete disappearance of the starting material (**2-10**), conversion to a small quantity of **3-7,** and **3-8,** the major product. As the number of O_2 equivalents increased, so did the ratio of **3-7** to **3-8**. An approximate equivalence point between **3-7** and **3-8** was reached when **2-10** was charged with 2.3 equivalents of O_2. Finally, as stated above, when **2-10** was charged with a large excess of O_2 (1 atm, >10 equiv), the ratio of **3-7** to **3-8** inverted, and **3-7** became the major product. Although **3-8** could be synthesized by adding exactly one equivalent of O_2 to **2-10**, on a larger scale it was more convenient to react **3-7** with **2-10** in a 2:1 ratio, respectively.

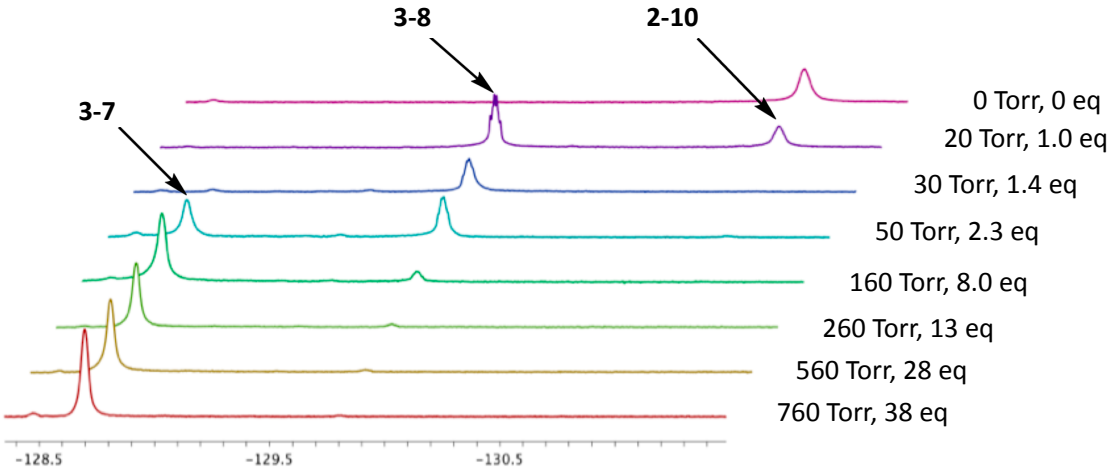

Figure 3.2 ^{19}F NMR spectra of the reactions of **2-10** with different amounts of O_2 in C_6D_6 collected after 5 min in direct sunlight.

3.2.2 Equilibrium between [(^{F}PNP^{iPr})PdO-]$_2$ and (^{F}PNP^{iPr})PdO$_2$

To determine if **3-7** and **3-8** were in equilibrium with each other, a solution of **3-7** in C_6D_6 under 1 atm O_2 was evacuated and stripped of its volatiles (**Scheme 3.6**). The solid was then redissolved in C_6D_6 and exposed to fluorescent lighting (lab lighting), after 3 h the solution of **3-7** became a mixture of **3-7** and **3-8**. The reverse was also tested by taking a degassed solution of **3-8** and exposing it to 1 atm of O_2. Upon irradiation, the solution was converted into **3-7** (>95%). These two experiments suggested that in the presence of light, **3-7** and **3-8** are in equilibrium with free oxygen. However, mixtures of **3-7** and **3-8** did not revert back into **2-10** under a deficiency of O_2. In other words, the conversion of **2-10** into **3-8** and **3-7** is an irreversible process.

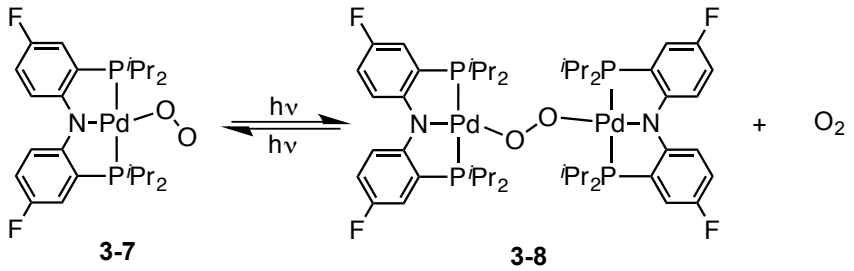

Scheme 3.6 Photolytic equilibrium between **3-7** and **3-8** and O_2.

3.2.3 Dependence on light

The dependence of this reaction on light is very pronounced, in the presence of light the reaction is rapid, however in the absence of it, **2-10** and O_2 exhibit no reaction. The type of light source can also have a profound influence on the rate of the transformation from **2-10** to **3-7** and **3-8**. Both solar light, and light from a halogen lamp (250-W or 500-W) rapidly convert **2-10** into **3-7** and **3-8**. Fluorescent lighting (lab lighting) also induces the transformation, but does so at a much slower rate. The majority of the reactions performed were done using a halogen lamp (250-W or 500-W), largely out of convenience, but also because the intensity of the lighting was much more reproducible with the halogen lamp than with sunlight. For example, a cloudy day could dramatically reduce the rate of the reaction. On the other hand, the light intensity from a halogen lamp varies very little from day to day or from light bulb to light bulb, making rates much more reproducible.

Both **3-7** and **3-8** are stable at room temperature and in the dark for many hours; however, exposure to light or heat for extended periods of time dramatically accelerates decomposition. This is especially severe when light sources such as the sun or a halogen

lamp are used. The main product of decomposition is **2-8**, however, other unidentifiable products are also formed. This is not surprising since even the simplest peroxide (H_2O_2) is known to be both photo and thermally sensitive. Despite their thermal and photolytic instability, we were able to obtain single-crystal X-ray structures of both **3-7** and **3-8**.

3.2.4 Structural analysis of $[(^{F}PNP^{iPr})PdO-]_2$ and $(^{F}PNP^{iPr})PdO_2$

The Pd-O bond lengths of 2.0096(13) and 2.046(14) for **3-7** and **3-8** respectively, are very similar (with differences <0.02 Å) to the analogous compound **2-5** (**Figure 3.3** and **3.4**).[135] These bond distances are consistent with a single bond between palladium and oxygen. In addition, the N-Pd in **3-7** and **3-8** is comparable to what is observed in **2-5**, suggesting that the *trans*-influence of peroxide (O^{2-}) and superoxide (O_2^-) is comparable to acetate ($^-$OAc). The distance between palladium and the oxygen most distal to it, in **3-7** and **3-8** is greater than 2.7 Å, too long to be considered a bonding interaction. This is indicative that both superoxo and peroxo behave as monohapto ligands. The Pd-O-O bond angles for both of these compounds are comparable (104-113°). The O-O bond length in **3-7** (1.293(2) Å) is longer that the reported O-O bond length for molecular oxygen (1.20 Å)[188] and significantly shorter than singly bound O-O peroxides and hydroperoxides (1.41-1.49 Å).[188,203-209] The O-O distance of 1.293(2) Å in **3-7** is close to the average O-O bond of a recently reported palladium bis(superoxide) (**3-3**; **Figure 3.1**) of 1.327(11), both of which lie within the typical range of other reported superoxo (O_2^-) moieties.[185,190,210-214] The O-O distance of 1.47(2) Å in **3-8** is within the range reported for other μ-peroxo complexes reported in the literature (**Figure 3.2**).[203-208]

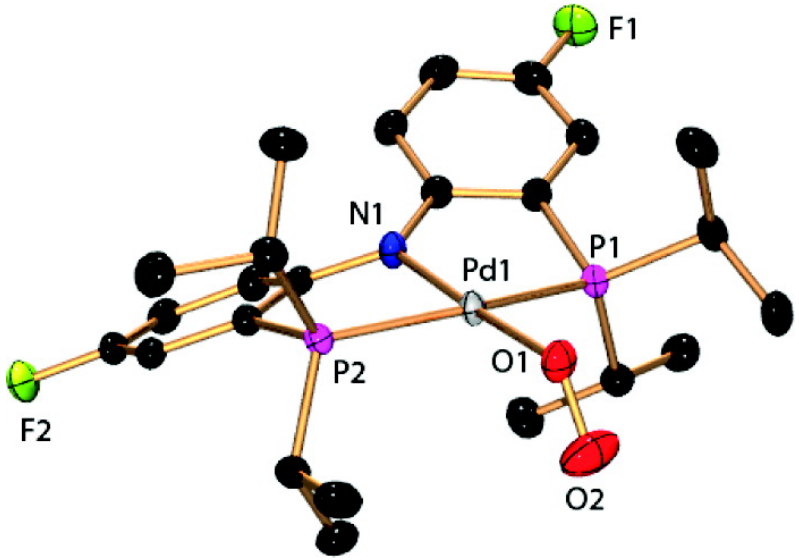

Figure 3.3 POV-Ray rendition of the ORTEP[162] drawing (50% thermal ellipsoids) of **3-7** showing selected atom labeling. Hydrogen atoms and the THF solvent molecule have been omitted for clarity. Selected bond distances (Å) and angles (deg): Pd1−P1, 2.2886(5); Pd1−P2, 2.2981(4); Pd1−O1, 2.0096(13); Pd1−N1, 2.0263(14); O1−O2, 1.293(2); P1−Pd1−P2, 165.129(17); O1−Pd1−N1, 176.49(6); Pd1−O1−O2, 113.79(12).

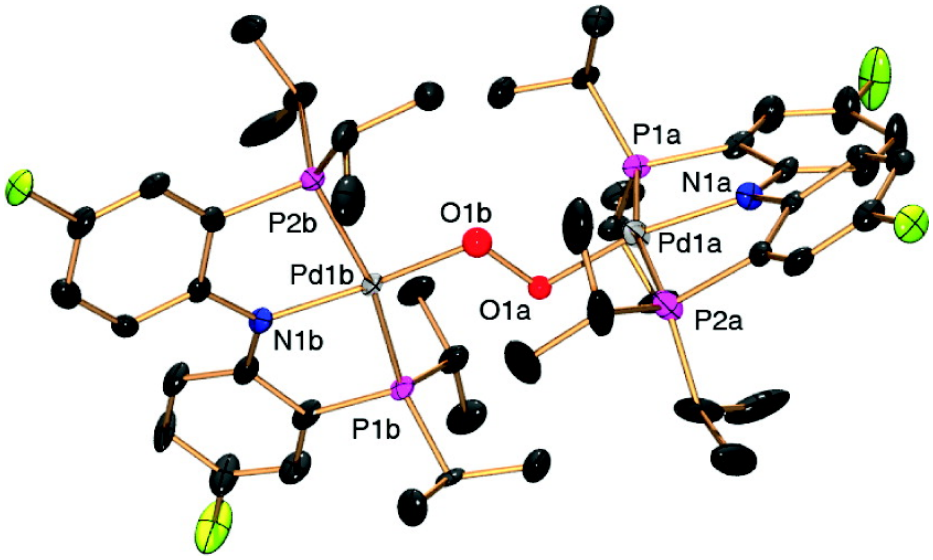

Figure 3.4 POV-Ray rendition of the ORTEP[162] drawing (50% thermal ellipsoids) of **3-8** showing selected atom labeling. Hydrogen atoms and the isopropyl Me groups have been omitted for clarity. Selected bond distances (Å) and angles (deg): O1a−O1b, 1.47(2); N1a−Pd1a, 2.032(8); O1a−Pd1a, 1.985(13); O1b−Pd1b, 2.046(14); P1a−Pd1a, 2.290(3); P2a−Pd1a, 2.288(3); O1a−Pd1a−N1a, 163.7(5); P2a−Pd1a−P1a, 166.51(11); O1b−Pd1b−N1b, 167.3(5).

3.2.5 Spectroscopic features of [(^{F}PNP^{iPr})PdO-]$_2$ and (^{F}PNP^{iPr})PdO$_2$

3-7 an open-shell, paramagnetic molecule with one unpaired electron shows a single peak by EPR with a g value of 2.06 (**Figure 3.5**). Due to its paramagnetic character, **3-7** is silent by ^{31}P NMR spectroscopy and shows very broad aliphatic ^{1}H NMR signals with relatively sharp, paramagnetically shifted, aromatic signals. However, the ^{19}F NMR spectrum of **3-7** is unperturbed, showing relatively sharp signals. The combination of EPR and ^{19}F NMR spectroscopic evidence suggests that the radical is in

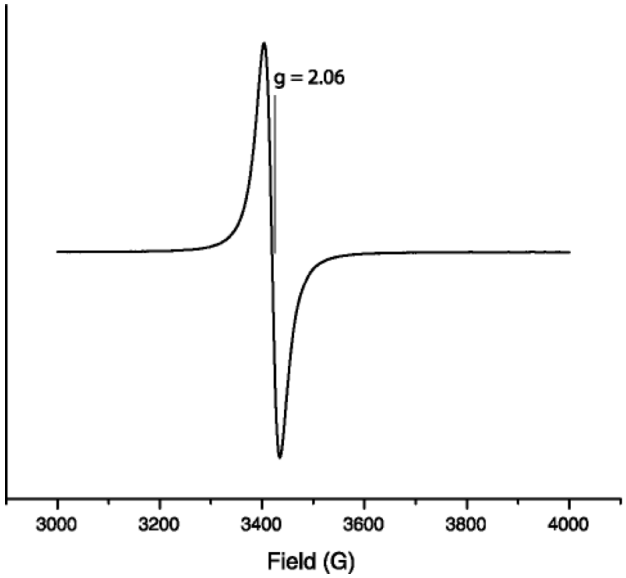

Figure 3.5 X-band EPR spectrum of **3-7**.

a remote and localized position, away from the fluorine atoms on the ancillary ligand, possibly on the O_2^- fragment. DFT calculations performed (by Prof. Christine M. Thomas at Brandeis University) on **3-7** predict a closed shell, anionic PNP ligand and an open-shell superoxide fragment (**Figure 3.6**), in keeping with the ^{19}F NMR and EPR spectroscopy evidence. The palladium peroxide **3-8**, a diamagnetic molecule, shows normal diamagnetic signals by ^{31}P, ^{1}H and ^{19}F NMR spectroscopy.

In addition to obtaining X-ray crystallographic evidence for **3-8**, we were interested in confirming the O_2^{2-} formulation by transferring the peroxide fragment from **3-8** to an organic fragment to make an organic peroxide. The idea was to extract the peroxide (O_2^{2-}) fragment with a sufficiently strong Lewis acid. Compound **3-8** was reacted with a variety of electrophiles such as, benzoyl chloride, Me_3SiCl and Me_3SiBr. The product from these reactions should be (^{F}PNP)PdCl (**2-28)**/Br and a corresponding

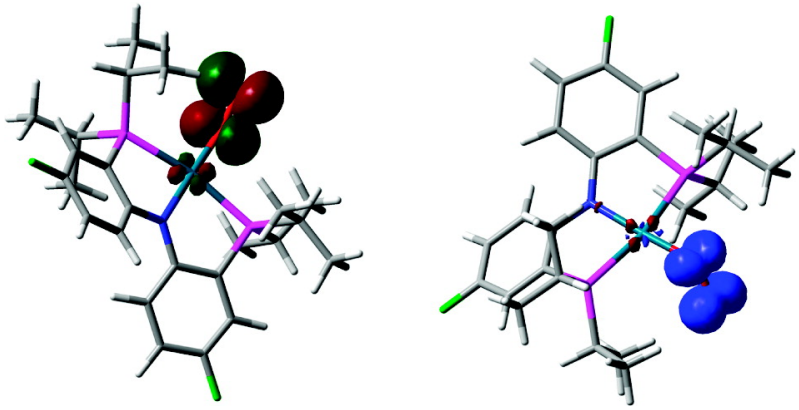

Figure 3.6 Calculated representation of (left) the singly occupied molecular orbital and (right) the spin density distribution in **3-7**.

organic peroxide, both easily identifiable by a combination of ^{19}F, ^{31}P and ^{1}H NMR spectroscopy. Although the reaction between **3-8** and Me_3SiCl or benzoyl chloride both gave quantitative conversion to **2-4**, the corresponding organic peroxide was not observed. It is likely that the organic peroxides produced in these reactions rapidly decompose, avoiding detection by NMR spectroscopy. However, the abstraction of the peroxide with Me_3SiBr successfully produced the organic peroxide $Me_3SiOOSiMe_3$. Addition of substoichiometric quantities of Me_3SiBr generates a mixture of (^{F}PNP)PdBr (**3-9**), (^{F}PNP)Pd-OO-$SiMe_3$ (**3-10**) and **3-8**, the starting material (**Scheme 3.7**).

In addition, to illustrate the capacity of this Pd system for catalytic O_2 activation, we found that **3-7** behaves as a catalyst for the oxidation of Ph_3P with O_2. In the presence of 2% **3-7**, we observed 95% conversion of Ph_3P to Ph_3PO after 3 days at ambient temperature in C_6D_6.[215] A control reaction in the absence of **3-7** led to only 5% conversion after 5 days. **3-7** remained the dominant species observed by NMR

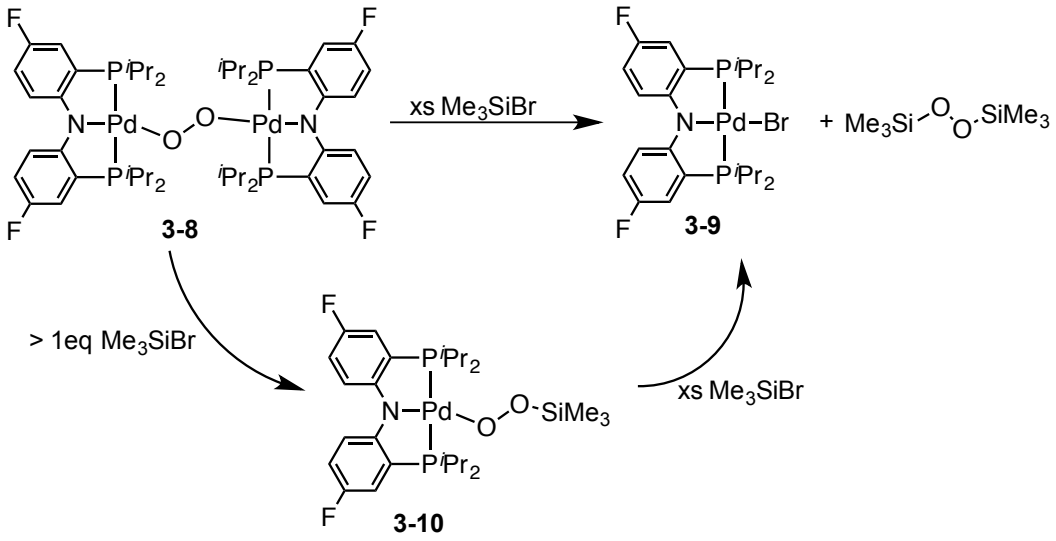

Scheme 3.7 Reaction of **3-8** with Me_3SiBr to generate **3-9** and $Me_3SiOOSiMe_3$.

spectroscopy during the Ph_3P oxidation, but this does not exclude the possibility that **3-8** or one of the decomposition products is the active catalyst.

3.2.6 Synthesis, characterization, and reactivity of [(^{F}PNP^{iPr})PdOH]$^{+}$ cation

The conversion of water into O_2 has been the topic of intense research for many years.[16,216-220] It is widely accepted that the key step in the conversion of H_2O into O_2 is the formation of an O-O bond.[221] Given the importance of this transformation we were curious if we could access the palladium peroxide, **3-8** from **2-8**. The path we envisioned would convert compound **2-8** into compound **3-8** involved the loss of an electron from **2-8** to produce [**2-8**]$^{+}$ followed by deprotonation to yield **3-8** (**Scheme 3.8**). As discussed in Chapter II, the synthesis of **2-8**[54] involves exchanging triflate for hydroxide by treating **2-6** with excess KOH.

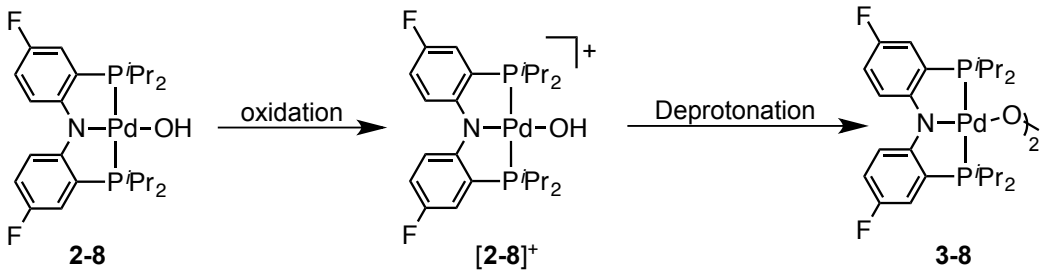

Scheme 3.8 Possible alternate synthesis of **3-8** via a one-electron oxidation followed by deprotonation.

To determine the oxidation potential of **2-8**, and to test whether this compound can undergo reversible oxidation/reduction, cyclic voltametric (CV) was performed. The CV of **2-8** in C_6H_5F revealed a broad quasi-reversible redox process with an approximate $E_{1/2}$ of 0.61 V versus Ag°/AgCl. In comparison, the CV of **2-4** in CH_2Cl_2 revealed a relatively narrow reversible redox wave with an $E_{1/2}$ of 0.59 V versus Ag°/AgCl (**Figure 3.7**). The large separation between the anodic and cathodic wave in **2-8** (relative to **2-4**) may be attributed to the acidic character (predicted by DFT calculations) of the **3-11** cation, and the presence of the relatively basic electrolyte $[Bu_4N]^+[PF_6]^-$ or residual water.

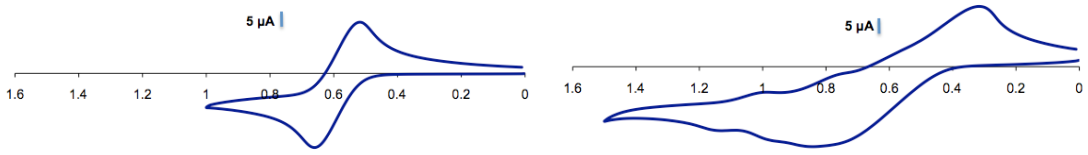

^{F}(PNP)PdCl vs. Ag°/AgCl ^{F}(PNP)PdOH vs. Ag°/AgCl

Figure 3.7 Cyclic Voltammetry of **2-4** in CH_2Cl_2 (left) and **2-8** in C_6H_5F (right). Conditions 50 mV/s; [electrolyte: 0.1 M $Bu_4N^+PF_6^-$].

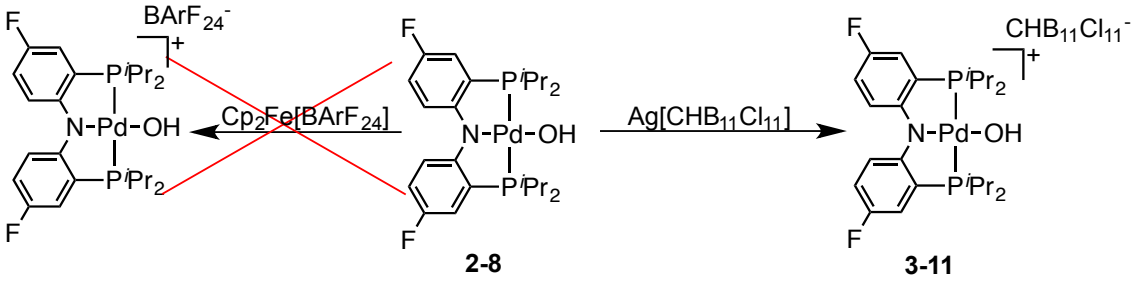

Scheme 3.9 Synthesis of **3-11** by chemical oxidation of **2-8** with $Ag[CHB_{11}Cl_{11}]$.

However, because the CVs of **2-4** and **2-8** were done in different solvents further comparison of the $E_{1/2}$ cannot be done accurately. Attempts to chemically oxidize **2-8** with $[Fc]^+[BArF_{20}]^-$ were unsuccessful (**Scheme 3.9**). However, chemical oxidation of **2-8** with $Ag[CHB_{11}Cl_{11}]$ evinced a rapid color change from orange to purple, consistent with oxidation potential determined by cyclic voltammetry. After filtering through a pad of Celite, to remove Ag(0), the solution was layered with pentane and placed in the freezer at −35 °C. Overnight the solution produced dark purple, X-ray quality, crystals that were analyzed by single-crystal X-ray analysis. The crystal structure of **3-11** shows a hydrogen bonding interaction between the proton on PdOH and the "meta" ring chloride of $[CHB_{11}Cl_{11}]^-$ (2.3 Å) (**Figure 3.8**). Unlike the quinoid type systems, where the C-C bonds on the aromatic framework alternate in length, the PNP ligand is structurally unperturbed. This is consistent with what is observed for $[(^{Me}PNP^{iPr})NiCl]^+[OTf]^-$.[60] The Pd-O bond length in **3-11** of 2.118(3) Å is significantly longer than what is observed in **3-7** (2.0096(13) Å) and the average of both Pd-O bond distances (2.0155 Å) in **3-8**, suggesting that oxidation of **2-8** significantly weakens the Pd-O bond. In addition, the Pd1-N1 (1.9973(3) Å) is comparable to the Pd-N bond

length observed in **3-7** and **3-8**. The average Pd-P bond length in **3-11** (2.320(12) Å) is also comparable to the average Pd-P bond in **3-8 (**2.289(3) Å). In contrast to the observed O-Pd-N bond angle in **3-8** (163.7(5)°) and **3-7** (176.49(6)°) in **3-11** the O-Pd-N angle is very close to linearity (178.46(12)°).

In addition to X-ray crystallography, **3-11** has also been characterized by room temperature X-band EPR spectroscopy. EPR analysis of **3-11** in a solution of C_6H_5F at room temperature gave a $g_{iso} = 2.02$ (see Section 3.4 for spectrum). This value is close to the free electron value of 2.0023 and to the value reported by Mindiola for $[(^{Me}PNP^{iPr})NiCl]^+[OTf]^-$.[58] This suggests that the electron hole is delocalized throughout the ligand framework and that Pd has an oxidation state of +II. Further substantiating this claim, Mirica et al.[222] revealed g-values ranging from 2.118 to 2.133 for Pd(III) complexes. The hyperfine observed in the EPR spectrum of **3-11** is likely due to a combination of both ^{19}F (S = 1/2) and ^{14}N (S = 1) coupling. However, isotropic simulations of the EPR in combination with spin density calculations coupled to EPR simulations must be done to substantiate this claim. In addition, $[(^{F}PNP)PdCl]^+[CHB_{11}Cl_{11}]^-$ (**3-12**) was also synthesized using the procedure used to synthesize **3-11** and an almost identical EPR spectrum was obtained.

DFT calculations (Computational Details: Gaussian09; B3LYP functional; Stuttgart basis set and ECP for Pd, P; 6-31G(d') for C, H, N, O, F; solvation correction: SCRF in THF) performed by Dr. Justin Walensky predict deprotonation of $[\mathbf{2\text{-}8}]^+$ with triethylamine to be a very favorable process (−48 kcal/mol). Given that $[\mathbf{2\text{-}8}]^+$ is

predicted to be a very strong acid, we anticipated that deprotonation could can be achieved using bases such as 2,6-di-*tert*-butyl pyridine and NaH.

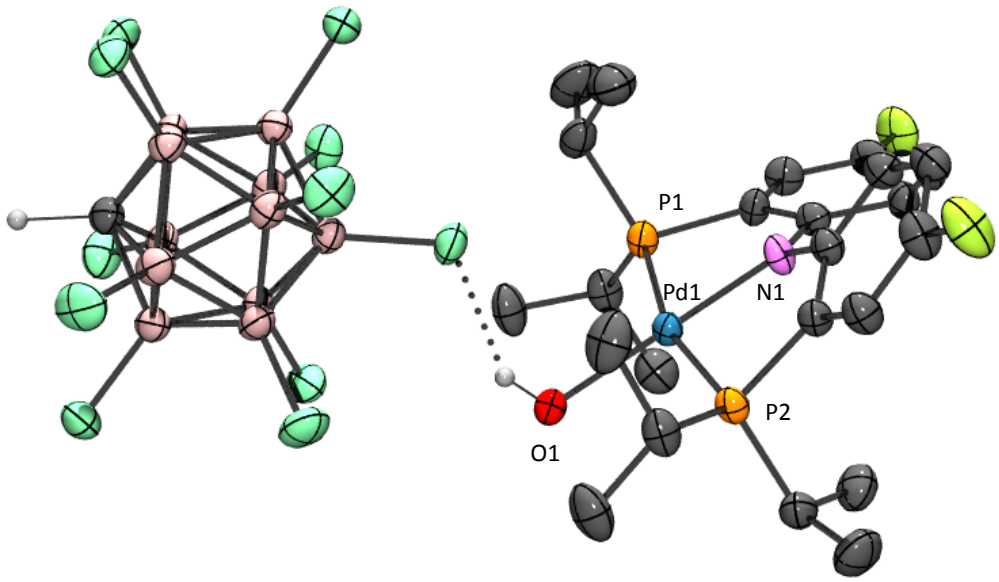

Figure 3.8 POV-Ray rendition of the ORTEP[162] drawing (50% thermal ellipsoids) of **3-11** showing selected atom labeling. Hydrogen atoms were omitted for clarity. Selected bond distances (Å) and angles (deg): Pd1−P1, 2.3217(11); Pd1−P2, 2.3180(12); Pd1−O1, 2.118(3); Pd1−N1, 1.997(3); O1-Cl11, 3.051; H1-Cl11, 2.367; P1−Pd1−P2, 164.78(4); O1−Pd1−N1, 178.46(12).

However, attempts to deprotonate **3-11** with poorly nucleophilic bases did not yield the expected product **3-8**. The reaction of **3-11** with NaH, a non-nucleophilic base, yields **2-7** instead. In addition, attempts to deprotonate **3-11** with bulky non-nucleophilic bases such as 2,2,6,6-tetramethylpiperidine were also unsuccessful. Although the identity of the product of this reaction is unclear (product silent NMR spectroscopy), it is certain that **3-8** is not among the observed products.

3.2.7 Reactivity of [(^{F}PNP^{iPr})Pd-]$_2$ with ethylene (C_2H_4)

Exposure of a solution of **2-10** in C_6D_6 to excess C_2H_4 (1 atm), followed by irradiation a 250-W halogen lamp, led to a slow color change from green to yellow/green color. As confirmed by ^{19}F and ^{31}P NMR spectroscopy, a mixture of **2-10** (46%), the starting material, and a second unknown product (56%) was produced. Based on ^{13}C, ^{1}H and ^{19}F NMR spectroscopic evidence, we tentatively assigned the new product to be the bridging ethylene palladium complex, [(^{F}PNP)Pd-CH_2-]$_2$ (**3-13**; **Scheme 3.10**). The relatively upfield ^{19}F NMR chemical shift at −131.3 ppm suggests that the ligand *trans* to the amido is an alkyl. In addition, the multiplets at 2.41 ppm by ^{1}H NMR and 24.7 ppm by ^{13}C NMR spectroscopy are consistent with the Pd-alkyl formulation. Unlike molecular oxygen, free ethylene is a singlet, diamagnetic molecule; however in the coordination sphere of some late metal complexes ethylene has been shown to behave as an open-shell, paramagnetic ligand.[223,224] In these complexes ethylene can be viewed as a redox non-innocent ligand and the electron can reside on either the metal[225] or the ethylene moiety.[223] This closely parallels the reactivity of **2-10** with oxygen to form superoxide an open-shell molecule or peroxide a closed shell molecule. We were curious whether the reaction of **2-10** with ethylene would generate an open-shell ethylene complex, akin to **3-7**. However, the sharp ^{1}H, ^{31}P and ^{19}F NMR chemical shifts are consistent with a diamagnetic species, ruling out an open-shell monohapto-ethylene complex.

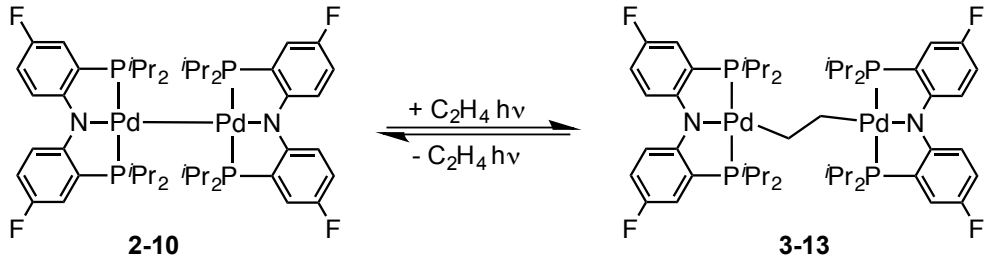

Scheme 3.10 Synthesis of **3-13** via insertion of C_2H_4 into the Pd-Pd bond of **2-10**; photolytic equilibrium between **3-13** and **2-10**.

This is similar to the reactivity reported by Wayland and coworkers in which [(Porph)Rh-]$_2$ with ethylene that produces a bridging ethylene complex, [(Porph)Rh-CH_2-]$_2$.[210] In addition, more sterically hindered [(TTEP)Rh-]$_2$ complexes (TTEP = [Tetrakis(1,3,5-triethylphenyl) porphyrinato)]), impede direct formation of the ethylene bridge and instead undergo carbon-carbon bond coupling of two C_2H_4 to form a butylene-bridged species, [(TTEPP)Rh-CH_2CH_2-]$_2$.[226]

If the volatiles in a solution containing the mixture of **2-10** and **3-13** are removed by vacuum and redissolved in C_6D_6 then covered in aluminum foil overnight no major change in the ratio of **3-13** and **2-10** is observed by NMR spectroscopy. However, if the sample is irradiated with light from a 250 W halogen lamp the product reverts back to **2-10** and free ethylene. This suggests that under photolytic conditions, **3-13** and **2-10** are in equilibrium with free C_2H_4 (**Scheme 3.10**).

3.2.8 Mechanistic discussion of O_2 and C_2H_4 activation with [(^{F}PNP^{iPr})Pd-]$_2$

Although the details of the mechanism of insertion of C_2H_4 and dioxygen into the Pd-Pd bond of **2-10** are not known, it is still interesting to speculate what the mechanism might be. There are two main mechanistic pathways (Path A and B) for the insertion of O_2 and C_2H_4 into the Pd-Pd bond of **2-10** (See **Scheme 3.11).** One possibility (Path A) is that irradiation of **2-10** generates a (PNP^{iPr})Pd(I) metalloradical intermediate (**A**) that then rapidly reacts with O_2 or C_2H_4 via radical coupling type mechanism. However, this pathway is unlikely because the cross-reaction between **2-10** and [(^{Me}PNP^{iPr})Pd-]$_2$ (**3-14**) is slow to generate the mixed product, [(^{Me}PNP^{iPr})Pd-Pd(^{iPr}PNP^{F})] (**3-15**) (**Scheme 3.11b**).[54] If the rate determining step in both the cross-reaction between **2-10** and **3-14** and the reaction between **2-10** and X_2 (X = O, CH_2) is the formation of intermediate **A** then their rates should be similar, which is not the case. The second possible pathway (Path B; **Scheme 3.11**) involves the photoexcitation of **2-10** (without Pd-Pd bond cleavage), which then reacts with X_2. This reaction can occur via a concerted type mechanism where O_2 or C_2H_4 first approaches the exited Pd-Pd fragment of **2-10** and via radical coupling mechanism intermediate **B** is formed with concomitant formation of the (PNP^{iPr})Pd(I) radical. Although not definitive, one way the two pathways might be differentiated is by testing alkenes of different sizes. In intermediate **A** the metal center is less sterically protected and would therefore be more likely be able to react with bulkier alkenes. C_2H_4 and O_2 are both small molecules that could more easily access the metal in intermediate **C** (Path B).

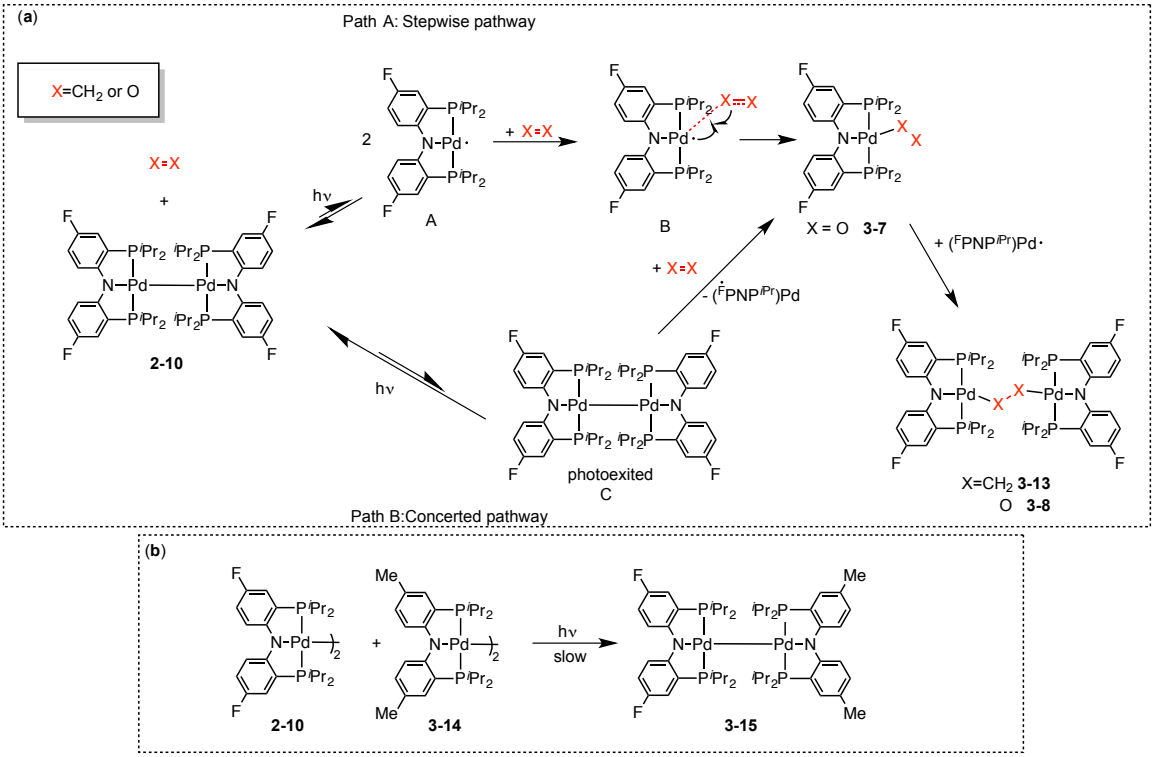

Scheme 3.11 Possible pathways for the insertion of O_2 and C_2H_4 into the Pd-Pd bond of **102**.

3.3 Conclusion

In summary, the first example of a structurally characterized monohapto palladium(II) superoxide (**3-7**) and the equilibrium with a μ-peroxide (**3-8**) was characterized. Compound **3-7**, was synthesized by irradiation of **2-10** under an atmosphere of excess O_2. Compound **3-7** is an open-shell, paramagnetic complex with the electron localized on the O_2 moiety. The associated μ-peroxide (**3-8)** was synthesized by irradiation of **2-10** and substoichiometric quantities of O_2. **3-8** is a closed shell, diamagnetic complex with well-defined ^{1}H, ^{31}P and ^{19}F NMR spectra. In addition, the first example of a palladium ethylene bridging complex (**3-13**) was synthesized by irradiating **2-10** under an atmosphere of ethylene. Although η^2-O_2-Pd and η^2-(C_2H_4)-Pd

have been observed previously, **3-7**, **3-8** and **3-13** are unique because of the η^1 binding mode. The PNP ligand's strong, tridentate, and meridional type coordination forces dioxygen and ethylene to bind to palladium in a unique η^1 fashion. Finally, the synthesis and characterization of $[(^{F}PNP^{iPr})PdOH]^+$ was also discussed. Although attempts to synthesize **3-8** via deprotonation of $[(^{F}PNP^{iPr})PdOH]^+$ were unsuccessful, DFT calculations of **2-8** suggest that $[(^{F}PNP^{iPr})PdOH]^+$ is a very acidic species.

3.4 Experimental

3.4.1 General considerations

All manipulations were performed under an argon atmosphere using standard Schlenk line or glovebox techniques. Toluene, THF, diethyl ether and C_6D_6 were dried over NaK/Ph_2CO/18-crown-6, distilled or vacuum transferred and stored over molecular sieves in an Ar-filled glovebox. **2-4**, **2-8** and **2-10** were prepared according to published procedures.[54,135,157] All other chemicals were used as received from commercial vendors. NMR spectra were recorded on a Varian iNova 400 (^{1}H NMR, 399.755 MHz; ^{19}F NMR, 375.912 MHz) and NMRS 500 (^{1}H NMR, 499.703 MHz; ^{13}C NMR, 125.697 MHz; ^{31}P NMR, 202.289 MHz; ^{19}F NMR, 470.069 MHz) spectrometer. Chemical shifts are reported in δ (ppm). For ^{1}H NMR spectra, the residual solvent peak was used as an internal reference. ^{19}F NMR spectra were referenced externally using 99% CF_3CO_2H at −78.5 ppm. For the purpose of clarity, the following abbreviations are defined: apparent (app.), doublet of virtual triplet (dvt). X-band EPR derivative spectra were recorded on a Bruker EMX spectrometer equipped with the Bruker standard cavity (ER4102ST) and

referenced to DPPH. Microwave frequencies were calibrated with a Hewlett-Packard frequency counter (HP5352B), and the field control was calibrated with a Bruker NMR field probe (ER035M). (EPR conditions for the collection of spectra: microwave power, 2.007 mW; microwave frequency, 9.858 GHz; modulation frequency, 100.00 kHz; modulation amplitude, 10.00 G.)

Synthesis of 3-7. An oven-dried, 200 mL polytetrafluoroethylene (PTFE)-valved flask was charged with 10 mL of THF. Compound **2-10** (40 mg, 37 μmol), and a stir bar were then added. The flask was closed off, and removed from the glovebox. It was degassed using three freeze-pump-thaw cycles, and O_2 was added at 1 atm from a flushed gas line. The flask was placed in an ice water bath on a stir plate, and allowed to stir in direct sunlight for 5 min until the solution was transparent orange. The flask was degassed and returned to the glovebox where the solution was transferred to an oven-dried, 250 mL Schlenk flask. The volatiles were removed. The resulting solid was redissolved in a minimum amount (approx. 1 mL) of THF, layered with pentane (approx. 3 mL) and placed in a freezer (−35 °C) for 2 d. The supernatant was decanted off revealing orange crystals. The purity of solid samples prepared in this fashion is difficult to judge because upon dissolution, **3-7** can equilibrate with **3-8** in the absence of excess O_2. **3-7** can be more conveniently generated in situ by treatment of solutions of **2-10** with excess O_2 under light (vide infra for details). Selected NMR data for **3-7** follow. ^{1}H NMR (C_6D_6): δ 7.55 (br, 2H, Ar-H), 6.13 (br, 2H, Ar-H), 5.66 (br, 2H, Ar-H) (**Figure 3.9**); ^{19}F NMR (C_6D_6): δ −128.7 (**Figure 3.10**); ^{31}P{^{1}H} NMR: no detectable signal.

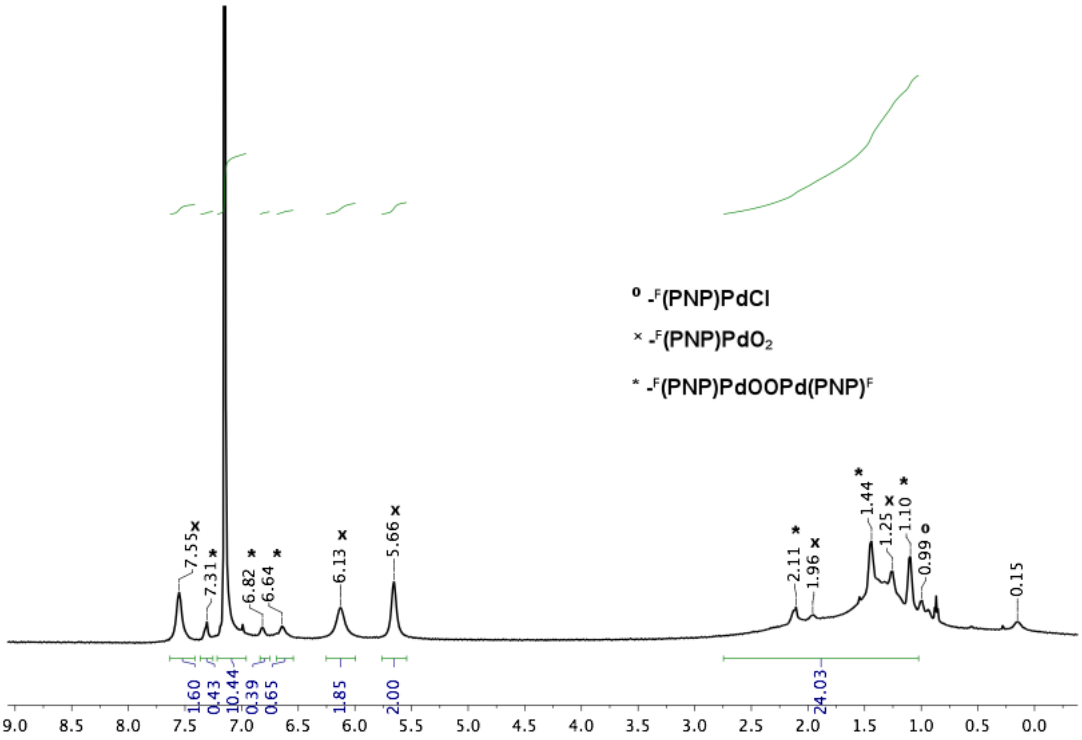

Figure 3.9 ^{1}H NMR spectrum of a solution of 3-7 in C_6D_6 that contains small amounts of 106 and 3-8 impurities.

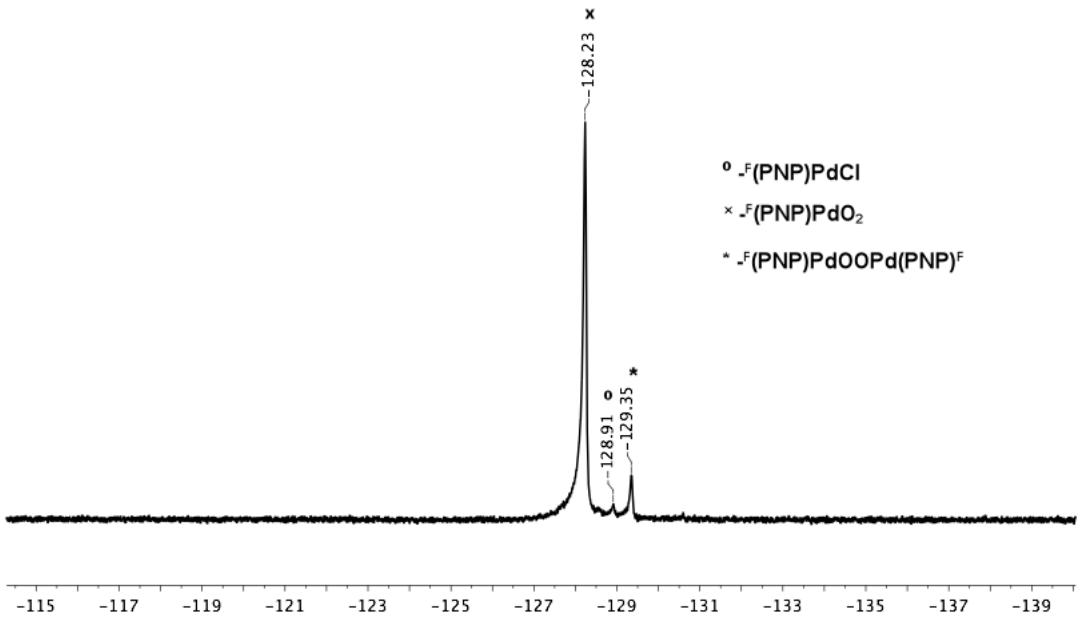

Figure 3.10 ^{19}F NMR spectrum of a solution of **3-7** in C_6D_6 that contains small amounts of **106** and **3-8** impurities.

Light dependency of 3-7 formation. Two oven-dried, J. Young tubes were each charged with 1 mL of a solution of **2-10** (4.7 mg, 4.0 μmol) in C_6D_6 which contained $PhCF_3$ as a standard. The solutions were removed from the glovebox and degassed with three freeze-pump-thaw cycles. One J. Young tube was wrapped in foil to prevent exposure to light, and O_2 was added to both samples at 1 atm from a flushed gas line. ^{19}F NMR spectroscopy was used to monitor the progress of the reaction comparing two identical solutions, one of which was kept in the dark, and the other was laid down flat on a white sheet of paper and exposed to fluorescent laboratory light for 1 h. The

reactions were periodically monitored by ^{19}F NMR spectroscopy (**Figures 3.11 and 3.12**). After 1 h, the solution that was exposed to light displayed nearly complete formation of **3-7**. The covered solution was left in the dark overnight and showed only **2-10** in the ^{19}F NMR spectrum. At the conclusion of the experiment, the covered solution was then exposed to light, and shaken for 3 min until it turned orange and displayed a nearly complete conversion to **3-7**.

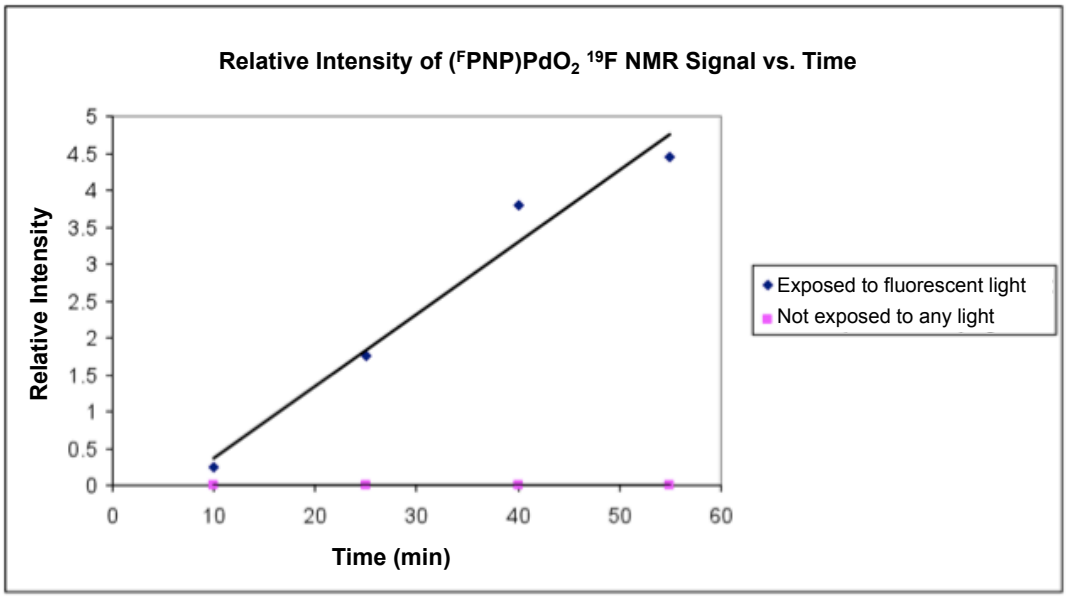

Figure 3.11 Light dependence of **3-7** formation. Linear relationship is not implied by the use of the trend line.

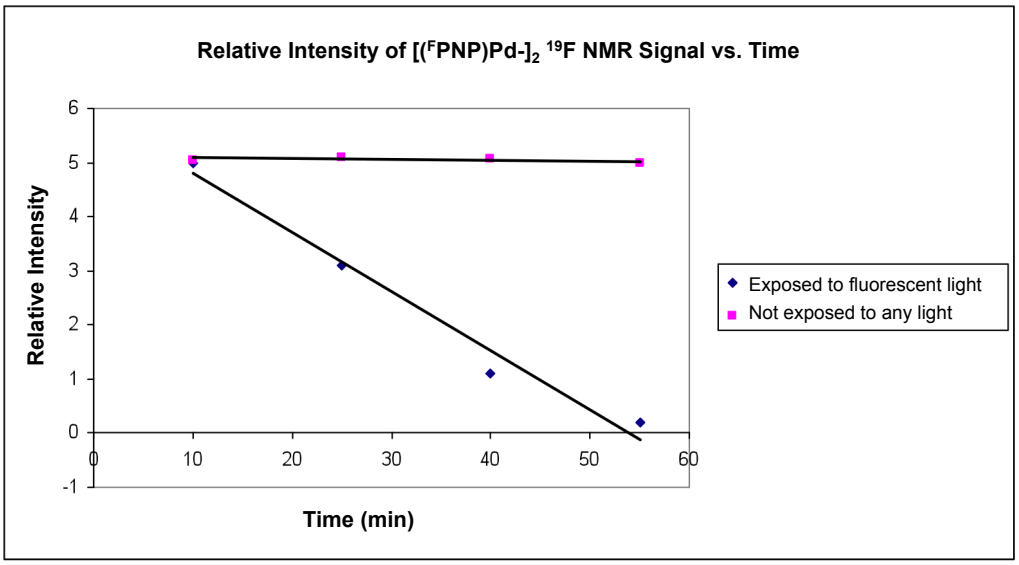

Figure 3.12 Light dependence of **2-10** consumption. Linear relationship is not implied by the use of the trend line.

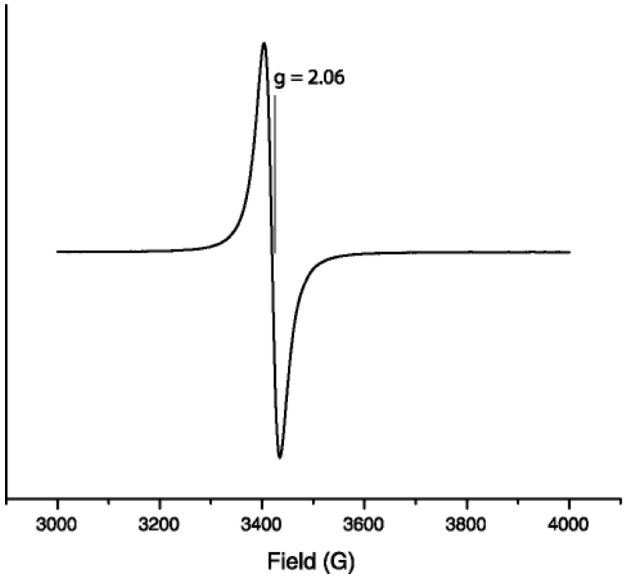

Figure 3.13 X-band EPR spectrum of **3-7** recorded on a Bruker EMX spectrometer

EPR spectrum of compound 3-7. Compound **2-10** (10.0 mg, 9.2 μmol) was placed in an oven-dried J. Young tube and dissolved in toluene. The solution was degassed, and then filled with O_2. It was placed in an acetone-dry ice bath inside a UV box for 15 min until it turned orange. An EPR spectrum was collected at 293 K (**Figure 3.13**).

VT NMR spectroscopy study of 3-7. Compound **2-10** (10.0 mg, 9.2 μmol) was placed in an oven-dried J. Young tube and dissolved fully in toluene-d^8. The sample was removed from the glovebox, degassed with three freeze-pump-thaw cycles, and O_2 was added at 1 atm from a flushed gas line. The J. Young tube was shaken in the sunlight until it turned orange (30 s), it was then placed in liquid N_2 as the NMR instrument was prepared. NMR spectra were collected in the −50 °C to +10 °C range. The residual solvent peak of $C_6D_5CD_2H$ was used as an internal standard, and the broad resonance at 5.66 ppm (at RT) was monitored (**Figure 3.14**). At the conclusion of the experiment, the presence of **3-7** was confirmed by ^{19}F NMR spectroscopy.

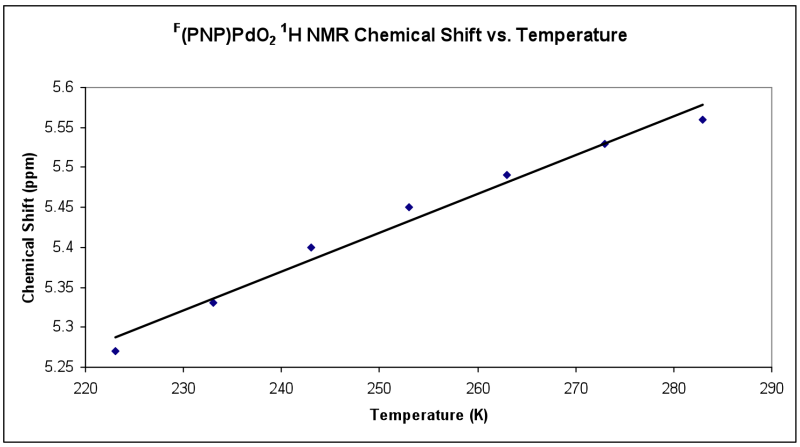

Figure 3.14 Temperature dependence of the chemical shift of one of the ^{1}H NMR resonances of **3-7**. Linear relationship is not implied by the use of the trend line.

Reaction of 3-7 with $CDCl_3$. An oven-dried J. Young tube was charged with **2-10** (5.0 mg, 4.6 μmol) and dissolved fully in C_6D_6. The J. Young tube was removed from the glovebox, and degassed with three freeze-pump-thaw cycles and O_2 was added at 1 atm from a flushed gas line. The solution was shaken in direct sunlight for 1 min until it turned orange. The solvent was stripped off and the solid was left under vacuum at room temperature for 5 min. The J. Young tube was returned to the glovebox, and dissolved in chloroform-d. **2-4** (90%) was observed after 24 h at ambient temperature. We have occasionally observed **2-4** as a trace impurity in our spectra and it may originate from the reactions with the traces of the vapors of chlorinated solvents present in the glovebox.

Decomposition of 3-7 under O_2 atmosphere. In an oven-dried J. Young tube, **2-10** (0.50 mL of a saturated solution in C_6D_6 with C_6F_5OMe as an internal standard, 2.4

μmol) was degassed with three cycles of freeze-pump-thaw. The solution was frozen with a dry ice, acetone bath and 760 torr of O_2 were added by rapidly opening and closing the J. Young tube. The solution was then irradiated with light from a 500-W halogen lamp for 8 min. The resulting solution of **3-7** was wrapped with aluminum foil, and left at room temperature. According to the ^{19}F NMR spectroscopy analysis, after 21 h the solution of **3-7** evolved into a mixture of **2-8** (11%), **3-7** (68%) and two other unknown products (21%). The sample was then placed in 50 °C oil bath for 2 h producing many unknown products. Percentages are percent fluorine content determined by ^{19}F NMR spectroscopy.

Decomposition of 3-7 under Ar atmosphere. In an oven-dried J. Young tube, **2-10** (0.50 mL of a saturated solution in C_6D_6 with C_6F_5OMe as an internal standard, 2.4 μmol) was degassed with three cycles of freeze-pump-thaw. The solution was frozen with a dry ice, acetone bath and 760 torr of O_2 where added by rapidly opening and closing the J. Young tube. The solution was then irradiated with light from a 500-W halogen lamp for 8 min. ^{19}F NMR spectroscopy confirmed quantitative conversion of **2-10** to **3-7**. The volatiles were removed *in vacuo* (under fluorescent lighting), and the solid was re-dissolved in 0.50 mL of C_6D_6. The solution of **3-7** equilibrated to a mixture of **3-8** (23%) and **3-7** (77%). The J. Young tube was wrapped with aluminum foil, and left at room temperature for 5 h. No measurable change was observed. The above mixture was then irradiated with a 500-W halogen light source for 5 min producing a

mixture of **2-8** (10%), **3-8** (45%) and 5 unknown products (13%). Percentages are percent fluorine content determined by ^{19}F NMR spectroscopy.

Catalysis of oxidation of Ph_3P with O_2. PPh_3 (25 mg, 94 μmol, 92 eq) was placed in a J. Young tube and left under vacuum for 5 min. It was then brought into a glovebox where **2-10** (1.0 mg, 0.9 μmol, 1.8 μmol Pd) was added along with 0.5 mL C_6D_6. The J. Young tube was removed from the glovebox, and degassed with three freeze-pump-thaw cycles. O_2 was added at 1 atm from a flushed gasline. The solution was irradiated in direct sunlight for 1 min until it turned orange. After 3 d at ambient temperature, 95% Ph_3PO was observed. The **3-7** produced a ^{19}F NMR resonance at −128.7 ppm was observed as the dominant NMR signal throughout the experiment. Control reaction: PPh_3 (25 mg, 94 μmol) was placed in a J. Young tube and left under vacuum for 5 min. It was then brought into a glovebox where it was dissolved in 0.5 mL C_6D_6. The J. Young tube was removed from the glovebox, and degassed with three freeze-pump-thaw cycles, and O_2 was added at 1 atm from a flushed gasline. After 5 d at room temperature in fluorescent light, 5% Ph_3PO was observed.

Synthesis of 3-8 via reaction of 2-10 with 3-7. A polytetrafluoroethylene (PTFE)-valved 100 mL flask was charged with **2-10** (10 mL of a 2.8 mM solution, 28 μmol). After three cycles of freeze-pump-thaw, the solution was frozen with a dry ice/acetone bath, and 760 torr of O_2 was added by rapidly opening and closing the flask. The solution was then irradiated with light from a 500-W halogen lamp for 8 min. The

volatiles were then removed *in vacuo*. To the resulting solid, **2-10** (7 mL of a 2.8 mM solution, 20 μmol) was added. The sample was then irradiated for 30 min with a fluorescent (ceiling lamps) light source. The volatiles were removed *in vacuo*, and the solid was washed with pentane. After thoroughly drying under vacuum the solid was dissolved in THF, layered with pentane, and placed in the freezer at −35 °C. Overnight the solution produced many dark-red X-ray quality crystals. The solution was decanted and the solid was washed with pentane. The solid was vacuum dried overnight and 27 mg of **3-8** was produced (27 mg, 0.024 mmol, 50%). ^{1}H NMR (C_6D_6): 7.33 (m, 2H, Ar-H), 6.82 (m, 2H, Ar-H), 6.65 (td), 2.13 (m, 4H, CH), 1.45 (app. quartet (dvt), 12H, J = 8 Hz, PCH*Me*$_2$), 1.12 (app. quartet (dvt), 12H, J = 8 Hz, PCH*Me*$_2$). ^{13}C{^{1}H} NMR (C_6D_6): δ 160.3 (t, J_{C-P} = 10 Hz, C-N), 154.3 (dvt, J_{C-F} = 236 Hz, J_{C-P} = 4 Hz, C-F), 120.7 (dvt, J_{C-P} = 14 Hz, J_{C-F} = 5 Hz), 118.4 (d, J_{C-F} = 22 Hz), 118.1 (d, J_{C-F} = 22 Hz), 116.0 (app. q, J_{C-F} = 7 Hz), 24.1 (t, J_{C-P} = 11 Hz, $CHMe_2$), 19.0 (br s, $CHMe_2$), 17.6 (s, $CHMe_2$) (**Figure 3.15**); ^{31}P{^{1}H} NMR (C_6D_6): δ 40.6; ^{19}F NMR (C_6D_6): δ –129.9 (m, C-F).

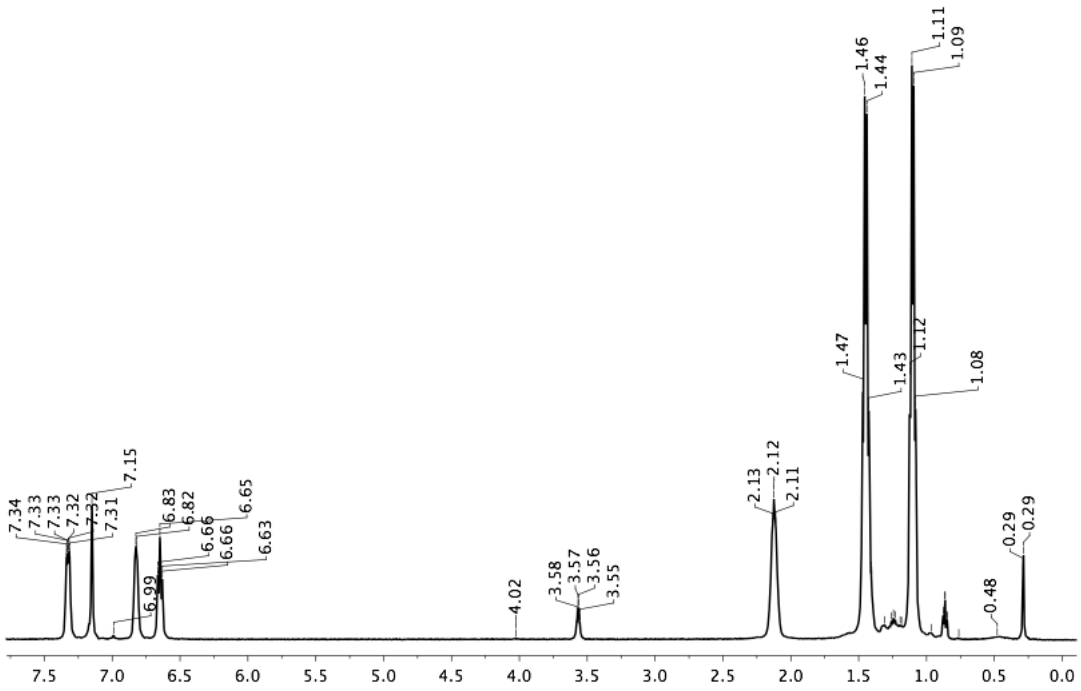

Figure 3.15 ^{1}H NMR spectrum of **3-8** in C_6D_6 (containing residual pentane, THF, and silicone grease).

Preparation of a saturated solution of 2-10. In an oven-dried vial, 5.0 mL of C_6D_6 were added to 30 mg **2-10**. The solution was stirred for 5 min and filtered through Celite. 4 μL of C_6F_5OMe was added as an internal standard. Based on the internal standard, the saturated solution was calculated to be approximately 4.8 mM.

Reaction of 2-10 with 20-760 torr of O_2. Seven oven-dried J. Young tubes were charged with **2-10** (0.50 mL of a saturated solution in C_6D_6 with pentafluoroanisole as an internal standard, 2.4 μmol) and degassed with three cycles of freeze-pump-thaw. Each solution was frozen with a dry ice/acetone bath, and by rapidly opening and closing

each J. Young tube, 20, 30, 50, 160, 260 and 760 torr of O_2 were added to each, respectively, and the tube was closed off. The solution was then irradiated with sunlight for 5 min. The ratio of **2-10**, **3-8**, **2-8** and **3-7** was monitored by ^{19}F NMR spectroscopy (see **Tables 3.1** and **3.2**).

Table 3.1 ^{19}F and ^{31}P NMR resonances in C_6D_6.

Compound	^{31}P NMR	^{19}F NMR
2-10	46.5[1]	−131.1
3-8	40.6	−129.4
2-8	40.4[2]	−129.4[b]
3-7	n/a	−128.7
(^{F}PNP)Pd-OO-SiMe$_3$	Unknown	−129.1

Table 3.2 Relative concentrations of **2-10**, **3-8**, **2-8**, and **3-7** at different pressures of O_2.

Added O_2 pressure (torr)	**2-10**	**3-8**	**2-8**	**3-7**
20	36	64	0	0
30	0	82	8	10
50	0	31	3	65
160	0	6	2	92
260	0	2	0	98
560	0	1	0	99
760	0	0	0	100

Evidence for equilibration of 3-7 and 3-8. In an oven-dried J. Young tube, **2-10** (0.50 mL of a saturated solution in C_6D_6, 2.4 μmol) was degassed with three freeze-pump-thaw cycles. To the solution, 160 torr of O_2 (8 eq) was added. The solution was irradiated with sunlight for 8 min until no further change by ^{19}F NMR spectroscopy was

observed. The ratio of **3-8** to **3-7** to **2-8** was 9:86:5 (^{19}F NMR spectroscopy evidence). The solution was then degassed with three freeze-pump-thaw cycles. After 3 h, the molar ratio changed to 19:76:5. Overnight the ratio changed to 23:59:17, and a small quantity (1%) of three other unknown products.

Reaction of 3-8 with excess Me_3SiBr. In an oven-dried J. Young tube, **3-8** (5.0 mg, 4.5 μmol) was dissolved in 0.5 mL of C_6D_6. To the above solution, C_6F_5OMe was added (10 μL of a 0.35 mM solution in C_6D_6, 35 μmol). The ratio of the starting material (**2-10**) to the internal standard was determined by ^{1}H and ^{19}F NMR spectroscopy. To the solution, Me_3SiBr (200 μL of a 0.18 M solution in C_6D_6, 36 μmol) was added via syringe. Based on ^{31}P, ^{19}F, and ^{1}H NMR spectroscopic observations, the reaction produced (^{F}PNP)PdBr (NMR yield: 100%) with concomitant $Me_3SiOOSiMe_3$ (NMR yield: 61%) and $Me_3SiOSiMe_3$ (NMR yield: 39%).

Decomposition of $Me_3SiOOSiMe_3$. In an oven-dried J. Young tube, $Me_3SiOOSiMe_3$ (2.0 μL, 9.3 μmol) was dissolved in C_6D_6. To the above solution, Me_3SiBr (2.0 μL, 15 μmol) was added. After overnight, the solution contained a mixture of $Me_3SiOSiMe_3$ (41%) and Me_3SiBr (59%).

Synthesis of (^{F}PNP^{iPr})PdBr (3-9) via reaction of 2-4 with Me_3SiBr. In an oven-dried J. Young tube, **2-4** (12 mg, 21 μmol) was dissolved in 0.5 mL of C_6D_6. To above solution, Me_3SiBr (60.0 μL of a 0.18 M solution in C_6D_6, 11.0 μmol) was added.

Based on ^{31}P NMR spectroscopic observations, a mixture of **2-4** (45%), and (^{F}PNP)PdBr (54%) was produced. This was done to establish that **2-4,** and (^{F}PNP$^{i\text{Pr}}$)PdBr were distinguishable by NMR spectroscopy. To the above solution, Me_3SiBr (80 μL of a 0.18 M solution in C_6D_6, 14.0 μmol) was added, and complete conversion to (^{F}PNP)PdBr was observed (Yield: not isolated, 100% conversion). ^{1}H NMR (C_6D_6): 7.30 (m, 2H, Ar-H), 6.70 (m, 2H, Ar-H), 6.63 (td), 2.11 (m, 4H, PC*H*Me_2), 1.31 (app. quartet (dvt), 12H, J = 8 Hz, PCH*Me*$_2$), 0.96 (app. quartet (dvt), 12H, J = 8 Hz, PCH*Me*$_2$); $^{13}C\{^{1}H\}$ NMR (C_6D_6): δ 160.5 (t, $J_{C\text{-}P}$ = 11 Hz, C-N), 154.8 (dvt, $J_{C\text{-}F}$ = 237 Hz, $J_{C\text{-}P}$ = 4 Hz, C-F), 121.3 (dvt, $J_{C\text{-}P}$ = 14 Hz, $J_{C\text{-}F}$ = 5 Hz), 118.6 (d, $J_{C\text{-}F}$ = 23 Hz), 118.2 (d, $J_{C\text{-}F}$ = 21 Hz), 115.9 (app. q, J = 7 Hz), 25.4 (t, $J_{C\text{-}P}$ = 13 Hz, *C*HMe_2), 18.7 (br s, CH*Me*$_2$), 17.8 (s, CH*Me*$_2$); $^{31}P\{^{1}H\}$ NMR (C_6D_6): δ 48.7; ^{19}F NMR (C_6D_6): δ –128.3 (m, C-F).

Stability of 3-8 in the dark. In an oven-dried J. Young tube, **3-8** (5.0 mg, 4.5 μmol) was dissolved in 0.50 mL of C_6D_6. The J. Young tube was then wrapped with aluminum foil and left at room temperature overnight. After 18 h, no change was observed by NMR spectroscopy.

Photochemical decomposition of 3-8. In an oven-dried J. Young tube, **3-8** (5.0 mg, 4.5 μmol) was dissolved in 0.50 mL of C_6D_6. The J. Young tube was then exposed to fluorescent lighting (laboratory lighting) at room temperature overnight. After 20 h, **3-8** evolved into a mixture of **3-8** (72%), and nine different products (28%), that could not

be reliably identified. Percentages are percent fluorine content determined by ^{19}F NMR spectroscopy.

Thermal decomposition of 3-8. In an oven-dried J. Young tube, **3-8** (5.0 mg, 4.5 μmol) was dissolved in 0.50 mL of C_6D_6. The J. Young tube was wrapped with aluminum foil, and placed in a 60 °C oil bath overnight. After 18 h, **3-8** evolved into a mixture of **2-8** (13%), **2-7** (19%), and 10 different unknown products (51%). Percentages are percent fluorine content determined by ^{19}F NMR spectroscopy.

Light source dependency. After experimenting with different sources of light it was determined that either sunlight or the halogen light source (250-W or 500-W) provided the fastest conversion rate from **2-10** to **3-8** or **3-7**. Although sunlight, and halogen light both are equally effective, using a halogen light source is more convenient. Using sunlight involves either walking outside or placing the reaction vessel next to a window and naturally the weather must have an influence on the rate of the reaction. Fluorescent light sources (lab lighting) also induces the conversion from **2-10** to **3-8** (or **3-7**), but the rate is approximately 10-15 times slower than sun or halogen light sources. However, the synthesis of **3-8** via the reaction of **2-10** with **3-7** should be done using fluorescent lighting because it reduces the amount of side products formed.

Reaction of 3-8 with Me_3SiCl (2.1 eq.). An oven-dried J. Young tube was charged with **2-10** (2 mg, 2 μmol), and dissolved in 0.5 mL of C_6D_6. The sample was then degassed with three cycles of freeze-pump-thaw. The solution was frozen with a

dry ice/acetone bath and 760 torr of O_2 were added by rapidly opening and closing the J. Young tube to a gas line. The solution was then irradiated with light from a 250-W halogen lamp for 5 min. The volatiles were removed *in vacuo*. To the solution, **2-10** (2 mg, 2 μmol) was added, and the resulting solution was irradiated with fluorescent light for 20 min. Me_3SiCl (24 μL of 0.16 M solution in C_6D_6, 3.8 μmol) was added to the resulting solution of **3-8**. Complete conversion to **2-4** was observed; however, no $Me_3SiOOSiMe_3$ was observed by ^1H NMR spectroscopy.

Reaction of 2-8 with benzoyl chloride. In an oven-dried J. Young tube, **2-8** (15 mg, 0.027 mmol) was dissolved in 0.5 mL of C_6D_6 to the solution benzoyl chloride (3 μL, 0.03 mmol) was added. Complete conversion to **2-4** was observed, but benzoic acid was not observed by ^1H NMR spectroscopy.

Synthesis of 3-11. In an oven-dried vial, **2-8** (31 mg, 0.056 mmol) was dissolved in 1 mL of C_6H_5F. To the resulting solution, $Ag[CHB_{11}Cl_{11}]$ (35 mg, 0.056 mmol) was added as a solid, and an immediate color change from orange to blue was observed. The solution was then filtered through Celite and the volatiles were removed by vacuum. The solid was redissolved in a minimal amount of C_6H_5F, and the resulting solution was carefully layered with pentane. After allowing the pentane to slowly diffuse for a few days, crystals were formed. A single crystal was selected for single-crystal X-ray analysis. The rest of the solid was dried under vacuum (37 mg, 0.034 mmol, 60%). A

small sample of the resulting solid was dissolved in C_6H_5F, and an EPR spectrum was obtained (**Figure 3.16**).

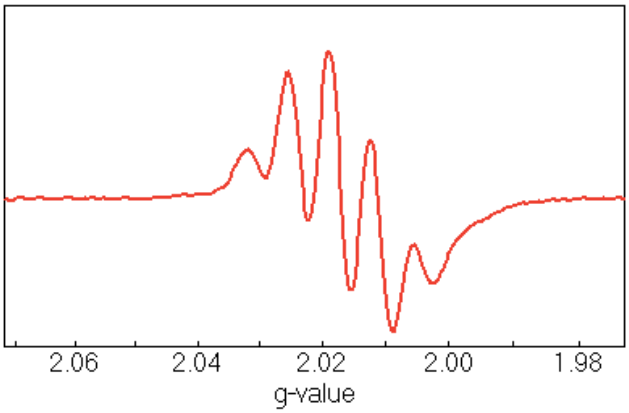

Figure 3.16 Room temperature X-band EPR spectrum of **3-11**.

Reduction of 3-11 with $(Cp^*)_2Fe$. In an oven-dried J. Young tube, **3-11** (5 mg, 5 μmol) was dissolved in C_6H_5F. To the resulting solution, $(Cp^*)_2Fe$ (3 mg, 9 μmol) was added as a solid, and the solution was analyzed by NMR spectroscopy. Based on ^{19}F NMR spectroscopy, there were a total of 14 products generated.

Attempted deprotonation of 3-11 with NaH. In an oven-dried J. Young tube, **3-11** (8.0 mg, 0.014 mmol) was dissolved in THF. To the resulting solution NaH (1 mg, 0.04 mmol) was added as a solid, and after properly mixing, the solution was analyzed by NMR spectroscopy. Based on ^{19}F NMR, ^{1}H NMR, and ^{31}P NMR spectroscopy the only product observed was ($^{F}PNP^{iPr}$)PdH.

Synthesis of [(^{F}PNP^{iPr})PdCl]$^{+}$[CHB$_{11}$Cl$_{11}$]$^{-}$ (3-12). In an oven-dried vial, **2-4** (31 mg, 0.035 mmol) was dissolved in 1 mL of C_6H_5F. To the resulting solution Ag[CHB$_{11}$Cl$_{11}$] (22 mg, 0.056 mmol) was added as a solid, and an immediate color change from red to purple was observed. The solution was filtered through Celite, and the volatiles were removed by vacuum. The solid was redissolved in a minimum amount of C_6H_5F, layered with pentane, and placed in the freezer overnight. The solution was decanted, and the solid was dried under vacuum (20 mg, 0.18 mmol, 52%). A small amount of the product was dissolved in C_6H_5F, and an EPR spectrum was taken at room temperature (**Figure 3.17**).

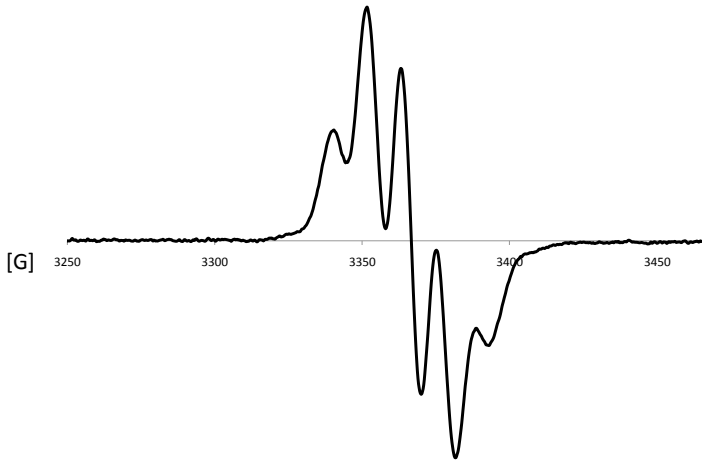

Figure 3.17 Room temperature X-band EPR spectrum of **3-12**.

Reduction of 3-12 with decamethylferrocene. In an oven-dried schlenk flask, **3-12** (16 mg, 0.015 mmol) was dissolved in 1 mL of C_6H_5F. To the resulting solution, (Cp*)$_2$Fe (4.0 mg, 0.015 mmol) was added as a solid. After a few minutes of stirring, a

color change from purple to a brown/red was observed. The volatiles were removed under vacuum, redissolved in toluene, filtered through Celite, and dried under vacuum. The product in the reaction was confirmed to be **2-4** by NMR spectroscopy.

Attempted deprotonation of 3-11 with 2,6-Di-*tert*-butypyridine. In an oven-dried J. Young tube, **3-11** (8.0 mg, 0.014 mmol) was dissolved in 0.5 mL of C_6H_5F. To the resulting solution, 2,6-di-*tert*-butypyridine (10 μL, 0.046 mmol) was added with a micro syringe. After properly mixing the reagents, no color change was observed. The product of the reaction was silent by ^{19}F, ^{1}H, and ^{31}P NMR spectroscopy.

Reaction of 2-10 with ethylene (C_2H_4). In a J. Young tube **2-10** (10 mg, 9 μmol) was dissolved in 0.50 mL of C_6D_6. After three cycles of freeze-pump-thaw, the J. Young tube was charged with 760 torr of ethylene. After the sample was irradiated with light from a 250-W halogen lamp for 180 min, a slight color change from a dark green to a lighter yellow/green was observed. ^{19}F, ^{31}P, and ^{1}H NMR spectroscopy confirm an incomplete conversion of **2-10** to a second product determined to be a bridging ethylene complex, **3-13** (56%). ^{1}H NMR (C_6D_6): 7.46 (m, 2H, Ar-H), 6.86 (m, 2H, Ar-H), 6.75 (m, 2H, Ar-H), 2.41 (m, 2H, Pd-CH_2), 2.09 (m, 4H, PCHMe$_2$), 1.24 (app. quartet (dvt), 12H, J = 8 Hz, PCHMe_2), 1.03 (app. quartet (dvt), 12H, J = 8 Hz, PCHMe_2) (**Figure 3.18**). $^{13}C\{^{1}H\}$ NMR (C_6D_6): δ 159.3 (t, J_{C-P} = 10 Hz, C-N), 154.8 (d, J_{C-F} = 235 Hz, C-F), 121.3 (dvt, J_{C-P} = 23 Hz, J_{C-F} = 3 Hz), 118.2 (d, J_{C-F} = 20 Hz), 118.1 (d, J_{C-F} = 19 Hz),

115.2 (s), 24.7 (s), 20.2 (s, *C*HMe$_2$), 19.4 (s, CH*Me*$_2$), 18.0 (s, CH*Me*$_2$); ^{31}P{^{1}H} NMR (C_6D_6): δ 35.37; ^{19}F NMR (C_6D_6): δ –131.3 (m, C-F).

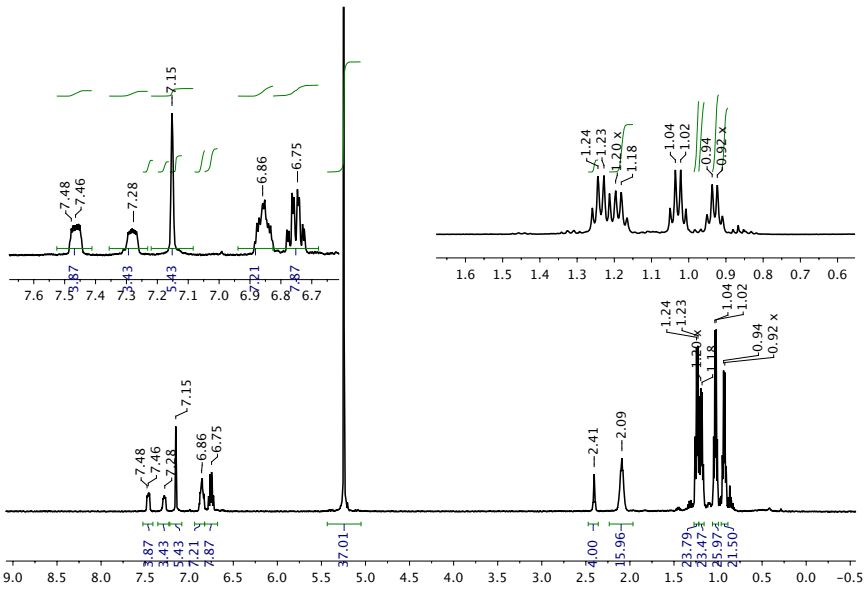

Figure 3.18 ^{1}H NMR of a mixture of **3-13** (44%) and **2-10** (66%).

Evidence for an equilibrium between 3-13 and 2-10. In a J. Young tube, **2-10** (10 mg, 9 μmol) was dissolved in 0.50 mL of C_6D_6. After three cycles of freeze-pump-thaw, the J. Young tube was charged with 760 torr of ethylene. After the sample was irradiated with light from a 250-W halogen lamp for 90 min, a slight color change from a dark green to a lighter yellow/green color was observed. ^{19}F, ^{31}P, and ^{1}H NMR spectroscopy confirmed formation of a mixture of **2-10** (44%), and **3-13** (56%). The volatiles were removed under vacuum, redissolved in C_6D_6, and then covered in aluminum foil. After 2 h, no major change in the ratio of **3-13** and **2-10**. The sample was

then irradiated with light from a 250-W halogen lamp for 180 min. During this time, the solution changed from a yellow/green color to a darker green color. ^{19}F, ^{31}P and ^{1}H NMR spectroscopy confirmed complete conversion back to **2-10** (100%).

3.4.2 X-ray diffraction experiments

X-Ray data collection, solution, and refinement for 3-7 (solved by Prof. Foxman, B. M. at Brandeis U.). A small quantity of compound **3-7** was dissolved in a minimum amount (approx. 1 mL) of THF, layered with pentane (approx. 3 mL), and placed in a freezer (−35 °C) for 2 d. The supernatant was decanted off revealing orange crystals. A single X-ray suitable crystal was selected, and all operations were performed on a Bruker-Nonius Kappa Apex2 diffractometer, using graphite-monochromated MoKα radiation. All diffractometer manipulations, including data collection, integration, scaling, and absorption corrections were carried out using the Bruker Apex2 software.[177] Preliminary cell constants were obtained from three sets of 12 frames. Data collection was carried out at 120 K, using a frame time of 10 s, and a detector distance of 60 mm. The optimized strategy used for data collection consisted of 8 phi and 7 omega scan sets, with 0.5° steps in phi or omega; completeness was 99.8%. A total of 5726 frames were collected. Final cell constants were obtained from the *xyz* centroids of 9949 reflections after integration.

From the systematic absences, the observed metric constants and intensity statistics, space group *P21/c* was chosen initially; subsequent solution and refinement confirmed the correctness of this choice. The structure was solved using SIR-92,[227] and refined (full-matrix-least squares) using the Oxford University Crystals for Windows program.[228] All non-hydrogen atoms were refined using anisotropic displacement parameters. Hydrogen atoms were fixed at calculated geometric positions and allowed to ride on the corresponding carbon atoms. The difference map showed a peak of 1.8 $e^{-}/Å^3$ at a distance of 0.7 Å from Pd1; it was not possible to model a minor component of a disordered molecule or contaminant based upon this peak and other lower-level peaks. The final least-squares refinement converged to $R1 = 0.0258$ ($I > 2\sigma(I)$, 7014 data), and $wR2 = 0.0733$ (F^2, 8753 data, 334 parameters).

Table 3.3 Crystal data and structure refinement for 3-7.

Empirical formula	$C_{28}H_{42}F_2N_1O_2P_2Pd$	
Formula weight	646.99	
Temperature	110(2) K	
Wavelength	0.71073 Å	
Crystal system	Monoclinic	
Space group	*P21/c*	
Unit cell dimensions	a = 17.97(2) Å	α = 90.0°
	b = 11.73(2) Å	β = 106.5060(10)°
	c = 14.7031(3) Å	γ = 90.0°
Volume	2971.85(12) $Å^3$	
Z	4	
Density (calculated)	1.446 Mg/m^3	
Absorption coefficient	0.774 mm^{-1}	
F(000)	1340	
Crystal size	0.06 × 0.27 × 0.43 mm^3	
Theta range for data collection	1.78 to 27.50°	
Index ranges	$-28 \le h \le 28$, $-26 \le k \le 26$, $-17 \le l \le 17$	
Reflections collected	59805	
Independent reflections	9949 [R(int) = 0.0885]	
Completeness to theta = 27.50°	99.8%	
Absorption correction	Semi-empirical from equivalents	
Max. and min. transmission	0.81 and 0.95	
Refinement method	Full-matrix least-squares on F^2	
Data / restraints / parameters	8753 / 0 / 334	
Goodness-of-fit on F^2	1.0055	
Final R indices [I>2σ(I)]	$R1$ = 0.0409, wR2 = 0.1321	
R indices (all data)	$R1$ = 0.0365, wR2 = 0.1261	
Absolute structure parameter	0.28(4)	
Largest diff. peak and hole	1.432 $eÅ^{-3}$ and −1.495 $eÅ^{-3}$	

X-Ray data collection, solution, and refinement for 3-8 (solved by Prof. Foxman, B. M. at Brandeis U. and Dr. Herbert, D.). A small quantity of **3-8**, was dissolved in a minimum of THF, layered with pentane, and placed in the freezer at −35 °C. Overnight the solution produced many dark red X-ray quality crystals. A red, multi-faceted crystal of suitable size (0.30 × 0.19 × 0.16 mm) was selected from a representative sample of crystals of the same habit using an optical microscope, and mounted onto a nylon loop. Low temperature (150 K) X-ray data were obtained on a Bruker APEXII CCD based diffractometer (Mo sealed X-ray tube, K_α = 0.71073 Å). All diffractometer manipulations, including data collection, integration and scaling were carried out using the Bruker APEXII software.[177] An absorption correction was applied using SADABS.[178] The space group was determined on the basis of systematic absences, and intensity statistics and the structure was solved by direct methods and refined by full-matrix least squares on F^2. The structure was solved in the monoclinic *C2/c* space group using XS[179] (incorporated in SHELXTL). All non-hydrogen atoms except the O atoms were refined by using anisotropic displacement parameters. Hydrogen atoms were placed in idealized positions, and refined using a riding model. The structure was refined (weighted least squares refinement on F^2) to convergence.

The oxygen atoms of the peroxo bridge were found to be disordered. The center of the O–O bond lies on the crystallographic 2 axis at ~ (0, 0.185, ¼); hence the occupancies of the O atoms were fixed at 0.5. The two O atoms (O1A, O1B) were refined by using isotropic displacement parameters. Restraints were employed to treat the displacement parameters of some of the peripheral carbon atoms to acceptable sizes. Solvent accessible voids of 61 $Å^3$ were found in the structure with an electron count of 30 per cell, which were not treated further. The final least-squares refinement converged to $R1 = 0.0971$ ($I > 2\sigma(I)$, 4062 data) and $wR2 = 0.2289$ (F^2, 4367 data, 287 parameters). The final CIF file is available upon request; we note that the CheckCIF routine produced three Alert B items, related to a crystal quality and/or disorder issues. Accordingly, the CIF file and CheckCIF output contain validation reply form items, which address the Alert B issues. While we would have preferred to have found a crystal of high quality, the present data collection and solution represent the best of repeated data collections using a number of different crystals.

Table 3.4 Crystal data and structure refinement for 3-8.

Empirical formula	$C_{48}H_{68}F_4N_2O_2P_4Pd_2$	
Formula weight	1117.72	
Temperature	110(2) K	
Wavelength	0.71073 Å	
Crystal system	Monoclinic	
Space group	*Cc*	
Unit cell dimensions	a = 21.59(2) Å	α = 90°
	b = 20.65(2) Å	β = 125.387(10)°
	c = 13.770(14) Å	γ = 90°
Volume	5005(9) $Å^3$	
Z	4	
Density (calculated)	1.483 Mg/m^3	
Absorption coefficient	0.900 mm^{-1}	
F(000)	2296	
Crystal size	0.296 × 0.187 × 0.162 mm^3	
Theta range for data collection	1.78 to 27.50°	
Index ranges	$-28 \le h \le 28$, $-26 \le k \le 26$, $-17 \le l \le 17$	
Reflections collected	26886	
Independent reflections	10961 [R(int) = 0.0885]	
Completeness to theta = 27.50°	99.8%	
Absorption correction	Semi-empirical from equivalents	
Max. and min. transmission	0.7456 and 0.5585	
Refinement method	Full-matrix least-squares on F^2	
Data / restraints / parameters	10961 / 26 / 576	
Goodness-of-fit on F^2	1.128	
Final R indices [I>2σ(I)]	$R1$ = 0.0609, wR2 = 0.1455	
R indices (all data)	$R1$ = 0.0765, wR2 = 0.1561	
Absolute structure parameter	0.28(4)	
Largest diff. peak and hole	1.644 $eÅ^{-3}$ and −1.495 $eÅ^{-3}$	

X-Ray data collection, solution, and refinement for 3-11 (solved by McCulloch, B.). Crystals of **3-11** were grown from a concentrated solution in fluorobenzene layered with pentane. A blue block of suitable size (0.21 × 0.19 × 0.16 mm), and quality was selected from a representative sample of crystals of the same habit using an optical microscope, mounted onto a nylon loop, and placed in a cryocooled stream of nitrogen (110 K). Room-temperature X-ray data were obtained on a Bruker APEXII CCD based diffractometer (Mo sealed X-ray tube, K_α = 0.71073 Å). All diffractometer manipulations, including data collection, integration, and scaling were carried out using the Bruker APEX2 software. An absorption correction was applied using SADABS.[178] The space group was determined on the basis of systematic absences and intensity statistics. The structure was solved by direct methods, and refined by full-matrix least squares on F^2. The structure was solved in the triclinic *P1* space group using XS (incorporated in SHELXTL). A check for missed symmetry was run using the ADDSYM program within PLATON,[180] revealing no apparent higher symmetry. All non-hydrogen atoms were refined with anisotropic thermal parameters. Hydrogen atoms bound to carbon were placed in idealized positions, and refined using a riding model. The hydrogen atom bound to oxygen was found to be disordered over two chemically equivalent sites, each hydrogen-bonded to a chlorine atom of a carborane cage, and were located in the difference maps and refined with AFIX constraints on the O-H bonds. The structure was refined (weighted least squares refinement on F^2) to convergence.

Table 3.5 Crystal data and structure refinement for 3-11.

Empirical formula	$C_{25}H_{36}B_{11}Cl_{11}F_2NOP_2Pd$	
Formula weight	1081.75	
Temperature	110(2) K	
Wavelength	0.71073 Å	
Crystal system	Triclinic	
Space group	*P-1*	
Unit cell dimensions	a = 9.660(4) Å	α = 92.653(6)°
	b = 12.695(6) Å	β = 102.900(5)°
	c = 19.526(9) Å	γ = 97.263(6)°
Volume	2308.6(18) $Å^3$	
Z	2	
Density (calculated)	1.556 Mg/m^3	
Absorption coefficient	1.141 mm^{-1}	
F(000)	1074	
Crystal size	0.21 × 0.19 × 0.16 mm^3	
Theta range for data collection	1.87 to 27.51°	
Index ranges	$-12 \le h \le 12$, $-15 \le k \le 16$, $-25 \le l \le 25$	
Reflections collected	23523	
Independent reflections	10396 [R(int) = 0.0362]	
Completeness to theta = 25.00°	99.3%	
Absorption correction	Semi-empirical from equivalents	
Max. and min. transmission	0.7456 and 0.6031	
Refinement method	Full-matrix least-squares on F^2	
Data / restraints / parameters	10396 / 0 / 496	
Goodness-of-fit on F^2	1.082	
Final R indices [I>2σ(I)]	$R1$ = 0.0383, wR2 = 0.0938	
R indices (all data)	$R1$ = 0.0528, wR2 = 0.1075	
Largest diff. peak and hole	0.476 $eÅ^{-3}$ and −0.679 $eÅ^{-3}$	

3.4.3 Computational details

Calculations on 3-7 (Calculations performed by Prof. Thomas C. at Brandeis University). All calculations were performed using Gaussian03-E.01[71] for the Linux operating system. Density functional theory calculations were performed using a hybrid functional the three parameter exchange functional of Becke (B3),[229] and the correlation functional of Lee, Yang, and Parr (LYP)[230] (B3LYP). A mixed basis set was employed, using the LANL2DZ basis set and effective core potentials of Hay and Wadt for palladium and phosphorus,[231,232] the D95V basis set for carbon, hydrogen, and fluorine,[233] and the cc-pVDZ basis set for oxygen and nitrogen.[234] Using the crystallographically determined geometry of **3-7** as a starting point, the geometry was optimized to a minimum, followed by analytical frequency calculations to confirm that no imaginary frequencies were present. To obtain the most useful depiction of the SOMO, a restricted open-shell calculation (ROB3LYP) was performed.

Table 3.6 Comparison of calculated and experimental geometrical parameters in **3-7**.

	Calculated (DFT)	**Experimental (X-ray)**
Pd1-P1	2.358 Å	2.2886(5) Å
Pd1-P2	2.372 Å	2.2981(4) Å
Pd1-O1	2.061 Å	2.0096(13) Å
Pd1-N1	2.092 Å	2.0263(14) Å
O1-O2	1.298 Å	1.293(2) Å
P1-Pd1-P2	165.70 Å	165.129(17) Å
O1-Pd1-N1	178.73 Å	176.49(6) Å
Pd1-O1-O2	112.5 Å	113.79(12) Å

CHAPTER IV

SYNTHESIS AND REACTIVITY OF $[(PNP)Pd(L)]^+$ CATIONS

4.1 Introduction

As discussed in Chapter I, three-coordinate, 14-electron, d^8, Pt and Pd complexes have been implicated as intermediates in many catalytic reactions such as C-C[235], C-O[236], C-N[28,104,237] bond coupling and C-H activation. Typically, these highly electrophilic complexes undergo dimerization, coordination of solvent or formation of agostic interactions.[27,93-99,236,238] Because of their elusive behavior, significant effort has been devoted towards isolating and characterizing these complexes.[23-26,28] This chapter will describe the results of abstracting a coordinating anion from $(PNP^R)PdX$ (X = H, Cl, F or OTf; R = ^{i}Pr, ^{t}Bu) with a variety of cations (e.g. Na^+, R_3Si^+) in combination with weakly-coordinating anions such as $[BArF_{24}]^-$ or $[CRB_{11}X_{11}]^-$ (X = H, Cl; R = H, Me, Et and Bu). In addition, the DFT predictions on the structure and electronics of a theoretical three-coordinate, T-shaped palladium(II), cationic complex will also be discussed. As will be discussed in Section 4.2.3, the most comparable analog to the three-coordinate $[(PNP)Pd]^+$ cation is Hartwig's three-coordinate species (**1-64**). Compound **1-64** is an intermediate in C-N coupling, and as such, undergoes reductive elimination of (anisyl)N(3,5-$(CF_3)_2C_6H_3)_2$ with concomitant formation Pd(0). Although the three-coordinate $[(PNP)Pd]^+$ cation is not an not an intermediate in a catalytic cycle, it is also supported by both a diarylamido and a phosphine ligand, however, the rigid PNP pincer framework forces the diarylamido ligand to be *trans* to the empty

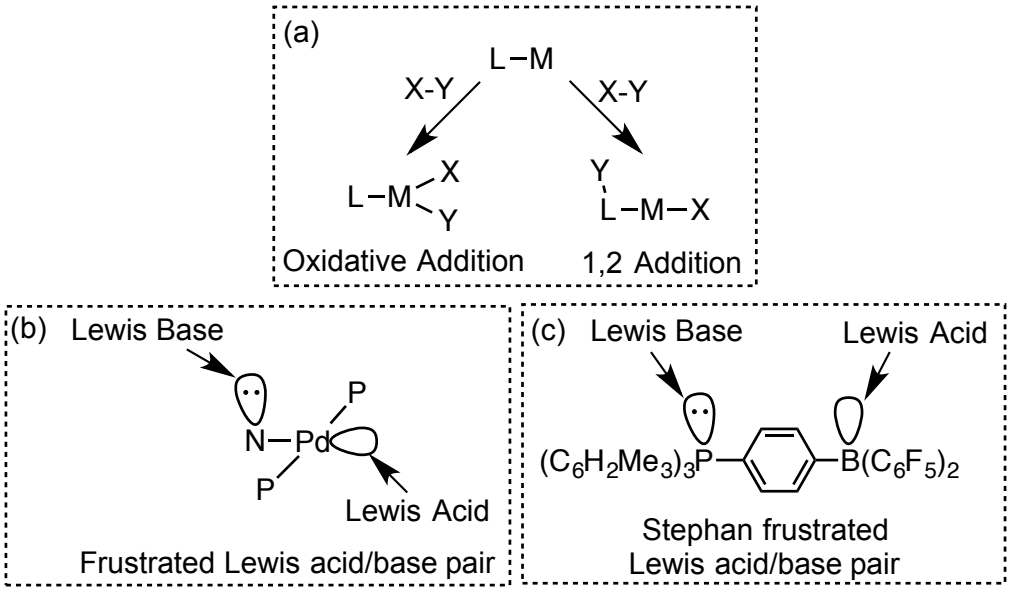

Scheme 4.1 Oxidative addition and 1,2-addition (a); Frustrated Lewis acid/base pairs $[(PNP)Pd]^+$ cation (b), and Stephan example (c).

coordination site. This structural difference produces a highly electrophilic cation that is capable of coordinating even extremely poor Lewis bases such as arenes and haloarenes. This chapter will discuss the chemistry of these unusual Lewis acid base adducts.

Our group has previously reported that the $[(PNP^{iPr})Pd]^+$ fragment is capable of heterolytically cleaving X-H bonds such as alkynyl C-H, S-H, B-H and B-B.[66,67] These reactions can be viewed as the product of a 1,2-addition rather than conventional oxidative addition of X-H (**Scheme 4.1**). In conventional oxidative addition an overall metal oxidation change of +2 is required,[103,239] however, in 1,2-addition there is no net change in the oxidation state. Oxidative addition also requires both an empty and a filled metal orbital, but in $[(PNP^{iPr})Pd]^+$ cation, the metal has only an empty metal orbital; the

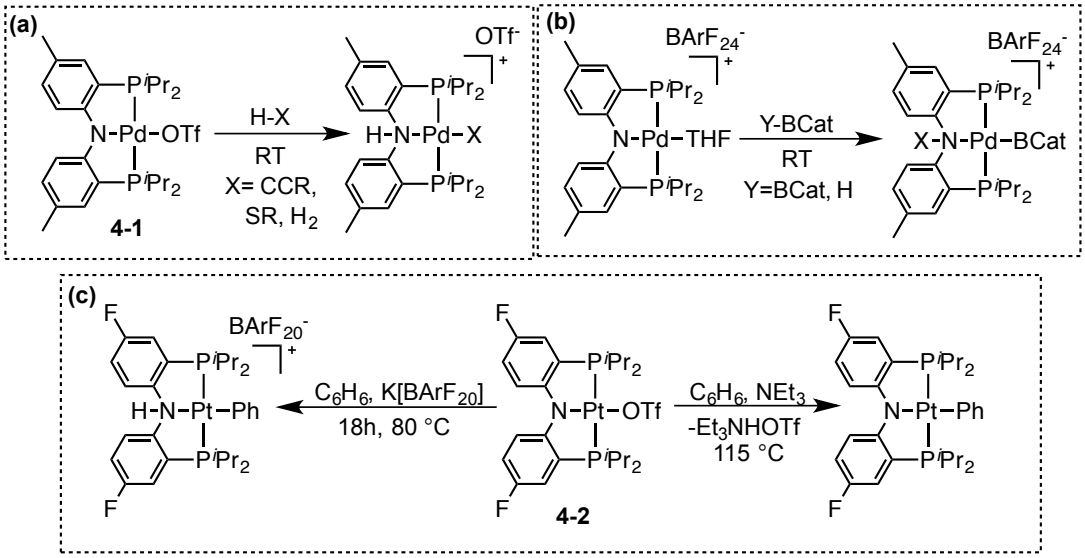

Scheme 4.2 Heterolytic cleavage of H-X (X = CCR, SR, H_2) and Y-Bpin using $[(PNP)Pd]^+$ cation (top), and H-Ph cleavage using $[(PNP)Pt]^+$ cation (bottom).

filled orbital is located on the amido ligand. The $[(PNP^{iPr})M]^+$ cations can be viewed in very much the same way as the frustrated Lewis acid-base pairs reported by Stephan et al (**Scheme 4.1c**).[240,241] The reactivity of $[(PNP^{iPr})M]^+$ fragment (M = Ni, Pd, or Pt) depends on both the metal and the basicity of the counter anion. For example, in compounds **2-6** and ($^{Me}PNP^{iPr}$)PdOTf (**4-1**) the frustrated Lewis acid/base pair in $[(PNP^{iPr})Pd]^+$ is able to activate substrates such as H_2, thiols, and terminal alkynes (**Scheme 4.1b**).[66] However, more innocent anions such as $[CHB_{11}H_{11}]^-$ or $[BArF_{20}]^-$ are needed to cleanly activate bonds like B-H and B-B (**Scheme 4.2b**).[67] Also, whereas ($^{F}PNP^{iPr}$)PtOTf (**4-2**) requires an external base and elevated temperatures to cleave C-H bonds in arenes, the use of weakly-coordinating anions such as $[BArF_{20}]^-$ allows the $[(^{F}PNP^{iPr})Pt]$ fragment to undergo1,2-addition of arenes under mild conditions (**Scheme 4.2c**).[65] The role of weakly-coordinating anions (see Section 4.2.4 for definition)

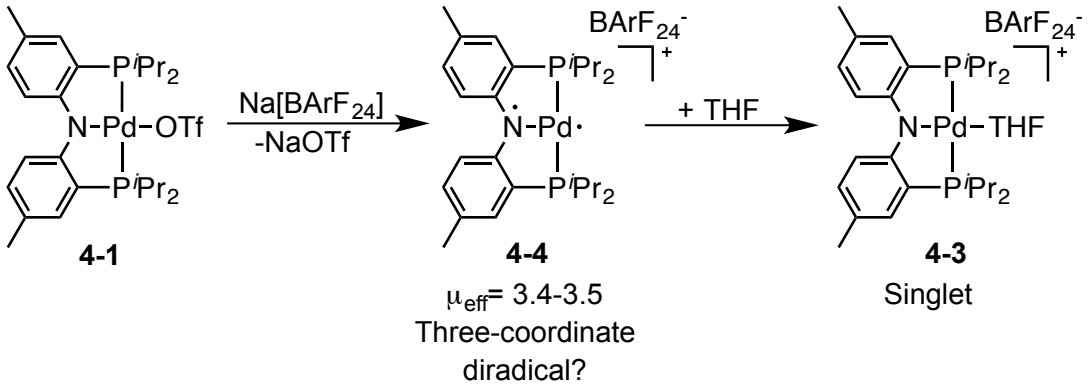

4-1 **4-4** **4-3**

μ_{eff}= 3.4-3.5

Three-coordinate diradical?

Singlet

Scheme 4.3 Initial discovery of hypothesized triplet three-coordinate species (**4-4**) and quenching with THF.

is twofold: to facilitate access to an empty coordination site on Pd, and to avoid a reaction between the resulting cation and the anion. Although the reactivity of $[(PNP^{iPr})M]^+$ (M = Pd, Pt) fragment with substrates like H_2, RCC-H, RSH, CatBH, CatB-BCat and Ar-H has been thoroughly explored, there is little understanding of the product of the reaction between **4-1** and Na[WCA] (WCA = [$BArF_{24}$], [$CRB_{11}Cl_{11}$] (R = H, alkyl)) in the absence of the above substrates. This chapter will focus on the synthesis, reactivity, and structural characterization of $[(PNP^R)Pd(L)]^+$ (R = ^{t}Bu, ^{i}Pr; L = arene, haloarene, etc.) cations with weakly-coordinating anions with an overall goal to isolate a three-coordinate, 14-electron $[(PNP)Pd]^+$ cation.[d]

[d] Note: The following nomenclature is in addition to the nomenclature established in Chapter I (footnote b): The term "three-coordinate $[(PNP)Pd]^+$" cation refers to the hypothetical three-coordinate, 14-electron complex species. However, the term $[(PNP)Pd(L)]^+$ refers to the cation with ligand L coordinated to Pd. The term (PNP)Pd[WCA] does not imply a specific structure (i.e. solvent adduct or anion adduct).

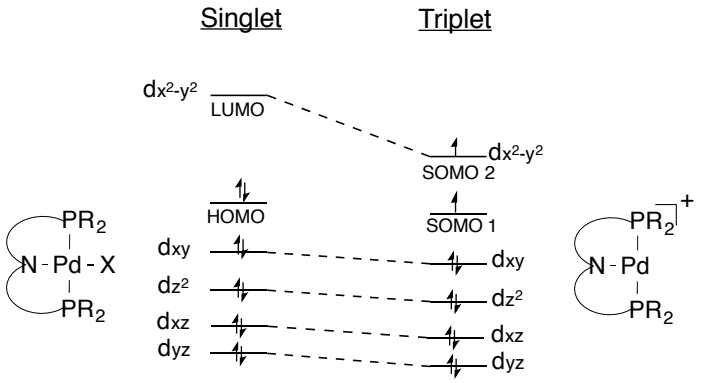

Figure 4.1 Molecular orbital diagram of theoretical triplet, three-coordinate $[(PNP)Pd]^+$ cation.

4.2 Results and Discussion

4.2.1 Initial discovery of $[(PNP)Pd]^+$ cation

Dr. Lei Fan, a former coworker in the Ozerov group, discovered that the reaction between **4-1** and $Na[BArF_{20}]$ ($Na[B(C_6H_3(CF_3)_2)_4]$) produces a green solution that is silent by NMR spectroscopy. Addition of THF to the above solution evinced an immediate color change from green to blue, and concomitant reemergence of NMR signals corresponding to $[(^{Me}PNP^{iPr})Pd(THF)]^+[BArF_{24}]^-$ (**4-3**). Elemental analysis of the green solid was in agreement with the formulation $[(^{Me}PNP^{iPr})Pd]^+[BArF_{20}]^-$ (**Scheme 4.3**). In addition, preliminary Evans method magnetic susceptibility measurements, collected by Dr. Fafard,[173] determined a μ_{eff} of 3.4-3.5, consistent with a triplet species.[242-244] These results led to the hypothesis that the product made in the reaction in **Scheme 4.3** was a paramagnetic, 14-electron, three-coordinate $[(^{Me}PNP^{iPr})Pd]^+[BArF_{20}]^-$ complex (**4-4**).

4.2.2 DFT analysis of three-coordinate $[(PNP)Pd]^+$ cations

In an effort to further understand the structure and electronics of the predicted three-coordinate $[(PNP)Pd]^+$ cation, DFT calculations were performed by Prof. Dmitry Gusev at Wilfrid Laurier University.

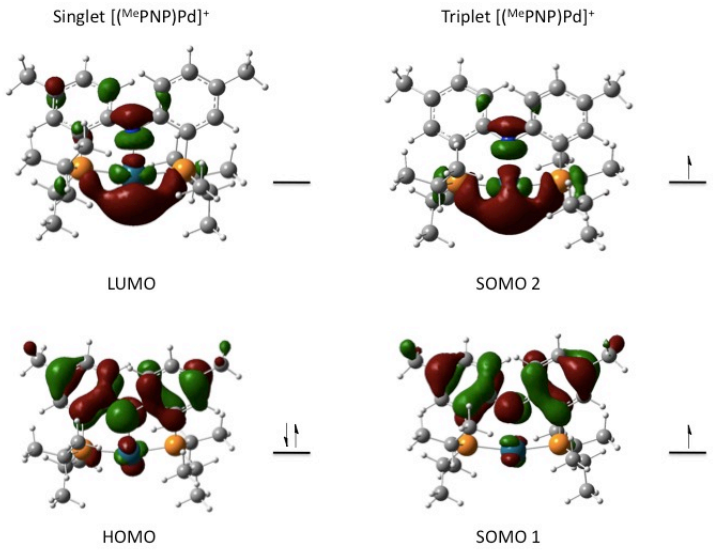

Figure 4.2 Frontier molecular orbitals of singlet and triplet $[(PNP)Pd]^+$ cation.

The results of these calculations (computational details: MPW1PW91/BS2: SDD+ECP (Pd); 6-311+g(d,p)(N,P); 6-31g(d) (C); 6-31g (H)) and the analogous Pt calculations (Functionals used: PBE1PBE (also known as PBE0)[245] and M06-L5,[246] The basis sets used: Def2-QZVPP (with the corresponding ECP) for Pt, 6-311+G(2df) for the N, F, and P atoms, and 6-31+G(d,p) for all other atoms with Gaussian 04)[65,71,247] determined that in a three-coordinate $[(PNP)Pd]^+$ cation, the metal-based LUMO (x^2-y^2) drops in energy

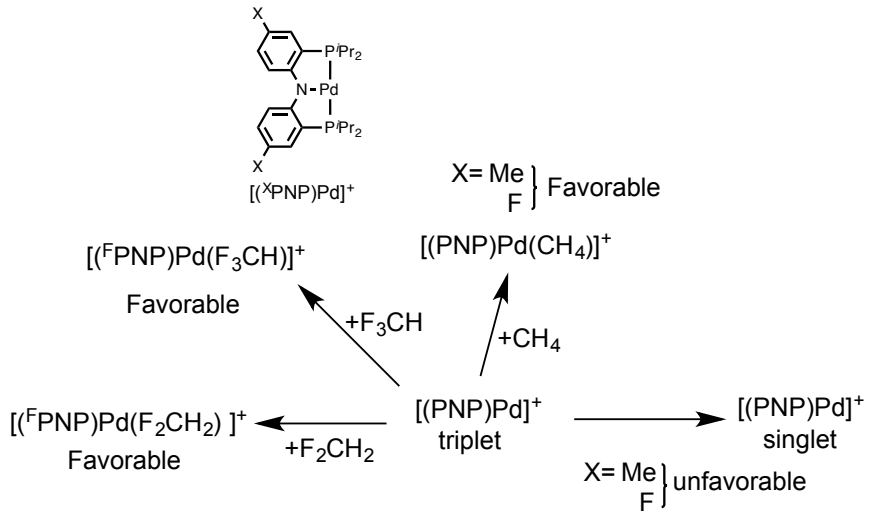

Scheme 4.4 Favorability of Lewis base coordination to $[(PNP)Pd]^+$ cation.

relative to the HOMO; compared to a four-coordinate PNP)PdX complex (**Figure 4.1** and **4.2**). This occurs because the diarylamido in PNP is a weak *trans*-influence ligand that lowers the energy of the *trans* empty orbital. The drop in energy of the LUMO $d(x^2-y^2)$ decreases the HOMO-LUMO gap enough to give access to a low-lying triplet state (akin to a high-spin metal complex). DFT calculations performed on $[(^{X}PNP)Pd]^+$ (X = Me, F and CF_3) determined that when X = Me, F and CF_3 the triplet and the singlet species are relatively close in energy. In addition, DFT calculations also predict that coordination of ligands, even as poor as CH_4 and CF_2H_2, is thermodynamically favorable with respect to the three-coordinate, triplet $[(PNP^{iPr})Pd]^+$ cation. Therefore, Lewis bases such as arenes, ethers, nitriles etc. are likely to form Lewis acid/base adducts with the $[(PNP^{iPr})Pd]^+$ cation, and thus prevent formation of the triplet state (**Scheme 4.4**).

4.2.3 Comparison of calculated three-coordinate [(PNP)Pd]$^+$ cation to Hartwig's three-coordinate complex

As discussed in Chapter I, there are several examples of three-coordinate, Pd(II) and Pt(II) complexes reported in the literature.[18,23-28] However, the closest analog to the calculated three-coordinate [(^{F}PNP^{iPr})Pd]$^+$ cation (**4-5**) is likely Hartwig's example of a 14-electron, three-coordinate species (**1-64**; **Figure 4.3**).[28] When comparing these two

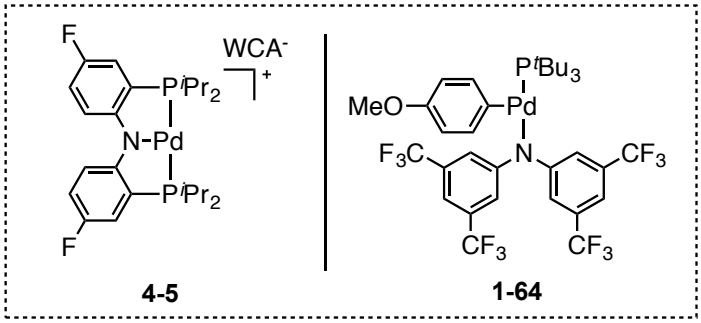

Figure 4.3 Calculated three-coordinate [(PNP)Pd]$^+$ cation (left); Hartwig's three coordinate species (**1-64**).

complexes, there are several differences that must be taken into consideration. The most obvious difference between **4-5** and **1-64** is the charge. **1-64** contains one L-type type ligand (P^tBu_3) and two X-type ligands (diarylamido and aryl), making an overall neutral Pd(II) complex. In contrast, **4-5** is a Pd(II) species with two L-type ligands, one inner-sphere X-type ligand and one non-coordinating X-type ligand making an overall cationic complex. As such, a truly three-coordinate [(PNP)Pd]$^+$ cation would require the use of a weakly-coordinating anion (see Section 4.2.4).

The anion's degree of "non-coordination" will greatly influence the ability to isolate a stable three-coordinate $[(PNP)Pd]^+$ complex (see Section 4.2.4). Whether or not the anion coordinates depends on both the WCA and the nature of the cation. Factors such as the sterics and electronics of the cation ultimately determine whether or not the anion will coordinate to the metal center. Another important difference is that **1-64** contains bulky ligands such as P^tBu_3 and $N(3,5\text{-}(CF_3)_2C_6H_3)_2$ which help prevent formation of dimers or solvent adducts. In contrast, the isopropyl groups in **4-5** are not as bulky. However, as discussed in Chapter II, the sterics around the metal center in $(^FPNP^R)PdX$ complexes can be tweaked by varying the substituent R on the phosphine with substituents such as Et, Ph, ^{i}Pr, ^{t}Bu, and adamantyl (Ad). The ^{t}Bu and Ad substituents are significantly bulkier than ^{i}Pr and can dramatically change the coordination environment around the metal center.

Although the basicity of the anion, and the sterics of the ligand are both critical factors in determining the structure of the cation, a third factor is the ligand *trans* to the empty site. Compared to the aryl ligand in **1-64**, the diarylamido moiety on **4-5** is a weak *trans*-influence ligand, and the nitrogen is electronegative (vs. carbon). A strong *trans*-influence ligand, as the name implies, weakens the bond *trans* to it. Therefore, a strong *trans*-influence ligand should favor formation of a three-coordinate species; whereas a weak *trans*-influence ligand will destabilize a three-coordinate species.

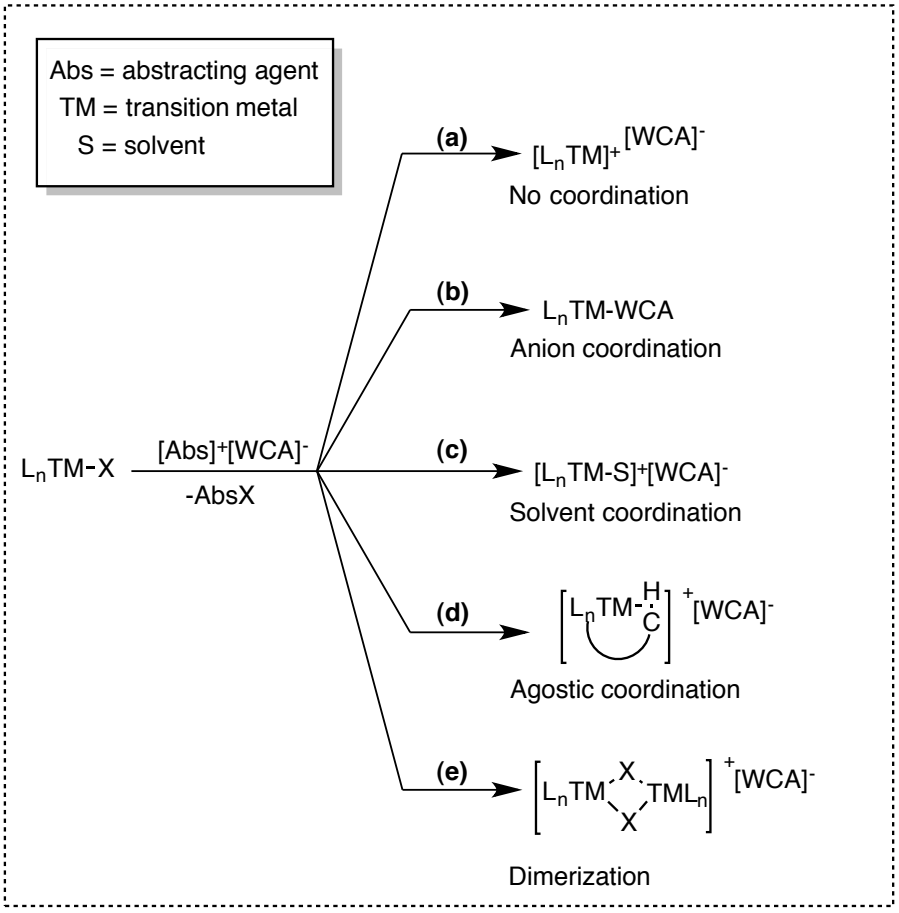

Scheme 4.5 Possible products of anion abstraction from L_nTM-X.

4.2.4 Weakly-coordinating anions and solvents

Scheme 4.5 illustrates the different possible outcomes when abstracting an anion (X) from a transition metal complex (L_nTM-X). The first possibility is that the product is an unsaturated complex and no adducts are formed (**a**). However, there are four other possible outcomes form this reaction. The WCA itself can coordinate to the metal center (**b**), the solvent forms an adduct to the metal center (**c**), an agostic interaction may form (**d**), or the product may dimerize (**e**). As discussed in Chapter I, the formation of dimers

is controlled by the sterics of the supporting ligands. In addition, formation of agostic interactions is a factor that is controlled by the accessibility of the C-H bonds to the metal center.

Whether the anion coordinates to the metal complex is highly dependent on the anion's degree of "weakly-coordinating" character. Weakly-coordinating anions have been the topic of intense research in the past 40 years.[248-250] Anions such as $[BPh_4]^-$, $[CF_3SO_3]^-$, $[BF_4]^-$, $[ClO_4]^-$, $[AlCl_4]^-$, $[PF_6]^-$ and $[SbF_6]^-$, although considered very poor bases, do not fall into the category of weakly-coordinating anions (WCA).[249,251] More recent examples of WCAs such as $[B_{12}Cl_{12}]$ and $[CRB_{11}X_{11}]$ (**Figure 4.4a-c**),[250,252] fluorinated tetraarylborates (BArFs) (**Figure 4.4d**),[253-255] and perfluorinated alkoxyaluminates ($[Al\{OC(CF_3)_3\}_4]^-$) have been developed (**Figure 4.4e**).[256,257] These anions are much larger and contain more diffuse charges; making them much more weakly coordinating than their predecessors. Though the basicity of these anions is extremely low,[256,258,259] it is widely accepted that the term "non-coordinating" is not suitable because many of these anions have been shown to coordinate to transition metal complexes.[256] The two most common fluorinated tetraarylborate anions are tetrakis(pentafluorophenyl)borate ($BArF_{20}$) and tetrakis[(3,5-trifluoromethyl)phenyl] borate ($BArF_{24}$) (**Figure 4.4d**).[254,255,260,261] These WCAs are significantly more weakly-coordinating, and stable than their non-fluorinated $[BPh_4]^-$ anion counterparts,[262] but do decompose under Bronsted/Lewis acidic conditions. For example, $[H(OEt_2)_2]^+[BArF_{24}]^-$ slowly decomposes producing BAr_3 (Ar = 3,5-$C_6H_3(CF_3)_2$) and *m*-$C_6H_4(CF_3)_2$.[262]

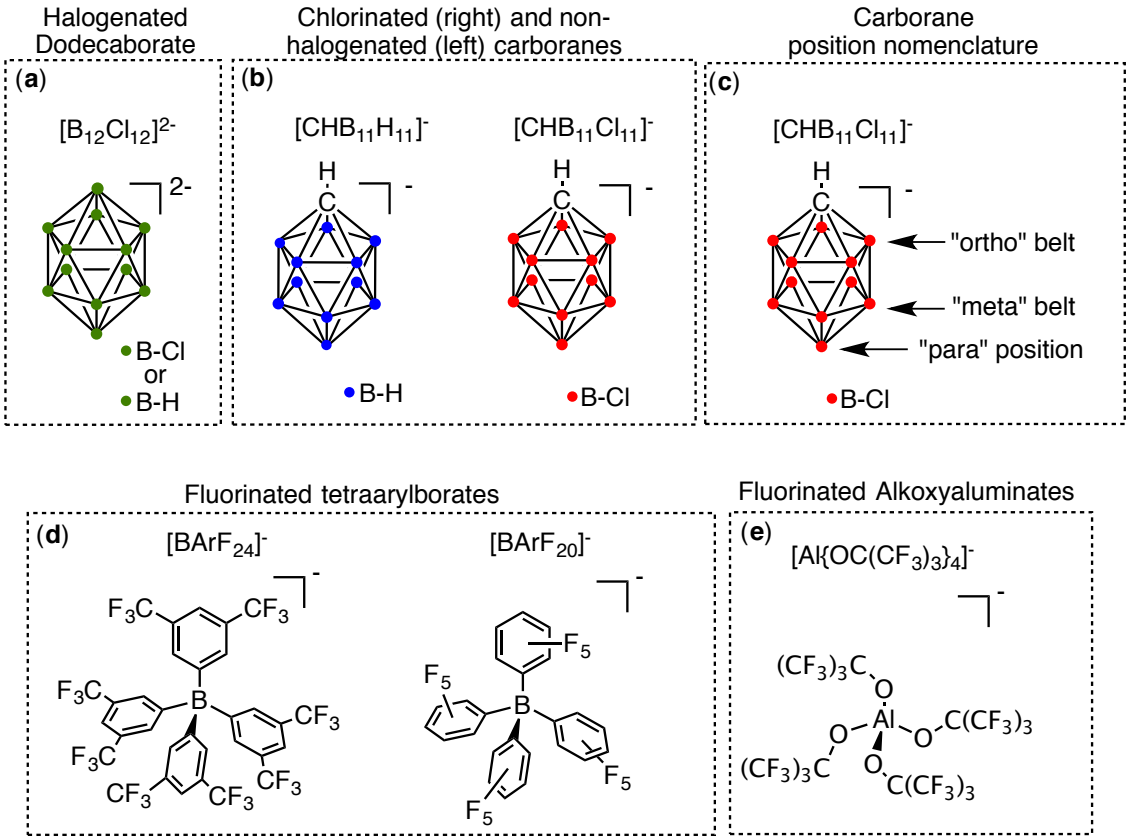

Figure 4.4 Examples of weakly coordinating anions (WCAs).

In addition, because $BArF_{24}$ contains C(sp3)-F bonds, the silylium salts with these anions readily decompose.[254,255] Even when $BArF_{20}$ (which contains only sp^2 type C-F bonds) is used, decomposition still occurs over prolonged periods of time.[263] These anions are very lipophilic, and are useful phase transfer agents.[255,264] Unfortunately, the higher solubility and the poorer ability to form lattices make growing X-ray quality crystals of cationic organometallic complexes less favorable. In contrast, $[B_{12}H_{12}]^-$ and $[CHB_{11}H_{11}]^-$ (**Figure 4.4a,b**), and their halogenated analogs, $[B_{12}X_{12}]^-$ and $[CHB_{11}X_{11}]^-$

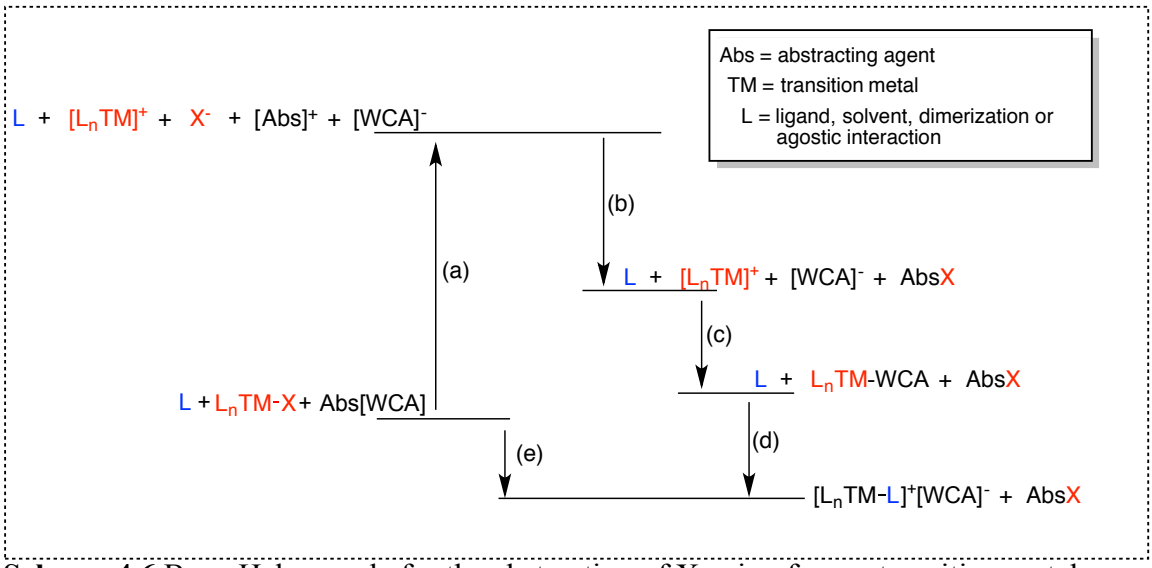

Scheme 4.6 Born-Haber cycle for the abstraction of X anion from a transition metal complex (L_nTM-X) in the presence of a Lewis basic solvent.

(X = Cl, Br) are known to be less soluble and more crystalline than the BArF anions.

This family of halogenated carborane anions are more weakly coordinating, and resistant towards oxidation (vs. $[B_{12}H_{12}]^-$ and $[CHB_{11}H_{11}]^-$),[252] and have been used to stabilize highly electrophilic cations.[250,258,259,265] Unfortunately, these anions are not commercially available, and their non-halogenated precursors are relatively expensive. For the sake of clarity in later sections of this chapter, the nomenclature for the different positions ("*ortho*" belt, "*meta*" belt and the "*para*") on the carborane is illustrated in **Figure 4.4c**. Perfluorinated alkoxyaluminates ($[Al\{OC(CF_3)_3\}_4]^-$; **Figure 4.4e**) is another class of anions that has received considerable attention in the field of WCAs.[256,257] These anions have the advantage over carboranes and BArFs that they are easily synthesized in large scale from commercially available precursors.[257] The synthesis, although not devoid of potential hazards, does not require the use of relatively

dangerous precursors that can be potentially explosive (i.e. fluorinated aryllithium) or toxic.[254] Despite their utility, the reactivity of these anions is not explored in this dissertation. The main reason why our group has not adopted these anions is because, like $BArF_{24}$, the corresponding silylium salts cannot be synthesized; these anions contain $C(sp^3)$-F bonds that are susceptible to the highly fluorophilic silylium cation.[257]

The basicity of the solvent also plays a critical role in the stability of highly unsaturated species and the favorability of the abstraction of X from L_nTMX. Although abstraction may take place, the generated product will not always be an unsaturated species and as illustrated in **Scheme 4.5c**, abstraction of X from L_nTM-X can also generate a solvent adduct ($[L_nTM\text{-}S]^+[WCA]^-$). If this is the case, the solvent's basicity can be a key factor in determining the favorability of abstracting X from L_nTM-X. As illustrated by the Born-Haber cycle in **Scheme 4.6**, the higher the Lewis basicity of L the more favorable Step d will be, and as a result the overall abstraction of X from L_nTM-X will be more favorable (Step e). Solvents that contain free lone pairs such as THF are known to form strong adducts with transition metal complexes making the ΔG for Step d more favorable. However, solvents such as toluene and benzene that do not contain obvious free electron lone pairs are significantly less basic, and are therefore weaker ligands to transition metal complexes (ΔG for Step d less negative). However, polar solvents with lone pairs such as bromobenzene and fluorobenzene are necessary to solubilize the resulting cationic species. Fluorobenzene is a good solvent because it is sufficiently polar to solubilize the cationic complexes, but the lone pairs on the fluorine substituent are very weak bases and therefore poor ligands. Even then aromatic solvents

do not have obvious lone pairs, they do contain unsaturated bonds that can serve as ligands to transition metal complexes.[266-273] Solvents such as C_6H_5Br and *o*-$C_6H_4Br_2$ are likely better ligands than toluene and fluorobenzene because the lone pairs on bromine are much more readily accessible.[274] Alkanes, on the other hand, are extremely poor ligands to transition metals; however, alkanes are also extremely poor solvents for cationic complexes. The best solvent is one that is polar enough to be able to solubilize the cationic complex, but at the same time does not contain strongly Lewis basic sites. For the purpose of the $[(PNP^{iPr})Pd(L)]^+$ cations the best solvents appear to be benzene, fluorobenzene and toluene. However, as will discussed later in this chapter these solvents still form adducts to $[(PNP^{iPr})Pd]^+$ cations. In summary, the degree Lewis basicity of both the solvent and the anion plays a critical role in the ability to abstract X from L_nTM-X (see **Scheme 4.6**). The more coordinating the solvent (or anion) the more favorable the abstraction of X from L_nTM-X is. Furthermore, abstraction of X to an empty site is even less favorable. When WCAs such as BArFs or $[CHB_{11}Cl_{11}]$ are used the basicity of the solvent becomes a more dominant factor in the ability to abstract X.

4.2.5 Reagents for anion abstraction

Halide and pseudo halide anions abstracting agents. Scheme 4.7 illustrates the reagents that can be used for the abstraction of different X-type (**a-e**) and L-type ligands (**f**) from transition metals. Each type of ligand be it halide, pseudo halide, hydride, alkyl or neutral ligand requires a specific type of abstracting agent. This section

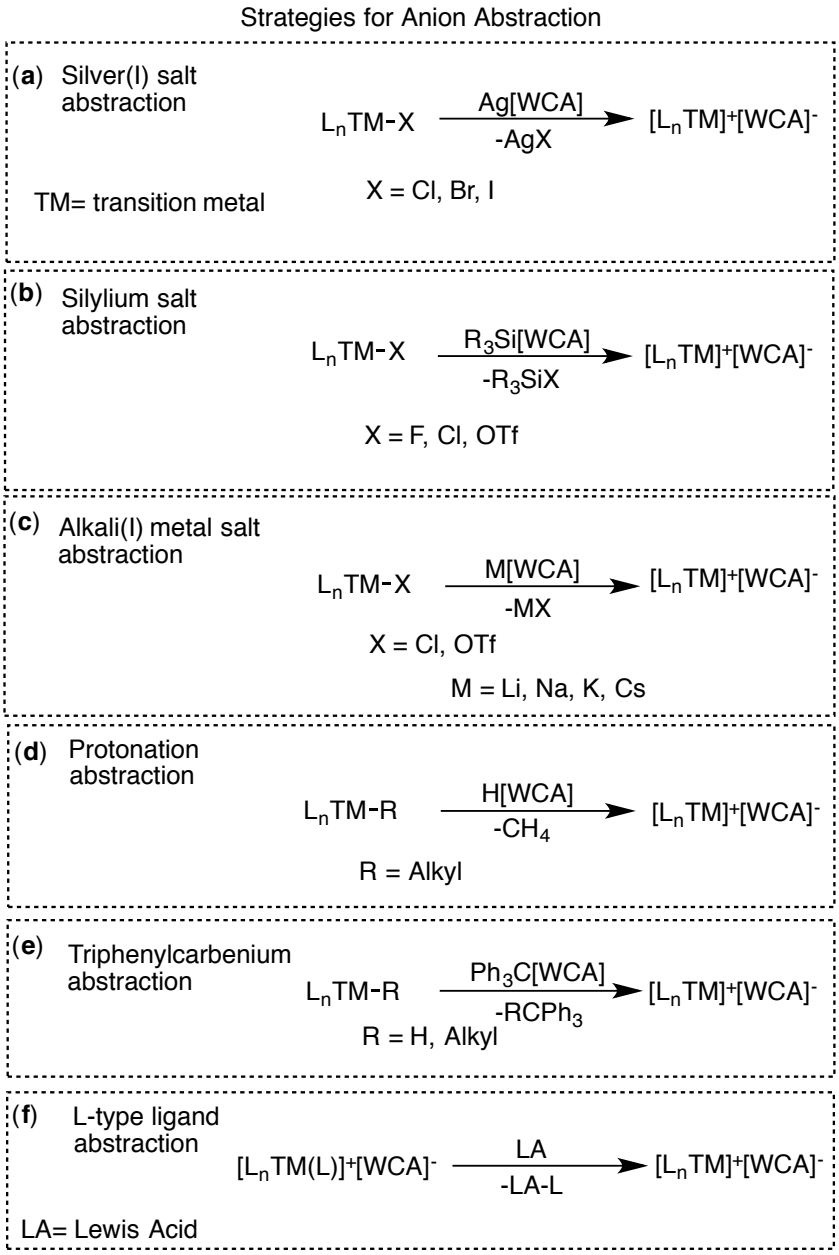

Scheme 4.7 Anion abstracting agents; silver(I) salts (a); silylium salts (b); alkali(I) metal salts (c); proton abstraction(d); triphenylcarbenium abstraction (e); L-type ligand abstraction (f).

will discuss the use of different types of abstracting agents and ligands from transition metal complexes.

Although abstraction of neutral ligands is not very common (**f**), the use of dehydrating agents such as molecular sieves to absorb water in non-polar solvents is widely known.[275,276] Such a technique can potentially be used to remove water from a metal complex. In addition, reagents such as 9-BBN have also been used to abstract phosphines from transition metal complexes.[277] However, these techniques are dependent on the L ligand being able to dissociate from the metal center.

Silver(I) salt metathesis has historically been the preferred method to abstract Cl, Br and I anions from organometallic complexes.[278] Even as early as 1973 silver(I) salts were already being used abstract chloride anions.[279] Silver(I) salts with anions such as $[CF_3SO_3]^-$, $[BF_4]^-$, $[ClO_4]^-$, $[AlCl_4]^-$, $[PF_6]^-$ and $[SbF_6]^-$ are able to abstract halide anions. However, when silver salts are used in combination with more WCAs (in weakly-coordinating solvents) halide abstraction becomes less favorable. This is due to the fact that anion coordination (Step c) and solvent coordination (Step d) become less thermodynamically favorable, and reduce the overall favorability of abstraction (Step 3, **Scheme 4.6**). For example, in 1989 Reed and coworkers reported that addition of $Ag[CHB_{11}H_{11}]$ (**4-6**) to **1-1** does not abstract Cl, and instead generates a product with an Ag-Ir bond (**4-7**).[280] In addition, silver(I) cations can also function as one-electron oxidants, which in some cases can be competitive with halide anion abstraction.[281] In contrast, thallium and lighter alkali metal cations have the advantage that they do not function as oxidants.[282,283] However, thallium salts are known to be highly toxic, and are

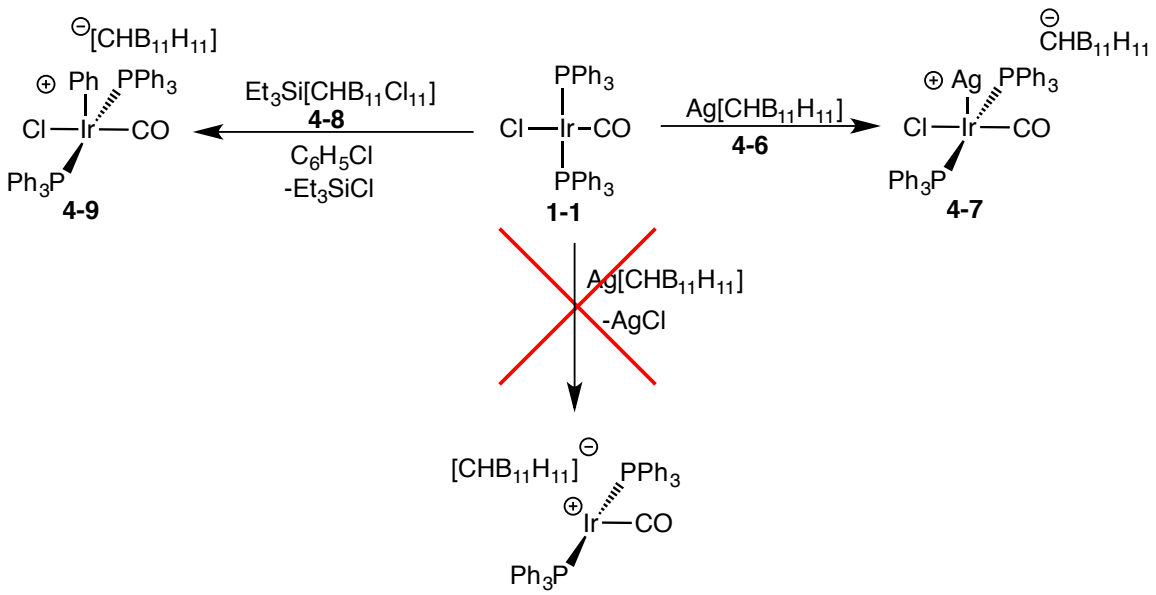

Scheme 4.8 Reactivity of Vaska's complexes with **4-6** and **4-8**.

therefore less appealing as abstracting reagents.[284] Alkali metal cations, in combination with weakly-coordinating anions (i.e. $Na[BArF_{20}]$) are commonly used in organometallic chemistry to abstract halides and pseudo halides.[262,285-287] In addition, these salts are quite useful because they can be used to make other useful reagents such as triphenylcarbenenium salts (e.g. $Ph_3C[BArF_{20}]$)[288] and $[H(OEt_2)_2]^+[BArF_{24}]^-$).[262]

Silyl reagents such as Me_3SiOTf have been used in organometallic chemistry to exchange ligands such as acetate and halides for triflate (^-OTf), a more weakly-coordinating ion.[289] Less prevalent in the field of organometallic chemistry is the use of silylium in combination with weakly-coordinating anions such as $[BAr^F_4]^-$ or carboranes.[280,290] In contrast to Ag(I) salts, silylium salts are powerful, non-redox active, halide and pseudohalide abstracting agents,[250] and are therefore ideal candidates for the abstraction of anions such as triflate. Silylium salts have been shown to be capable of abstracting chloride from organometallic complexes when traditional halide abstracting

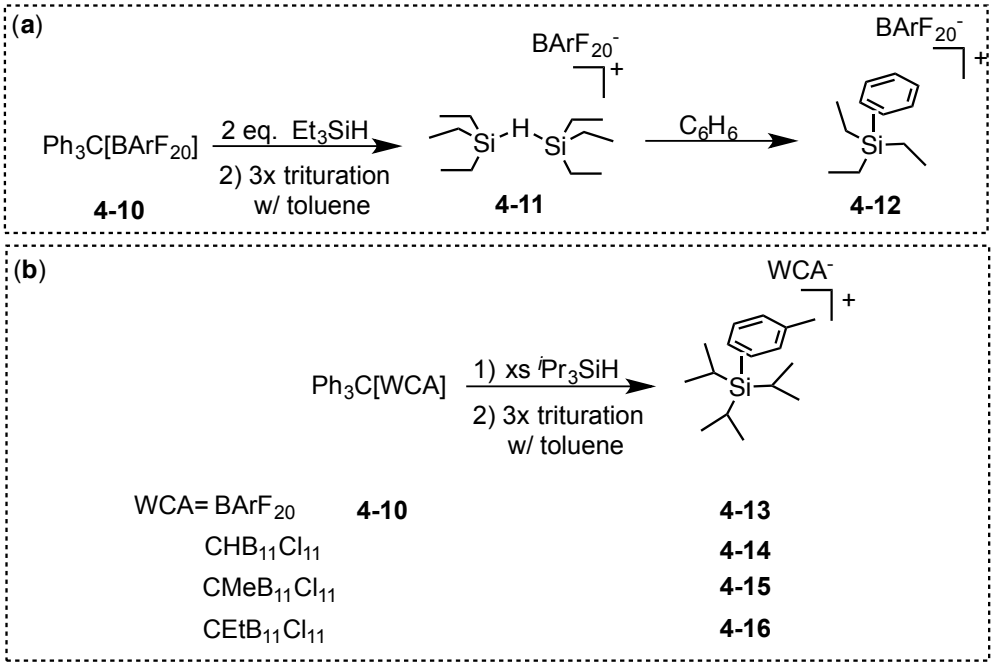

Scheme 4.9 Synthesis of silylium salts (**4-[12-16]**).

agents such as silver(I) salts fail. As illustrated in **Scheme 4.8**, **4-6** is not capable of abstracting chloride from Vaska's complex (**1-1**). However, $Et_3Si[CHB_{11}Cl_{11}]$ (**4-8**) cleanly abstracts chloride from **1-1** to produce **4-9** with concomitant formation of Et_3SiCl.[280]

Silylium salts ($R_3Si[WCA]$) can be synthesized by treating $Ph_3C[WCA]$ with excess silane. In 2011, Reed et al. reported that triethylsilyl perfluorotetraarylborate ($[BArF_{20}]^-$), a reagent widely used in the literature, can be synthesized by treating $Ph_3C[BArF_{20}]$ with excess Et_3SiH. To fully convert $Ph_3C[BArF_{20}]$ (**4-10**) into silylium at least 2 equivalents of Et_3SiH must be used, but the product formed is $[Et_3Si\text{-}H\text{-}SiEt_3]^+[BArF_{20}]^-$ (**4-11**), and not "$[Et_3Si]^+[BArF_{20}]^-$".[290] In the presence of solvents, even as weakly coordinating as benzene, Et_3SiH is displaced from **4-11**, producing

$[Et_3Si(C_6H_6)]^+[BArF_{20}]^-$ (**4-12; Scheme 4.9**). Removal of the volatiles under vacuum induces the decomposition of $[BArF_{20}]^-$; in the absence of a stabilizing ligand such as silane or arene the $[BArF_{20}]^-$ anion decomposes.[290] In addition, silylium salts with $BArF_{20}$ anion such as **4-13** are difficult to synthesize in large quantities because over longer periods of time they decompose. In contrast, silylium salts with more robust weakly anions such as $[^iPr_3Si(toluene)][CHB_{11}Cl_{11}]$ (**4-14**),[263] do not decompose upon removal of the volatiles and can be stored without decomposition for longer periods of time. For the purposes of generating highly unsaturated species, such as a three-coordinate $[(^FPNP^{iPr})Pd]^+$ cation, it is important to avoid potential ligands such as silanes.[291] Therefore, a silylium salt with as weak a base as possible coordinated to the silicon center was necessary. Arenes, typically considered very poor Lewis bases are likely the best option to generate these unsaturated species. In 2006, Reed and coworkers reported the synthesis of silylium salts with adducts such as SO_2 and *ortho*-dichlorobenzene (ODCB).[263]

In addition to **4-13** and **4-14**, the Ozerov group has developed protocols for the synthesis of silylium salts with alkylated carboranes. Initially $[Me_3NH]^+[CMeB_{11}Cl_{11}]^-$ was synthesized using a modified version of the procedure used to alkylate $[CHB_{11}F_{11}]^-$.[292] This procedure involves the use of a 5% NaOH solution in combination with Me_2SO_4 as the alkylating agent. However, in 2012 Ramirez et al. reported a simple protocol for the alkylation of $[CHB_{11}Cl_{11}]^-$ using common reagents like KO^{t}Bu and alkyl iodides.[293] Using this procedure, $[Me_3NH]^+[CRB_{11}Cl_{11}]^-$ (R = Me, Et and ^{n}Bu) could be made in good yields. In addition to increasing the steric bulk of the carborane cage,

alkylation has the added benefit of increasing the solubility of the anions. Trityl and silylium salts $[^{i}Pr_3Si(toluene)]^{+}[CRB_{11}Cl_{11}]^{-}$; R = Me (**4-15**), R = Et (**4-16**) with alkylated carboranes can be made using a procedure analogous to that reported for the synthesis of **4-10** and **4-12**.[288,294]

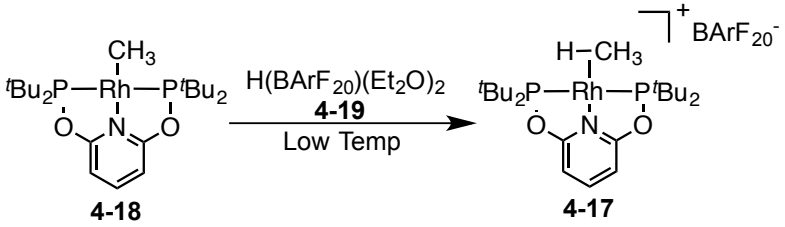

4-18 **4-17**

Scheme 4.10 Synthesis of rhodium-methane complex **4-17**.

Abstraction of alkyls and hydrides from (^{F}PNP^{iPr})PdX (X = H, Me). As illustrated in Scheme 4.7e, alkyl and hydride ligands can be abstracted using triphenylcarbenium salts.[295] However, like silver(I) salts, triphenylcarbenium cations can also function as a one-electron oxidants, generating Gomberg's dimer as a byproduct.[281] Another strategy for the abstraction of transition metal alkyls involves the protonation of the alkyl with a strong acid in combination with a weakly-coordinating anion (H[WCA]). The byproduct of this reaction is an alkane, which is a poor ligand for transition metals. This makes this technique ideal for abstraction because the byproduct readily dissociates and if lighter alkanes such as methane are produced they can be easily removed under vacuum.

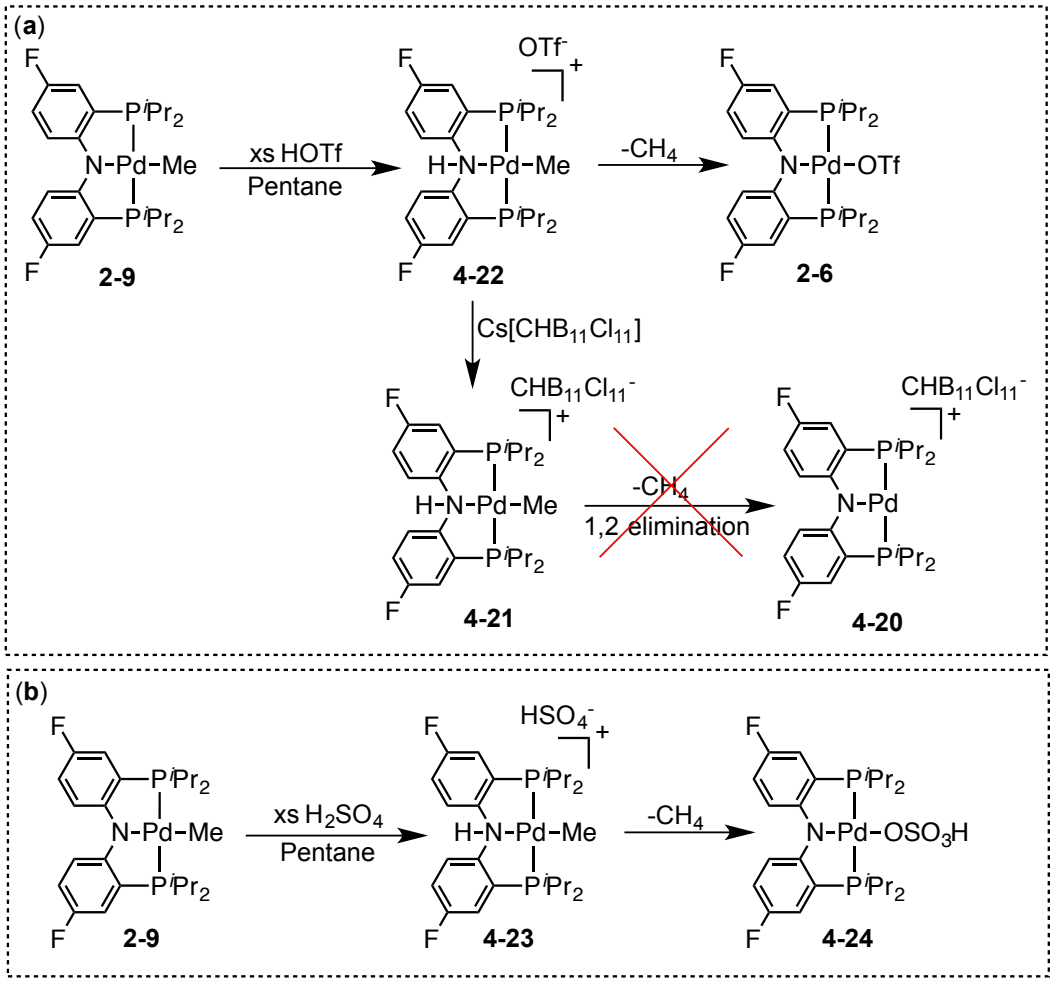

Scheme 4.11 Synthesis of **4-21, 4-22** and **4-24**.

This technique was applied by Brookhart and Goldberg towards the synthesis and characterization of a Rh(I) methane complex.[160] The authors synthesized $[(PONOP)Rh(CH_4)]^+[BArF_{20}]^-$ (**4-17**) via protonation of $(PONOP)RhCH_3$ (**4-18**) with $H(BArF_{24})\bullet(Et_2O)_2$ (**4-19**) (**Scheme 4.10**). The resulting methane complex is stable enough to be observed at low temperatures; at room temperature the product readily eliminates methane and binds solvent. Although the intent of the authors was not to

generate an unsaturated complex, and the final product (upon release of methane) appears to be a solvent adduct, it is reasonable that under the right conditions (i.e. solvent and acid precursor) an unsaturated complex could be generated using this technique.

4.2.6 Reactivity of (PNP)PdX complexes with anion abstracting agents

Attempted synthesis of $[(PNP)Pd(L)]^+$ cation via protonation of ($^{F}PNP^{iPr}$)Pd-Me. We surmised that the protonation technique could be applied towards the isolation of a three-coordinate $[(^{F}PNP^{iPr})Pd]^+[CHB_{11}Cl_{11}]^-$ (**4-20**) cation by protonation of **2-9**. Compound **2-9** could be protonated with $H^+[CHB_{11}Cl_{11}]^-$ to produce **4-21**. However, the synthesis of $H^+[CHB_{11}Cl_{11}]^-$ is relatively long and synthetically inconvenient. To avoid this, **4-21** was synthesized via protonation of **2-9** with triflic acid (HOTf) a commercially available acids (**Scheme 4.11a**). The reaction between triflic acid, and **2-9** produces $[(PN(H)P)PdMe]^+[OTf]^-$ (**4-22**) which undergoes 1,2-elimination of methane to generate **2-6**. However, at lower temperatures formation of **2-6** occurs at a significantly slower rate, allowing **4-22** to be isolated as a relatively clean product. The analogous reaction between **2-9** and H_2SO_4 aq. produces what is tentatively assigned to ($^{F}PNP^{iPr}$)PdOSO_3H (**4-24**), with concomitant formation of methane. The OSO_3H proton in **4-24** resonates at 11.5 ppm consistent with formulation shown in **Scheme 4.11b**. In addition to NMR spectroscopy, **4-22** was also characterized by single-crystal X-ray crystallography. With the exception of the tetrahedral environment around the N, the structure of **4-22** is unremarkable. The Pd-C bond in **4-22** (2.064(6) Å) is statistically equivalent to the

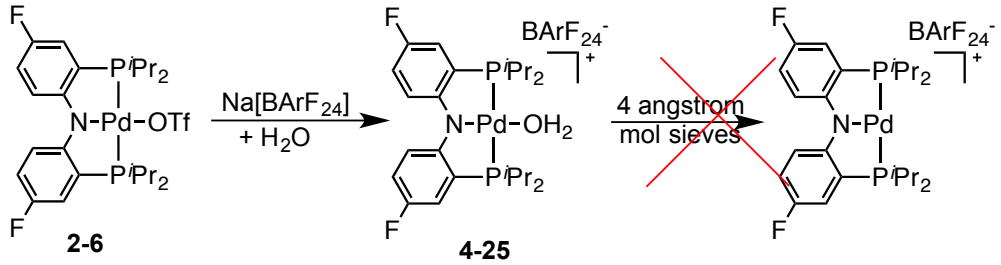

Scheme 4.12 Attempted abstraction of H_2O from **4-25** with 4 Å molecular sieves.

observed Pd-C in **2-9** (2.061(2) Å).[8]

Consistent with the amine formulation in **4-22**, the Pd1−N1 bond distance (2.182(5) Å) is considerably longer that what is observed in **2-9** (2.094(4) Å) (**Figure 4.5**). In addition, the distance between the amine proton, and the closest oxygen on the triflate is 2.671 Å, consistent with hydrogen bonding between the triflate anion, and the proton on the amine.[67] The outer sphere triflate anion in compound **4-22** can then be easily exchanged for $[CHB_{11}Cl_{11}]^-$ via salt metathesis with $Cs[CHB_{11}Cl_{11}]$ to produce **4-21**. However, unlike the triflate analog, **4-21** does not undergo 1,2-elimination of methane in weakly-coordinating solvents. It is not clear whether **4-21** is the thermodynamically favored product, or if 1,2-elimination is simply kinetically inaccessible. It is possible that 1,2-elimination requires a Bronsted base to "shuttle" the proton from the amine to the methyl.

As discussed above, one of the strategies to generate the $[(PNP)Pd]^+$ cation involves the dissociation of a labile ligand (L) from $[(PNP)Pd(L)]^+$. Unfortunately, when $[(^{F}PNP^{iPr})Pd(OH_2)]^+[BArF_{24}]^-$ (**4-25**) is placed in molecular sieves no change is

observed by NMR spectroscopy (**Scheme 4.12**). It is likely that dissociation of H_2O from $[(^{F}PNP^{iPr})Pd]^{+}$ is not favorable enough to allow removal with molecular sieves.

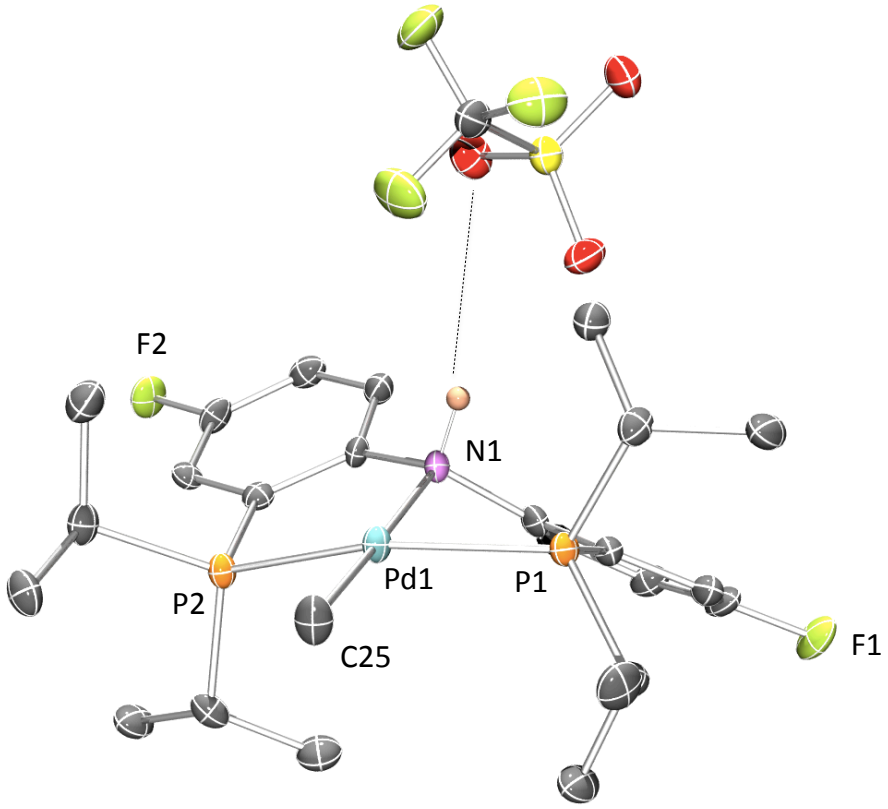

Figure 4.5 POV-Ray rendition of the ORTEP[162] drawing (50% thermal ellipsoids) of **4-22** showing selected atom labeling. Hydrogen atoms (except N-H) were omitted for clarity. Selected bond distances (Å) and angles (deg): Pd1-C25 2.064(6); Pd1−P1, 2.2779(16); Pd1−P2, 2.3035(17); Pd1−N1, 2.182(5); N1-O1, 3.537(5); NH1-O1 2.870(3); P1−Pd1−P2, 160.21(6).

Reactivity of (^{F}PNP^{iPr})PdCl/H with silver and triphenylcarbenium salts. As discussed in Section 4.2.5 both silver and trityl salts are capable of abstracting halides and hydrides respectively. However, attempts to abstract a chloride anion from **2-4** using **4-6**, and hydride from **2-7** with $Ph_3C[CHB_{11}Cl_{11}]$ (**4-26**) were unsuccessful due to the PNP ligand's redox non-innocence.[60] Instead of abstracting chloride or hydride from **2-4**

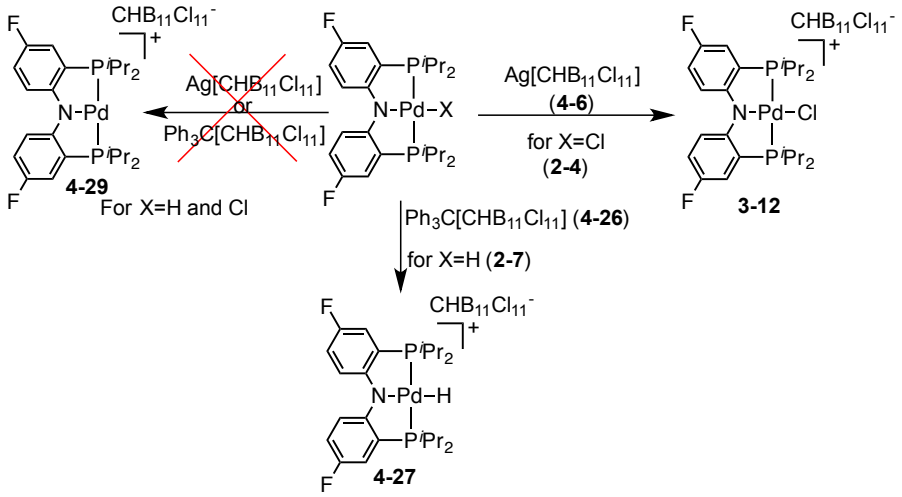

Scheme 4.13 Chemical oxidation of **2-4** and **2-7** with silver and trityl cations.

and **2-7** both silver(I) and triphenylcarbenium cations function as oxidants, respectively. Addition of **4-6** to **2-4** produces **3-12**, and the reaction between **4-26** and **2-7** is believed to produce $[(^{F}PNP^{iPr})PdH]^{+}[CHB_{11}Cl_{11}]^{-}$ (**4-27**) (**Scheme 4.13**).[173] It is not clear if **4-27** is the thermodynamically favorable product, and Pd-H is simply not hydridic enough for abstraction with trityl or if hydride abstraction is simply kinetically less favorable than oxidation.

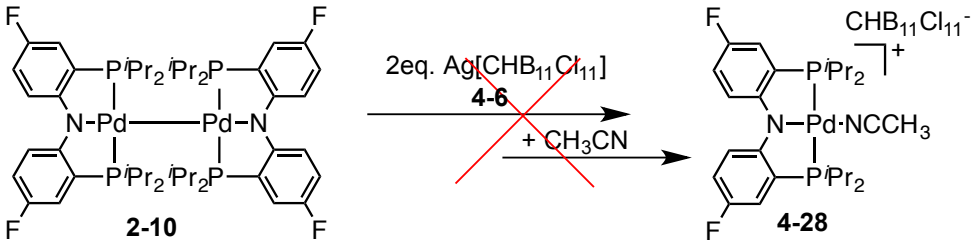

Scheme 4.14 Chemical oxidation of **2-10** with **4-6**.

Based on the observed reactivity of silver and trityl salts towards **2-4** and **2-7**, we hypothesized that our target three-coordinate [(^{F}PNP)Pd]$^+$ cation could potentially be generated via a two electron oxidation of **2-10**. By taking advantage of the redox non-innocence of the PNP ligand, the problem of abstraction of X^- could be circumvented. Oxidation of **2-10** would theoretically cleave the Pd-Pd bond by removal of the two electrons involved in bonding and generate [(^{F}PNP)Pd]$^+$. However, oxidation of **2-10** with **4-6** followed by addition of acetonitrile did not yield the expected acetonitrile adduct [(^{F}PNP^{iPr})PdNCMe]$^+$[CHB$_{11}$Cl$_{11}$]$^-$ **(4-28)**, indicating that (^{F}PNP^{iPr})Pd [CHB$_{11}$Cl$_{11}$] is not formed (**4-29**; **Scheme 4.14**).

Reactivity of (^{F}PNP^{iPr})PdX (X = OTf and F) with silylium salts. Addition of ^{i}Pr$_3$Si[CRB$_{11}$Cl$_{11}$] (R = H (**4-14**), Me (**4-15**), Et (**4-16**) to **2-6** evinces an immediate color change from purple to green (**Scheme 4.15**). The color change is accompanied by a disappearance of the ^{19}F, ^{31}P and ^{1}H NMR ligand signals and the formation of ^{i}Pr$_3$SiOTf, presumably generating **4-29**, **4-30** and **4-31**, respectively. Addition of THF produces a color change from green to blue and reemergence of the ^{19}F, ^{31}P and ^{1}H NMR signals of

the THF adduct (**4-32**).[173] Analogously, the reaction between **2-28** and **4-15** produces a green NMR silent solution with concomitant formation of $^{i}Pr_3SiF$ suggesting that **4-30** is formed. Surprisingly, single-crystal X-ray analysis of **4-29** determined that in the solid state, $[CHB_{11}Cl_{11}]^-$ coordinates to the metal centre through an "*ortho*" belt chloride.[173] This result is inconsistent with the Evans method magnetic susceptibility measurements made by Dr. Claudia Fafard,[173] and the apparent silence by NMR spectroscopy; a four-coordinate complex such as ($^{F}PNP^{iPr}$)Pd[κ^1-Cl-$CHB_{11}Cl_{10}$] (**4-29a**) should be diamagnetic. We surmised that in the solid state, $[CHB_{11}Cl_{11}]^-$ coordinates to Pd and forms a four-coordinate **4-29**a, and in solution $[CHB_{11}Cl_{11}]^-$ is displaced by the aromatic solvent and forms an arene adduct [($^{F}PNP^{iPr}$)Pd(arene)]$^+$[$CHB_{11}Cl_{11}$]$^-$ (**4-29b**). It was therefore conceivable that the use of alkylated carboranes anion could impede coordination of the anion to the metal center. The X-ray structure of ($^{F}PNP^{iPr}$)Pd[κ^1-Cl-$CHB_{11}Cl_{10}$] shows coordination of $[CHB_{11}Cl_{11}]^-$ via the Cl on the "*ortho*" belt, and the CH points towards the isopropyl groups in the (PNP)Pd fragment. The Pd-Cl bond length in **4-29a** (2.4442(9) Å) is comparable to other reported complexes such as Pd(κ^1-Cl-CH_2Cl) (**4-33**; 2.49 Å).[274] We surmised that the reason an "*ortho*" belt chloride preferentially coordinates to Pd is because of the lack steric hindrance on the *ipso* CH. Therefore, using bulkier C-alkylated carboranes can make anion coordination less favorable and allow for characterization by single-crystal X-ray analysis of a [($^{F}PNP^{iPr}$)Pd(arene)]$^+$ complex. Unfortunately, attempts to grow X-ray quality crystals of (($^{F}PNP^{iPr}$)Pd(arene)]$^+$[$CMeB_{11}Cl_{11}$]$^-$ (**4-30b)** using the silylium protocol for abstraction were unsuccessful.

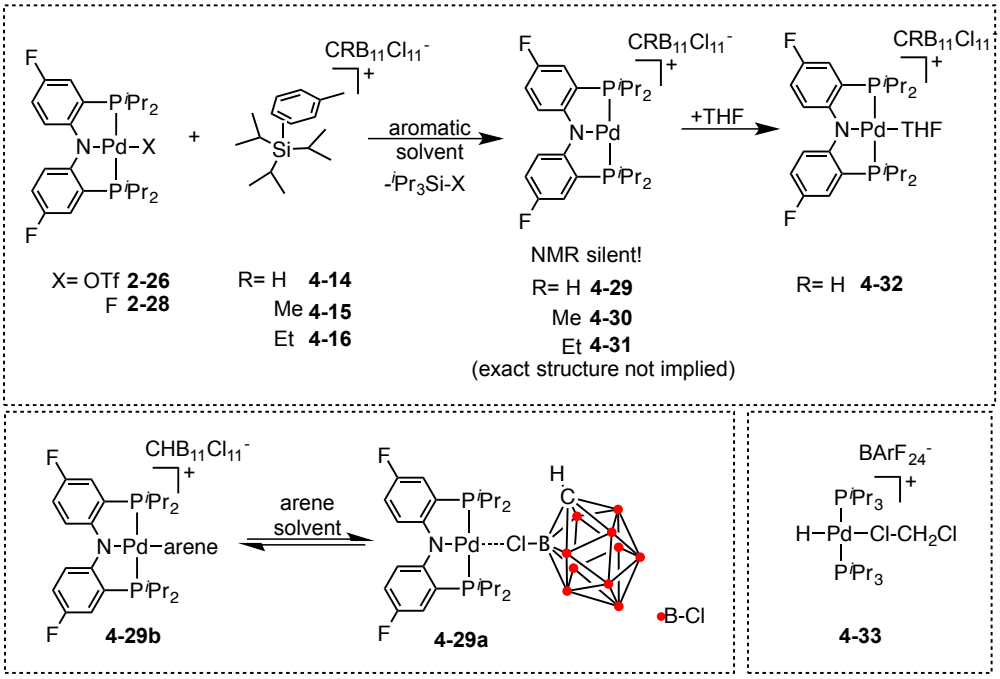

Scheme 4.15 Abstraction of triflate from **2-26** and fluoride from **2-28** with silylium salts with alkylated carboranes.

Reactivity of (^{F}PNP^{iPr})PdX (X = Cl, OTf) with alkali metal salts. Because Na[BArF$_{24}$] (**4-35**) was not capable of fully abstracting chloride from **2-4** (**Scheme 4.16**), we moved to **2-6** as a precursor for the [(^{F}PNP^{iPr})Pd]$^{+}$ cation. Triflate ($CF_3SO_3^-$), a "harder" and more weakly coordinating than chloride, can be more easily abstracted by alkali metals. There are a variety of different weakly-coordinating anions that are commercially available, each with different counter cations: K[BArF$_{20}$] (**4-34**), Na[BArF$_{24}$] (**4-35**) and Cs[CHB$_{11}$H$_{11}$] (**4-36**). Although [CHB$_{11}$Cl$_{11}$]$^-$ is not a commercially available carborane, it is typically isolated as the Cs[CHB$_{11}$Cl$_{11}$] (**4-37**) salt.[252] Therefore, for practical purposes we thought it logical to explore the reactivity of all of the above salts with **2-6**.

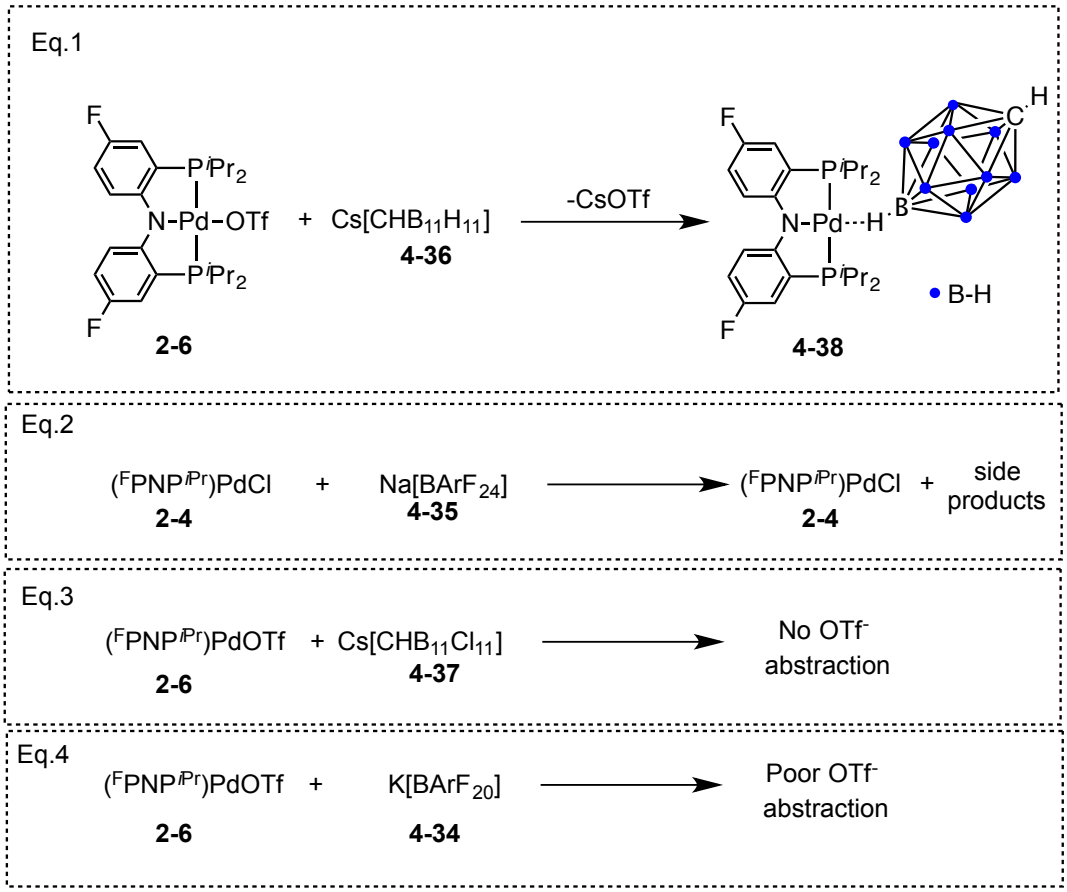

Scheme 4.16 Reaction between **2-4, 2-6** and M[WCA] (**4-34**, **4-35**, **4-36**, **4-37**).

Our group has previously reported the synthesis of ($^{F}PNP^{iPr}$)Pd[$CHB_{11}H_{11}$] (**4-38**) via the reaction of **2-6** with **4-37**. However, single-crystal X-ray analysis of this complex showed that in the solid state, $CHB_{11}H_{11}$ coordinates to the metal through the para B-H fragment of [$CHB_{11}H_{11}$].[67] Unlike **4-29**, **4-38** shows well defined ^{1}H, ^{31}P, and ^{19}F NMR spectra, consistent with a non-fluxional species in solution. In light of the above mentioned reactivity, it is clear that $[CHB_{11}H_{11}]^{-}$ forms a strong adduct to $[(PNP)Pd]^{+}$, and that more weakly-coordinating carborane anions such as $[CHB_{11}Cl_{11}]^{-}$ are necessary.[250] Unfortunately, Cs[$CHB_{11}Cl_{11}$] was not capable of abstracting triflate

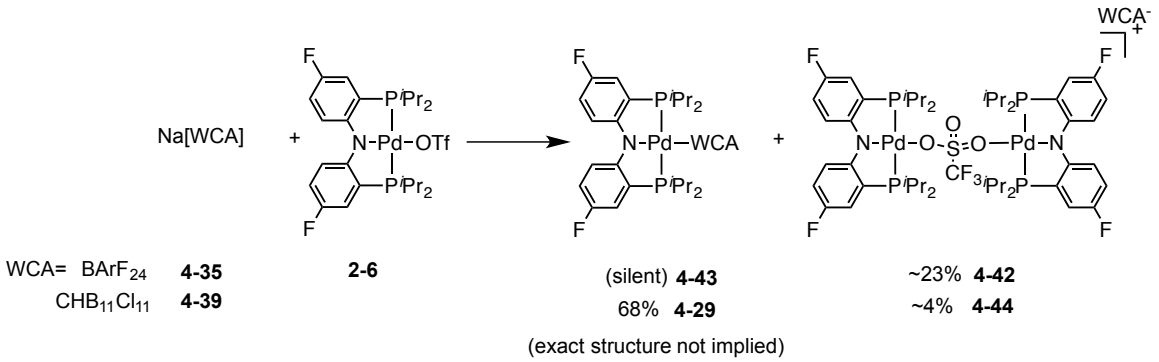

Scheme 4.17 Abstraction of triflate from **2-6** with Na[WCA] (**4-35** and **4-39**).

from **2-6**.[173] We believe that the reason for this is that cesium, a "soft" cation, is not a sufficiently strong triflate abstracting agent. However, sodium and potassium cations are "harder" Lewis acids, and should therefore be a stronger triflate abstracting agent.[296] Addition of a small excess of **4-34** to **2-6** produces a slight color change from purple to blue. The ^{19}F NMR spectrum of the product shows a broad ^{F}PNP^{iPr} signal at −124.0 ppm with a (^{F}PNP^{iPr}):[BArF$_{20}$] ratio of 2:1. In addition, residual triflate signals at −74.8 ppm and −77.6 ppm with a (^{F}PNP^{iPr}):(OTf) ratio of 1:2 and 4:2 respectively (see experimental section). The blue color, the presence of residual [OTf], and the broad (^{F}PNP^{iPr}) ^{19}F NMR signal indicates that **4-34** is not capable of abstracting triflate from **2-6**.

The reactions between **2-6** and Na[WCA] (WCA = [BArF$_{24}$] (**4-35**), [CRB$_{11}$Cl$_{11}$] (R = H (**4-39**), Me (**4-40**), ^{n}Bu (**4-41**))) all yield an immediate color change from purple to green (**Scheme 4.17**). The reaction between **2-6** and **4-35** produces a solution that at first sight appears not to contain ^{19}F or ^{31}P NMR signals pertaining to the (^{F}PNP^{iPr})Pd fragment. However, close inspection of the ^{19}F NMR spectrum reveals two residual

triflate signals at −75.1 and −78.0 ppm in a 2.4:1 ratio. With each residual triflate signal a corresponding ^{F}PNP signal is observed at −124.4 and −125.4 ppm by ^{19}F NMR spectroscopy. The two signals at −75.1 and −124.4 ppm with a 2.4:3.3 ratio are tentatively assigned to [(^{F}PNP$^{i\text{Pr}}$)Pd(μ-OTf)Pd($^{i\text{Pr}}$PNP^{F})]$^{+}$[BArF$_{24}$]$^{-}$ (**4-42**). This is not surprising since there are several examples of μ-triflate Pd complexes reported in the literature.[297-299] The second set of ^{19}F NMR spectroscopic signals at −78.0 and −125.4 ppm are tentatively assigned to **2-6**. To test this hypothesis, the above mixture was treated with substoichiometric portions of **2-6** (see experimental). With each addition of **2-6**, the intensity of the signals at −75.1 and −124.4 ppm increased relative to the signals at −78.0 and −125.4 ppm. Although these experiments clearly demonstrate an incomplete abstraction of triflate from **2-6**, the observed triflate resonance accounts only about 23% of the expected signal intensity with respect to the ^{19}F NMR signals of [BArF$_{24}$]. It is possible that (^{F}PNP$^{i\text{Pr}}$)Pd[BArF$_{24}$] (**4-43)** is not observable by NMR spectroscopy because of intense broadening.

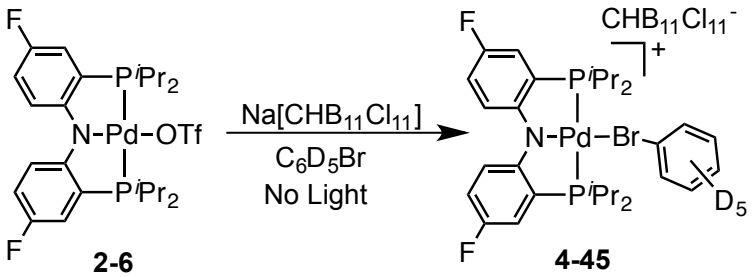

Scheme 4.18 Reactivity of **4-36** with **4-39** in C_6D_5Br.

Analogously, the reaction between **2-6** and **4-39** in C_6D_6, with C_6H_5F as an internal standard, also produces two ^{19}F NMR signals at −77.2 and −123.8 ppm that account for 4% and 68% of the original triflate and ($^{F}PNP^{iPr}$) signals, respectively. In addition, a smaller set of signals at −125.0 and −125.6 ppm, which account for less than 1% (based on an internal standard) of the original ($^{F}PNP^{iPr}$), are also observed. This tells us that although the abstraction is incomplete, the majority of triflate (96%) is likely converted into NaOTf. In addition, the major product in this reaction (at −123.8 ppm, by ^{19}F NMR spectroscopy) also shows a broad ^{1}H NMR spectrum and a relatively sharp ^{31}P NMR resonance at 58.1 ppm. This suggests that the reaction produces reaction produces a mixture of diamagnetic products. In addition, although the solid state structure of **4-29** shows coordination of $[CHB_{11}Cl_{11}]$ to $[(^{F}PNP^{iPr})Pd]^{+}$, this may not be the case in solution. It is likely that the product of this reaction is a mixture of solvent adduct (**4-29b**) and carborane adduct (**4-29a**) and μ-OTf (**4-44**).

Upon treating **2-6** with **4-39** in C_6D_5Br an immediate color change from purple to green is also observed. However, in contrast to the reaction in C_6D_6, no residual triflate signals are observed; indicative of a complete abstraction of triflate from **2-6**. The complete abstraction, and the solution state ^{19}F, ^{31}P and ^{1}H NMR spectroscopy analysis suggests the product is a diamagnetic bromobenzene adduct $[(^{F}PNP^{iPr})Pd(\kappa^{1}\text{-Br-}C_6D_5)]^{+}[CHB_{11}Cl_{11}]^{-}$ (**Scheme 4.18**; **4-45**). The relatively downfield shift at −122.6 ppm by ^{19}F NMR spectroscopy is indicative that the ligand *trans* to the amido is a very weak *trans*- influence ligand. In addition, the sharp ^{31}P (at 59.3 ppm) and ^{1}H NMR spectroscopic signals suggest that the observed product is a diamagnetic and non-

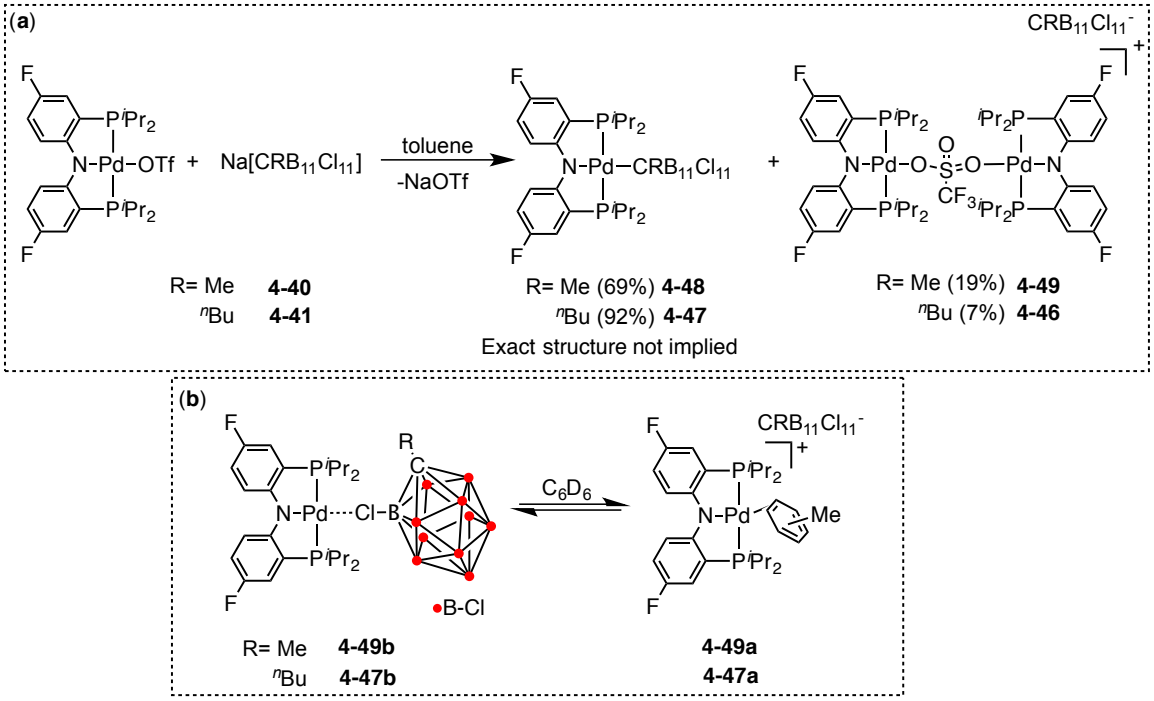

Scheme 4.19 Triflate abstraction from **4-36** with **4-40** and **4-41**.

fluxional. Although aryl halides are very poor Lewis bases, Pd(II), and Pt(II) *trans*-diphosphine haloarene complexes have been characterized previously.[274,300,301] Based on these results, in poorly basic solvents such as toluene and C_6D_6, triflate abstraction with Na[WCA] salts is incomplete and residual triflate is observed by ^{19}F NMR spectroscopy. However, in more Lewis basic solvents such as C_6D_5Br a complete abstraction of triflate is observed.

The reaction between **2-6** and **4-41** in toluene gives a sharp ^{31}P NMR signal resonating at 57.7 ppm. In addition, the ^{19}F NMR spectrum reveals a major signal at −123.6 ppm (92%) and minor signals at −77.1 ppm and −124.8 and −125.3 ppm (7%) (see **Scheme 4.19)**. This is consistent with an incomplete abstraction of triflate from **2-6** producing **4-46**, as observed in the reactions between **2-6** and **4-39** or **4-35**. Based on

solution state NMR spectroscopy, it is likely that the major product in this reaction is a four-coordinate diamagnetic complex. The major product's significant ^{19}F NMR downfield shift (−123.6 ppm) relative to **2-6** (−126.5 ppm) is consistent with a very weak *trans*-influence ligand *trans* to the diarylamido N.[156] However, based solely on NMR spectroscopy it is not clear whether the major product in solution is a solvent (i.e. toluene) adduct (**4-47a**) or a carborane adduct (**4-47b**). In the solid state, however, formation of **4-47a** appears to be more favorable (see Section 4.2.6.5). The reaction between $Na[CMeB_{11}Cl_{11}]$ (**4-40**) and **2-6** in toluene gave very similar results, with only minor deviations in chemical shifts of the observed products (< 0.2 ppm). In the reaction between **2-6** and **4-40**, however, the ^{19}F NMR signal intensity of the major product ($^{F}PNP^{iPr}$)Pd$[CMeB_{11}Cl_{11}]$ (**4-48**) (−123.5 ppm) relative to Pd(μ-OTf) (**4-49**) is lower, which is likely due to the lower solubility of **4-48** versus **4-47.**

Solid state characterization of [($^{Me}PNP^{iPr}$)Pd(toluene)]$^{+}$[$CEtB_{11}Cl_{11}$]$^{-}$. In an effort to characterize ($^{X}PNP^{iPr}$)Pd$[CRB_{11}Cl_{11}]$ (X = Me or F; R = Me, ^{n}Bu, Et) by single-crystal X-ray crystallography, a series of solutions of **2-6** and **4-1** in toluene were treated with a slight excess of $Na[CRB_{11}Cl_{11}]$ (R = Me (**4-40**), ^{n}Bu (**4-41**) or Et (**4-50**)) (**Scheme 4.20**). The solutions were allowed to stir for a few minutes, filtered through Celite, then layered with pentane, and placed in the freezer at −35 °C. In addition, attempts to isolate crystals of [($^{F}PNP^{iPr}$)Pd][$CHB_{11}Br_{11}$] (**4-51**) and [($^{F}PNP^{iPr}$)Pd]$_2$[$B_{12}Cl_{12}$] (**4-52**) ([($^{F}PNP^{iPr}$)Pd(OH_2)][$B_{12}Cl_{12}$]Na (**4-52a**) was obtained see experimental**)** were undertaken by layering a solution of **4-43** in $C_6H_4F_2$ with [$^{n}Bu_4N$]$^{+}$[$B_{12}Cl_{12}$]$^{-}$ (**4-53**) and

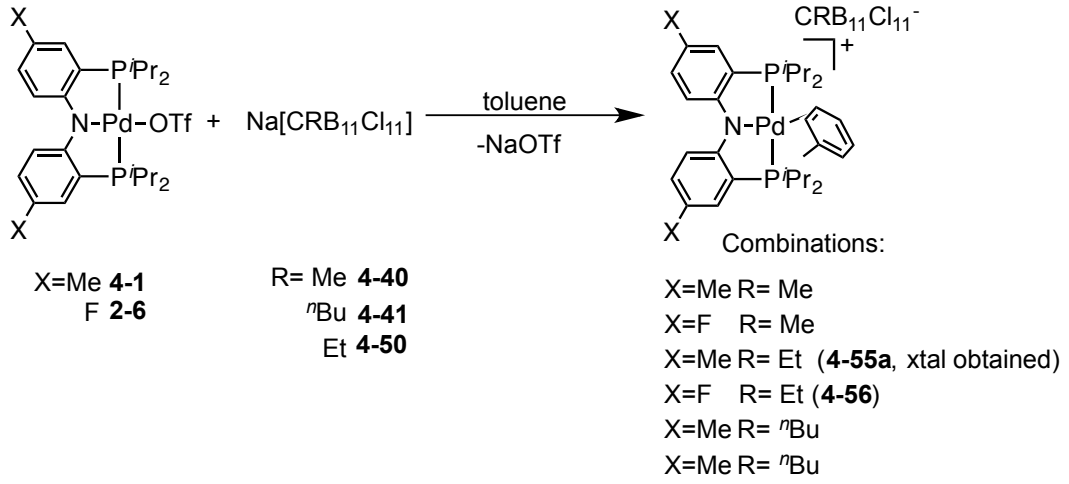

Scheme 4.20 Attempted crystal growth of (PNP^{iPr})Pd[WCA] with different WCAs.

$[Me_3NH]^+[CHB_{11}Br_{11}]^-$ (**4-54**). From this series of reactions, several X-ray quality crystals were obtained from the reaction between **4-1** and **4-50**. The structure of a toluene adduct $[(^{Me}PNP)Pd(toluene)]^+[CEtB_{11}Cl_{11}]^-$ (**4-55a**) was obtained (**Figure 4.6**). Although the analogous complex ($^{F}PNP^{iPr}$)Pd[$CEtB_{11}Cl_{11}$] (**4-56**) cation could not be characterized by single-crystal X-ray crystallography, it is likely that it also exists as a toluene adduct; the steric and electronic differences between $^{F}PNP^{iPr}$ and $^{Me}PNP^{iPr}$ are very small.[92] Transition metal-arene complexes have been shown to be intermediates in arene C-H activation.[107,267,268,270,302-305] In 2013, DeMott and coworkers demonstrated that upon abstraction of triflate from **4-2** with **4-34**, the $[(^{F}PNP)Pt]^+$ undergoes heterolytic cleavage of aromatic C-H bonds (**Scheme 4.21**).[65] It was proposed that the mechanism of this reaction first involves coordination of the aromatic solvent to $[(^{F}PNP)Pt]^+$ cation to form an intermediate arene adduct (**4-57**). The resulting arene complex could either directly be deprotonated by the amido to form **4-58** or first undergo

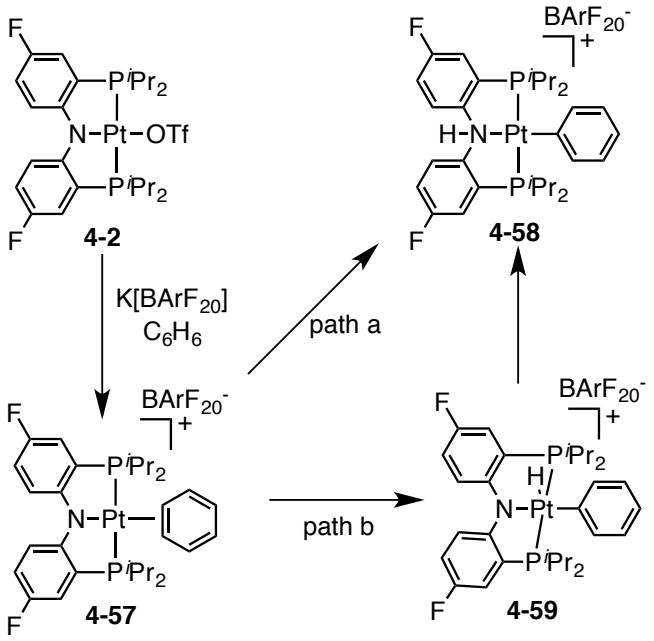

Scheme 4.21 Possible pathways for arene C-H activation by (^{F}PNP^{iPr})Pt[$BArF_{20}$].

oxidative addition to form an acidic Pt(IV) hydride (**4-59)**. Inspired by this work, and the work of Brookhart et al.[268] we were curious if [(^{F}PNP^{iPr})Pd(arene)]$^{+}$ complexes could also undergo 1,2-addition of the coordinated arene. Preliminary data indicates that thermolysis of **2-6** with an equivalent of **4-39** in $C_6H_4F_2$ appears to heterolytically cleave a C-H bond in $C_6H_4F_2$ (see Chapter V experimental).

The hapticity of arene ligands can vary from η^1-η^6; η^6 and η^4 metal-arene complexes are relatively common, whereas η^2 and η^1 are less prevalent.[267,268,272,273,306,307] Arene ligands bind to the metal center by a combination of sigma donation from the arene to the metal, and by metal backbonding into the π^* orbitals of arenes. Metal back bonding into the π^* orbital of an arene typically elongates the C-C bond length of the carbons directly bound to the metal. However, in **4-55a** that is not the case; starting from

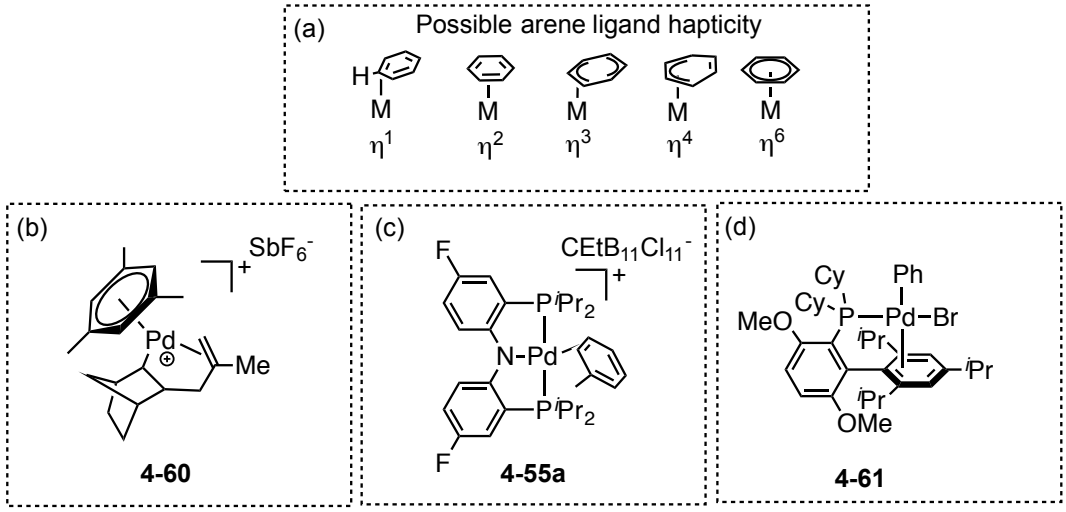

Figure 4.6 Possible hapticity of arene complexes (a); example of palladium arene adduct (b); solid state structure of **4-55a** (c).

the C-C bond directly bound to Pd, the C-C bond distances in the toluene are 1.396, 1.409, 1.376, 1.384, 1.375 and 1.400 Å. The small deviation in bond length between C-C bonds in bound toluene and free toluene suggests that metal backbonding into π* of thearomatic ring is only a small contribution to the bonding between Pd and toluene. This is consistent with the high C-O stretching frequency in Pt(II) and Pd(II)-CO complexes which is indicative that Pd and Pt cations are weak π bases.[308] The structure of **4-55a** has two different Pd-C distances of 2.470(4) Å and 2.369(3) Å. The two Pd-C bond distances in **4-55a** are marginally longer than the two shortest Pd-C bond distances in the η^6-mesitylene palladium complex (**4-60**), but significantly shorter than the three longest Pd-C bond distances in compound **4-60**.[266] Starting from the shortest, the Pd-C bond distances in **4-60** are 2.331(6), 2.435(6), 2.594(6), 2.607(6) and 2.677(6) Å. The significant difference in bond lengths between Pd-C27 and Pd-C33 (0.100 Å), suggests that complex **4-55a** is between a η^1 and a η^2 arene adduct. The three shortest Pd-C bond

distances in Buchwald's η^1 arene adduct (**4-61**) are 2.485(3), 2.983(3), 2.861(3) Å (**Figure 4.6**). The shortest of these bonds is relatively close to the longer of the two Pd-C bonds in complex **4-55a** (**Figure 4.7**).[309] In addition, to accommodate the molecule of toluene into the coordination sphere of Pd, the $^{Me}PNP^{iPr}$ ligand in **4-55a** undergoes a series of distortions. Close inspection of the bond angles of P^iPr_2 in **4-55a** reveals that one phosphine arm has a $^{iPr}C\text{-}P^1\text{-}C^{iPr}$ bond angle of 106.25° whereas the second phosphine has an unusually wide $^{iPr}C\text{-}P^2\text{-}C^{iPr}$ bond angle of 110.98°. As a control, these two angles were compared further with the phosphine bond angles of **2-27**,[70] which we can assume has minimal distortions. The $^{iPr}C\text{-}P\text{-}C^{iPr}$ bond angle of 106.23° in **2-27** tells us that $P^1(i\text{Pr}_2)$ in **4-55a** is relatively unperturbed with respect to the $^{iPr}C\text{-}P\text{-}C^{iPr}$ angles seen in **2-27**. However, the $^{iPr}C\text{-}P^2\text{-}C^{iPr}$ angle in $P^2(i\text{Pr}_2)$ is 4.57° wider than the angle in $P^1(i\text{Pr}_2)$. This distortion is brought about by the rotation of a P(2)-C(24) bond in $P^2(i\text{Pr}_2)$. The rotation brings C(23) and C(25) into close proximity of each other. To minimize the steric repulsion between the two methyl groups, the $^{iPr}C\text{-}P^2\text{-}C^{iPr}$ angle increases. Not surprisingly, the bite angle in **4-55a** decreases to allow the toluene into the coordination sphere of Pd (**Table 4.1**).

Table 4.1 Bond angles in **4-55a** and **2-27**.

Bond Angle	**4-55a**	($^{Me}PNP^{iPr}$)PdCl (**2-27**)
$^{iPr}C\text{-}P^1\text{-}C^{iPr}$	106.28(17)°	106.23(9)°
$^{iPr}C\text{-}P^2\text{-}C^{iPr}$	110.99(16)°	106.23(9)°
P-Pd-P	161.28(3)°	163.54(2)°

So far, this section has detailed the abstracting ability of several alkali metal salts (i.e. Cs^+, K^+ and Na^+) in combination with weakly-coordinating anions. Assuming the differences in Lewis basicity between $[BArF_{20}]^-$, $[BArF_{24}]^-$ and $[CHB_{11}Cl_{11}]^-$ are relatively small, one can deduce the relative triflate abstracting abilities of different alkali metal cations. Based on the above-mentioned observations, Na^+ cations are best for triflate abstraction, followed by K^+ cations, and then Cs^+, the poorest triflate abstracting agent. This is not surprising since the abstracting ability of alkali metals is likely directly related to the lattice energy of the salt produced. For example, in the case of chloride anion the lattice energy of the salts produced with alkali metals follows a simple trend in decreasing lattice energy of: LiCl, NaCl, KCl, RbCl, CsCl and FrCl.[310] This trend could be explained using simple Hard-Soft acid-base (HSAB) theory.[296,311] Triflate a "harder" anion than chloride forms a stronger interaction with harder cations such as Li^+ and Na^+ as compared to softer alkali metals like Cs^+ and Rb^+. Based on this trend, Li[WCA] salts would likely be ideal triflate abstracting agents, however further investigation is necessary to verify this hypothesis.

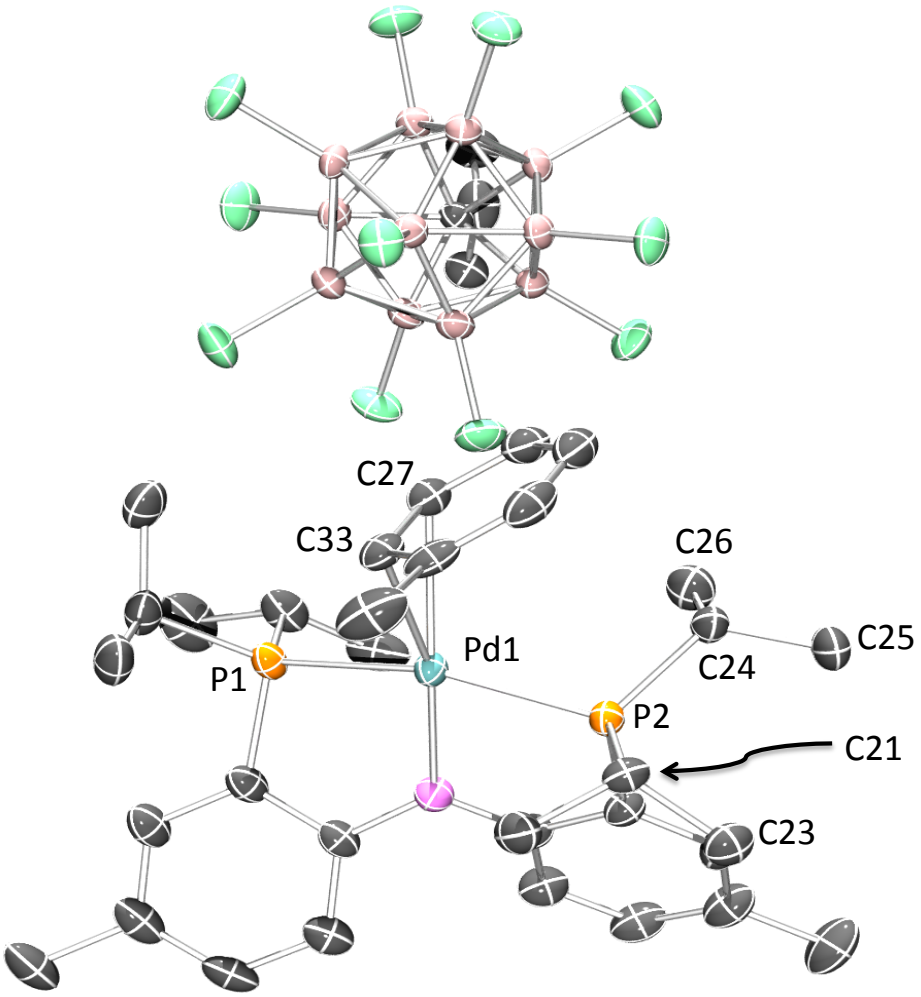

Figure 4.7 POV-Ray rendition of the ORTEP[162] drawing (50% thermal ellipsoids) of **4-55a** showing selected atom labeling. Hydrogen atoms and solvent have been omitted for clarity. Selected bond distances (Å) and angles (deg): Pd1-C33 2.364(3); Pd1-C27, 2.465(4); Pd1−P1, 2.3395(14); Pd1−P2, 2.3461(13); Pd1−N1, 2.027(3); P1−Pd1−P2, 161.28(3).

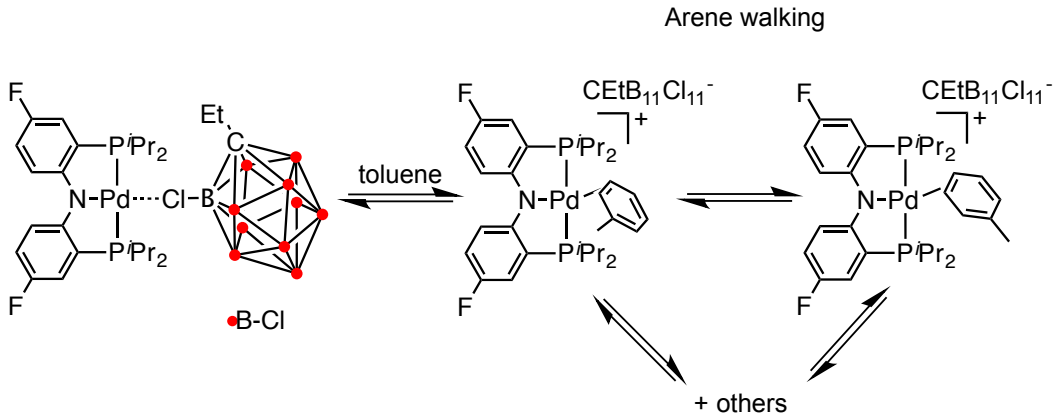

Scheme 4.22 Equilibrium between carborane adduct ($[CEtB_{11}Cl_{11}]^-$) and toluene solvent coordination with ring walking.

Broadening of NMR spectra in (^{F}PNP^{iPr})Pd[WCA]. Presumably, the reaction between **2-6** and **4-16** in toluene also generates $[(^{F}PNP^{iPr})Pd(toluene)]^+[CEtB_{11}Cl_{11}]^-$ (**4-56a**). This four-coordinate complex is expected to be diamagnetic, however the resulting solution is silent by ^{31}P NMR and ^{19}F NMR spectroscopy, and the ^{1}H NMR spectrum shows resonances corresponding to only $[CEtB_{11}Cl_{11}]^-$. The apparent silence by NMR spectroscopy can be due to intense broadening brought about by an equilibrium between different adducts such as the carborane adduct, a toluene adduct, and possibly agostic interactions. Although X-ray crystallographic evidence indicates that in the solid-state **4-55a** coordinates toluene to $[(^{Me}PNP^{iPr})Pd]^+$, in solution it is possible that coordination of both toluene and $[CEtB_{11}Cl_{11}]^-$ are in equilibrium with each other (**Scheme 4.22**). The toluene ligand could also undergo "ring-walking", which would further broaden the NMR spectra.

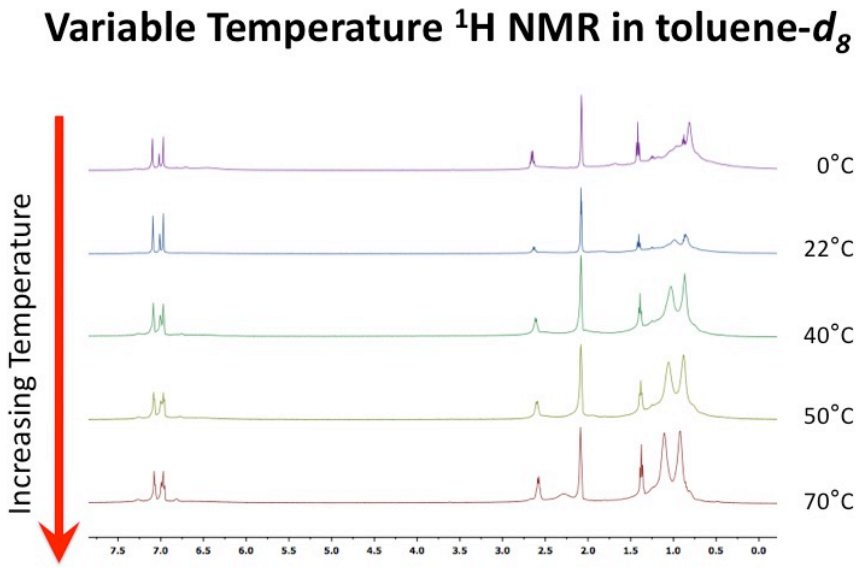

Figure 4.8 Variable temperature ^{1}H NMR of [(^{F}PNP^{iPr})Pd(toluene)]$^{+}$ (**4-56a**) cation in toluene d_8.

In an effort to answer these questions, **4-56** was analyzed by variable temperature ^{19}F, and ^{1}H NMR spectroscopy (**Figure 4.8**). At 0 °C two sharp signals, a quartet at 2.67 ppm and a triplet at 1.43 ppm, belonging to [CEtB$_{11}$Cl$_{11}$] can be seen by ^{1}H NMR spectroscopy. In addition, two broad humps can be seen at 0.98 ppm and 0.83 ppm, presumably belonging to the (^{F}PNP^{iPr}) ligand. However, as the temperature is increased from 0 °C to 70 °C, the ^{1}H NMR spectrum becomes more resolved. Unfortunately, compound **4-56** remains silent by ^{31}P NMR spectroscopy even at elevated temperatures. At 70 °C two aromatic signals at 7.26 ppm and 6.81 ppm, a methine signal at 2.28 ppm and two methyl resonances at 1.11 and 0.81 are observed. These results suggest that at higher temperatures the mixture of adducts rapidly exchange with each other, and the average of all these complexes is observed. The increase in signal intensity is also likely

the result of an increase in solubility of **4-56** at higher temperatures. Another factor that may contribute to the broadening of the NMR spectrum of the reaction between **4-16** and **2-6** could be the presence of residual silane in **4-16**.

Based on the results discussed above it is clear that Lewis bases, even as weak as toluene, are capable of forming adducts with $[(PNP^{iPr})Pd]^+$ cations. The use of weakly-coordinating anions, such as $[CHB_{11}Cl_{11}]^-$ leads to the formation of $(PNP^{iPr})Pd[\kappa^1\text{-Cl-}CHB_{11}Cl_{10}]$ a carborane adduct. The alkylation at the *ipso* carbon of $[CHB_{11}Cl_{11}]^-$ leads to bulkier and more soluble carboranes that in the solid state appear to not coordinate to $[(PNP^{iPr})Pd]^+$, and instead aromatic solvents such as toluene, fluorobenzene, and benzene coordinate to the metal center. A simple change in $[CRB_{11}Cl_{11}]^-$ from R = H to R = Et decreases the favorability of carborane binding to Pd, allowing arenes to coordinate more favorably. It also appears that less weakly-coordinating solvents (i.e. bromobenzene), and anions (e.g. $[CHB_{11}H_{11}]$) facilitate the abstraction of triflate from **2-6**. It is also clear that to generate a truly three-coordinate $[(PNP^{iPr})Pd]^+$ cation, arene coordination to Pd must become less favorable. To prevent arene coordination there are two things that could be done: use bulkier arenes such as mesitylene (a poor solvent), or increase the steric bulk (cone angle) of the phosphine arms on (PNP^R).

The chemistry of bulky $[(^FPNP^{tBu})Pd]^+$ cations. To avoid the formation arene complexes with the $[(^FPNP^R)Pd]^+$ cation we decided the best solution was to increase the steric bulk around the metal. Although there are many options for bulky phosphines available in the literature, a bulky alkyl group would have a minimal perturbation on the

electronics of the $[(PNP)Pd]^+$cation. The most obvious choice is to substitute -P^{i}Pr$_2$ in $[(^F PNP^{iPr})Pd]^+$ for more sterically imposing alkyl phosphines such as -P^{t}Bu$_2$ and -PAd$_2$. The details of the synthesis of the bulky ^{F}PN(Me)P$^{t Bu}$ (**2-20**) and ^{F}PN(Me)P^{Ad} (**2-21**) ligands, and their palladium complexes are discussed in Chapter II. Based on the observed reactivity of the $[(PNP^{iPr})Pd]^+$ cation, it is clear that a bulkier ligand will reduce the favorability of coordination of ligands such as arenes. The reaction between **2-25** and **4-39** in C_6D_6 produces a color change from dark blue to a lighter blue/green color. Along with the color change a large chemical shift is observed by ^{19}F and ^{31}P NMR spectroscopy (**Scheme 4.23**). Surprisingly, the OTf:^{F}PNP$^{t Bu}$ ratio of 3:2 in **2-25** does not change upon addition of **4-39**. The large change in chemical shift (more downfield) observed by ^{19}F and ^{31}P NMR spectroscopy, and the observed OTf:^{F}PNP$^{t Bu}$ ratio of 3:2 suggest **4-62** is formed. Although it is not clear what the exact structure of **4-62** is, one possibility is that the oxygen of the triflate group coordinates to the Na^+, but does not dissociate from palladium. Regardless of the structure, this indicates that **4-39** is not capable of abstracting triflate from **2-25**. It is likely that abstraction of triflate with sodium(I) salts is driven by the coordination of the anion or solvent suggesting that the bulky ^{t}Bu phosphines in **2-25** prevent coordination of $[CHB_{11}Cl_{11}]$ or aromatic solvents (e.g. toluene), therefore impeding the abstraction of triflate.

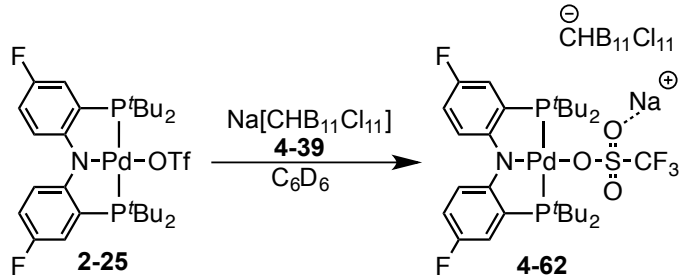

Compound	^{19}F NMR		^{31}P NMR	^{1}H NMR (^{t}Bu signal)
(^{F}PNP^{tBu})PdOTf	-77.3 ppm	-126.0 ppm	68.4 ppm	1.30 ppm
(^{F}PNP^{tBu})PdOTf + Na[CHB$_{11}$Cl$_{11}$]	-75.0 ppm	-124.9 ppm	72.1 ppm	1.33 ppm

Scheme 4.23 Reaction between **2-25** and **4-39** in C_6D_6 and corresponding ^{31}P and ^{19}F NMR chemical shifts.

Based on the reactivity of silylium salts with **2-6** we know that silylium salts are effective triflate abstracting agents. In addition, the reactivity of **2-25** with **4-39** suggests that $[CHB_{11}Cl_{11}]^-$ does not coordinate to the $[(^{F}PNP^{tBu})Pd]^+$ cation. The $[CHB_{11}Cl_{11}]^-$ anion's high crystallinity will also be advantageous in our efforts to obtain a crystal structure of the $[(^{F}PNP^{tBu})Pd]^+$ cation. The reaction between **2-25** and **4-14** in toluene produces an immediate color change from dark blue to a brown/yellow. Addition of C_6H_5F to the above solution produces a color change from brown/yellow to a dark green.

Unfortunately, the product from this reaction is NMR silent and only $^{i}Pr_3SiOTf$ is observed by ^{19}F NMR spectroscopy. As will be discussed in Section 4.2.7 each L in $[(PNP^{iPr})Pd(L)]^+$ cation gives a unique color, and based on the colors of the known $[(PNP^{iPr})Pd(L)]^+$ complexes, we can make an educated guess of the identity of L in the above reaction. The green color obtained upon addition of C_6H_5F to $[(^{F}PNP^{tBu})Pd]^+$ can

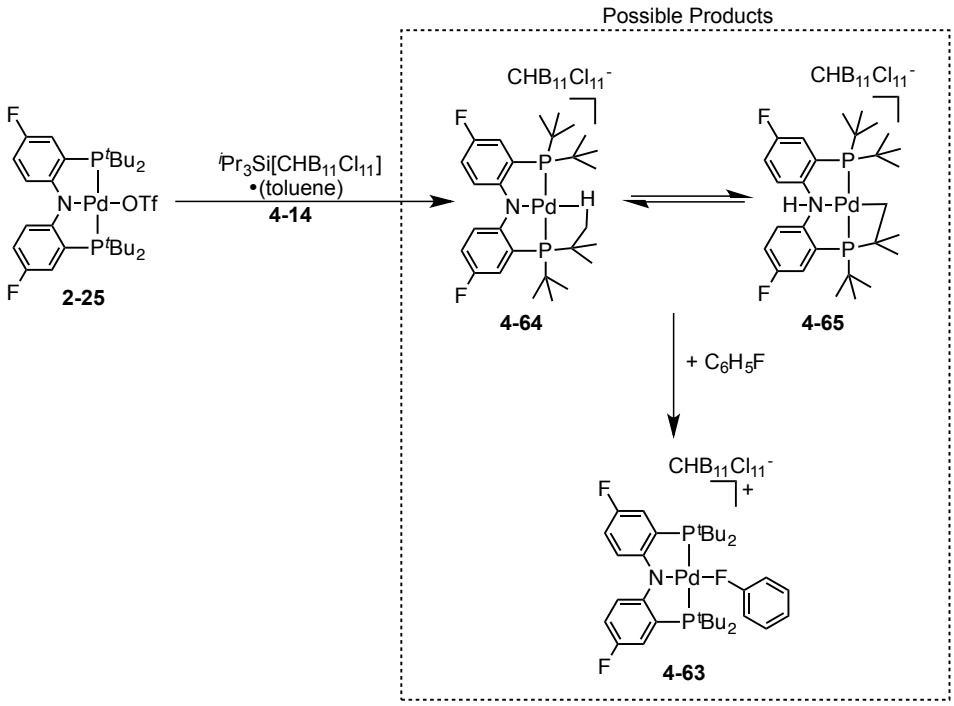

Scheme 4.24 Possible products from triflate abstraction from **2-25** with **4-14**.

be attributed to the formation of an fluorobenzene adduct, [(PNP^{tBu})Pd(κ^1-F-C$_6$H$_5$)] (**Scheme 4.24; 4-63**). However, the yellow/brown color, prior to adding C$_6$H$_5$F, is not observed in any known [(PNP^{iPr})Pd(L)]$^+$ complexes. As one moves from coordinating anions (i.e. Cl$^-$) to more weakly-coordinating ligands (i.e. toluene and [CHB$_{11}$Cl$_{11}$]$^-$) there is a shift in the absorbed light from red to green. Based on this trend, one would expect that a [(PNP)Pd]$^+$ cation with a very weak *trans*-influence ligand such as an agostic interaction (**4-64**) might be light yellow (or nearly colorless) product (**Table 4.2**). A second possibility is a cyclometalated product such as **4-65**. This product should also be colorless because the nitrogen lone-pair (the active chromophore) is protonated.

Table 4.2 Observed and absorbed color of (^{F}PNP^{iPr})PdX complexes.

(^{F}PNP^{iPr})PdX Complex	**Observed Color**	**Absorbed Color**
(^{F}PNP^{iPr})PdCl (**2-4**)	Red (620-780 nm)	Green
(^{F}PNP^{iPr})PdOTf (**2-6**)	Blue (450-495 nm)	Orange
(^{F}PNP^{iPr})Pd[$CHB_{11}Cl_{11}$]	Blue/green	Red/orange
[(^{F}PNP^{iPr})Pd(Toluene)]$^{+}$	Green (495-570 nm)	Red
?	Light Yellow/brown (570-590 nm)	Near IR?

4.2.7 Reactivity of [(^{F}PNP^{iPr})Pd]$^{+}$ cations

Not surprisingly, addition of Lewis bases such as pyridine, THF or H_2O generates the corresponding Lewis acid/base product. The color of [(^{F}PNP^{iPr})Pd(L)]$^{+}$ is highly dependent on the ligand L. Each ligand L in [(^{F}PNP^{iPr})Pd(L)]$^{+}$[WCA]$^{-}$ gives a unique color that allows for a convenient way of identifying the resulting product. For example, when L is a weakly-coordinating ligand such as toluene, or a WCA (i.e. $[CHB_{11}Cl_{11}]$), the color of the complex is green. However, more strongly bound ligands like H_2O and pyridine generate blue and purple solutions, respectively. **Scheme 4.25** illustrates some of the different adducts that can be synthesized such as [(^{F}PNP^{iPr})Pd(L)]$^{+}$[WCA]$^{-}$ (WCA = $BArF_{24}$; L = H_2O (**4-66**)); (WCA = $BArF_{24}$; L = THF (**4-67**)), (WCA = $CMeB_{11}Cl_{11}$; L = pyridine (**4-68**)); and (WCA = $BArF_{24}$; **2-8** (**4-69**)).

Given that the DFT calculations predict the [(^{F}PNP^{iPr})Pd]$^{+}$ cation is a triplet, diradical species, we expected to see reactivity consistent with a metalloradical. With this in mind, we decided to explore the reactivity of [(^{F}PNP^{iPr})Pd]$^{+}$ cation with substrates

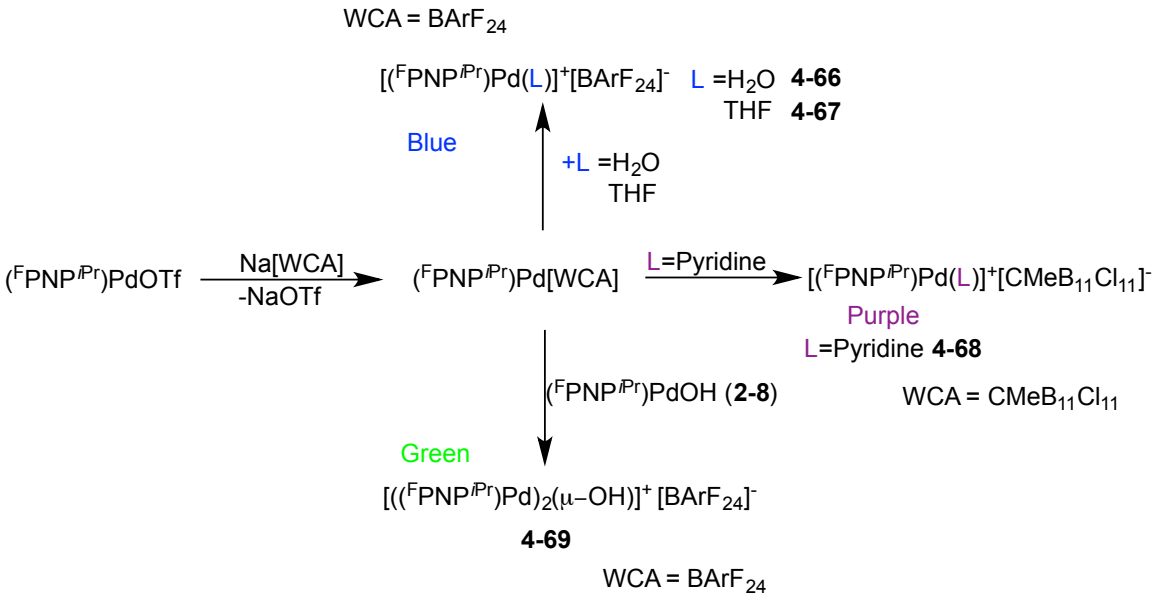

Scheme 4.25 Formation of $[(^{F}PNP^{iPr})Pd(L)]^{+}$ adducts: **4-66**, **4-67**, **4-68**, **4-69**.

such as O_2 and C_6D_6Br. These reagents essentially function as a radical trap to the triplet $[(^{F}PNP^{iPr})Pd]^{+}$ cation. In Section 4.2.6.4 the synthesis of **4-45** was discussed. When protected from light and at room temperature compound **4-45** appears to be stable, however if exposed to lab lighting for an extended period of time (2 weeks), a gradual color change to a dark green is observed.

Irradiation with a 250-W halogen lamp accelerates the decomposition, and produces an immediate color change from a light green to dark green. If the sample is irradiated overnight, treated with excess Cp_2Fe, and then filtered through a pad of silica gel, the major product is **3-9** (81%). Based on these observations, we surmise that upon irradiation of **4-45** the compound undergoes homolytic C-Br bond cleavage to generate $[(^{F}PNP^{iPr})PdBr]^{+}[CHB_{11}Cl_{11}]^{-}$ (**Scheme 4.26**; **4-70**). The abstraction of a bromine atom

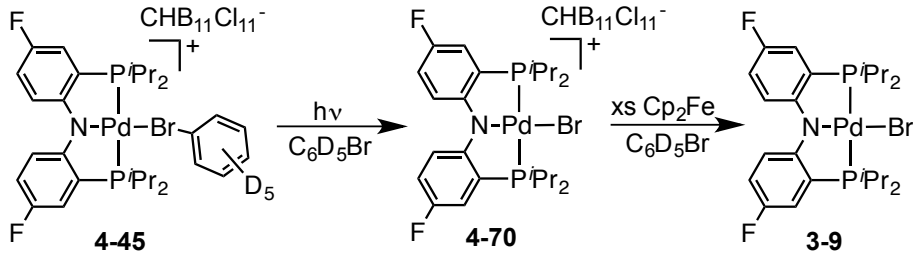

Scheme 4.26 Photo-induced bromine atom abstraction from C_6D_5Br in **4-45**.

from bromobenzene is consistent with a metalloradical species. However, it is not clear if an intermediate, diradical $[(^{F}PNP^{iPr})Pd]^{+}$ cation is formed prior to the abstraction, or if abstraction is a concerted process.

Exposure of **4-43** to an atmosphere of O_2 produces an immediate color change from aqua-blue to a dark green color. Unlike the acid/base reactions mentioned in the previous section, addition of O_2 gas to **4-43** does not produce a diamagnetic product. This suggests that O_2 is not acting as a two-electron donor, as is the case with bases such as H_2O and CH_3CN. Our hypothesis is that under an atmosphere of O_2, **4-43** generates a cationic η^1 superoxide $[(^{F}PNP)Pd(O_2)]^{+}[BArF_{20}]^{-}$ (**4-71**). X-band EPR spectroscopy of compound **4-71** under an atmosphere of O_2 produces a relatively complex spectrum, as is expected for a diradical.

Based on the reactivity exhibited between $(^{F}PNP)PdO_2$ and $[(^{F}PNP)PdO\text{-}]_2$ (see Chapter III), it is conceivable that removal of the oxygen headspace from **4-71** produces a mixture of a cationic superoxide (**4-71)** and a dicationic peroxide (**4.72**) (**Scheme 4.27**). However, further characterization is needed to substantiate this hypothesis. If a degassed sample of **4-71** is treated with excess CH_3CN to a quantitative conversion to

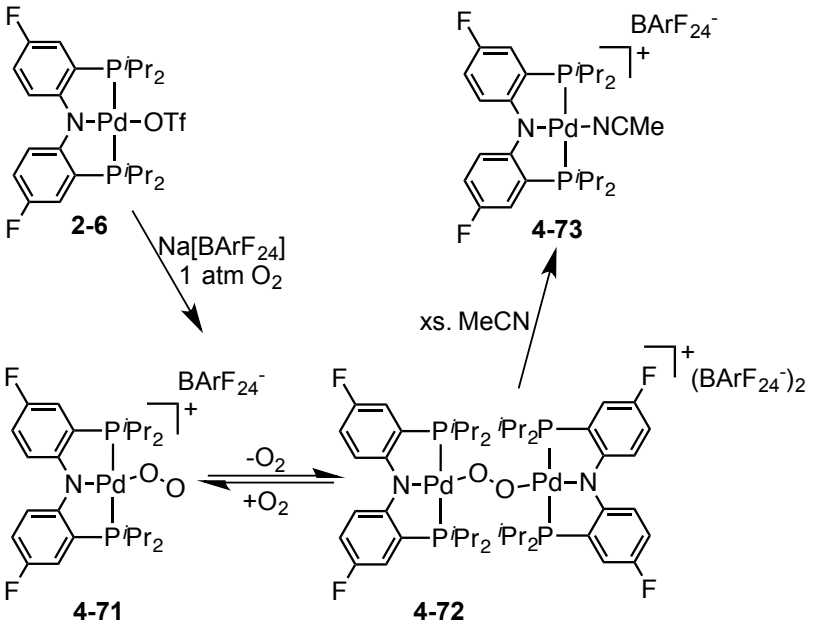

Scheme 4.27 Reactivity of **4-43** with molecular oxygen; possible equilibrium between **4-71** and **4-72**.

$[(^{F}PNP)Pd(NCCH_3)]^+[BArF_{20}]^-$ (**Scheme 4.27**; **4-73**). In contrast, addition of a saturated solution of H_2O in C_6H_6F to **4-71** does not yield the expected $[(^{F}PNP)Pd(OH_2)]^+[BArF_{20}]^-$ (**4-66**). This suggests that either O_2 binds more strongly than H_2O to $[(^{F}PNP)Pd]^+$ cation or that the resulting superoxide/peroxides undergo hydrolysis. Unfortunately, attempts to grow X-ray quality crystals of **4-71** were unsuccessful, preventing characterization by single-crystal X-ray crystallography.

4.3 Conclusion

This chapter discussed the attempts to synthesize and characterize a three-coordinate $[(PNP)Pd]^+$ cation. Abstraction of triflate from **2-6** with silylium reagents generates a green solution that appears to be silent by NMR spectroscopy. Based on

preliminary experiments by Dr. Claudia Fafard it was hypothesized that a three-coordinate paramagnetic $[(PNP^{iPr})Pd]^+$ cation was formed.[173] However, X-ray crystallographic evidence of **4-29** indicates that the carborane anion coordinates to the metal center. In addition, abstraction of triflate from **2-6** with **4-39** generates a green diamagnetic solution. In the presence of Lewis basic solvents such as C_6D_5Br a κ^1-Br bromobenzene adduct **4-45** is formed. To prevent coordination of the carborane anion to Pd, bulkier and more soluble alkylated carboranes were employed. Abstraction of triflate in toluene using Na^+ salts in combination with alkylated carboranes ($[CRB_{11}Cl_{11}]^-$; R = Me, Et, ^{n}Bu) appear to generate arene complexes, and **4-55** was characterized by X-ray crystallography. The combination of these observations suggests that the apparent silence by NMR spectroscopy is in fact the result of an equilibrium between a mixture of diamagnetic products. However, the possibility that paramagnetic complexes exist in solution cannot be completely ruled out. Although the desired three-coordinate $[(PNP)Pd]^+$ cation was not obtained, several unusual complexes such as η^1-arene-Pd and κ^1-haloarene-Pd complexes were obtained. These complexes are particularly interesting because they offer insight into the binding modes of halogenated and non-halogenated arenes to palladium complexes. These complexes are particularly interesting in the context of C-H and C-Br activation, because they give a glimpse of what the possible structures are of the intermediates in C-H and C-Br activation. The DFT calculations of $[(PNP^{iPr})M]^+$ (M = Pd or Pt) cations[65] suggests the possibility of a low-lying triplet state. The reactivity of $[(PNP^{iPr})Pd]^+$ cations with C_6D_5Br, and molecular oxygen corroborates the metalloradical character of $[(PNP^{iPr})Pd]^+$ cations.

Finally, to disfavor arene coordination to the metal center, bulkier (PNP)Pd complexes such as **2-25** and **2-26** were synthesized. Unfortunately, attempts to abstract, triflate from **2-25** with **4-39** were unsuccessful; presumably because the ^{t}Bu groups are too large to allow arene, or anion coordination to occur. However, **4-14** does fully abstract triflate from **2-25**, and the product of this reaction is silent by NMR spectroscopy. It is not clear why the resulting solution is silent by NMR spectroscopy; however, it could be due to poor solubility, or fluxional processes which lead to intense broadening. Further characterization is needed to determine if $[(^{F}PNP^{tBu}Pd]^{+}$ cations are indeed three-coordinate, or if cyclometalation or agostic interactions take place.

4.4 Experimental

4.4.1 General considerations

Unless specified otherwise, all manipulations were performed under an argon atmosphere using standard Schlenk line or glovebox techniques. Toluene, pentane, and C_6D_6 were dried over NaK/Ph_2CO/18-crown-6, distilled or vacuum transferred, and stored over molecular sieves in an Ar-filled glovebox. Diethyl ether and THF were dried, and deoxygenated (by purging) using a solvent purification system, and stored over molecular sieves in an Ar-filled glovebox. Fluorobenzene, pyridine, acetonitrile, bromobenzene and CD_2Cl_2 were dried over CaH_2, distilled or vacuum transferred, and stored over molecular sieves in an Ar-filled glove box. **4-14**,[263] **2-4**,[135] **2-7**,[70] **2-9**,[70] **2-6**[157] were prepared according to published procedures. Compounds **4-40** and **4-41** were synthesized according to published procedures.[293] $Na[CHB_{11}Cl_{11}]$ (**4-39**),[312] potassium

tetrakis(pentafluorophenyl) borate (K[$BArF_{20}$]) (caution: shock sensitive), and sodium tetrakis[(3,5-trifluoromethyl)phenyl]borate (Na[$BArF_{24}$]) were dried under vacuum overnight at ambient temperature, and stored in an Ar-filled glovebox. All other chemicals were used as received from commercial vendors. NMR spectra were recorded on a Varian iNova 300 (^{1}H NMR, 299.951 MHz; ^{13}C NMR, 75.426 MHz; ^{31}P NMR, 121.422 MHz; ^{19}F NMR, 282.211 MHz), and NMRS 500 (^{1}H NMR, 499.703 MHz; ^{13}C NMR, 125.697 MHz; ^{31}P NMR, 202.289 MHz; ^{19}F NMR, 470.069 MHz) spectrometer. Chemical shifts are reported in δ (ppm). For ^{1}H NMR and ^{13}C NMR spectra, the residual solvent peak was used as an internal reference. ^{1}H NMR spectra in C_6D_5Br were referenced by setting the most downfield signal to 7.30 ppm. ^{19}F NMR spectra were referenced externally using 99% CF_3CO_2H at −78.5 ppm. For the purpose of clarity, the following abbreviations are defined: apparent (app.), doublet of virtual triplet (dvt). Elemental analyses were performed by CALI Labs, Inc. (Parsippany, NJ).

Synthesis of [(^{F}PN(H)P^{iPr})PdMe]$^{+}$[$CHB_{11}Cl_{11}$]$^{-}$ (4-21). In an oven-dried flask, **2-9** (60 mg, 0.11 mmol) was dissolved in 4 mL of CH_2Cl_2. To the resulting solution, HOTf (10 μmol, 0.11 mmol) was syringed in, and the volatiles were removed by vacuum. The resulting solid was redissolved in CD_2Cl_2, Cs[$CHB_{11}Cl_{11}$] (72 mg, 0.11 mmol) was added as a solid, and the solution was sonicated for 5 min. The solution was then filtered through Celite, and the volatiles were removed by vacuum. ^{1}H NMR (CD_2Cl_2): δ 7.27 (broad m, 6H, Ar-H), 6.95 (s, 1H, N-H), 3.19 (broad s, 1H, H-CB), 2.69 (broad m, 4H, PC*H*Me_2), 1.41 (app. q, 6H, J_{P-H} = 10 Hz, PCH*Me*$_2$), 1.29 (app. q,

6H, J_{P-H} = 7 Hz, PCH*Me*$_2$), 1.27 (app. q, 6H, J_{P-H} = 10 Hz, PCH*Me*$_2$), 1.16 (app. q, 6H, J_{P-H} = 10 Hz, PCH*Me*$_2$) (**Figure 4.9**); $^{31}P\{^1H\}$ NMR (CD_2Cl_2): δ 38.8 (s); ^{19}F NMR (CD_2Cl_2): δ −112.4 (2F, s).

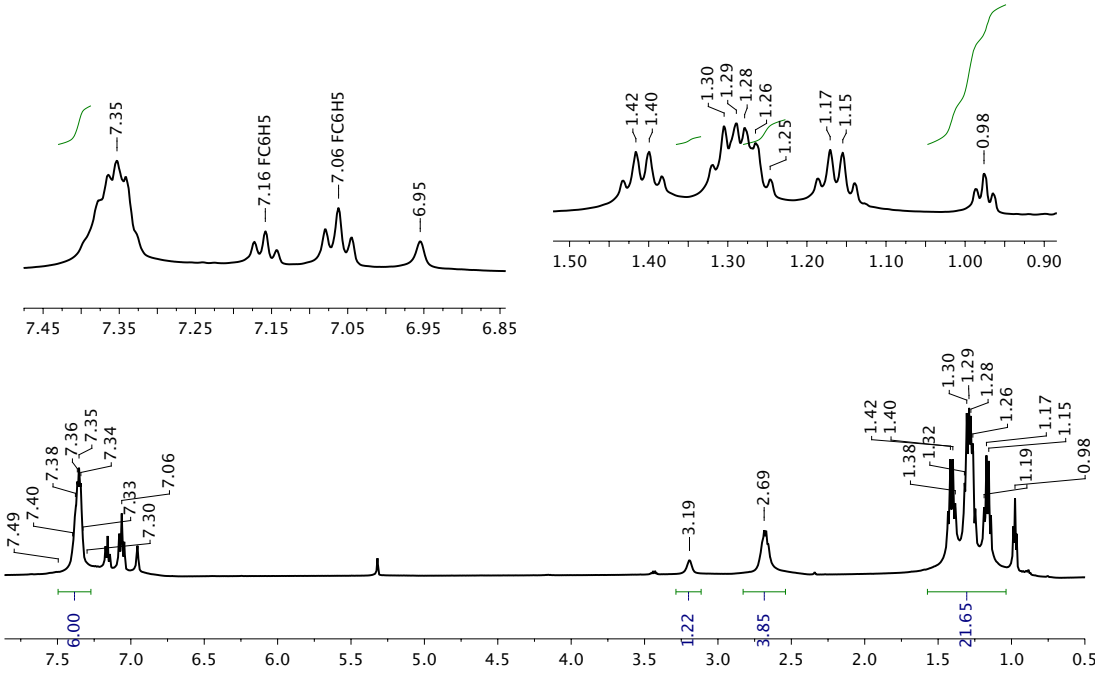

Figure 4.9 ^1H NMR spectrum of **4-21** in C_6D_6.

Synthesis of [(^{F}PN(H)P^{iPr})PdMe]$^{+}$[OTf]$^{-}$ (4-22). In an oven-dried flask, **2-9** (50 mg, 0.090 mmol) was dissolved in 10 mL of pentane. To the resulting solution, HOTf (8.0 μmol, 0.090 mmol) was syringed in and a precipitate was formed. The solid was isolated using filtration, and dried under vacuum. ^{1}H NMR (C_6D_6): δ 10.33 (s, 1H, N-H), 7.27 (m, 2H, Ar-H), 6.78 (m, 2H, Ar-H), 6.75 (broad s, 2H, Ar-H), 2.53 (m, 2H, PC*H*Me$_2$), 1.80 (m, 2H, PC*H*Me$_2$), 1.15 (app. q, 6H, J_{P-H} = 5 Hz, PCH*Me*$_2$), 0.98 (app. q, 6H, J_{P-H} = 5 Hz, PCH*Me*$_2$), 0.81 (app. q, 6H, J_{P-H} = 5 Hz, PCH*Me*$_2$), 0.62 (app. q, 6H, J_{P-H} = 5 Hz, PCH*Me*$_2$) (**Figure 4.10**); ^{31}P{^{1}H} NMR (C_6D_6): δ 38.1 (s); ^{19}F NMR (C_6D_6): δ −115.1 (2F, s), −78.5 (3F, s).

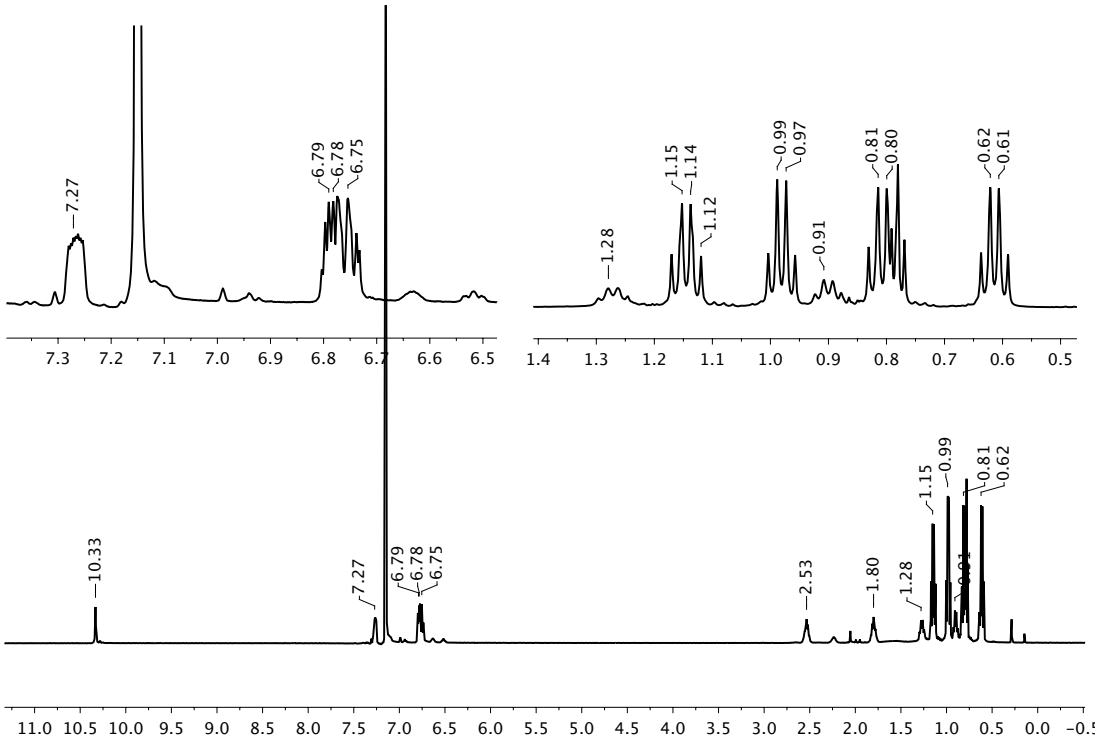

Figure 4.10 ^{1}H NMR spectrum of 4-22 with 2-6 impurity and residual pentane in C_6D_6.

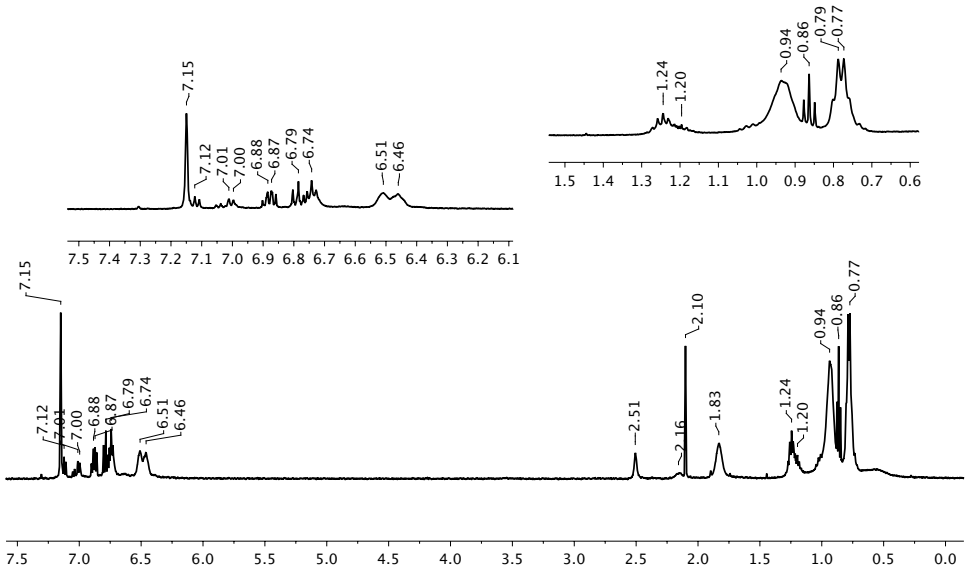

Figure 4.11 ^{1}H NMR spectrum of **4-29** with residual toluene and C_6H_5F.

Reaction between 2-9 and H_2SO_4(aq) (observation of 4-24). In a 25 mL flask, **2-9** (20 mg, 0.054 mmol) was dissolved in 5 mL of THF. To the resulting solution H_2SO_4 (3 μL, 18 M) was added and an immediate color change to yellow was observed. After allowing the solution to stir for 5 min, the solution turned to a maroon color. The volatiles were removed, the sample was redissolved in C_6D_6, and was analyzed by NMR spectroscopy. ^{1}H NMR (C_6D_6): δ 11.53 (s, 1H, H-OSO$_3$), 7.15 (m, 2H, Ar-H), 6.66 (m, 2H, Ar-H), 6.52 (m, 2H, Ar-H), 2.26 (m, 4H, PC*H*Me$_2$), 1.37 (app. q, 12H, $J_{P\text{-}H}$ = 9 Hz, PCH*Me*$_2$), 0.95 (app. q, 6H, $J_{P\text{-}H}$ = 9 Hz, PCH*Me*$_2$); ^{31}P{^{1}H} NMR (C_6D_6): δ 50.7 (s); ^{19}F NMR (CD_2Cl_2): δ −127.4 (2F, s).

Reaction of 2-6 with 4-39 in C_6D_6 in the dark (observation of 4-29). In an oven-dried J. Young tube, **2-6** (11 mg, 0.016 mmol) was dissolved in 0.5 mL of C_6D_6. To the resulting solution, **4-39** (10 mg, 0.018 mmol) was added. The J. Young tube was shaken to assure proper mixing of the reagents. As the reagents mixed, a color change from purple to green was observed. The product was covered with aluminum foil overnight and no change was observed by NMR spectroscopy. ^{1}H NMR (C_6D_6): δ 7.10 (m, 2H, Ar-H; overlapping with residual toluene), 6.51 (broad t, 2H, Ar-H), 6.46 (broad s, 2H, Ar-H), 2.51 (s, 1H, HCB), 1.83 (broad s, 4H, C-H), 1.04 (broad m, 12H, PCH*Me*$_2$)), 0.78 (app. quartet (dvt), 12H, J = 10 Hz, PCH*Me*$_2$); ^{31}P{^{1}H} NMR (C_6D_6): δ 58.14 (s); ^{19}F NMR (C_6D_6): δ −123.8 (see **Figure 4.11**).

Reaction between 2-6 and ^{i}Pr$_3$Si[CMeB$_{11}$Cl$_{11}$]•1.6(CH$_3$C$_6$H$_5$) (4-15) (possible synthesis of 4-30). In an oven-dried J. Young tube, **2-6** (8.0 mg, 0.012 mmol) was dissolved in a mixture of C_6D_6/C_6H_5F. Addition of **4-15** (11 mg, 0.014 mmol) to the solution produces an immediate color change from purple to green. No ^{F}PNP$^{i\text{Pr}}$ signals are observed by ^{1}H, ^{31}P, or ^{19}F NMR spectroscopy. The disappearance of ^{F}PNP$^{i\text{Pr}}$ NMR signals is accompanied by the formation of ^{i}Pr$_3$SiOTf; as confirmed by ^{19}F NMR, and ^{1}H NMR spectroscopy.

Reaction between (^{F}PNP$^{i\text{Pr}}$)PdF (2-28) and 4-15 (possible synthesis of 4-30). In an oven-dried J. Young tube, **2-28** (8.7 mg, 0.016 mmol) was dissolved in 0.5 mL of C_6H_5F. Upon addition of **4-15** (16 mg, 0.020 mmol) to the solution, the color changed

color from red to green. No $^{F}PNP^{iPr}$ signals were observed by ^{1}H, ^{31}P, or ^{19}F NMR spectroscopy. The disappearance of $^{F}PNP^{iPr}$ NMR signals was accompanied by the formation of $^{i}Pr_3SiF$; as confirmed by ^{19}F NMR spectroscopy.

Reaction between 2-6 and $^{i}Pr_3Si[CEtB_{11}Cl_{11}]\bullet 1.6(CH_3C_6H_5)$ (4-16) (possible observation of 4-31 and VT study). In an oven-dried J. Young tube, **2-6** (16 mg, 0.023 mmol) was dissolved in $C_6D_6CD_3$. Addition of **4-16** (21 mg, 0.025 mmol) to the solution produces an immediate color change from purple to green. No $^{F}PNP^{iPr}$ signals were observed by ^{1}H, ^{31}P or ^{19}F NMR spectroscopy at room temperature. The solution was triturated with excess pentane, and then dried under vacuum. The solid was redissolved in toluene-d_8 and variable temperature ^{1}H NMR (**Figure 4.8**) and ^{19}F NMR spectra (**Figure 4.12**) were acquired (silent by ^{31}P NMR spectroscopy).

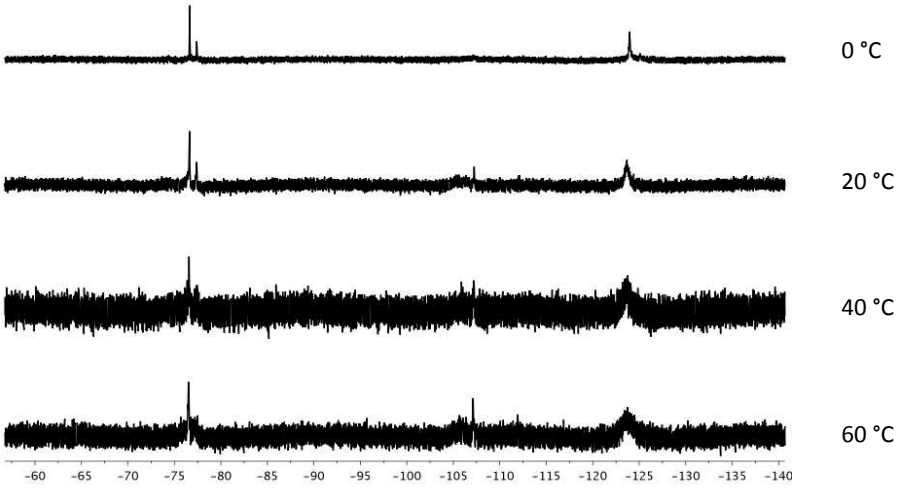

Figure 4.12 Variable temperature ^{19}F NMR spectrum of reaction between **2-6** and **4-16**.

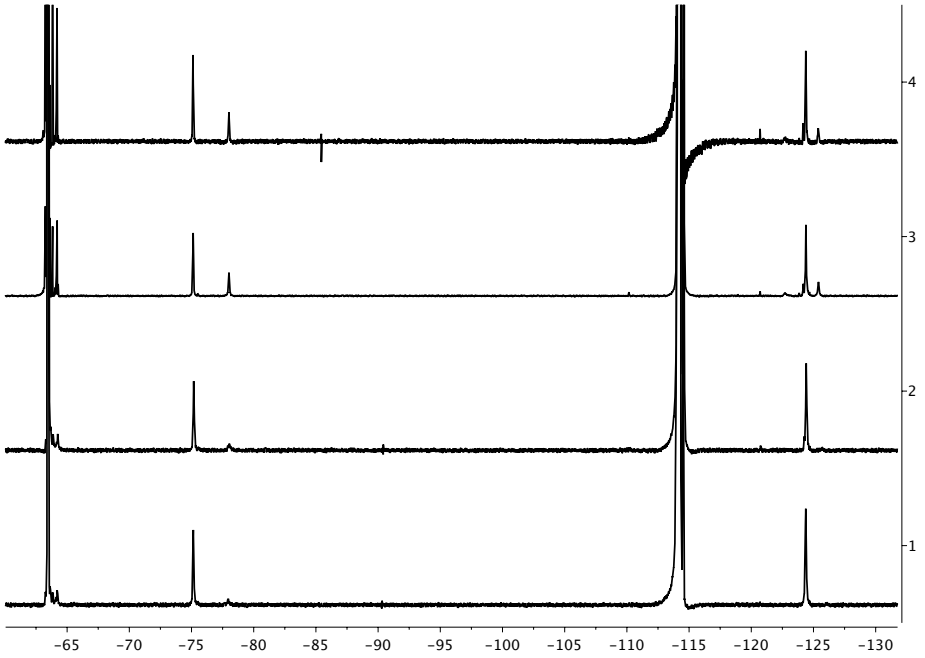

Figure 4.13 Monitoring the incremental addition of **2-6** to **4-43 (**observation of **4-42)** by ^{19}F NMR spectroscopy.

Reaction between 2-6 and 4-35 and incremental addition of 2-6 to 4-43 (observation of 4-42). In an oven-dried J. Young tube, **2-6** (5 mg, 0.007 mmol) was dissolved in 0.5 mL of C_6H_5F. To the resulting solution, **4-35** (7 mg, 8 μmol) was added as a solid, and the tube was shaken to assure proper mixing of the reagents. The product was then analyzed by ^{19}F NMR spectroscopy (**Figure 4.13**, column 4). To the resulting solution, **2-6** was added in increments of 2 mg (3 μmol), each time taking a ^{19}F NMR spectrum. The results are shown in **Figure 4.13**, columns 3-1. After adding a total of 9 μmol of **2-6** (**Figure 4.13**, column 1), the two resonances at −75.1 ppm and −124.4 ppm became the major product.

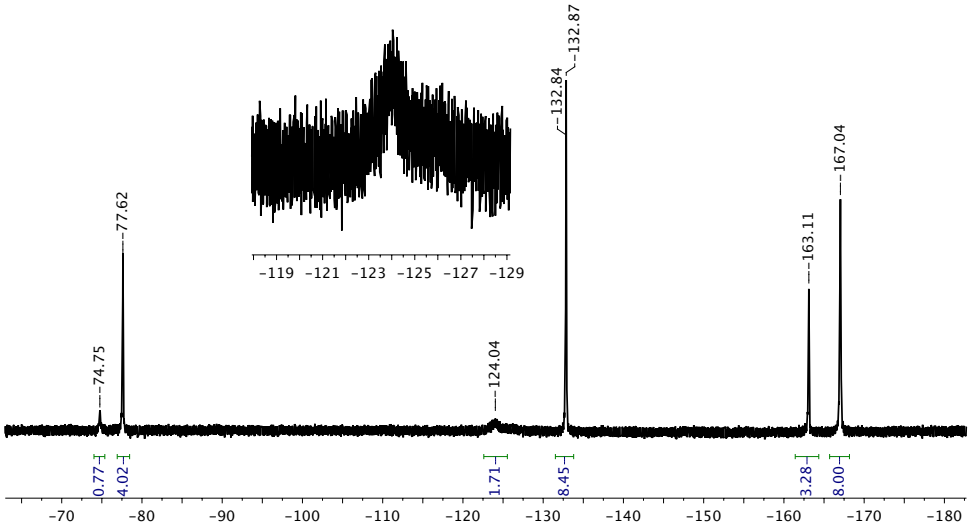

Figure 4.14 ^{19}F NMR spectrum of the reaction between **2-6** and **4-34**.

Reaction between (^{F}PNP^{iPr})PdCl (2-4) and 4-35 (attempted synthesis of 4-43). In an oven-dried J. Young tube, **2-4** (15 mg, 0.030 mmol) was dissolved in C_6D_6. To the resulting solution, **4-35** (23 mg, 0.030 mmol) was added as a solid. After allowing the resulting mixture to react overnight a mixture of two minor unknown products, and **2-4** was observed by ^{19}F and ^{31}P NMR spectroscopy.

Reaction between 2-6 and 4-34. In an oven-dried J. Young tube, **2-6** (10 mg, 0.014 mmol) was dissolved in 0.5 mL of toluene. To the resulting solution, **4-34** (11 mg, 0.015 mmol) was added as a solid. A slight color change from purple to blue was

observed upon mixing the above reagents. Analysis of the resulting solution gave no observable signals by ^{31}P NMR spectroscopy, and ^{19}F NMR spectrum was obtained (shown in **Figure 4.14**). The ^{19}F NMR spectrum shows a broad signal at −124.0 ppm.

Reaction of 2-6 with 4-39 in C_6D_5Br in the dark (observation of (4-45)). In an oven-dried J. Young tube, **2-6** (15 mg, 0.022 mmol) was dissolved in 0.5 mL of C_6D_5Br. To the solution **4-39** (13 mg, 0.023 mmol) was added and allowed to react for 5 min. The resulting green solution was covered in aluminum foil, and left undisturbed at ambient temperature overnight. No change was observed. ^1H NMR (C_6D_5Br): δ 7.10 (m, 2H, Ar-H, overlapping with residual toluene), 6.75 (broad t, 2H, Ar-H), 6.62 (broad s, 2H, Ar-H), 2.85 (s, 1H, HCB), 1.87 (broad s, 4H, CH), 1.04 (app. quartet (dvt), 12H, J = 10 Hz, PCH*Me*$_2$)), 0.93 (app. quartet (dvt), 12H, J = 10 Hz, PCH*Me*$_2$) (**Figure 4.15**); $^{31}P\{^1H\}$ NMR (C_6D_5Br): δ 59.3 (s); ^{19}F NMR (C_6D_5Br): δ −122.6.

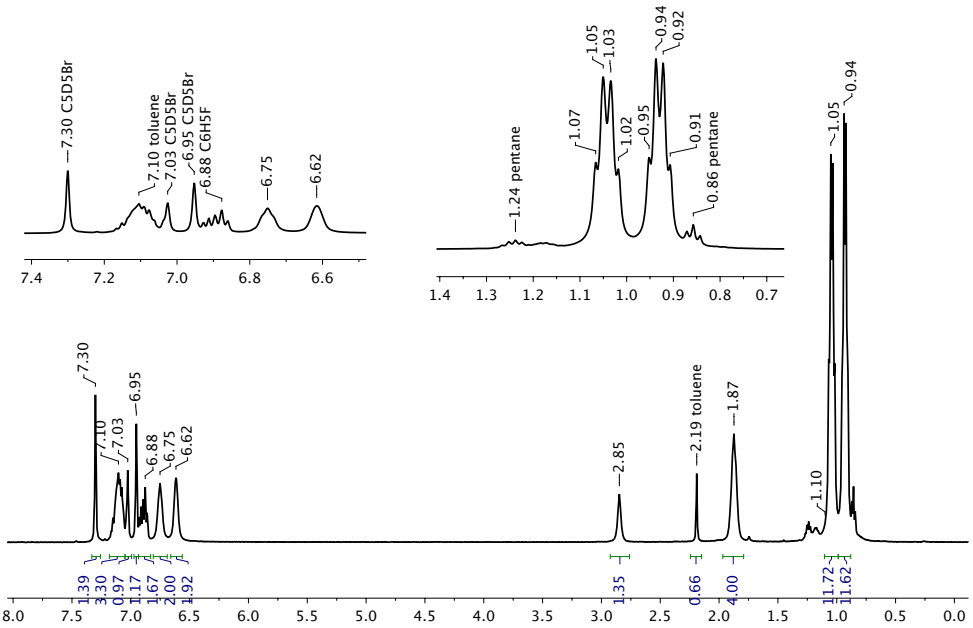

Figure 4.15 ^{1}H NMR spectrum of **4-45** in C_6D_5Br.

Reaction of 2-6 with 4-39 in C_6H_5Br under photolysis (photolysis of 4-45). An oven-dried, J. Young tube was charged with **2-6** (15 mg, 0.022 mmol), and 0.5 mL of C_6D_5Br. To the solution, **4-39** was added and allowed to react for 5 min, producing a green solution. Upon exposure to light from a 250-W halogen lamp the solution began to change color from the original light green to a dark green color. The J. Young tube was then placed in a 250 mL water bath to maintain the temperature below 60 ˚C. After irradiating the sample overnight, ^{31}P, ^{1}H, and ^{19}F NMR spectroscopy confirmed that **4-45** was consumed. The sample was then treated with excess Cp_2Fe (8.0 mg, 0.043 mmol), and the solution was passed thru silica gel. After removing the volatiles, the solid was washed with pentane and re-dissolved in 0.5 mL of C_6D_6. Based on ^{19}F, ^{31}P, and ^{1}H

NMR the major product was (^{F}PNP)PdBr (**3-9**) (81%), and three minor unknown products (19%) (**Figure 4.16**).

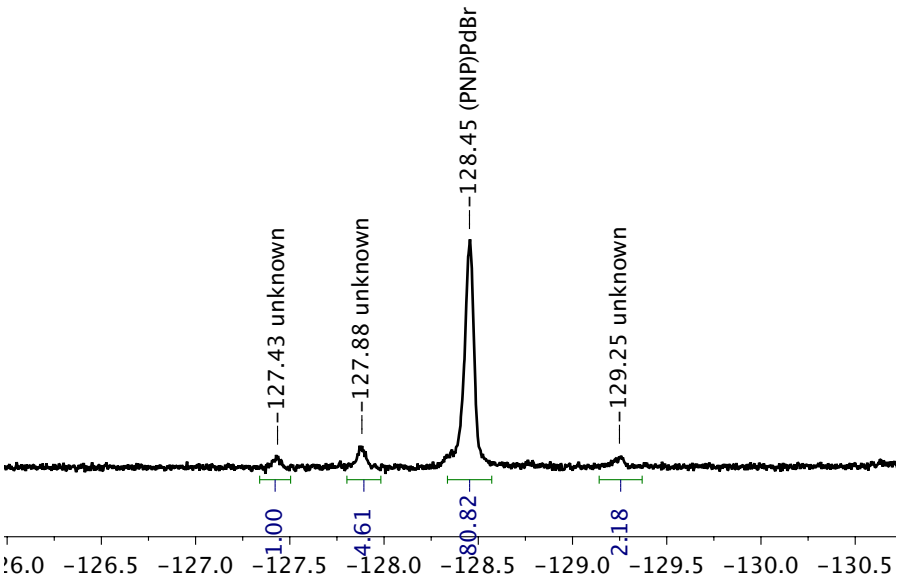

Figure 4.16 ^{19}F NMR spectrum of product mixture after irradiation of **4-45** followed by reduction with excess Cp_2Fe.

Reaction between 2-6 and 4-41 in $CH_3C_6H_5$ (observation of 4-47). In an oven-dried J. Young tube, **2-6** (10 mg, 0.015 mmol) was dissolved in 0.5 mL of toluene. To the resulting solution **4-41** (11 mg, 0.018 mmol) was added as a solid, and allowed to thoroughly mix, producing a green solution. $^{31}P\{^1H\}$ NMR ($CH_3C_6H_5$): δ 57.7 (s); ^{19}F NMR ($CH_3C_6H_5$): δ −123.6 (broad s) (major product) and two minor signals at −124.8 ppm and −125.3 ppm (**Figure 4.17**).

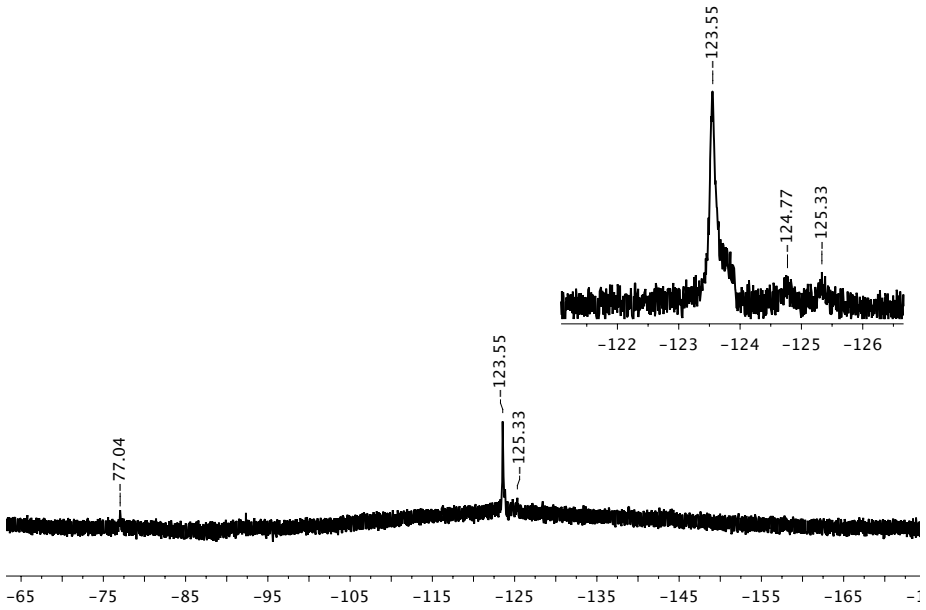

Figure 4.17 ^{19}F NMR spectrum of the product mixture of the reaction between **2-6** and **4-47**; observed products: **4-47** and **4-48**.

Reaction between 2-6 and Na[$CMeB_{11}Cl_{11}$] (4-40) in $CH_3C_6H_5$ (observation of 4-48). In an oven-dried J. Young tube, **2-6** (10 mg, 0.015 mmol) was dissolved in 0.5 mL of toluene and **4-40** (8.0 mg, 0.014 mmol) was added. The J. Young tube was shaken

to assure proper mixing of the reagents. As the reagents mixed a color change from purple to green was observed. $^{31}P\{^{1}H\}$ NMR ($CH_3C_6H_5$): δ 57.9 (s); Two major products were observed by ^{19}F NMR spectroscopy in $CH_3C_6H_5$ (**Figure 4.18**):

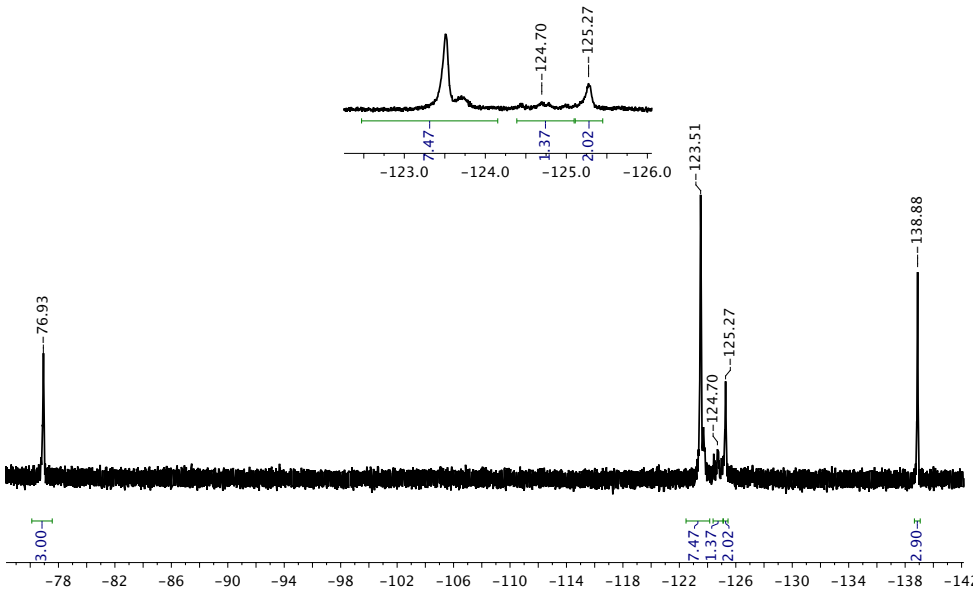

Figure 4.18 ^{19}F NMR spectrum of the product mixture of the reaction between **2-6** and **4-40**.

Reaction between 2-25 and 4-39 (observation of 4-62). In an oven-dried J. Young tube, **2-25** (10 mg, 0.013 mmol) was dissolved in 0.5 mL of C_6D_6. To the solution, **4-39** (3 mg, 0.02 mmol) was added as a solid, and the solution was thoroughly mixed. As the reaction was mixed, the solution changed from a blue to a light blue/green color. ^{1}H NMR (C_6D_6): δ 6.95 (broad s, 4H, Ar-H), 6.43 (broad s, 2H, Ar-H), 2.54 (s,

1H, HCB), 1.33 (t, 36H, $C(CH_3)_3$, J_{P-H} = 8 Hz) (**Figure 4.19**); $^{31}P\{^1H\}$ NMR (C_6D_6): δ 72.1 (s); ^{19}F NMR (C_6D_6): δ −124.9 (2F, s), −75.0 (3F, s).

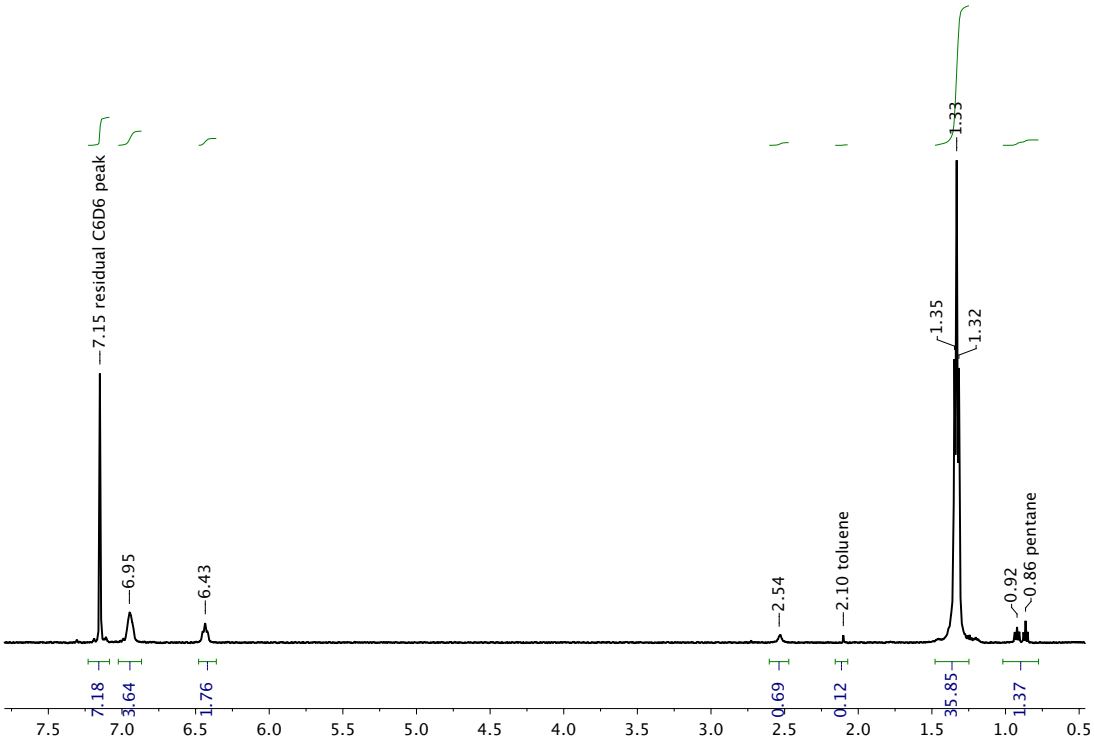

Figure 4.19 ^1H NMR spectrum of reaction between **2-25** and **4-39** in C_6D_6 (observation of **4-62**).

Reaction between 2-25 and $[^iPr_3Si(CH_3C_6H_5)]^+[CHB_{11}Cl_{11}]^-$ (4-39) (potential observation of 4-63, 4-64, 4-65) . In an oven-dried J. Young tube, **2-25** (8 mg, 0.01 mmol) was dissolved in 0.5 mL of C_6D_6. To the resulting solution, **4-39** (8 mg, 0.01 mmol) was added as a solid, and the solution was thoroughly mixed by shaking the J. Young tube vigorously. Upon mixing, a brown/yellow precipitate was formed from a

yellow/brown solution. The solution was dried under vacuum, and redissolved in C_6H_5F. Upon contact with C_6H_5F, the solution changed to a dark green color. The product of the reaction was silent by ^1H, ^{31}P, and ^{19}F NMR spectroscopy; $^iPr_3SiOTf$ was observed by ^1H and ^{19}F NMR spectroscopy.

Synthesis of [(^{F}PNP^{iPr})Pd(OH$_2$)]$^+$[BArF$_{24}$]$^-$ (4-66). In an oven-dried J. Young tube, **2-6** (10 mg, 0.014 mmol) was dissolved in CD_2Cl_2. To the resulting solution, **4-35** (14 mg, 0.016 mmol) was added. Upon mixing, the solution turned a light green color. and a precipitate formed. The sample was filtered through Celite, and treated with degassed water (2.0 μL, 0.11 mmol) outside of the glovebox with an argon flow over the J. Young tube. After shaking the J. Young tube to mix the reagents, a blue solution was produced. The volatiles were removed under vacuum, and the solid was collected. (10 mg, 0.007 mmol, 49%). ^1H NMR (CD_2Cl_2): δ 7.34 (broad s, 2H, Ar-H), 6.86 (broad s, 4H, Ar-H), 2.48 (m, 4H, C*H*Me$_2$), 1.36 (m, 12H, CH*Me*$_2$), 1.27 (m, 12H, CH*Me*$_2$); $^{31}P\{^1H\}$ NMR (CD_2Cl_2): δ 53.0 (s); ^{19}F NMR (CD_2Cl_2): δ −63.6 (24F, s), −126.2 (2F, s).

Reaction of [(^{F}PNP^{iPr})Pd(OH$_2$)]$^+$[BArF$_{24}$]$^-$ (4-66) with molecular sieves 4 Å. In an oven-dried J. Young tube, **4-66** (10 mg, 6.0 μmol) was dissolved in C_6D_6 (0.5 mL). To the resulting solution two beads of 4 Å molecular sieves were added. After leaving the reaction overnight, no change was observed by NMR spectroscopy.

Synthesis of [(^{F}PNP^{iPr})Pd(THF)]$^{+}$[CHB$_{11}$Cl$_{11}$]$^{-}$ (4-67). In an oven-dried, 10 mL flask, **2-6** (15 mg, 0.022 mmol) was dissolved in 0.3 mL C_6D_6. To the resulting solution, **4-39** (15 mg, 0.028 mmol) and THF (145 mg, 163 mL, 0.160 mmol) were added and allowed to stir for 5 min. The volatiles were removed under vacuum. The resulting solid was dissolved in 0.5 mL of CD_2Cl_2, and filtered through a pad of Celite. The solution was concentrated by partial removal of the solvent under vacuum, layered with pentane, and placed in the freezer at −35 °C overnight. The supernatant was decanted, and the solid was dried (23 mg, 0.015 mmol, 70%). ^{1}H NMR (CD_2Cl_2): 7.30 (m, 2H), 6.86 (m, 4H), 3.99 (m, OC*H*$_2$CH$_2$, 4H), 2.47 (m, PC*H*Me$_2$, 4H), 2.10 (m, OCH$_2$C*H*$_2$), 1.41 (dvt, 12H, CH*Me*$_2$), 1.30 (dvt, 12H, CH*Me*$_2$); ^{13}C{^{1}H} NMR (CD_2Cl_2): δ 162.0 (t, J = 10 Hz), 157.8 (dt, J = 245 Hz, J = 5 Hz), 122.0 (d, J = 23 Hz), 120.3 (m, overlapping signals), 120.0 (d, J = 23 Hz), 117.5 (d, J = 21 Hz), 79.8 (s), 49.7 (s, H*C*B$_{11}$Cl$_{11}$), 27.6 (s), 27.7 (s), 20.9 (s, PCH*Me*$_2$), 19.9 (s, PCH*Me*$_2$).

Synthesis of [(^{F}PNP^{iPr})Pd(Py)]$^{+}$[CMeB$_{11}$Cl$_{11}$]$^{-}$ (4-68). In an oven-dried J. Young tube, **2-6** (15 mg, 0.022 mmol) was dissolved in 0.5 mL of C_6H_5F. To the resulting solution, **4-40** (13 mg, 0.023 mmol) was added as a solid. After shaking the J. Young tube vigorously the solution changed from a blue/purple to a green color. The solution was then filtered through a pad of Celite. Excess pyridine (0.2 mL) was added, and an immediate color change from green to purple was observed. The solution was crashed out with pentane, and the resulting solid was dried under vacuum (Yield: not isolated). ^{1}H NMR (CD_2Cl_2): δ 8.65 (*o*-Py, d, J = 4 Hz), 8.10 (*p*-Py, t, J = 9 Hz), 7.72 (*m*-

Py, t, J = 7 Hz), 7.41 (m, 2H, Ar-H), 6.91 (t, 2H, J = 7 Hz, Ar-H), 6.84 (m, 2H, Ar-H), 2.40 (m, 4H, PC*H*Me$_2$), 1.57 (s, 3H, CH$_3$-CB), 1.21 (app. quartet (dvt), 12H, J = 8 Hz, PCH*Me*$_2$), 1.03 (app. quartet (dvt), 12H, J = 8 Hz, PCH*Me*$_2$); ^{31}P{^{1}H} NMR (CD_2Cl_2): δ 51.1 (s); ^{19}F NMR (CD_2Cl_2): δ −126.4 (m, C-F).

Synthesis of [(^{F}PNP^{iPr})Pd(μ-OH)Pd(^{iPr}PNP^{F})]$^+$[BArF$_{24}$]$^-$ (4-69). In an oven-dried J. Young tube, **2-6** (10 mg, 0.014 mmol) was dissolved in C_6H_5F and **4-35** (14 mg, 0.016 mmol) was added as a solid and allowed to react for a few minutes. To the resulting solution **2-8** (8.0 mg, 0.014 mmol) was added as a solid, and an immediate color change from blue/green to a darker green was observed. The volatiles were removed under vacuum, redissolved in a minimum amount of C_6H_5F, carefully layered with pentane, and placed in the freezer at −35 °C. The solid was collected, and dried under vacuum (15 mg, 0.008 mmol, 55%). ^{1}H NMR (C_6H_5F): δ (aromatic signals overlapping with solvent), 2.36 (m, 4H, C*H*Me$_2$), 1.56 (m, 12H, CH*Me*$_2$), 1.22 (m, 12H, CH*Me*$_2$), −3.02 (bs, 1H, OH); ^{31}P{^{1}H} NMR (C_6H_5F): δ 47.3 (s); ^{19}F NMR (C_6H_5F): δ −63.3 (24F, s), −125.1 (2F, s).

Attempted deprotonation of 4-69 with NaH. In an oven-dried J. Young tube, **2-6** (10 mg, 0.014 mmol) was dissolved in C_6H_5F, and **4-35** (14 mg, 0.016 mmol) was added, and allowed to react for a few minutes. **2-8** (8.0 mg, 0.014 mmol) was added as a solid, and an immediate color change from blue/green to a darker green was observed. The resulting solution was treated with NaH (1.0 mg, 0.014 mmol), and allowed to react

overnight. No change was observed by NMR spectroscopy. The sample was placed in an 86 °C oil bath, and allowed to react for 24 h. During this time, the solution turned an orange color; NMR spectroscopy confirmed the formation of **2-7.**

Synthesis of 4-71 and 4-72 mixture. In an oven-dried J. Young tube, **2-6** (50 mg, 0.072 mmol) was dissolved in 0.6 mL of C_6H_5F. To the resulting solution **4-35** (64 mg, 0.072 mmol) was added as a solid. The resulting solution was treated with O_2 (760 torr, 0.072 mmol); upon contact with O_2 the solution turned a dark green color. The solution was filtered through a pad of Celite, the volatiles were removed, and the solid was dried by vacuum. The solid was then redissolved in a minimum amount of C_6H_5F, layered with pentane, and placed in the freezer at −35 °C. The supernatant was removed, and the solid was dried under vacuum (52 mg, 0.036 mmol, 50%; assuming **4-71** is the structure). The solid was analyzed by EPR spectroscopy (**Figure 4.20**).

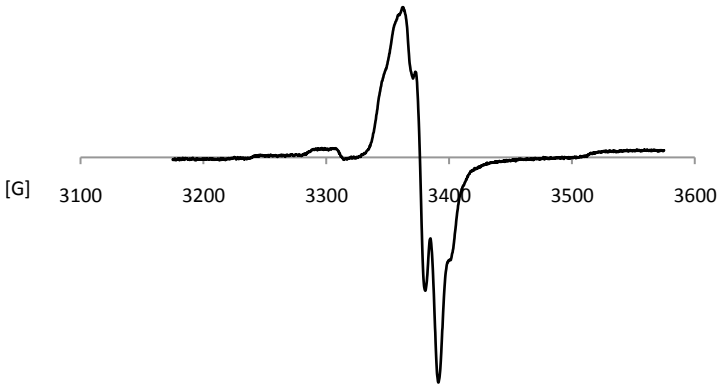

Figure 4.20 Room-temperature EPR spectrum of a mixture of **4-71** and **4-72**.

Reaction between 4-71 and MeCN. In an oven-dried J. Young tube, **4-71** (10 mg, 7 μmol) was dissolved in 0.5 mL C_6H_5F. The resulting solution was treated with a large excess of MeCN. Overnight, the reaction color changed from dark green to purple, and formation of **4-73** was confirmed by ^{19}F and ^{31}P NMR spectroscopy.

Reaction between 4-71 and 4-72 and H_2O. In an oven-dried J. Young tube, **4-71** (10 mg, 7 μmol) was dissolved in 0.5 mL C_6H_5F. The resulting solution was treated with a saturated solution of H_2O in C_6H_5F. After leaving the reaction overnight, no **4-66** was observed by ^{19}F and ^{31}P NMR spectroscopy. The resulting solution was silent by NMR spectroscopy.

Reaction between [(^{F}PNP^{iPr})Pd-]$_2$ (2-10) and Ag[$CHB_{11}Cl_{11}$] (4-6). In an oven-dried J. Young tube, **2-10** (14 mg, 0.013 mmol) was dissolved in 0.50 mL of C_6H_5F. To the resulting solution **4-6** (14 mg, 0.024 mmol) was added as a solid. After allowing the solution to stir for 10 min, excess CH_3CN (0.2 mL) was added. Three unknown products were observed by ^{19}F NMR spectroscopy (silent by ^{31}P NMR spectroscopy).

Attempted crystal growth from reactions between 4-1 and 4-40, 4-41, 4-50. Three oven-dried vials were charged with **4-1** (10 mg, 0.015 mmol), and dissolved in 0.50 mL of toluene ($C_6H_5CH_3$). Each of the resulting solutions was treated with **4-40** (0.017 mmol), **4-50** (0.017 mmol) or **4-41** (0.017 mmol). After stirring the solutions for

5 min, the solutions were filtered through a plug of Celite into a small oven-dried vial. The solutions were carefully layered with pentane and placed in the glovebox freezer at −35 °C. After leaving the solution from the reaction between **4-50** and **4-1** in the freezer for over a week, small rhombus-like crystals were formed at the bottom of the vial. A single X-ray quality crystal was selected, and the X-ray structure was determined to be **4-55a** (**Figure 4.7;** see crystallographic section for data).

Attempted Crystal Growth of (^{F}PNP^{iPr})Pd[CHB$_{11}$Br$_{11}$] (4-51). In an oven-dried 10 mL vial, **2-6** (7.0 mg, 0.11 mmol) was dissolved in C_6H_5F. **4-35** (10 mg, 0.11 mmol) was added, and allowed to stir for 5 min. The solution was filtered through Celite. The resulting solution was carefully layered with a saturated solution of **4-54** in $C_6H_4F_2$ and allowed to slowly diffuse. After 2 d, no crystals were produced in the reaction. The solution was then layered with pentane, and placed in the freezer at −35 °C. No crystals were produced.

Attempted crystal growth of [(^{F}PNP^{iPr})Pd]$_2$[B$_{11}$Cl$_{12}$] (4-52). In a 25 mL vial, **2-6** (10 mg, 0.014 mmol) was dissolved in $C_6H_4F_2$. **4-35** (13 mg, 0.015 mmol) was added and the solution was allowed to stir for 30 min. The solution was filtered through a pad of Celite. In a separate vial, **4-53** (15 mg, 0.014 mmol) was dissolved in $C_6H_4F_2$. The solution with **4-43** was carefully layered with the solution of **4-53**. After allowing the solution to mix by diffusion, no crystals were formed. The same experiment was run, but instead the solution of **4-53** was layered with the solution of **4-43**. After allowing the

solution to mix by diffusion, several X-ray quality crystals grew from the solution. Based on single-crystal x-ray diffraction analysis, the structure was determined to be $[(^{F}PNP^{iPr})PdOH_2]^{+}[B_{12}Cl_{12}]^{2-}Na^{+}$ (**4-52a**) (see **Figure 4.21** for ORTEP image).

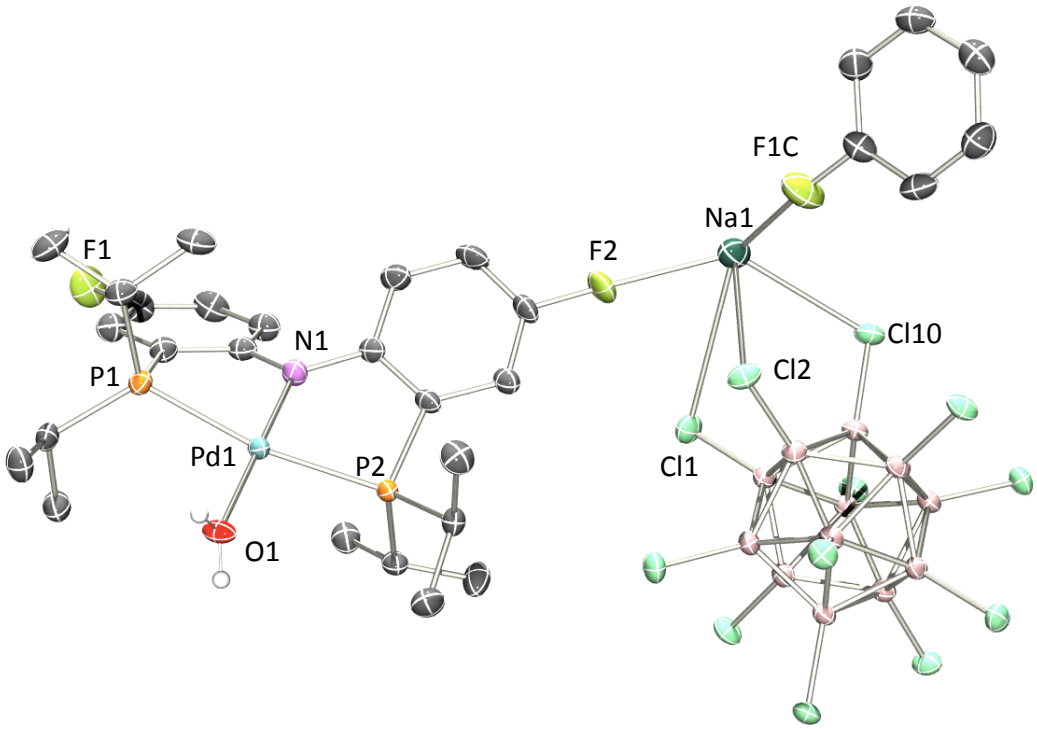

Figure 4.21 POV-Ray rendition of the ORTEP[162] drawing (50% thermal ellipsoids) of **4-52a** showing selected atom labeling. Hydrogen atoms (except for OH_2) and disordered *o*-$C_6H_4F_2$ were omitted for clarity. Selected bond distances (Å) and angles (deg): Pd1−P1, 2.3317(9); Pd1−P2, 2.3229(9); Pd1−O1, 2.1057(15); Pd1−N1, 1.9937(18); Na1-F2, 2.3742(17); Na1-F1C, 2.3470(18); P1−Pd1−P2, 162.32(2); O1−Pd1−N1, 179.53(7).

Attempted crystal growth of (^{F}PNP^{iPr})Pd[CRB$_{11}$Cl$_{11}$] (R = Me (4-48), Et (4-56), ^{n}Bu (4-47)). Three oven-dried vials were charged with **2-6** (10 mg, 0.014 mmol) and dissolved in 0.50 mL of toluene ($C_6H_5CH_3$). Each of the resulting solutions was treated with **4-40** (10 mg, 0.017 mmol), **4-50** (10 mg, 0.017 mmol) or **4-41** (10 mg, 0.017 mmol). After stirring the solutions for 5 min, the solution was filtered through a plug of Celite into a small oven-dried vial. The solutions were carefully layered with pentane and placed in the glovebox freezer at −35 °C. After leaving the solution in the freezer for over a week no X-ray quality crystals were formed.

Synthesis of ^{i}Pr$_3$Si[CMeB$_{11}$Cl$_{11}$]•(CH$_3$C$_6$H$_5$) (4-15). In an oven-dried vial, $Ph_3C[CMeB_{11}Cl_{11}]$ (40 mg, 0.051 mmol) was treated with a minimal amount of toluene. $^{i}Pr_3SiH$ (247 mg, 1.60 mmol) was added and the solution was allowed to stir over the weekend. The solution was triturated with pentane. The solid was redissolved with ODCB, and again triturated using pentane. This was repeated a total of three times. ^{1}H NMR spectroscopy in C_6D_5Br revealed residual silane. The solid was redissolved in minimum amount of toluene (approx. 0.05 mL) and triturated with pentane a total of three times. The solid was dried by gentle ventilation of argon using a pipette (16 mg, 0.020 mmol, 40%). A second ^{1}H NMR spectrum in C_6D_5Br no longer showed residual silane. The resulting solid was used as is in subsequent reactions. ^{1}H NMR (C_6D_5Br): δ 1.24 (m, 3H, C*H*Me$_2$), 0.81 (d, $J_{H\text{-}H}$ = 7 Hz, 18H, CH*Me*$_2$).

Synthesis of $^{i}Pr_3Si[CEtB_{11}Cl_{11}]\bullet(CH_3C_6H_5)$ (4-16). In an oven-dried vial, $Ph_3C[CEtB_{11}Cl_{11}]$ (105 mg, 0.130 mmol) was dissolved in a minimal amount of toluene. To the solution, $^{i}Pr_3SiH$ (315 mg, 2.00 mmol) was added, and allowed to stir over the weekend. The solution was triturated with pentane. The solid was redissolved in toluene, and triturated with pentane a total of three times. The solid was dried by gentle ventilation using a pipette (75 mg, 0.94 mmol, 72%). A ^{1}H NMR spectrum in C_6D_5Br showed no residual silane. The resulting solid was used as is in subsequent reactions. ^{1}H NMR (C_6D_5Br): δ 2.63 (q, J_{H-H} = 8 Hz, 2H, CH_3CH_2C), 1.44 (t, J_{H-H} = 8 Hz, 3H, CH_3CH_2C), 1.18 (m, 3H, $CHMe_2$), 0.79 (d, J_{H-H} = 8 Hz, 18H, $CHMe_2$).

Synthesis of $[^{n}Bu_4N]_2^{+}[B_{12}Cl_{12}]^{2-}$ (4-53). In 10 mL vial, $Cs_2B_{12}Cl_{12}$ (139 mg, 0.170 mmol) was dissolved in 2 mL of H_2O. In a separate vial, $^{n}Bu_4NCl$ (56 mg, 0.20 mmol) was dissolved in 1 mL of H_2O. Upon mixing both solutions, a white precipitate was formed. The solid was isolated by filtration, and dried under vacuum overnight. The solid was used as is in subsequent reactions.

4.4.2 X-ray diffraction experiments

Data collection for 4-22 (solved by Dr. Reibenspies, J. H.). In an oven-dried vial, a small quantity of **4-22** was dissolved in a minimum amount of toluene and was carefully layered with pentane and placed in the freezer at −35 °C and overnight several colorless crystals were formed. A Leica Z microscope was used to identify a suitable colorless cube 0.085 × 0.068 × 0.063 mm from a representative sample of crystals of the

same habit. The crystal was coated in a cryogenic protectant (paratone), and was then fixed to a loop, which in turn was fashioned to a copper-mounting pin. The mounted crystal was then placed in a cold nitrogen stream (Oxford) maintained at 110 K.

A BRUKER SMART X-ray three-circle diffractometer was employed for crystal screening, unit cell determination and data collection. The goniometer was controlled using the SMART1000 software suite (Microsoft operating system). The sample was optically centered with the aid of a video camera such that no translations were observed as the crystal was rotated through all positions. The detector was set at 5.0 cm from the crystal sample (CCD, 512 × 512 pixel). The X-ray radiation employed was generated from a Mo sealed X-ray tube (K_α = 0.70173 Å with a potential of 50 kV and a current of 40 mA), and filtered with a graphite monochromator in the parallel mode (175 mm collimator with 0.8 mm pinholes).

Dark currents were obtained for the appropriate exposure time 10 s, and a rotation exposure was taken to determine crystal quality and the X-ray beam intersection with the detector. The beam intersection coordinates were compared to the configured coordinates and changes were made accordingly. The rotation exposure indicated acceptable crystal quality, and the unit cell determination was undertaken. Forty data frames were taken at widths of 0.5° with an exposure time of 10 s. Over 200 reflections were centered and their positions were determined. These reflections were used in the auto-indexing procedure to determine the unit cell. A suitable cell was found and refined by nonlinear least squares and Bravais lattice procedures and reported. The unit cell was

verified by examination of the *h k l* overlays on several frames of data, including zone photographs. No super-cell or erroneous reflections were observed.

After careful examination of the unit cell, a standard data collection procedure was initiated. This procedure consists of collection of one hemisphere of data collected using omega scans, involving the collection over 2400 0.3° frames at fixed angles for φ, 2θ, and χ (2θ = −28°, χ = 54.73°), while varying omega. Each frame was exposed for 20 s and contrasted against a 20 s dark current exposure. The total data collection was performed for duration of approximately 12 h at 110 K. No significant intensity fluctuations of equivalent reflections were observed. After data collection, the crystal was measured carefully for size, morphology and color.

Table 4.3 Crystal data and structure refinement for 4-22.

Empirical formula	$C_{26}H_{38}F_5NO_3P_2PdS$	
Formula weight	707.97	
Temperature	110(2) K	
Wavelength	0.71073 Å	
Crystal system	Monoclinic	
Space group	*P2(1)/c*	
Unit cell dimensions	a = 15.615(6) Å	α = 90°
	b = 12.698(5) Å	β = 116.656(5)°
	c = 16.996(6) Å	γ = 90°
Volume	3011.8(19) $Å^3$	
Z	4	
Density (calculated)	1.561 Mg/m^3	
Absorption coefficient	0.851 mm^{-1}	
F(000)	1448	
Crystal size	0.08 × 0.06 × 0.06 mm^3	
Theta range for data collection	1.46 to 25.00°	
Index ranges	$-18 \le h \le 18$, $-15 \le k \le 15$, $-20 \le l \le 20$	
Reflections collected	28083	
Independent reflections	5258 [R(int) = 0.0957]	
Completeness to theta = 25.00°	99.2%	
Absorption correction	Semi-empirical from equivalents	
Max. and min. transmission	0.9915 and 0.9350	
Refinement method	Full-matrix least-squares on F^2	
Data / restraints / parameters	5258 / 0 / 362	
Goodness-of-fit on F^2	1.007	
Final R indices [I>2σ(I)]	$R1$ = 0.0429, $wR2$ = 0.0914	
R indices (all data)	$R1$ = 0.0889, $wR2$ = 0.1263	
Extinction coefficient	0.0005(2)	
Largest diff. peak and hole	0.746 $eÅ^{-3}$ and −0.597 $eÅ^{-3}$	

Data collection for 4-52a (solved by Dr. Reibenspies, J. H.). In a 25 mL vial, **2-6** (10 mg, 0.014 mmol) was dissolved in $C_6H_4F_2$. To the resulting solution, **4-35** (13 mg, 0.015 mmol) was added and allowed to stir for 30 min and then filtered through a pad of Celite. In a separate vial, **4-53** (15 mg, 0.014 mmol) was dissolved in $C_6H_4F_2$. The solution with **4-53** was carefully layered with the solution of **4-43**. After allowing the solution to mix by diffusion (approx. 5 d), several X-ray quality crystals grew from the solution. A Leica Z microscope was used to identify a suitable colorless cube 0.170 × 0.160 × 0.130 mm from a representative sample of crystals of the same habit. The crystal was coated in a cryogenic protectant (paratone), and was then fixed to a loop, which in turn was fashioned to a copper-mounting pin. The mounted crystal was then placed in a cold nitrogen stream (Oxford) maintained at 110 K.

A BRUKER SMART X-ray three-circle diffractometer was employed for crystal screening, unit cell determination, and data collection. The goniometer was controlled using the SMART1000 software suite (Microsoft operating system). The sample was optically centered with the aid of a video camera such that no translations were observed as the crystal was rotated through all positions. The detector was set at 5.0 cm from the crystal sample (CCD, 512 × 512 pixel). The X-ray radiation employed was generated from a Mo sealed X-ray tube (K_α = 0.70173 Å with a potential of 50 kV and a current of 40 mA) and filtered with a graphite monochromator in the parallel mode (175 mm collimator with 0.8 mm pinholes).

Dark currents were obtained for the appropriate exposure time 10 s, and a rotation exposure was taken to determine crystal quality, and the X-ray beam

intersection with the detector. The beam intersection coordinates were compared to the configured coordinates, and changes were made accordingly. The rotation exposure indicated acceptable crystal quality, and the unit cell determination was undertaken. Forty data frames were taken at widths of 0.5° with an exposure time of 10 s. Over 200 reflections were centered and their positions were determined. These reflections were used in the auto-indexing procedure to determine the unit cell. A suitable cell was found, and refined by nonlinear least squares and Bravais lattice procedures. The unit cell was verified by examination of the *h k l* overlays on several frames of data, including zone photographs. No super-cell or erroneous reflections were observed.

After careful examination of the unit cell, a standard data collection procedure was initiated. This procedure consists of collection of one hemisphere of data collected using omega scans, involving the collection over 2400 0.3° frames at fixed angles for φ, 2θ, and χ (2θ = −28°, χ = 54.73°), while varying omega. Each frame was exposed for 20 s, and contrasted against a 20 s dark current exposure. The total data collection was performed for duration of approximately 12 h at 110 K. No significant intensity fluctuations of equivalent reflections were observed. After data collection, the crystal was measured carefully for size, morphology and color.

Table 4.4 Crystal data and structure refinement for 4-52a.

Empirical formula	$C_{36}H_{45}B_{12}Cl_{12}F_5NNaOP_2Pd$	
Formula weight	1344.37	
Temperature	110(2) K	
Wavelength	0.71073 Å	
Crystal system	Monoclinic	
Space group	*P21/c*	
Unit cell dimensions	a = 13.315(5) Å	α = 90°
	b = 28.952(12) Å	β = 96.974(4)°
	c = 14.729(6) Å	γ = 90°
Volume	5636(4) $Å^3$	
Z	4	
Density (calculated)	1.584 Mg/m^3	
Absorption coefficient	1.011 mm^{-1}	
F(000)	2679	
Crystal size	0.170 × 0.160 × 0.130 mm^3	
Theta range for data collection	1.541 to 27.527°	
Index ranges	$-17 \le h \le 17$, $-37 \le k \le 37$, $-19 \le l \le 19$	
Reflections collected	65865	
Independent reflections	12971 [R(int) = 0.0554]	
Completeness to theta = 25.242°	100.0%	
Absorption correction	Semi-empirical from equivalents	
Max. and min. transmission	0.7456 and 0.6495	
Refinement method	Full-matrix least-squares on F^2	
Data / restraints / parameters	12971 / 270 / 712	
Goodness-of-fit on F^2	1.030	
Final R indices [I>2σ(I)]	$R1$ = 0.0292, wR2 = 0.0724	
R indices (all data)	$R1$ = 0.0371, wR2 = 0.0771	
Extinction coefficient	n/a	
Largest diff. peak and hole	0.878 $eÅ^{-3}$ and −0.643 $eÅ^{-3}$	

Data collection for 4-55a (solved by Dr. Bhuvanesh, N.). An oven-dried vial was charged with **2-6** (10 mg, 0.015 mmol), and dissolved in 0.50 mL of toluene ($C_6H_5CH_3$). The resulting solution was treated with **4-50** (0.017 mmol). After stirring the solutions for 5 min, the solutions were filtered through a plug of Celite into a small oven-dried vial. The solutions were carefully layered with pentane and placed in the glovebox freezer at −35 °C. After leaving the solution in the freezer for over a week, small rhombus like crystals were formed at the bottom of the vial. A Leica MZ 75 microscope was used to identify a suitable green block with very well defined faces with dimensions (max, intermediate, and min) 0.24 × 0.14 × 0.08 mm from a representative sample of crystals of the same habit. The crystal mounted on a nylon loop was then placed in a cold nitrogen stream (Oxford) maintained at 150 K.

A BRUKER APEX2 X-ray (three-circle) diffractometer was employed for crystal screening, unit cell determination, and data collection. The goniometer was controlled using the APEX2 software suite, v2008-6.0.[177] The sample was optically centered with the aid of a video camera such that no translations were observed as the crystal was rotated through all positions. The detector was set at 6.0 cm from the crystal sample (APEX2, 512 × 512 pixel). The X-ray radiation employed was generated from a Mo sealed X-ray tube (K_α = 0.70173 Å with a potential of 40 kV and a current of 40 mA) fitted with a graphite monochromator in the parallel mode (175 mm collimator with 0.5 mm pinholes).

Sixty data frames were taken at widths of 0.5°. These reflections were used in the auto-indexing procedure to determine the unit cell. A suitable cell was found, and

refined by nonlinear least squares and Bravais lattice procedures. The unit cell was verified by examination of the *h k l* overlays on several frames of data by comparing with both the orientation matrices. No super-cell or erroneous reflections were observed. After careful examination of the unit cell, a standard data collection procedure was initiated using omega and phi scans.

Data reduction, structure solution, and refinement. Integrated intensity information for each reflection was obtained by reduction of the data frames with the program APEX2.[177] The integration method employed a three dimensional profiling algorithm, and all data were corrected for Lorentz and polarization factors, as well as for crystal decay effects. Finally the data was merged and scaled to produce a suitable data set. The absorption correction program SADABS[178] was employed to correct the data for absorption effects.

Systematic reflection conditions and statistical tests of the data suggested the space group *P21/n*. A solution was obtained readily using SHELXTL (XS).[179] Absence of additional symmetry or voids was confirmed using PLATON (ADDSYM).[180] Hydrogen atoms were placed in idealized positions and were set riding on the respective parent atoms. All non-hydrogen atoms were refined with anisotropic thermal parameters. Elongated thermal ellipsoids on C35 and C36 along with residual electron density near C35 indicated possible disorder, which was modeled between two positions with an occupancy ratio of 62:38. Restraints and constraints were used to keep the bond lengths, angles, and thermal ellipsoids meaningful. Also, we suspected bonding of C27 and C33 to Pd1 would cause the hydrogen atoms attached to the former atoms will be out of plane of the toluene ring atoms. The corresponding hydrogen atoms were located from the difference Fourier maps and then were set riding on the parent carbon atoms. Accordingly, the angle between the planes formed by C27, C29, C30, C33, and C27 C33, H33, H27 is 15.86 degrees. The structure was refined (weighted least squares refinement on F^2) to convergence.

Table 4.5 Crystal data and structure refinement for 4-55a.

Empirical formula	$C_{36}H_{53}B_{11}Cl_{11}NP_2Pd$	
Formula weight	1176.99	
Temperature	150(2) K	
Wavelength	0.71073 Å	
Crystal system	Monoclinic	
Space group	*P21/n*	
Unit cell dimensions	a = 9.751(5) Å	α = 90°
	b = 33.768(18) Å	β = 107.346(6)°
	c = 16.327(10) Å	γ = 90°
Volume	5131(5) $Å^3$	
Z	4	
Density (calculated)	1.524 Mg/m^3	
Absorption coefficient	1.027 mm^{-1}	
F(000)	2376	
Crystal size	0.24 × 0.14 × 0.08 mm^3	
Theta range for data collection	1.78 to 27.50°	
Index ranges	$-12 \le h \le 12$, $-43 \le k \le 43$, $-20 \le l \le 21$	
Reflections collected	56296	
Independent reflections	11729 [R(int) = 0.0638]	
Completeness to theta = 27.50°	99.5%	
Absorption correction	Semi-empirical from equivalents	
Max. and min. transmission	0.9223 and 0.7906	
Refinement method	Full-matrix least-squares on F^2	
Data / restraints / parameters	11729 / 5 / 579	
Goodness-of-fit on F^2	1.034	
Final R indices [I>2σ(I)]	$R1$ = 0.0425, wR2 = 0.0884	
R indices (all data)	$R1$ = 0.0704, wR2 = 0.0968	
Largest diff. peak and hole	0.659 $eÅ^{-3}$ and −0.556 $eÅ^{-3}$	

4.4.3 Computational details (Performed by Prof. Gusev at Wilfrid Laurier University)

System	State	Relative Energy (kcal/mol)	Pd-N	Pd-P^1	Pd-P^2	P^1-C^1	P^2-C^2	N-C^1	N-C^2	A
D.Gusev	S	ΔH = 4.0	2.003	2.318	2.366	1.802	1.816	1.403	1.395	
	T		2.131	2.337	2.337	1.838	1.838	1.374	1.374	

Computational details, D.Gusev, MPW1PW91/BS2: SDD+ECP (Pd); 6-311+g(d,p) (N, P); 6-31g(d) (C); 6-31g (H).

CHAPTER V

PHOTO-INDUCED LIGAND ISOMERIZATION OF $[(PNP^{iPr})Pd]^+$ CATIONS

5.1 Introduction

Metal phosphine complexes in the context of catalysis have been the topic of intense research for the past 50 years.[103,159,197] The use of tertiary phosphines has led to the discovery of many industrially relevant catalysts with applications such as hydroformylation, hydrogenation and polymerization.[103,197] In part, their success in catalysis is due to their capacity to stabilize transition metals in variable oxidation states. Traditionally, tertiary phosphines have been viewed as spectator ligands acting only as supporting ligands for transition metal complexes.[313] However, decomposition does occur, and phosphine ligands have been shown to undergo oxidation (**Scheme 5.1, Eq.1**),[314] cyclometalation (**Scheme 5.1, Eq.2**)[3,315,316] or C-P bond cleavage (**Scheme 5.1, Eq. 2-8**)[317-319]

The topic of C-P bond cleavage has been discussed thoroughly in several reviews by Parkins,[320] Garrou,[319] Michman,[317] and more recently by Macgregor.[318] Most of the examples reported in Garrou's review are limited to P-C(Ar) bond cleavage and involve the formation of bimetallic complexes or clusters with bridging phosphido ligands via the transfer of a substituent from the phosphine to the metal center (e.g. **Scheme 5.1**, **Eq. 5-7**). Typically, P-C(sp) bonds are the easiest to cleave followed by P-C(sp^2) and P-C(sp^3). There are relatively few examples of P-C(sp^3) bond cleavage, but the examples that have been reported are limited to activation of PMe_3 (e.g. **Scheme 5.1, Eq. 7**).[321-326]

Eq.1

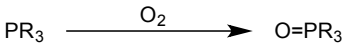

Eq.2

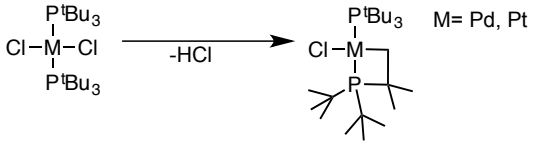

Eq.3

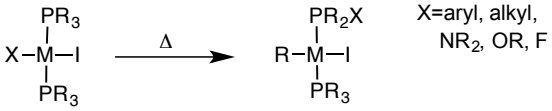

Eq.5

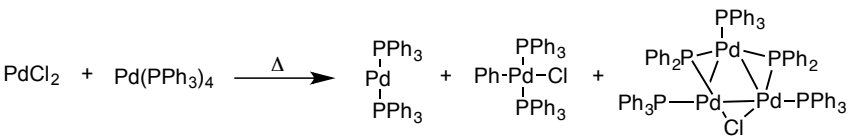

Eq.6

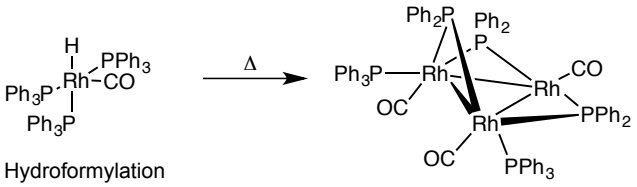

Hydroformylation catalyst **5-1**

Eq.7

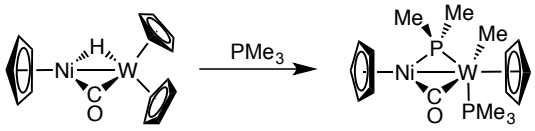

Eq.8

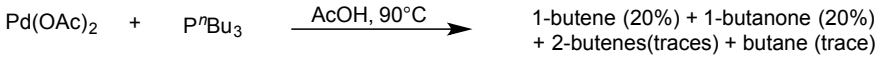

Scheme 5.1 Examples of phosphine decomposition.

In addition, Matsuda and coworkers reported the formation of butene (20%), 1-butanone (20%), 2-butenes (traces), and butane (trace) upon thermolysis of P^nBu_3 with $Pd(OAc)_2$ in acetic acid (**Scheme 5.1**, **Eq. 8**).[327]

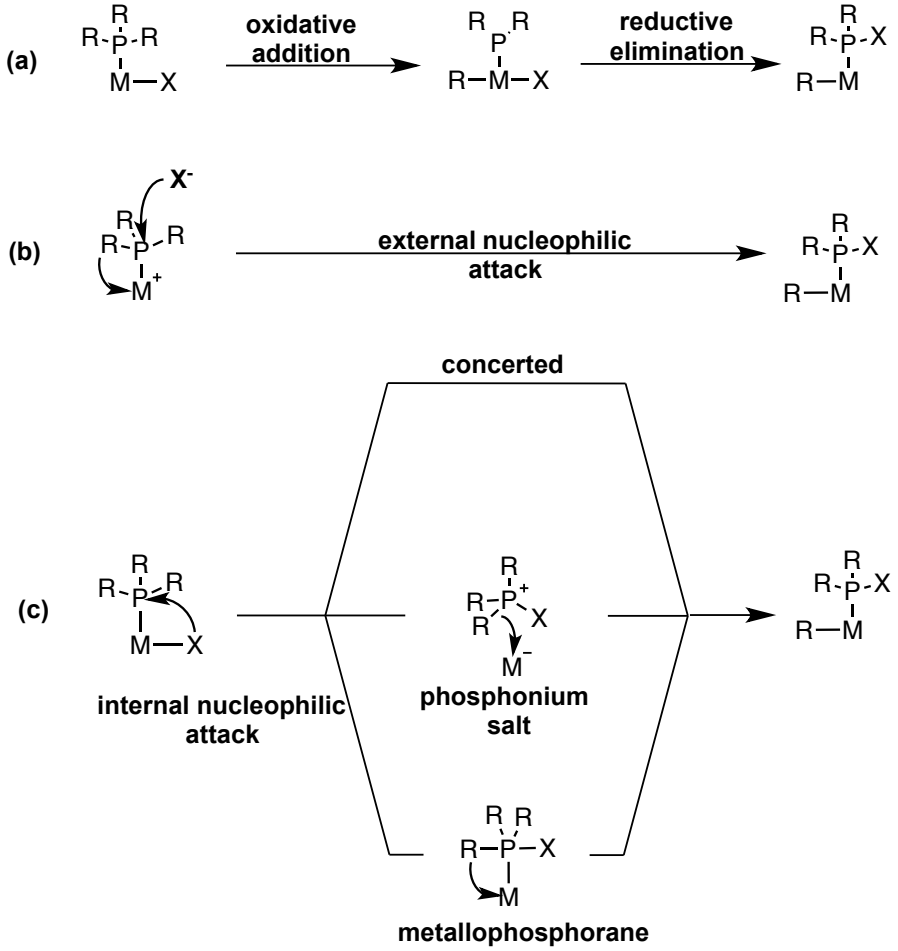

Scheme 5.2 Possible mechanisms for R/X exchange in complexes with the general formula $[L_nM\text{-}PR_3]$ (X = aryl, alkyl, NR_2, OR, F).

In contrast to the reactions discussed in Garrou's review, where the substituent R on the phosphine is transferred to the metal forming a phosphido, in the examples discussed in Macgregor's review the R group in complexes with the general formula [L_nM-PR_3] is exchanged for X (X = aryl, alkyl, NR_2, OR, F) (**Scheme 5.1**, **Eq. 3**). These reactions are believed to occur via, oxidative addition (**a**), nucleophilic attack by X^- (**b**), or by formation of a phosphonium salt (**c**) (**Scheme 5.2**). The mechanism for these reactions is likely dependent on the substituent X. The reactions discussed above are especially relevant in the field catalysis, as phosphine activation via C-P bond cleavage often leads to catalyst deactivation. For example, C-P bond activation has been shown occur upon thermolysis of $(Me_3P)_3RhH(CO)$ (**5-1**), a hydroformylation catalyst (**Scheme 5.1**, **Eq. 6**).[328,329]

This chapter will discuss the unprecedented photo-induced isomerization of the *i*-propyl groups on $[(PNP^{iPr})Pd]^+$ cations to *n*-propyl. The synthesis of $[(PNP^{iPr})Pd]^+$ cations using alkylated carboranes as weakly-coordinating anions was discussed Chapter IV. This unusual isomerization of the ancillary ligand appears to be driven by the coordination of the arene to metal center in $[(^{F}PNP^{iPr})Pd]^+$ cations. The isomerization decreases the steric pressure around the metal center, and as a result allows for tighter coordination of the arene. Although it is not clear whether the isomerization occurs via C-C or C-P bond cleavage, the latter pathway seems more plausible. As discussed above, in most examples of C-P bond cleavage a bridging phosphido complex is formed or P-C/X exchange occurs. In contrast, in the isomerization of $[(^{F}PNP^{iPr})Pd]^+$ cations the final product remains as a tertiary phosphine. The ability of the -P^iPr_2 phosphines in

[(^{F}PNP^{iPr})Pd]$^{+}$ cation to isomerize into the less sterically imposing -P^{n}Pr$_2$ phosphines is quite extraordinary. The phosphines in (^{F}PNP^{iPr})PdX complexes are typically considered spectator ligands; however, the isomerization of [(^{F}PNP^{iPr})Pd]$^{+}$ cations showcases the ability of phosphines to behave, under certain conditions, as non-innocent ligands by modifying the cone angle of the phosphine to accommodate the fourth ligand (e.g. arene).

5.2 Results and Discussion

5.2.1 Initial discovery of isomerization

During our attempts to characterize [(^{F}PNP^{iPr})Pd(arene)]$^{+}$ complexes by single-crystal X-ray crystallography, solutions of (^{F}PNP^{iPr})Pd[CRB$_{11}$Cl$_{11}$] (see Chapter IV, Section 4.2.6.5) were allowed to crystallize for extended periods of time (4 weeks). During this time X-ray quality crystals were obtained and subsequently analyzed by single-crystal X-ray crystallography. To our surprise, the results of this study determined that the crystal structure (**Figure 5.1**) was not the expected product, but instead was an isomer. Although quite surprising, the crystallographic evidence for this unusual isomerization was undeniable. Perplexed and intrigued by this reaction we decided to concentrate our research on further understanding the details of unusual this transformation. Although the isomerization of (^{F}PNP^{iPr})Pd[CHB$_{11}$Cl$_{11}$] can be monitored by ^{31}P NMR spectroscopy (see experimental section), we determined the most effective way to analyze the different isomers was to convert them to the corresponding neutral

(^{F}PNP^{isom})PdCl complexes by treating mixtures resulting the isomerization with excess CsCl (**Scheme 5.3**).

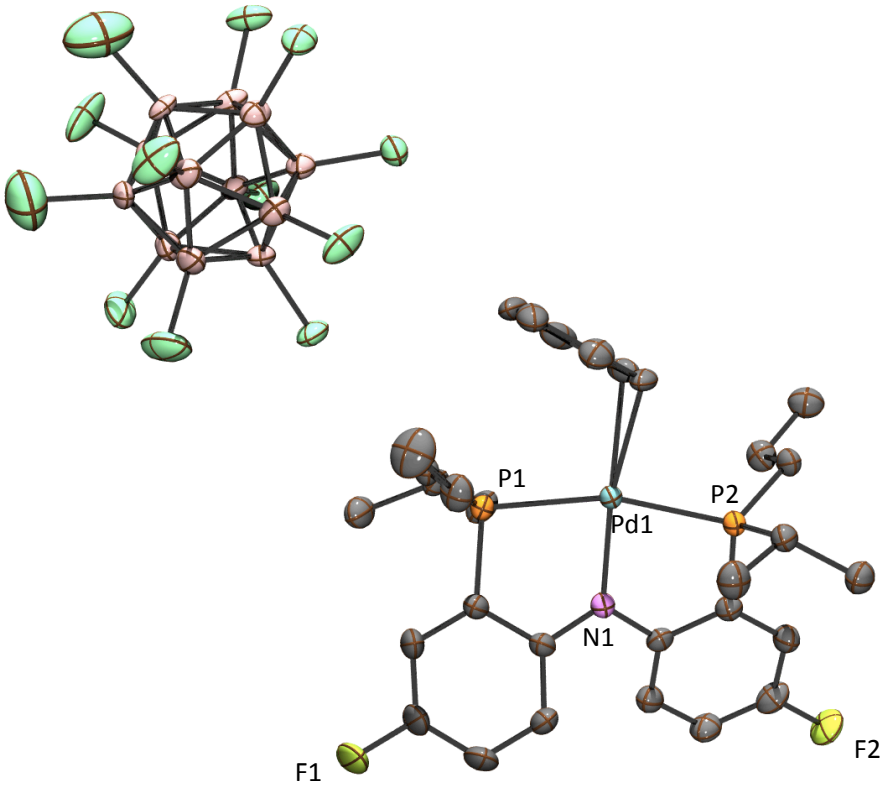

Figure 5.1 POV-Ray rendition of the ORTEP[162] drawing (50% thermal ellipsoids) of **5-1** showing selected atom labeling. Hydrogen atoms and solvent have been omitted for clarity. Selected bond distances (Å) and angles (deg): Pd1-C23 2.378(4); Pd1-C18, 2.376(5); Pd1−P1, 2.3494(18); Pd1−P2, 2.3053(18); Pd1−N1, 2.033(5); P1−Pd1−P2, 163.18(5).

The resulting (^{F}PNP^{Pr})PdCl complexes are more amenable to NMR characterization because they are significantly more soluble and do not have any fluxional chemical character (see Chapter IV). In addition, **2-4** is a known compound which makes it easier to identify the unisomerized (^{F}PNP^{iPr})Pd fragment within a mixture of different isomers.

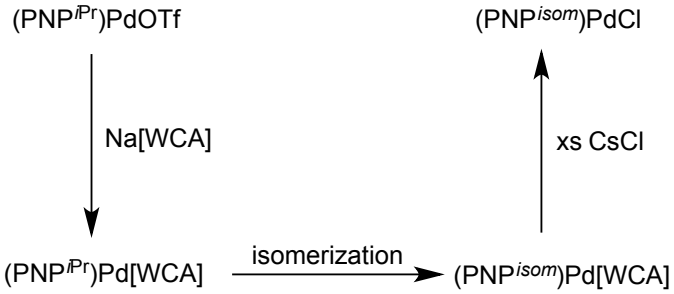

Scheme 5.3 Isomerization of (PNP^{iPr})Pd[WCA] and conversion to (PNP^{Pr})PdCl.

5.2.2 Possible regio, stereo and enantio isomers in (^{F}PNP^{Pr})Pd[WCA] isomerization

There are a total of nine possible isomers of (^{F}PNP^{Pr})PdCl (**Figure 5.2**) that can potentially be generated in the isomerization of [(^{F}PNP^{iPr})Pd]$^{+}$ cations. Each of these isomers differs by either the number and/or the arrangement of *n*-propyls and *i*-propyls: 1×(0*n*Pr,4*i*Pr) (**2-4**), 2×(1*n*Pr,3*i*Pr) (**5-2**, **5-3**), 3×(2*n*Pr,2*i*Pr) (**5-4**, **5-5, 5-7**), 2×(3*n*Pr,1*i*Pr) (**5-8, 5-9**) and 1×(4*n*Pr,0*i*Pr) (**5-10**). Both the tetra-*i*-propyl (0*n*Pr,4*i*Pr) (**2-4**) and the tetra-*n*-propyl (4*n*Pr,0*i*Pr) (**5-10**) exist as a single stereoisomer. However, the mono-*n*-propyl (1*n*Pr,3*i*Pr) has two possible enantiomers R (**5-2**) and S (**5-3**); as does the tri-*n*-propyl (3*n*Pr,1*i*Pr): R (**5-8**) and S (**5-9**). There are a total of 4 isomers of the bis-*n*-

propyl (2*n*Pr,2*i*Pr) (**5-[4-7]**). Isomers **5-[4**,**6]** are an enantiomeric pair, and 5-5 is their diastereomer; **5-7** exists as a single isomer. Although in the static state **2-4** is C_2-chiral on the NMR time scale the 2-4 is C_{2v}; this also applies to isomers **5-[2-10]**.

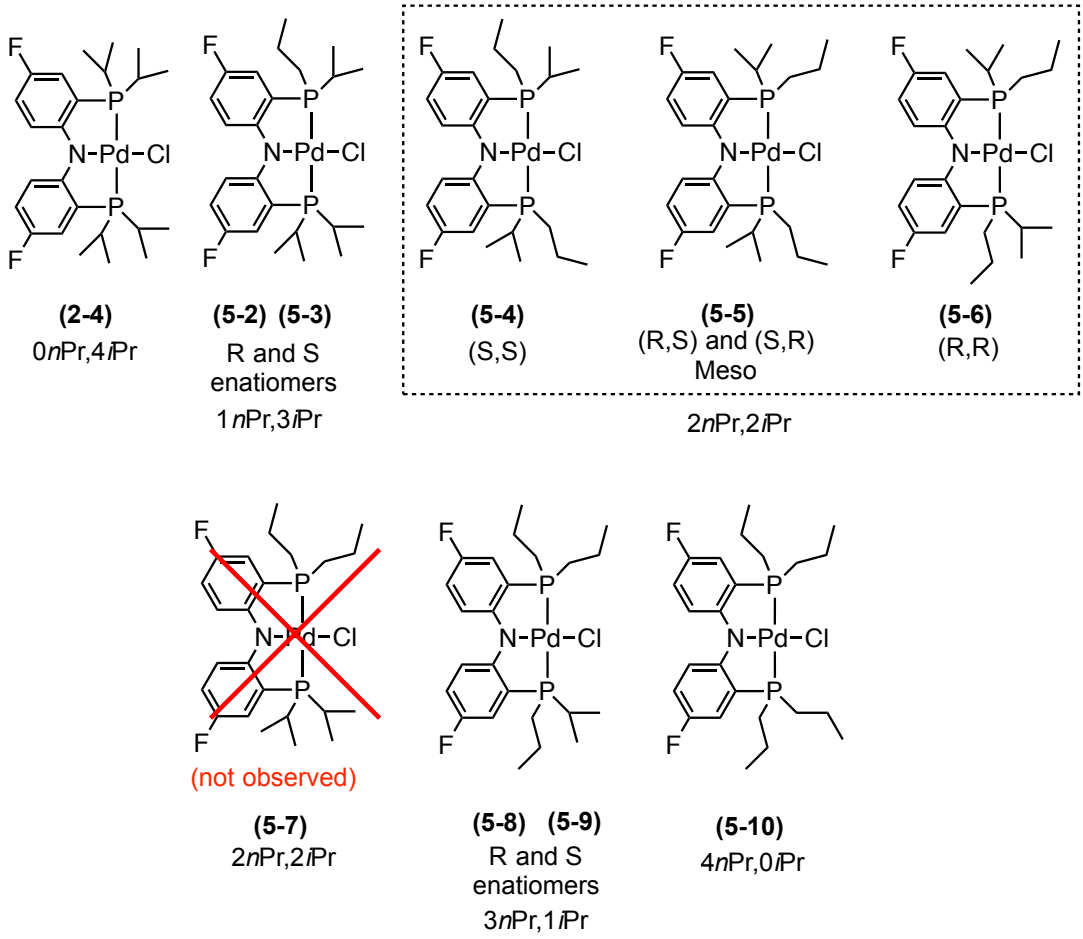

Figure 5.2 Possible ($^{F}PNP^{isom}$)PdCl products from the isomerization of [($^{F}PNP^{iPr}$)Pd]$^{+}$ cations.

As discussed in Chapter IV, addition of $Na[CEtB_{11}Cl_{11}]$ (**4-50**) to a solution of **2-6** generates ($^{F}PNP^{iPr}$)Pd[$CEtB_{11}Cl_{11}$] (**4-56**) which in the solid state forms a toluene adduct (**Figure 4.7**). It was discovered that when the resulting solution is allowed to stand under ambient temperature and lighting for a period of 4 weeks, followed by quenching with CsCl, it yielded a mixture of isomers **5-[4,6]** (70%) and **2-4** (30%) (**Scheme 5.4**, **Eq.1**). However, extending the reaction time did not yield a greater conversion; even after a period of 60 days the conversion did not exceed 76% (**Scheme 5.4**, **Eq. 3**). At room temperature and under ambient lighting conditions the rate of isomerization is very slow and reaches only 70% conversion. As expected, when the reaction time of the isomerization was cut in half (2 weeks), so did the conversion to the isomers **5-[4,6]** (34%) (**Scheme 5.4**, **Eq. 2**). This suggests that the isomerization of [($^{F}PNP^{iPr}$)Pd]$^{+}$ cations reaches an equilibrium between [($^{F}PNP^{iPr}$)Pd]$^{+}$ and [($^{F}PNP^{isom}$)Pd]$^{+}$ after approximately 4 weeks. However, to truly determine if the reaction is indeed reversible, the reaction must be approached from the other side of the equation. Unfortunately, the synthesis of ($^{F}PN(Me)P^{nPr}$) is complicated by the fact that $ClP(^{n}Pr_2)$, a necessary precursor, is not commercially available or easily synthesized.

If a solution of ($^{F}PNP^{iPr}$)Pd[$CHB_{11}Cl_{11}$] (**4-29**) in C_6D_6 is irradiated with a 250-W halogen lamp the rate of isomerization increases dramatically (**Scheme 5.4**, **Eq. 4**). Whereas under standard temperature and fluorescent lab lighting the isomerization took up to 4 weeks to reach 70% conversion, under irradiation with a 250-W halogen lamp the reaction reaches a similar conversion overnight.

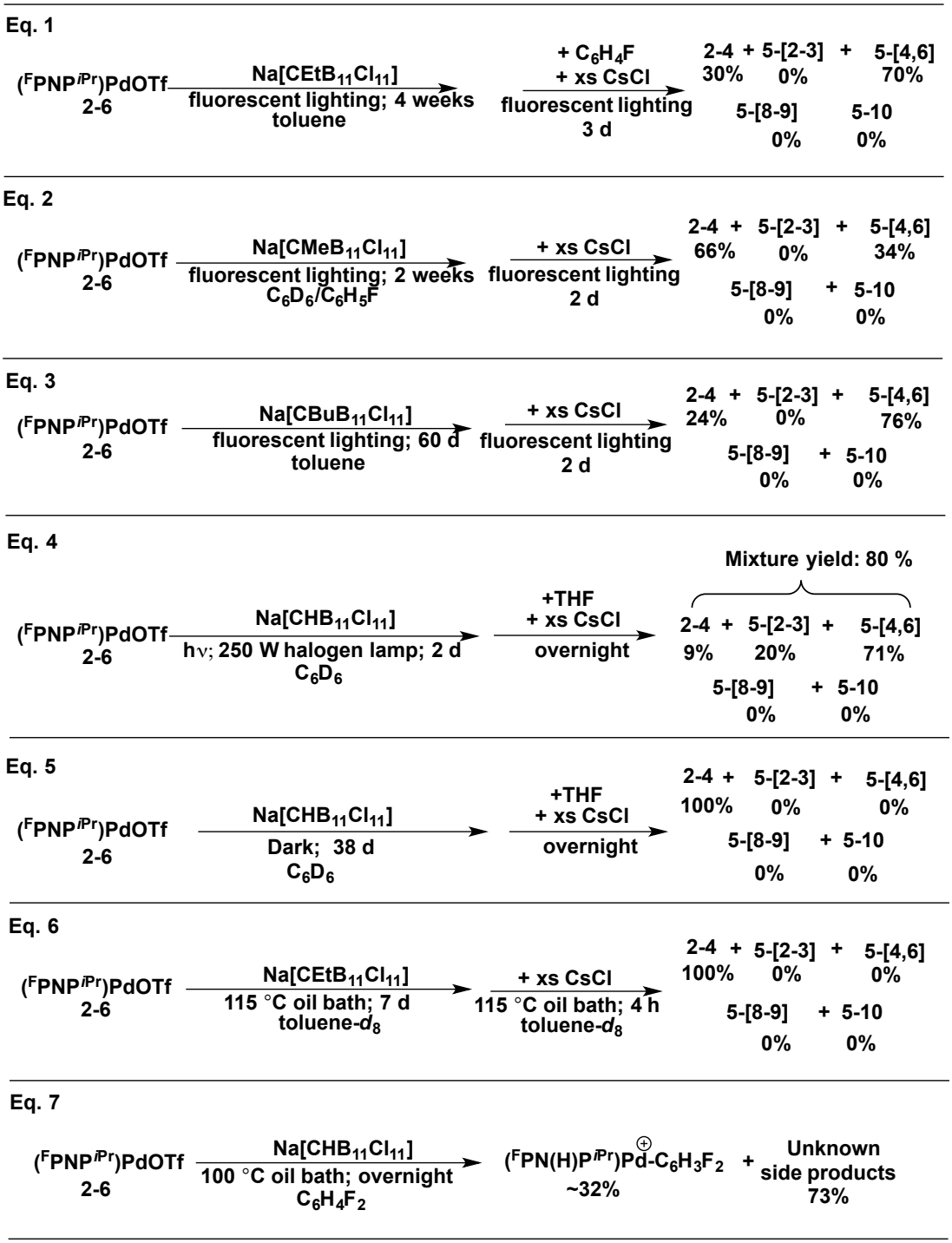

Scheme 5.4 Isomerization of (^{F}PNP^{iPr})Pd[WCA] under different conditions such at temperature and lighting.

When the reaction between **2-6** and **4-39** is protected from light with aluminum foil and allowed to react for 38 days, then quenched with excess CsCl, the observed product is **2-4** and no other isomers were observed (**Scheme 5.4**, **Eq. 5**). In addition, refluxing the reaction between **2-6** and **4-56** in $C_6D_5CD_3$ for 7 days followed by quenching with excess CsCl yielded only **2-4** and no other isomers (**Scheme 5.4**, **Eq. 6**).

From this series of experiments, it is clear that the isomerization of (^{F}PNP$^{i\text{Pr}}$)Pd[WCA] is light driven. Exposing [(^{F}PNP$^{i\text{Pr}}$)Pd]$^{+}$ cations to fluorescent lighting does induce the isomerization, albeit very slowly. This result is not surprising since there are several examples of (^{F}PNP$^{i\text{Pr}}$)Pd-X complexes that require photoexcitation to induce reactivity.[54,63] For example, in Chapter III we discussed the reaction between **2-10** and O_2 and its dependence on light.[69] In addition, in Chapter IV we discussed how irradiation of **4-45** cation with a 250-W halogen lamp homolytically abstracts a bromine atom from bromobenzene and produces [(^{F}PNP$^{i\text{Pr}}$)PdBr]$^{+}$ (**4-70**). It is therefore reasonable that the isomerization of (^{F}PNP$^{i\text{Pr}}$)Pd[WCA] is induced by light and that using a high intensity light source, such as a halogen lamp dramatically accelerates the reaction.

Interestingly, thermolysis of the (^{F}PNP$^{i\text{Pr}}$)Pd[WCA] does not accelerate the rate of isomerization (**Scheme 5.4**, **Eq. 6**). One possible explanation could be that thermolysis of (^{F}PNP$^{i\text{Pr}}$)Pd[WCA] in arene solvents such as toluene induces 1,2-addition of the aromatic solvent. Once the cation undergoes 1,2-addition of the solvent it falls into a thermodynamic well that prevents isomerization from occuring. This is corroborated by preliminary results that suggest that thermolysis of the reaction between

2-6 and **4-39** in $C_6H_4F_2$ cleaves a C-H bond of $C_6H_4F_2$ in 1,2-addition fashion (**Scheme 5.4**, **Eq. 7**). This is not unexpected since 2013 Demott and coworkers reported analogous reactivity with the [(^{F}PNP$^{i\text{Pr}}$)Pt] fragment.[65]

5.2.3 Selectivity of (^{F}PNP$^{i\text{Pr}}$)Pd[WCA] isomerization

Given the number of possible products, it is surprising that prolonged irradiation of **4-48** with fluorescent lighting (lab lighting) followed by quenching with CsCl produces almost exclusively the bis-*n*-propyl regioisomer (**5-[4,6]**) (**Scheme 5.4**, **Eq. 1-3**). As stated in Section 5.2.2, the bis-*n*-propyl regioisomer (**5-[4,6]**) consists of a mixture of enantiomers and diastereomers. Although it is possible that the reaction produces a mixture of diastereomers, it is more likely the reaction produces a single diastereomer that is observable by ^{31}P NMR spectroscopy as a singlet (38.9 ppm). In addition, this diastereomer is composed of enantiomers that cannot be differentiated by NMR spectroscopy. It is possible that addition of a chiral ligand might assist in differentiating the enantiomers by NMR spectroscopy. Based on NMR spectroscopy, it is clear that the regioisomer (**5-8**) is not formed in the reaction. As will be detailed later in this chapter, the -P^{n}Pr$_2$ shows up significantly more upfield (26.9 ppm) by ^{31}P NMR spectroscopy than the mixed –P(^{n}Pr)(^{i}Pr) (38.9 ppm) product.

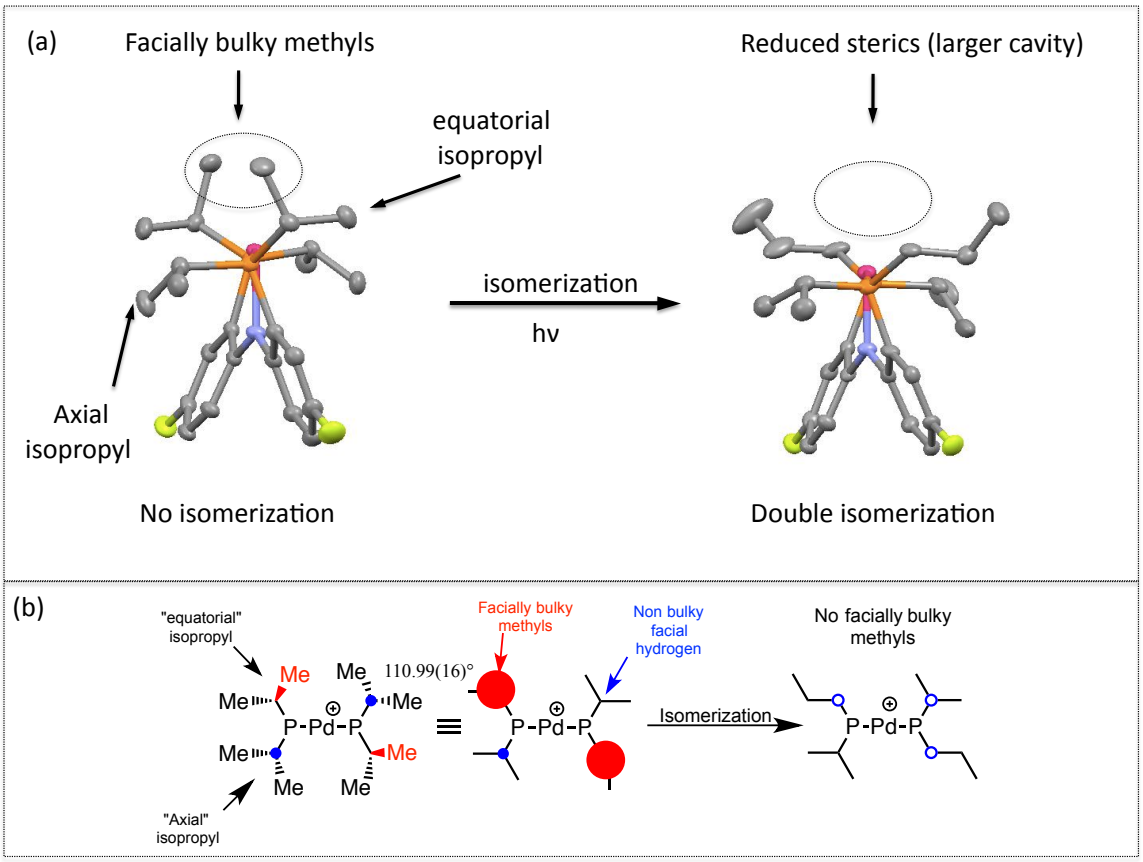

Figure 5.3 Illustration of reduction of sterics in (^{F}PNP$^{i\text{Pr}}$)Pd[WCA] around the metal; elimination of facially bulky equatorial isopropyl substituents upon isomerization.

Having said this, we were still interested in understanding why under ambient lighting the only isomers produced were (**2-4**) and (**5-[4,6]**) (**Scheme 5.4**, **Eq. 1-3**). A possible explanation came from looking at the arrangement of the isopropyl groups in the crystal structures of **2-4**, and [(^{F}PNP$^{2i\text{Pr}2n\text{Pr}}$)Pd($C_6D_6$)]$^{+}$[$CMeB_{11}Cl_{11}$] (**5-1**) (**Figure 5.1**) Typically (^{F}PNP$^{i\text{Pr}}$)PdX complexes, such as **2-4**, have two "axial" and two "equatorial" isopropyls. The two "equatorial" isopropyl groups exert the majority of the steric pressure on the ligand *trans* to the nitrogen. As shown in **Figure 5.3**, each of the

equatorial isopropyl groups in the unisomerized (^{F}PNP^{iPr})Pd fragment (partial structure of **2-4**) has a methyl group pointing towards the fourth coordination site. The two "facially" bulky methyls contribute greatly to the steric pressure on the fourth coordination site, making it more difficult for ligands such as arenes to coordinate to the metal center. However, as can be seen in **Figure 5.3**, upon isomerization of the equatorial *i*-propyl groups to *n*-propyls, the sterics around the fourth coordination site are greatly decreased. The new *n*-propyl groups no longer contain methyl groups pointing towards the fourth coordination site (**Figure 5.3b**). The larger cavity produced by the isomerization facilitates the coordination of arene ligands. This explains the observed selectivity for isomers (**5-[4,6]**). In essence, the reason for the observed selectivity is due to the fact that the two "equatorial" isopropyl groups on (^{F}PNP^{iPr})Pd[WCA] pose the greatest steric pressure on the fourth coordination site. Therefore, isomerization of the two equatorial isopropyl groups produces the greatest decrease in sterics, hence the selectivity.

5.2.4 The role of the anion in the isomerization

In Chapter IV we discussed the differences in coordinating ability between anions such as $[OTf]^-$, $[CHB_{11}H_{11}]^-$, $[CRB_{11}Cl_{11}]^-$ (R = H, Me, Et, Bu) and $[BArF_{24}]^-$. Both $[OTf]^-$ and $[CHB_{11}H_{11}]^-$ bind quite strongly to metal center in $[(PNP)Pd]^+$ cations, and in the solid state $[CHB_{11}Cl_{11}]^-$ also coordinates to the $[(^{F}PNP^{iPr})Pd]^+$ cation. However, the use of alkylated carboranes $[CRB_{11}Cl_{11}]^-$ (R = Me, Et, Bu) led to the characterization of a η^1-toluene adduct (**4-55a**).

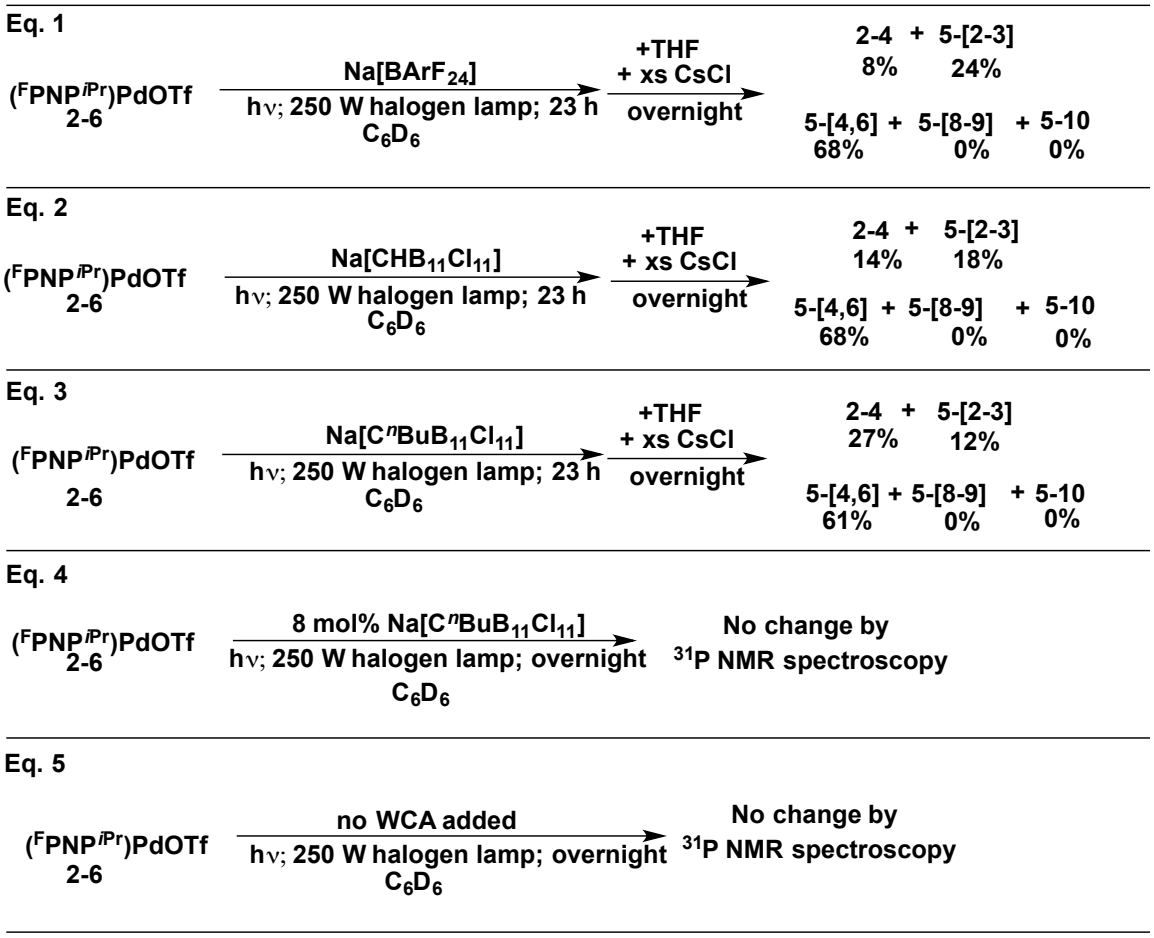

Scheme 5.5 The role of the anion in the isomerization of $[(PNP^{iPr})Pd]^+$ cations.

It was therefore a natural next step to study the role of the WCA in the isomerization of $(^{F}PNP^{iPr})Pd[WCA]$. To determine the function of the anion in the isomerization of $(^{F}PNP^{iPr})Pd[WCA]$, a series of solutions of **2-6**, **4-43**, **4-29**, **4-41** in C_6D_6 were irradiated using a 250-W halogen lamp overnight (**Scheme 5.5**).

The reactions between **2-6** and **4-35**, **4-39**, **4-41** (**Scheme 5.5**, **Eq. 1-3**) all produce different distributions of isomers (**2-4, 5-[2-11]**). However, one common factor between all of these reactions is the maximum extent of the isomerization. When using

4-35 (**Scheme 5.5**, **Eq. 1**), **4-39** or **4-41** (**Scheme 5.5**, **Eq. 2,3**)) as a counter anion we see that the maximum number of *i*-propyl groups converted to *n*-propyl groups is two. As discussed previously, the reason for this is likely because the two "equatorial" isopropyl groups on (^{F}PNP$^{i\text{Pr}}$)Pd[WCA] pose the greatest steric pressure on the fourth coordination site.

The differences in the observed isomer distributions can be due to inherent differences in the isomerization rate between the different anions. For example, some anions might produce more soluble (^{F}PNP$^{i\text{Pr}}$)Pd[WCA], which may lead to an increased rate in isomerization. In addition, there are also slight variations in coordinating ability (especially in different solvents) between the different anions that might lead to the observed differences in isomer distribution. Finally, it is also possible that the variations in isomer distribution are simply due to differences in the exposure to the light source that can be attributed to spatial arrangement of the J. Young tubes with respect to the light source. If **2-6** is irradiated with a 250-W halogen lamp overnight no reaction is observed (**Scheme 5.5**, **Eq. 5**). Additionally, if a deficiency of Na[C^{n}BuB$_{11}$Cl$_{11}$] (**4-41**) (8 mol%) is added to a solution of **2-6** and irradiated overnight with a 250-W halogen lamp no change is observed by ^{31}P NMR spectroscopy (**Scheme 5.5**, **Eq. 4**). This suggests that Na[WCA] is not functioning as a catalyst in the isomerization of (^{F}PNP$^{i\text{Pr}}$)Pd[WCA] and that stoichiometric quantities of Na[WCA] are needed for isomerization to occur. In addition, the results of these experiments (**Scheme 5.5**) suggest that triflate is not weakly coordinating enough to allow for isomerization to

occur. Less coordinating anions such as carboranes and $BArF_{24}$ are necessary for the isomerization to take place.

5.2.5 Solvent dependence of the isomerization

The results detailed in the previous section suggest that for isomerization to occur, an open coordination site must be accessible on Pd. While the anion is a key factor in the ability to access the empty coordination site, to have a more complete picture it is also important to take into consideration the role of the solvent. The basicity (and sterics) of the solvent can have a profound effect on the ability to access the empty coordinating site on $[(^{F}PNP^{iPr})Pd]^{+}$ cation. To determine the effect of the solvent on the isomerization of $(^{F}PNP^{iPr})Pd[WCA]$, several solvents with varying basicity and sterics were used in the reaction between **2-6** and **4-39** under irradiation with a 250-W halogen lamp for 23 h. The solvents in the reactions (**Scheme 5.6, Eq.1-6**) were benzene (C_6H_6), toluene ($C_6H_5CH_3$), mesitylene (C_9H_{12}), fluorobenzene (C_6H_5F) and tetrahydrofuran (THF). Surprisingly, the reactions between **2-6** and **4-39** in benzene and toluene gave relatively high conversions of isomers (**5-[4,6]**), 87% and 81% respectively upon quenching with cesium chloride. This suggests that the conversion of 70% in the reactions of under ambient lighting conditions (**Scheme 5.4**, **Eq. 1**) might be due to the fact that fluorescent lighting is a much lower intensity light source than the 250-W halogen lamp. However, what does remain consistent is the fact the fact that isomerization does not exceed two *i*Pr groups in benzene or toluene. However, as can be seen from (**Scheme 5.4**, **Eq. 4**), the use of C_6H_5F as a solvent produces a small amount

of isomer (**5-10**). Mesitylene, a bulkier arene than benzene or toluene, yields a mixture of all the possible isomers (**2-4, 5-[2-8]**, **5-[10-12])** in the same time period that the reactions in benzene and toluene yields only isomers (**2-4, 5-[2-8]**).

Eq. 1

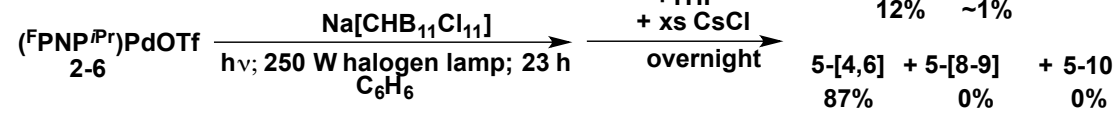

Eq. 2

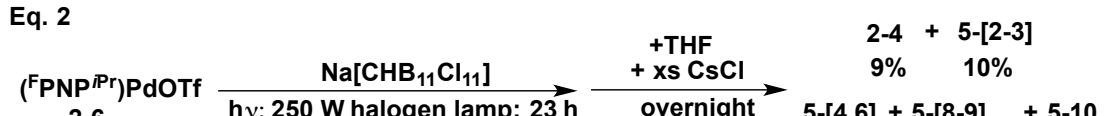

Eq. 3

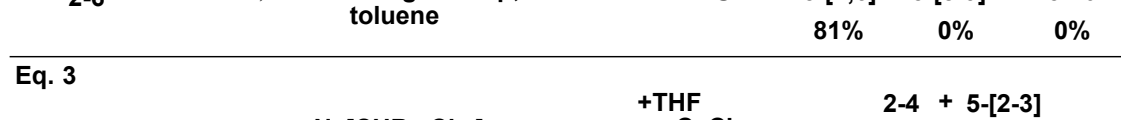

Eq. 4

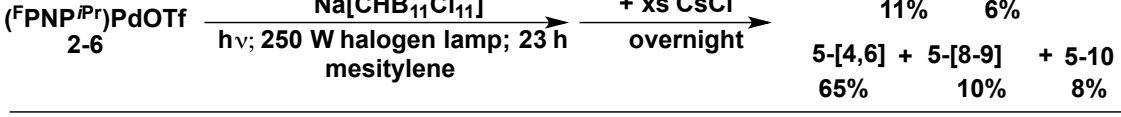

Eq. 5

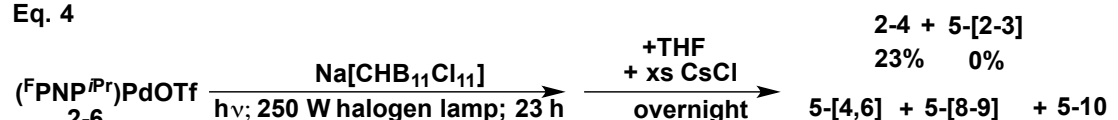

Eq. 6

Scheme 5.6 Solvent dependence in the isomerization of ($^{F}PNP^{iPr}$)Pd[$CHB_{11}Cl_{11}$].

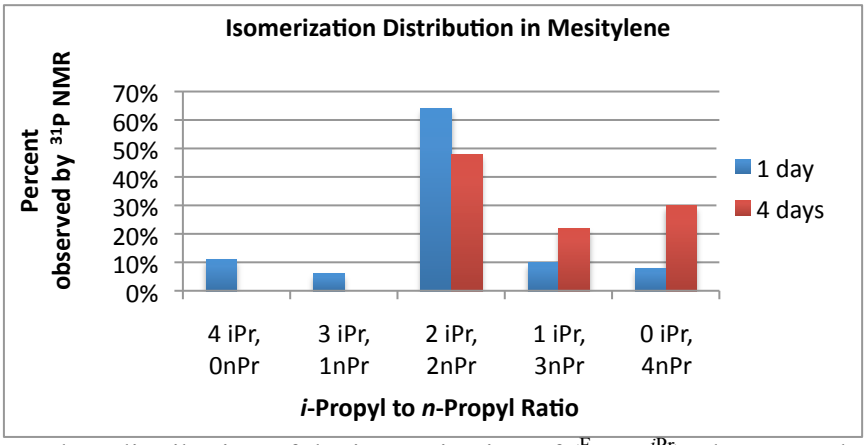

Figure 5.4 Product distribution of the isomerization of (^{F}PNP^{iPr})Pd[$CHB_{11}Cl_{11}$] in mesitylene after 1 and 4 days.

In addition, if the reaction time between **2-6** and **4-39** in mesitylene is extended for a total of 4 days the isomer distribution is pushed closer to complete isomerization and the only isomers observed are (**5-[4,6]**) and (**5-[8-9]**) (see **Figure 5.4** and **Scheme 5.6**, **Eq.3-5**). However, in more coordinating solvents such as THF, the reaction between **2-6** and **4-39** under irradiation for 20 h, and subsequent quenching with CsCl produces a mixture of isomers (**A**) (88%) and (**5-[4,6]**) (14%) (**Scheme 5.6**, **Eq.6**). These results (**Scheme 5.6**, **Eq.1-6**) suggest that both the sterics and basicity of solvent have a profound effect on the extent of isomerization. Although the difference in isomer distribution between benzene and toluene is minimal, the use of mesitylene as a solvent has a significant effect on the extent of isomerization. The reason for the increased extent of isomerization in solvents like mesitylene is likely due in large part to the bulkiness of the solvent. Compared to toluene or benzene, bulky arene solvents such as mesitylene might have more difficulty coordinating to (^{F}PNP^{iPr})Pd[WCA], even when two *i*-propyl groups

are converted to *n*-propyl groups. Therefore, further isomerization to tri-*n*-propyl and tetra-*n*-propyl allows mesitylene to coordinate to the $[(^{F}PNP)Pd]^{+}$ cation more effectively. Unlike in arene solvents such as benzene, toluene and mesitylene, the isomerization of $(^{F}PNP^{iPr})Pd[WCA]$ in THF produces significantly less products of isomerization. We hypothesize that for isomerization to occur, an empty coordination site must be accessible. Therefore, under Lewis basic conditions (i.e. using THF as solvent) the empty coordination site is occupied by THF, and the isomerization is inhibited. Although the isomerization is not completely quenched, it is clear that the use of THF as solvent greatly reduces the rate. It is likely that the isomerization is not completely inhibited because THF is capable of dissociating from the Pd center to allow the isomerization to occur.

Based on the results discussed thus far, we can conclude that the isomerization requires weakly-coordinating anions such as $CRB_{11}Cl_{11}$ (R = H, alkyl) and $BArF_{24}$, and does not occur with more basic anions such as triflate. In addition, it was determined that bulkier arenes such as mesitylene give access to isomers (**5-[10-12]**). However, the use of more Lewis basic solvents such as THF greatly inhibits the isomerization, presumably because the fourth coordination site in $[(PNP)Pd]^{+}$ cation is blocked by THF. In weakly Lewis basic solvents like arenes it appears that the major factor mediating the extent of the isomerization is the sterics or the arene. This suggests that the driving force for the isomerization in aromatic solvents is the formation of a more stable $[(^{F}PNP^{R})Pd(arene)]^{+}$ complex. Based on the current experiments, it is not clear whether the isomerization is a thermodynamically favorable process and the use of WCAs and weakly-coordinating

solvents simply makes the reaction kinetically accessible, or if the reaction is thermodynamically unfavorable and light serves as a source of energy driving the isomerization forward.

5.2.6 Solid-state characterization of isomerized arene adducts

So far, we have discussed the isomerization based on the results produced by quenching the (^{F}PNP$^{i\text{Pr}}$)Pd[WCA] with CsCl. However, the isomerized cations were also characterized by X-ray crystallography. The structural parameters of the η^1-arene complex (**4-55a**) were discussed in Chapter IV. The structure of compound **4-55a** revealed two different Pd-C bond lengths, 2.470(4) Å and 2.369(3) Å. In contrast to this, the Pd-C bond distances in [(^{F}PNP$^{2i\text{Pr}2n\text{Pr}}$)Pd($C_6D_6$)]$^{+}$[$CBuB_{11}Cl_{11}$]$^{-}$ (**5-11**) (2.364(5) Å and 2.346(5) Å) are close enough to be considered statistically equivalent. In addition, the shorter of the two Pd-C bond lengths in **4-55a** is close to the average Pd-C bond length in **5-11** (2.355(3) Å), consistent with an η^2-arene complex. In addition, the arene ring parameters of the bound toluene do not diverge from those of free toluene.

Table 5.1 Bond angles in **4-55a** and **2-27**.

Bond Angle	**4-55a**	(^{Me}PNP$^{i\text{Pr}}$)PdCl (**2-27**)
$^{i\text{Pr}}$C-P^1-C$^{i\text{Pr}}$	106.28(17)°	106.23(9)°
$^{i\text{Pr}}$C-P^2-C$^{i\text{Pr}}$	110.99(16)°	106.23(9)°
P-Pd-P	161.28(3)°	163.54(2)°

Table 5.2 Bond angles in **5-11**, **2-7**, and **2-5**.

Bond Angle	**5-11**	(^{F}PNP$^{i\text{Pr}}$)PdH (**2-7**)	(^{F}PNP$^{i\text{Pr}}$)PdOAc (**2-5**)
$^{i\text{Pr}}$C-P^{1}-C$^{i\text{Pr}}$	106.4(2)°	106.3(3)°	110.0(5)°
$^{i\text{Pr}}$C-P^{2}-C$^{i\text{Pr}}$	105.6(3)°	107.0(3)°	108.1(3)°
P^{1}-Pd-P^{2}	162.77(5)°	168.38(5)°	168.16(6)°

Starting from the C-C bond directly bound to Pd, the C-C bond distances in the toluene are 1.396(5), 1.400(5), 1.375(5), 1.384(5), 1.376(5), and 1.409(5) compared to the average bond length in free toluene of 1.40 Å. In addition, the planarity of the toluene ligand, suggests that metal backbonding into π* of the aromatic ring is not an important contribution to the bonding between Pd and toluene.[330,331]

As discussed previously (Chapter IV), **4-55a** underwent a series of distortions to accommodate toluene into the coordination sphere of Pd. One significant distortion was the expansion of the $^{i\text{Pr}}$C-P-C$^{i\text{Pr}}$ bond angle (110.99 Å) as compared to the relatively unstrained angles in **2-27** (106.23 Å; see **Table 5.1**). To gain insight into the level of strain in **5-11** the structural parameters were compared to other less strained complexes such as **2-5**[70] and **2-7**[8] (see **Table 5.2**). In some sense both the bite angle and the C-P-C angle can indicate the level of strain in the metal complex. Compound **2-7** can serve as a good base line because the hydride is the least sterically imposing ligand and thus imposes the least amount of steric strain on the (^{F}PNP$^{i\text{Pr}}$)Pd fragment. The parameters of **2-5** were also used as a secondary point of reference. The results of the comparison show a large contraction of bite angle of PNP, indicative of a small amount strain in the metal

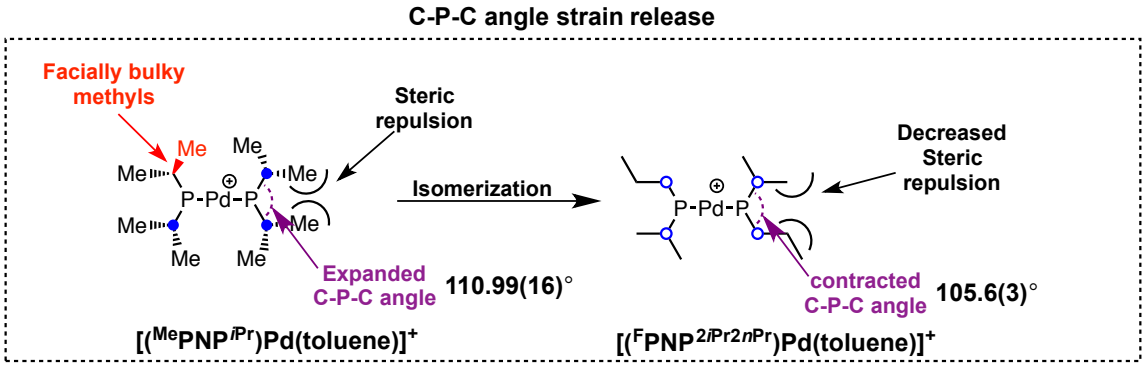

Figure 5.5 Strain release in isomerization of (^{F}PNP^{iPr})Pd]$^{+}$ cations.

complex. In addition, the average C-P-C angle of compound **5.14** (106.0(3)°) is comparable to the average C-P-C angle in **2-7** (106.7 (3)°) indicate of a low level of strain on the phosphine ligands. This angle is smaller than what is observed in **4-55a** (110.99(16)°). This suggests that some strain is released in the ^{iPr}C-P-C^{iPr} upon isomerization; this strain release can contribute to the favorability of the isomerization. In general the bond angles and distances of **5-1** are quite similar to what is observed in the structure of **5-11**. The Pd-C distances in **5-1** are 2.378(4) Å and 2.376(7) Å, which are comparable to the Pd-C distance observed in **5-11** (2.364(5) Å and 2.346(5) Å). The P2-Pd1-P1 bond angle in **5-1** is 163.18(5)°, which is marginally smaller than what is observed for **5-11** (162.77(5)°). Finally the C-C bond lengths for the C-C directly bound to Pd for compounds **4-55a**, **5-1 and 5-11** are all relatively close to each other and close to the average C-C bond length in free toluene (**Table 5.3**). However, the C-C bond lengths in compounds **4-55a**, **5-1 and 5-11** are marginally shorter than that of compound **4-60** (**Figure 5.6**).

Table 5.3 Pd-C and C-C bond distances in Pd-arene complexes **4-55a**, **5-1**, **5-11**, and **4-60**.

Compound	C-C (Å)	Pd-C_1 (Å)	Pd-C_2 (Å)
4-55a	1.395(6)	2.369(4)	2.468(4)
5-11	1.412(13)	2.306(8)	2.306(8)
5-1	1.402(7)	2.373(7)	2.376(5)
4-60	1.438(9)	2.331(6)	2.435(6)

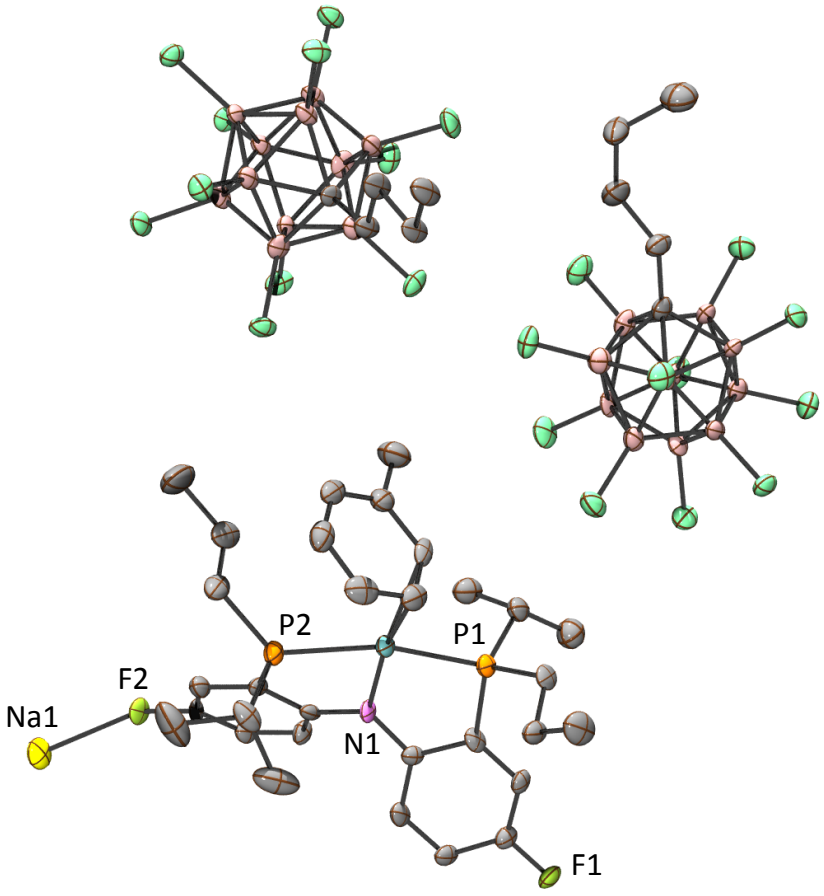

Figure 5.6 POV-Ray rendition of the ORTEP[162] drawing (50% thermal ellipsoids) of **5-11** cocrystallized with **4-41** showing selected atom labeling. Hydrogen atoms have been omitted for clarity. Selected bond distances (Å) and angles (deg): Pd1-C14 2.364(5); Pd1-C15 2.346(5); Pd1−P1, 2.2952(15); Pd1−P2, 2.3523(16); Pd1−N1, 2.021(4); P1−Pd1−P2, 162.77(5).

5.2.7 Mechanistic discussion

The isomerization of (^{F}PNP^{iPr})Pd[WCA] is an unprecedented transformation, and as such, the mechanistic details are still unknown. To properly rule out possible mechanisms, more detailed studies must be done such as: isotope labeling, kinetic and computations. For example, labeling the isopropyl methine carbon with ^{13}C can help differentiate between C-C and C-P bond cleavage (**Scheme 5.7**). If the isomerization occurs via C-P bond cleavage, the ^{13}C label in the isomerized product will no longer be attached to the phosphorus. However, if the ^{13}C label remains attached to the phosphorus after isomerization it suggests that the isomerization is occurring via C-C bond cleavage.

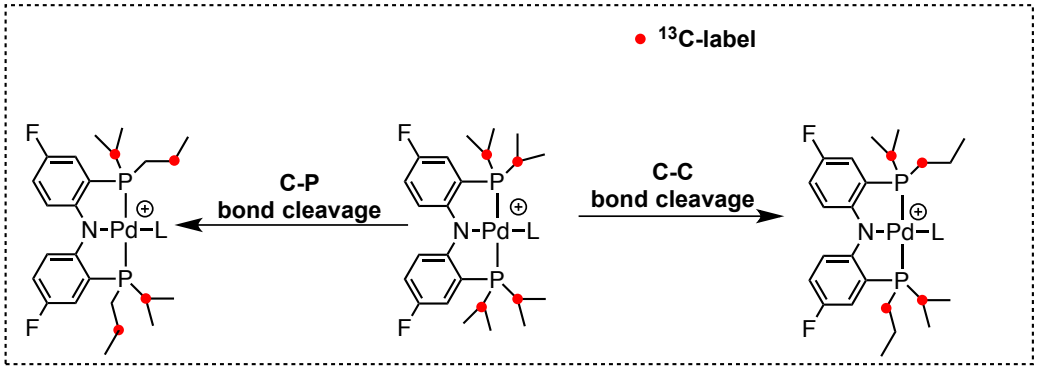

Scheme 5.7 Possible pathways for (^{F}PNP^{iPr})Pd[WCA] isomerization; C-C bond cleavage (right) and C-P bond cleavage (left).

Unfortunately, the synthesis (^{F}PNP^{iPr})Pd-X complexes with ^{13}C labeled isopropyl groups is likely very expensive, not to mention highly time-consuming. In addition, kinetic experiments can also be conducted by determining the rate of isomerization in several concentrations of (^{F}PNP^{iPr})Pd[WCA]. Establishing whether the isomerization is 0th, 1st or

2^{nd} order with respect to the concentration of $[(^{F}PNP^{iPr})Pd]^{+}$ cation can determine whether the reaction is inter or intramolecular. However, these experiments are complicated due to the fact that the reaction is dependent on light. Therefore, to properly conduct such an experiment the lighting conditions would have to be very rigorously controlled. However, even without these experiments some hypotheses can be made based about the possible mechanisms. As stated above, the isomerization of $(^{F}PNP^{iPr})Pd[WCA]$ can be occurring by two possible routes, via C-C bond cleavage or by C-P bond cleavage, and without conducting experiments such as those described above, C-C bond cleavage cannot be ruled out. However, based purely on literature precedence it is more reasonable that the reaction is occurring via C-P bond cleavage rather than C-C bond cleavage.[332]

In his 2007 review, Macgregor discussed several possible mechanisms for C-P bond cleavage. One possibility is that C-P bond cleavage occurs via nucleophilic attack by the anion.[318] However, the use of weakly-coordinating anions such as carboranes or BArFs eliminates this possibility. The use of WCA does produce highly unsaturated $(^{F}PNP^{iPr})Pd[WCA]$ that can possibly undergo oxidative cleavage of C-P bonds to generate a formally Pd(IV) alkyl intermediate (**III**) (**Scheme 5.8a**). The first step of the mechanism could involve irradiation of the arene adduct (**I**) to generate a three-coordinate Pd^{2+} intermediate (**II**) which can undergo C-P oxidative cleavage to generate (**III**), a Pd(III) alkyl complex. Intermediate (**III**) can theoretically be stabilized by resonance delocalization throughout the ligand framework to form a metallaphosphaalkene (**Scheme 5.8b**).

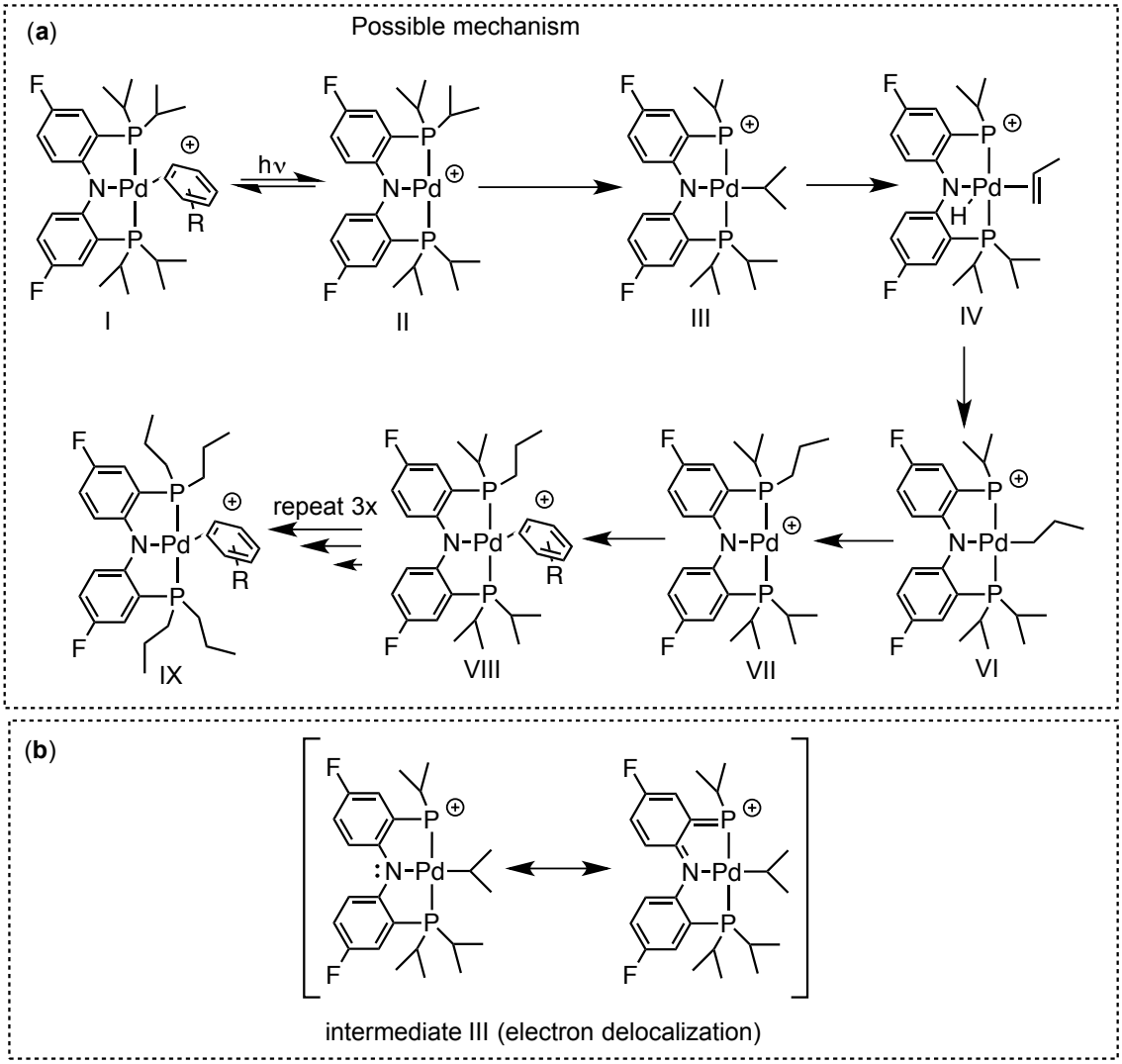

Scheme 5.8 Possible mechanism for (^{F}PNP^{iPr})Pd[WCA] isomerization (a); electron delocalization of intermediate **III** (b).

It is possible that electron delocalization helps minimize the energy barrier of C-P oxidative cleavage. The intermediate (**III**) can then undergo β-hydride elimination to form a hydrido propene complex (**IV**) that can undergo reinsertion into the hydride to form a linear *n*-propyl alkyl complex (**IV**). Finally, C-P reductive elimination and

subsequent coordination of the arene solvent can generate the mono-*n*-propyl palladium arene complex.

5.3 Conclusion

This chapter discussed the reactivity of (^{F}PNP^{iPr})Pd[WCA]. It was discovered that under photolytic conditions (using a 250-W halogen lamp) highly unsaturated (^{F}PNP^{iPr})Pd[WCA] undergoes an unprecedented isomerization of the di-isopropyl phosphines. Thermolysis of these cations in an aromatic solvent does not accelerate the isomerization. Preliminary evidence suggests that (^{F}PNP^{iPr})Pd[WCA] undergoes 1,2-addition of the aromatic solvent at elevated temperatures, preventing isomerization from occurring. Irradiation of **2-6** does not produce any isomerized products. However, the use of weakly-coordinating anions such as $[BArF_{24}]^-$ and $[CRB_{11}Cl_{11}]^-$ (R = H, Me, Et, ^{n}Bu) opens a coordination site at palladium and allows isomerization to occur. In solvents such as benzene and toluene isomers **2-4**, and **5-[2-8]** are exclusively produced. However, when mesitylene, a bulkier arene, is used the distribution of isomers is pushed further towards full isomerization and the full spectrum of isomers is produced (**2-4, 5-[2-8]**, **5-[10-12]**). These results have important implications about the driving force for the isomerization of (^{F}PNP^{iPr})Pd]$^+$ cations. They suggests that the driving force for isomerization is the coordination of the arene ligand to the metal center. Surprisingly, the isomerization of [(PNP)Pd]$^+$ cations also occurs with Lewis basic solvents such as THF, albeit very slowly. This suggests that the fourth coordination in [(^{F}PNP^{iPr})Pd]$^+$ must be accessible for the isomerization to occur.

5.4 Experimental

5.4.1 General considerations

All manipulations were performed under an argon atmosphere, using standard Schlenk line, or glovebox techniques. Toluene, pentane, and C_6D_6 were dried over NaK/Ph_2CO/18-crown-6, distilled, or vacuum transferred, and stored over molecular sieves in an Ar-filled glovebox. Diethyl ether and THF were dried, deoxygenated (by purging) using a solvent purification system, and stored over molecular sieves in an Ar-filled glovebox. Fluorobenzene, pyridine, acetonitrile, bromobenzene, and CD_2Cl_2 were dried over CaH_2, distilled or vacuum transferred, and stored over molecular sieves in an Ar-filled glove box. **2-4**, **2-7**, **2-9**, and **2-6** were prepared according to published procedures. Na[$CRB_{11}Cl_{11}$] (R = Me (**4-40**), Et (**4-50**), ^{n}Bu (**4-41**)) were synthesized according to published procedures.[293] Potassium tetrakis(pentafluorophenyl)borate (K[$BArF_{20}$]) (**4-34**), and sodium tetrakis[(3,5-trifluoromethyl)phenyl]borate (Na[$BArF_{24}$]; **4-35**) were dried under vacuum overnight at ambient temperature, and stored in an Ar-filled glovebox. All other chemicals were used as received from commercial vendors. NMR spectra were recorded on a Varian iNova 300 (^{1}H NMR, 299.951 MHz; ^{13}C NMR, 75.426 MHz; ^{31}P NMR, 121.422 MHz; ^{19}F NMR, 282.211 MHz), and NMRS 500 (^{1}H NMR, 499.703 MHz; ^{13}C NMR, 125.697 MHz; ^{31}P NMR, 202.289 MHz; ^{19}F NMR, 470.069 MHz) spectrometer. Chemical shifts are reported in δ (ppm). For ^{1}H NMR spectra, the residual solvent peak was used as an internal reference. ^{1}H NMR spectra in C_6D_5Br were referenced by setting the most downfield signal to 7.30 ppm. ^{19}F NMR spectra were referenced externally using 99% CF_3CO_2H at −78.5 ppm.

Monitoring the irradiation of 2-6 and 4-39. An oven-dried vial was charged with **2-6** (11 mg, 0.022 mmol), **4-39** (13 mg, 0.024 mmol), and 0.5 mL of C_6D_6. After properly mixing the reagents, the sample was placed in a water bath to protect the sample from the heat generated by the halogen lamp. The sample was irradiated for 2 h, and subsequently analyzed by NMR (see **Figure 5.7**). The sample was then irradiated for an additional 14 h, and then analyzed again by NMR. The reaction was then quenched with 2 mL of $C_6H_4F_2$, and CsCl (100 mg, 0.75 mmol), and placed on the NMR tube rotator[e] for 3 d. A mixture of **2-4** (7%), and **5-[4,6]** (88%) was observed by ^{31}P NMR spectroscopy.

[e] This apparatus is used to properly mix the reagents (in heterogeneous mixtures) in the NMR tubes. As the name implies, the NMR tube rotator slowly and continuously rotates the NMR tube. This motion allows the entire solution to come into contact with the insoluble CsCl. This specific device is not required for the reaction to occur. All that is required is proper mixing.

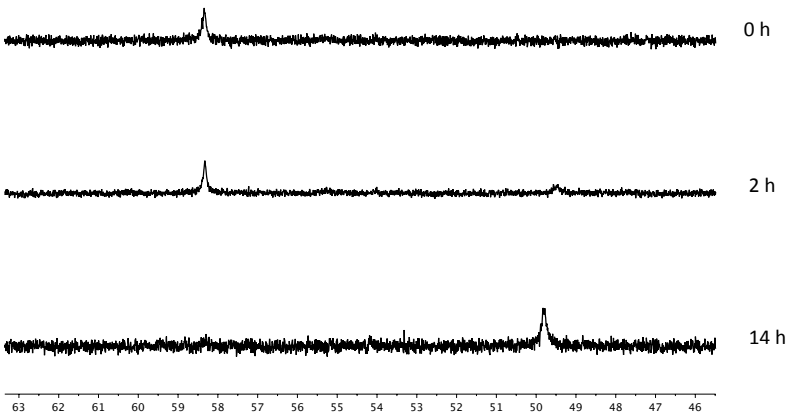

Figure 5.7 Monitoring the irradiation of **2-6** and **4-39** by ^{31}P NMR.

Synthesis of mixture of 2-4 (9%), 5-[2-3] (20%), and 5-[4,6] (71%). An oven-dried, 10 mL polytetrafluoroethylene (PTFE)-valved flask, **2-6** (104 mg, 0.15 mmol) and **4-39** (90 mg, 0.17 mmol) were dissolved in 2 mL of C_6D_6. After properly mixing the reagents, the sample was placed in a water bath to protect the sample from the heat generated by the halogen lamp. The solution was stirred and irradiated with a 250-W halogen lamp for 2 d. The sample was quenched with THF, and excess CsCl (100 mg, 0.59 mmol), and was then allowed to stir overnight. The solution was passed through a plug of Celite, and silica gel, the volatiles were removed under vacuum (69 mg, 0.12 mmol, 80%). The products observed were: **5-[4,6]** (71%), **5-[2-3]** (20%), and **2-4** (9%).

NMR data for **5-[4,6]**: ^1H NMR (C_6D_6): 7.28 (m, 2H, Ar-H), 6.68 (m, 2H, Ar-H), 6.63 (m, 2H, Ar-H), 2.00 (m, 2H, C*H*Me_2), 1.79 (m, 4H, PC*H*$_2$$CH_2CH_3$), 1.41 (m, 4H, PCH_2C*H*$_2$$CH_3$), 1.21(app. q (dvt), J = 8 Hz, CH*Me*$_2$) 1.05 (app. q (dvt), J = 8 Hz, CH*Me*$_2$), 0.87 (t, J = 8 Hz PCH_2CH_2C*H*$_3$); $^{13}C\{^1H\}$ NMR (C_6D_6): δ 159.9 (t, J_{C-P} = 11

Hz, C-N), 155.1 (dvt, J_{C-F} = 239 Hz, J_{C-P} = 4 Hz, C-F), 121.7 (dvt, J_{C-P} = 14 Hz, J_{C-F} = 5 Hz), 118.9 (d, J_{C-F} = 23 Hz), 117.5 (d, J_{C-F} = 21 Hz), 116.1 (app. q, J = 7 Hz), 29.1 (t, J_{C-P} = 12 Hz), 23.3 (t, J_{C-P} = 13 Hz), 18.5 (s), 18.4 (t, J_{C-P} = 2 Hz), 18.3 (t, J_{C-P} = 2 Hz), 15.9 (t, J_{C-P} = 7 Hz); $^{31}P\{^{1}H\}$ NMR (C_6D_6): δ 40.6 (s, $^{i}Pr^{n}Pr$*P*); ^{19}F NMR (C_6D_6): δ −127.9 (broad s, C-F). (**Figure 5.8** and **5.9**)

NMR data for **5-[2-3]**: $^{31}P\{^{1}H\}$ NMR (C_6D_6): δ 48.61 (d, J_{PP} = 424 Hz, $^{i}Pr_2$*P*); 39.75 (d, J_{PP} = 424 Hz, $^{i}Pr^{n}Pr$*P*); ^{19}F NMR (C_6D_6): δ −128.0 (broad s, C-F).

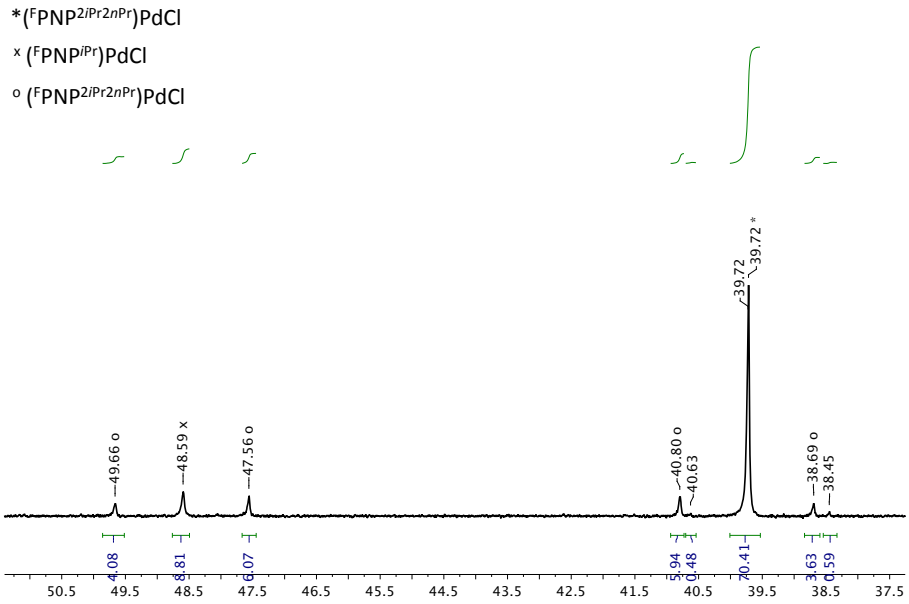

Figure 5.8 ^{31}P NMR spectrum of a mixture of **2-4**, **5-[4,6]**, and **5-[2-3]** in C_6D_6.

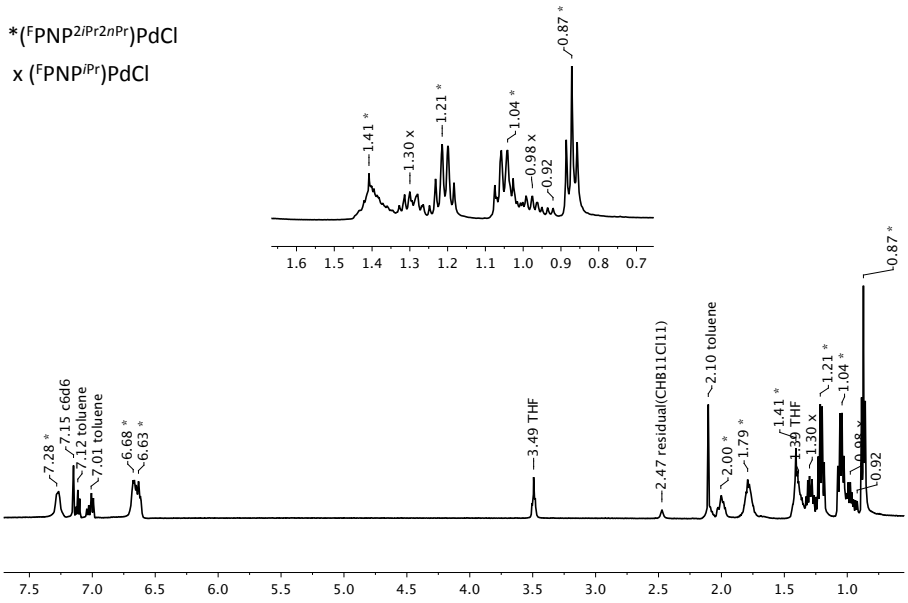

Figure 5.9 ^{1}H NMR spectrum of a mixture of **2-4**, **5-[2-3]**, and **5-[4,6]**.

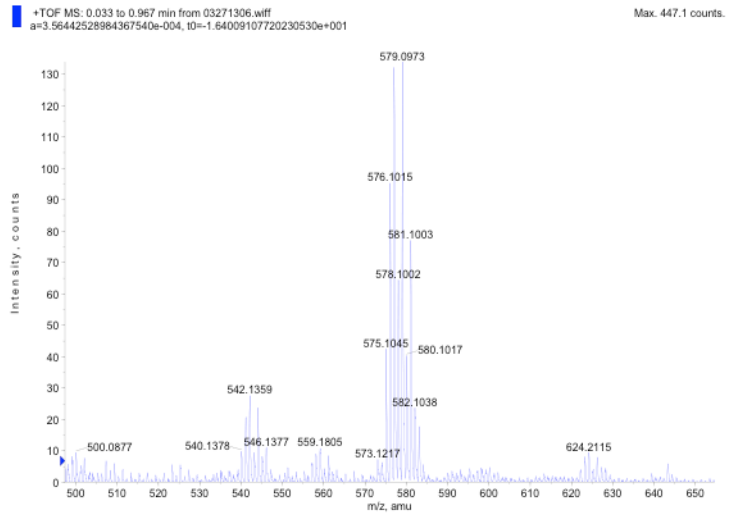

Figure 5.10 ESI Mass Spectrum in THF of a mixture of **2-6**, **5-[4,6]**, and **5-[2-3]**.

Reaction between 2-6 and Na[CEtB$_{11}$Cl$_{11}$] (4-50) for 4 weeks. In a 10 mL, oven-dried flask, **2-6** (73 mg, 0.11 mmol) was dissolved in 2 mL of toluene. Upon addition of **4-50** (67 mg, 0.12 mmol), the color gradually changed from purple to green. The reaction was stirred overnight, and then filtered through a pad of Celite to remove NaOTf. The reaction was allowed to stir for 4 weeks in a base free box. Over the course of this time, a green precipitate formed. The solution was decanted, and the solid was dried under vacuum. A small sample (5 mg) was taken from the dried solid, and dissolved with C_6H_5F (0.5 mL) in an oven-dried J. Young tube. Excess CsCl (90 mg) was added to the solution, and placed in an NMR tube rotator for 3 days. The products produced were **2-4** (30%) and **5-[4,6]** (70%), as determined by ^{31}P NMR and ^{19}F NMR spectroscopy.

Reaction between 2-6 and Na[CMeB$_{11}$Cl$_{11}$] (4-40) for 2 weeks. In an oven-dried vial, **2-6** (14 mg, 0.020 mmol) was dissolved in 2 mL of toluene. Upon addition of **4-40** (11 mg, 0.020 mmol), the color gradually changed from purple to green. The reaction was stirred for 5 min, and filtered through a pad of Celite to remove NaOTf. The reaction was allowed to stir for 2 weeks in a base free box. After this time, excess CsCl (24 mg) was added to the solution, and placed in an NMR tube rotator for 3 days. The products produced were **5-[4,6]** (34%) and **2-4** (66%), as determined by ^{31}P NMR and ^{19}F NMR spectroscopy.

Reaction between 2-6 and Na[C^{n}BuB$_{11}$Cl$_{11}$] (4-41) for 60 d. In an oven-dried vial, **2-6** (10 mg, 0.014 mmol) was dissolved in 2 mL of toluene. Upon addition of **4-41** (14 mg, 0.024 mmol) the color gradually changed from purple to green. The reaction was stirred for 25 min, and filtered through a pad of Celite to remove NaOTf. The reaction was allowed to stir for 60 d in a base free box. After this time, excess CsCl (50 mg) was added to the solution, and allowed to react for 2 d. The products produced were **5-[4,6]** (74%) and **2-4** (26%), as determined by ^{31}P NMR and ^{19}F NMR spectroscopy.

Thermolysis of 2-6 with 4-39 in C$_6$H$_4$F$_2$. In an oven-dried J. Young tube, **2-6** (16 mg, 0.023 mmol) was dissolved in $C_6H_4F_2$. **4-39** was added to the solution, and the J. Young tube was shaken. The sample was then placed in a 100 ˚C oil bath overnight. Two broad resonances were observed by ^{31}P NMR spectroscopy at 55.9 and 41.9 ppm, and two by ^{19}F NMR spectroscopy at −111.4 and −111.5 ppm (**Figure 5.11**).

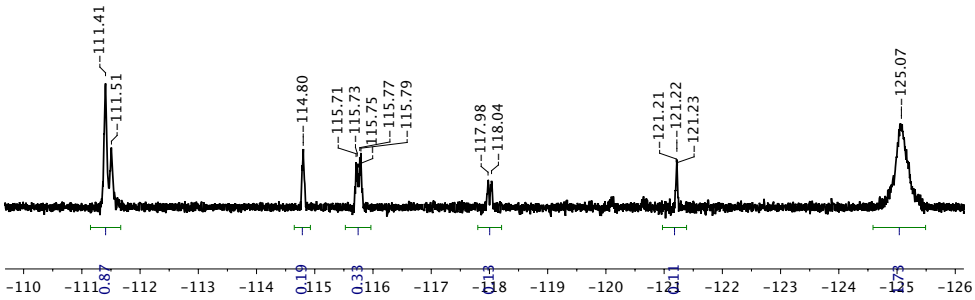

Figure 5.11 ^{19}F NMR spectrum of product mixture after thermolysis of **2-6** with **4-39** in $C_6H_4F_2$.

Thermolysis of 2-6 with 4-50 in $C_6D_5CD_3$. In an oven-dried J. Young tube, **2-6** (20 mg, 0.029 mmol) was dissolved in 0.5 mL of $C_6D_5CD_3$. To the solution, a small amount of C_6H_5F (3 mg) was added as an internal standard, and the ratio of C_6H_5F to **2-6** was determined by ^{19}F NMR spectroscopy. To the solution, **4-50** (40 mg, 0.070 mmol) was added, and the J. Young tube was vigorously shaken to allow the reagents to mix. The sample was then placed in a 115 °C oil bath for 7 days. During the course of the 7 days, a purple precipitate was formed on the walls of the J. Young tube. After adding excess CsCl (60 mg, 0.36 mmol), the sample was placed in the 115 °C oil bath for 4 h. No isomerization was observed, and **2-4** was the only product. However, based on the internal standard, only 30% of the initial ^{19}F NMR signal was recovered.

Isomerization solvent dependence. Four oven-dried, J. Young tubes were charged with **2-6** (15 mg, 0.022 mmol), and $NaCHB_{11}Cl_{11}$ (**4-39)** (13 mg, 0.024 mmol). Each sample was dissolved with 0.5 mL of C_6H_6, $C_6H_5CH_3$, C_6H_5F or 1,3,5-trimethylbenzene (mesitylene). The samples were sonicated for 1 h, and then placed in

an NMR tube rotator overnight. After irradiating the samples for 23 h with a 250-W halogen lamp, CsCl (85 mg, 0.50 mmol), and 0.25 mL of THF were added to each of the samples. The samples were placed on the NMR tube rotator for 48 h, and subsequently analyzed by ^{31}P, and ^{19}F NMR spectroscopy (see **Table 5.4** for product distribution).

Table 5.4 Product distribution from the isomerization of ($^{F}PNP^{iPr}$)Pd[$CHB_{11}Cl_{11}$] in C_6H_6, $C_6H_5CH_3$, C_6H_5F, and C_9H_{12} (mesitylene).

Solvent	**2-4**	**5-[2-3]**	**5-[4,6]**	**5-[8-9]**	**5-10**
Benzene (C_6H_6)	12%	1%	87%	0%	0%
Toluene ($C_6H_5CH_3$)	9%	10%	81%	0%	0%
Fluorobenzene (C_6H_5F)	22%	0%	72%	0%	6%
Mesitylene (C_9H_{12})	11%	6%	65%	10%	8%

Reaction between 2-6 with 4-39 in mesitylene. A J. Young tube was charged with **2-6** (15 mg, 0.022 mmol), and **4-39** (13 mg, 0.024 mmol). The mixture was then dissolved in 0.5 mL of mesitylene, and sonicated for 30 min. The sample was irradiated with a 250-W halogen lamp for a period of 4 d. Over the course of this time, a red oil began coating the inner part of the J. Young tube, leaving a light green solution. After treating the sample with 85 mg of CsCl, and 0.2 mL of THF, the sample was placed in the NMR tube rotator overnight. Analysis by ^{31}P NMR spectroscopy revealed formation of **5-[4,6]** (48%), **5-[8-3]** (20%), **5-10** (32%).

NMR data for **5-[8-9]**: $^{31}P\{^{1}H\}$ NMR (mesitylene/THF): δ 38.29 (d, J_{PP} = 446 Hz, $^{i}Pr^{n}PrP$); 26.36 (d, J_{PP} = 446 Hz, $^{n}Pr_{2}P$) (**Figure 5.12**); ^{19}F NMR (mesitylene/THF): (overlapping with **5-[4**,**6]** and **5-10**).

NMR data for **5-10**: $^{31}P\{^{1}H\}$ NMR (mesitylene/THF): δ 26.43; ^{19}F NMR (C_6D_6): δ 128.43 (**Figure 5.12**).

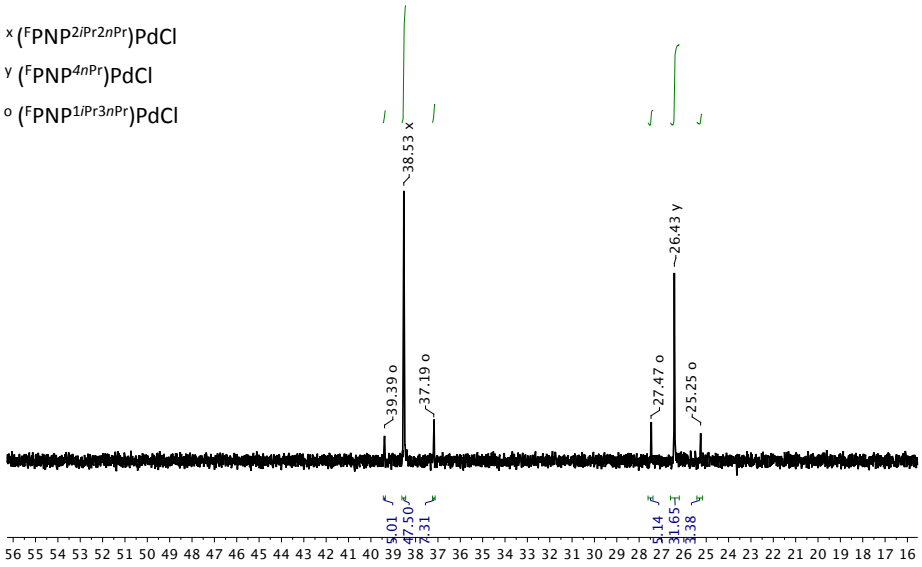

Figure 5.12 ^{31}P NMR spectrum (in mesitylene and THF) of mixture of **5-[4,6]**, **5-[8-9]**, and **5-10**.

Reaction between 2-6 with 4-39 in THF. A J. Young tube was charged with **2-6** (15 mg, 0.022 mmol), and **4-39** (13 mg, 0.024 mmol). The mixture was dissolved in 0.5 mL of THF and sonicated for 30 min. The solution was then irradiated with a 250-W halogen lamp for 20 h. After adding CsCl (85 mg, 0.50 mmol), the sample was placed in an NMR rotator overnight. ^{31}P NMR analysis revealed formation of **5-[4,6]** (14%), and **2-4** (86%)

Isomerization dependence on anion. Three oven-dried J. Young tubes were charged with **2-6** (15 mg, 0.022 mmol) and **4-35**, **4-39**, **4-41**; 0.024 mmol), each sample was then dissolved with 0.5 mL of C_6D_6. The samples were sonicated for 1 h, and then placed in an NMR rotator overnight. After irradiating the samples for 23 h with a 250-W halogen lamp, CsCl (85 mg) and 0.25 mL of THF were added to each of the samples. The samples were placed on the NMR rotator for 48 h, and subsequently analyzed by ^{31}P and ^{19}F NMR spectroscopy (see **Table 5.5** for product distribution).

Table 5.5 Product distribution from the isomerization of (^{F}PNP^{iPr})Pd[WCA] (WCA = $CHB_{11}Cl_{11}$, $BArF_{24}$, and $C^{n}BuB_{11}Cl_{11}$) in C_6D_6.

Anion	2-4	5-[2-3]	5-[4,6]	5-[10-11]	5-10
$[BArF_{24}]^-$	8%	24%	68%	0%	0%
$[CHB_{11}Cl_{11}]^-$	14%	18%	68%	0%	0%
$[C^{n}BuB_{11}Cl_{11}]^-$	27%	12%	61%	0%	0%

Irradiation of 2-6 in C_6D_6. In a J. Young tube **2-6** (10 mg, 0.022 mmol) was dissolved in 0.5 mL of C_6D_6. After 30 min of sonication, the sample was irradiated with a 250-W halogen lamp overnight. No change was observed by ^{31}P and ^{19}F NMR spectroscopy.

Irradiation of 2-6 with 4-41 (9 mol%) in C_6D_6. In a J. Young tube, **2-6** (16 mg, 0.022 mmol) and **4-41** (1 mg, 0.002 mmol) we dissolved in 0.5 mL of C_6D_6. After 30 min of sonication the sample was irradiated with a 250-W halogen lamp overnight. No change was observed by ^{31}P and ^{19}F NMR spectroscopy.

Reaction between 2-6 with 4-39 in the dark. An oven-dried vial was charged with **2-6** (15 mg, 0.022 mmol), **4-39** (13 mg, 0.024 mmol), and 0.7 mL of C_6D_6. The vial was then covered with enough aluminum foil to prevent light from entering the sample. After allowing the sample to stir for 1 h, the solution was filtered through Celite into a second oven-dried vial. The vial was then covered in aluminum foil and left in the glovebox. After 38 days, the sample was treated with excess CsCl (20 mg, 0.12 mmol), and 0.2 mL of THF and allowed to stir overnight while covered with aluminum foil. **2-4** was confirmed to be the only product by ^{31}P and ^{19}F NMR spectroscopy.

Role of light. Based on the control experiments, it is clear that the isomerization is induced by light. Exposing ($^{F}PNP^{iPr}$)Pd[WCA] to fluorescent lighting induces the isomerization, albeit very slowly. However, irradiation of ($^{F}PNP^{iPr}$)Pd[WCA] with a 250-

W halogen lamp source dramatically accelerates the conversion rate by approximately 30×. Thermolysis of (^{F}PNP^{iPr})Pd[WCA] does not seem to accelerate the isomerization; however, it is not clear because there is significant loss of ^{19}F NMR signal based on an internal standard experiment.

5.4.2 X-ray diffraction experiments

Data collection for 5-1 (solved by Dr. Bhuvanesh, N.). In an oven-dried vial, **2-6** (14 mg, 0.020 mmol) was dissolved in 2 mL of C_6D_6. Upon addition of **4-40** (11 mg, 0.020 mmol), the color gradually changed from purple to green. The solution was filtered through Celite into an NMR tube, layered with pentane, and then allowed to diffuse for approximately 4 weeks. After this time, several crystals were formed at the bottom of the NMR tube. A Leica MZ 75 microscope was used to identify a suitable green block with very well defined faces with dimensions (max, intermediate, and min) 0.22 × 0.18 × 0.15 mm from a representative sample of crystals of the same habit. The crystal mounted on a nylon loop was then placed in a cold nitrogen stream (Oxford) maintained at 110 K.

A BRUKER APEX2 X-ray (three-circle) diffractometer was employed for crystal screening, unit cell determination, and data collection. The goniometer was controlled using the APEX2 software suite, v2008-6.0.[177] The sample was optically centered with the aid of a video camera such that no translations were observed as the crystal was rotated through all positions. The detector was set at 6.0 cm from the crystal sample (APEX2, 512 × 512 pixel). The X-ray radiation employed was generated from a

Mo sealed X-ray tube (K_α = 0.70173 Å with a potential of 40 kV and a current of 40 mA) fitted with a graphite monochromator in the parallel mode (175 mm collimator with 0.5 mm pinholes).

Sixty data frames were taken at widths of 0.5°. These reflections were used in the auto-indexing procedure to determine the unit cell. A suitable cell was found, and refined by nonlinear least squares and Bravais lattice procedures. The unit cell was verified by examination of the *h k l* overlays on several frames of data by comparing with both the orientation matrices. No super-cell or erroneous reflections were observed. After careful examination of the unit cell, a standard data collection procedure was initiated using omega and phi scans.

Data reduction, structure solution, and refinement. Integrated intensity information for each reflection was obtained by reduction of the data frames with the program APEX2.[177] The integration method employed a three dimensional profiling algorithm and all data were corrected for Lorentz and polarization factors, as well as for crystal decay effects. Finally the data was merged and scaled to produce a suitable data set. The absorption correction program SADABS[178] was employed to correct the data for absorption effects.

Systematic reflection conditions and statistical tests of the data suggested the space group *P-1*. A solution was obtained readily using SHELXTL (XS).[179] Absence of additional symmetry or voids was confirmed using PLATON (ADDSYM).[180] Hydrogen atoms were placed in idealized positions and were set riding on the respective parent

atoms. All non-hydrogen atoms were refined with anisotropic thermal parameters. The larger thermal ellipsoids of several chlorine atoms indicated partial occupancy and correspondingly the location of C-Me group (also partially occupied); our efforts to model the disorder of C-Me and B-Cl groups in several positions started diverging even with strong restraints (EADP, EXYZ, SUMP, etc). Hence, we refined the occupancies of chlorine atoms in the initial stages and fixed to the refined valued in the final least square cycles. The C-Me group could not be located uniquely because of the multiple disorder of the $CMeB_{11}Cl_{11}$. Note that, accordingly, the formula (and associated quantities such as density, etc.) in the tables and the CIF file is not correct (The formulation is kept as in the refined .RES file to avoid additional Alerts in CHECKCIF). Several residual electron densities around the solvated toluene and benzene indicated further disorder of these molecules. No efforts were taken to further model this disorder. The structure was refined (weighted least squares refinement on F^2) to convergence.[179] [181] Olex2 was employed for the final data presentation and structure plots.[181]

Table 5.6 Crystal data and structure refinement for 5-1.

Empirical formula	$C_{43.86}H_{54.86}B_{12}Cl_{11.35}F_2NP_2Pd$	
Formula weight	1334.47	
Temperature	110(2) K	
Wavelength	0.71073 Å	
Crystal system	Triclinic	
Space group	*P-1*	
Unit cell dimensions	a = 11.848(3) Å	α = 88.817(7)°
	b = 14.273(3) Å	β = 75.117(6)°
	c = 18.955(4) Å	γ = 75.795(6)°
Volume	3000.1(11) $Å^3$	
Z	2	
Density (calculated)	1.477 Mg/m^3	
Absorption coefficient	0.908 mm^{-1}	
F(000)	1344	
Crystal size	0.22 × 0.18 × 0.15 mm^3	
Theta range for data collection	1.81 to 27.49°	
Index ranges	$-15 \le h \le 15$, $-18 \le k \le 18$, $-24 \le l \le 24$	
Reflections collected	34357	
Independent reflections	13423 [R(int) = 0.0527]	
Completeness to theta = 27.49°	97.4%	
Absorption correction	Semi-empirical from equivalents	
Max. and min. transmission	0.8759 and 0.8253	
Refinement method	Full-matrix least-squares on F^2	
Data / restraints / parameters	13423 / 0 / 603	
Goodness-of-fit on F^2	1.022	
Final R indices [I>2σ(I)]	$R1$ = 0.0558, wR2 = 0.1432	
R indices (all data)	$R1$ = 0.0942, wR2 = 0.1669	
Largest diff. peak and hole	1.255 $eÅ^{-3}$ and −0.860 $eÅ^{-3}$	

Data collection of 5-11 (solved by Dr. Bhuvanesh, N.). In an oven-dried vial, **2-26** (10 mg, 0.015 mmol) was dissolved in approx. 0.5 mL of toluene, the treated with **4-41** (0.017 mmol) and allowed to stir for a few minutes. The resulting solution was filtered through Celite into an oven-dried NMR tube and subsequently layered with pentane. After allowing the solution to diffuse/react for approx 4 weeks several crystals were formed at the bottom of NMR tube. A Leica MZ 75 microscope was used to identify a suitable green block with very well defined faces with dimensions (max, intermediate, and min) 0.18 × 0.15 × 0.12 mm from a representative sample of crystals of the same habit. The crystal mounted on a nylon loop was then placed in a cold nitrogen stream (Oxford) maintained at 110 K. A BRUKER APEX2 X-ray (three-circle) diffractometer was employed for crystal screening, unit cell determination, and data collection. The goniometer was controlled using the APEX2 software suite, v2008-6.0.[177] The sample was optically centered with the aid of a video camera such that no translations were observed as the crystal was rotated through all positions. The detector was set at 6.0 cm from the crystal sample (APEX2, 512 × 512 pixel). The X-ray radiation employed was generated from a Mo sealed X-ray tube (K_α = 0.70173 Å with a potential of 40 kV and a current of 40 mA) fitted with a graphite monochromator in the parallel mode (175 mm collimator with 0.5 mm pinholes).

Sixty data frames were taken at widths of 0.5°. These reflections were used in the auto-indexing procedure to determine the unit cell. A suitable cell was found and refined by nonlinear least squares and Bravais lattice procedures. The unit cell was verified by examination of the *h k l* overlays on several frames of data by comparing with both the

orientation matrices. No super-cell or erroneous reflections were observed. After careful examination of the unit cell, a standard data collection procedure including higher angles was initiated using omega scans.

Data reduction, structure solution, and refinement. Integrated intensity information for each reflection was obtained by reduction of the data frames with the program APEX2.[177] The integration method employed a three dimensional profiling algorithm and all data were corrected for Lorentz and polarization factors, as well as for crystal decay effects. Finally the data was merged and scaled to produce a suitable data set. The absorption correction program SADABS[178] was employed to correct the data for absorption effects.

Systematic reflection conditions and statistical tests of the data suggested the space group *P-1*. A solution was obtained readily using SHELXTL (XS).[179] Disordered solvent was found and identified as toluene in at least two positions, with a total of 1 molecule per unit cell. Hydrogen atoms were placed in idealized positions and were set riding on the respective parent atoms. All non-hydrogen atoms were refined with anisotropic thermal parameters. Solvated toluene was not stable through anistropic refinement in spite of significant restraints and constraints. Because the solvated toluene could not be modeled successfully they were SQUEEZEd out using PLATON.[180] This indicated 46 electrons, which is close to a molecule of toluene per unit cell. The formulation and the density given in CIF does not reflect the SQUEEZE'd content. The structure was refined (weighted least squares refinement on F^2) to convergence.[179,181] Olex2 was employed for the final data presentation and structure plots.[181]

Table 5.7 Crystal data and structure refinement for 5-11.

Empirical formula	$C_{41}H_{60}B_{22}Cl_{22}F_2NNaP_2Pd$	
Formula weight	1813.95	
Temperature	110(2) K	
Wavelength	0.71073 Å	
Crystal system	Triclinic	
Space group	*P-1*	
Unit cell dimensions	a = 16.823(9) Å	α = 100.128(9)°
	b = 17.236(9) Å	β = 108.721(9)°
	c = 17.520(15) Å	γ = 118.357(6)°
Volume	3892(4) $Å^3$	
Z	2	
Density (calculated)	1.548 Mg/m^3	
Absorption coefficient	1.079 mm^{-1}	
F(000)	1804	
Crystal size	0.18 × 0.15 × 0.12 mm^3	
Theta range for data collection	1.40 to 27.50°	
Index ranges	$-21 \le h \le 21$, $-22 \le k \le 22$, $-22 \le l \le 22$	
Reflections collected	45516	
Independent reflections	17658 [R(int) = 0.0837]	
Completeness to theta = 27.50°	98.8%	
Absorption correction	Semi-empirical from equivalents	
Max. and min. transmission	0.8815 and 0.8295	
Refinement method	Full-matrix least-squares on F^2	
Data / restraints / parameters	17658 / 0 / 838	
Goodness-of-fit on F^2	1.034	
Final R indices [I>2σ(I)]	$R1$ = 0.0565, wR2 = 0.1110	
R indices (all data)	$R1$ = 0.1083, wR2 = 0.1321	
Largest diff. peak and hole	0.694 $eÅ^{-3}$ and −0.979 $eÅ^{-3}$	

CHAPTER VI

CONCLUSION

During the course of our studies we have explored the chemistry of divalent (PNP)PdX complexes. The tridentate and meridional coordination of the diarylamido-PNP ligand restricts the reactivity in (PNP)PdX complexes to the fourth coordination site. This has provided the unique opportunity to study the reactivity of unusual ligands such as O_2 and C_2H_4. In addition, the pincer motif allows us to study the reactivity of a palladium complex with an empty coordination site *trans* to a weak *trans*-influence ligand such as diarylamido. This dissertation has predominantly focused on the reactivity of $[(^{F}PNP^{iPr})Pd\text{-}]_2$ and $(^{F}PNP^{iPr})Pd[WCA]$. The reactivity of these complexes can best be understood by viewing $[(^{F}PNP^{iPr})Pd\text{-}]_2$ and (PNP)Pd[WCA] as synthons for $(^{F}PNP^{iPr})Pd(I)$ radical monomer and $[(PNP)Pd]^{+}$ cation, respectively.

Irradiation of $[(^{F}PNP^{iPr})Pd\text{-}]_2$ under an atmosphere of molecular oxygen produces a mixture of $(^{F}PNP^{iPr})PdO_2$ (95%) and $[(^{F}PNP^{iPr})PdO\text{-}]_2$ (5%). If $[(^{F}PNP^{iPr})Pd\text{-}]_2$ is irradiated under a deficiency of O_2 the major product formed is $[(^{F}PNP^{iPr})PdO\text{-}]_2$. It was also determined that under photolytic conditions, $[(^{F}PNP^{iPr})PdO\text{-}]_2$ is in equilibrium with $(^{F}PNP^{iPr})PdO_2$ and free O_2. $(^{F}PNP^{iPr})PdO_2$ is an open-shell paramagnetic species with the electron localized on the O_2 fragment. $(^{F}PNP^{iPr})PdO_2$ was characterized by EPR spectroscopy and is silent by ^{31}P NMR spectroscopy, but exhibits a relatively sharp ^{19}F NMR spectrum, and a broad ^{1}H NMR spectrum. In contrast, $[(^{F}PNP^{iPr})PdO\text{-}]_2$ is a closed-shell, diamagnetic species that is observed by ^{1}H, ^{31}P and ^{19}F NMR spectroscopy.

In addition, if [(^{F}PNP^{iPr})Pd-]$_2$ is irradiated under an atmosphere of C_2H_4 a mixture of [(^{F}PNP^{iPr})Pd-CH$_2$-]$_2$ and [(^{F}PNP^{iPr})Pd-]$_2$ is observed. Although η^2-O_2-Pd and η^2-(C_2H_4)-Pd complexes are well known, [(^{F}PNP^{iPr})PdO-]$_2$, (^{F}PNP^{iPr})PdO$_2$ and [(^{F}PNP^{iPr})Pd-CH$_2$-]$_2$ are unique because they are rare examples of O_2 and C_2H_4 ligating to Pd in a η^1 fashion. This is possible because the tridentate, meridional coordination of the PNP ligand restricts the number of accessible coordination sites to one, and therefore limits the hapticity of dioxygen and ethylene to η^1.

This dissertation is also focused on the synthesis and reactivity of [(PNP)Pd]$^+$ cations. Although we were not able to isolate the desired three-coordinate, 14-electron, [(PNP)Pd]$^+$ cation, we were able to discover a rare example of an η^1 arene adduct. To avoid arene coordination, new bulkier (^{F}PN(Me)P^{R}) (R = Ad and ^{t}Bu) ligands were developed. These ligands were applied towards the synthesis of [(^{F}PNP^{tBu})Pd]$^+$ cations; further investigation is necessary to determine the structure of these complexes. It was also discovered that (^{F}PNP^{iPr})Pd[WCA] undergoes an unprecedented photo-induced isomerization of di-isopropyl groups on ^{F}PNP. In most examples of C-P bond activation, a bridging phosphido ligand is formed, or an R group on the phosphine is exchanged for another group (e.g. -NR$_2$, -OR). However, the isomerization of (^{F}PNP^{iPr})Pd[WCA] is unique in that the final product remains a tertiary phosphine. It is believed that the driving force for the isomerization of the [(^{F}PNP^{iPr})Pd]$^+$ cation is the reduction of the sterics around the metal that facilitates the coordination of the fourth ligand (i.e. arene). The phosphines in (^{F}PNP^{iPr})PdX complexes are typically considered spectator ligands; however, the isomerization of (^{F}PNP^{iPr})Pd[WCA] illustrates that under certain conditions

phosphines can behave as non-innocent ligands. The fact that the isomerization does not occur in complexes such as **2-4** and does in (^{F}PNP$^{i\text{Pr}}$)Pd[WCA] suggests that an empty coordination site is necessary for the isomerization to occur. Further investigation is necessary to determine the mechanism of this unusual isomerization.

REFERENCES

1. Moulton, C. J.; Shaw, B. L. *Dalton Trans.* **1976**, 1020.

2. van Koten, G.; Milstein, D., *Noninnocent Behavior of PCP and PCN Pincer Ligands of Late Metal Complexes*. Springer: Berlin Heidelberg, 2013; Vol. 40.

3. van der Boom, M. E.; Milstein, D. *Chem. Rev.* **2003**, *103*, 1759.

4. Morales-Morales, D.; Jensen, C. M., *The Chemistry of Pincer Compounds*. Elsevier: Amsterdam, The Netherlands, 2007.

5. Vaska, L. *Acc. Chem. Res.* **1968**, *1*, 335.

6. Vaska, L.; Diluzio, J. W. *J. Am. Chem. Soc.* **1962**, *84*, 679.

7. Choi, J.; MacArthur, A. H. R.; Brookhart, M.; Goldman, A. S. *Chem. Rev.* **2011**, *111*, 1761.

8. Ozerov, O. V.; Guo, C. Y.; Fan, L.; Foxman, B. M. *Organometallics* **2004**, *23*, 5573.

9. Zuideveld, M. A.; Swennenhuis, B. H. G.; Boele, M. D. K.; Guari, Y.; van Strijdonck, G. P. F.; Reek, J. N. H.; Kamer, P. C. J.; Goubitz, K.; Fraanje, J.; Lutz, M.; Spek, A. L.; van Leeuwen, P. *Dalton Trans.* **2002**, 2308.

10. Masuda, Y.; Hasegawa, M.; Yamashita, M.; Nozaki, K.; Ishida, N.; Murakami, M. *J. Am. Chem. Soc.* **2013**, *135*, 7142.

11. Weng, W.; Parkin, S.; Ozerov, O. V. *Organometallics* **2006**, *25*, 5345.

12. MacInnis, M. C.; McDonald, R.; Ferguson, M. J.; Tobisch, S.; Turculet, L. *J. Am. Chem. Soc.* **2011**, *133*, 13622.

13. Morgan, E.; MacLean, D. F.; McDonald, R.; Turculet, L. *J. Am. Chem. Soc.* **2009**, *131*, 14234.

14. Tulchinsky, Y.; Iron, M. A.; Botoshansky, M.; Gandelman, M. *Nature Chem.* **2011**, *3*, 525.

15. Khaskin, E.; Iron, M. A.; Shimon, L. J. W.; Zhang, J.; Milstein, D. *J. Am. Chem. Soc.* **2010**, *132*, 8542.

16. Kohl, S. W.; Weiner, L.; Schwartsburd, L.; Konstantinovski, L.; Shimon, L. J. W.; Ben-David, Y.; Iron, M. A.; Milstein, D. *Science* **2009**, *324*, 74.

17. Fan, H.; Fullmer, B. C.; Pink, M.; Caulton, K. G. *Angew. Chem., Int. Ed.* **2008**, *47*, 9112.

18. Fullmer, B. C.; Fan, H.; Pink, M.; Huffman, J. C.; Tsvetkov, N. P.; Caulton, K. G. *J. Am. Chem. Soc.* **2011**, *133*, 2571.

19. Fullmer, B. C.; Fan, H. J.; Pink, M.; Caulton, K. G. *Inorg. Chim. Acta* **2011**, *369*, 49.

20. Ingleson, M. J.; Pink, M.; Caulton, K. G. *J. Am. Chem. Soc.* **2006**, *128*, 4248.

21. Ingleson, M. J.; Pink, M.; Fan, H.; Caulton, K. G. *Inorg. Chem.* **2007**, *46*, 10321.

22. Ingleson, M. J.; Pink, M.; Fan, H.; Caulton, K. G. *J. Am. Chem. Soc.* **2008**, *130*, 4262.

23. Berthon-Gelloz, G.; de Bruin, B.; Tinant, B.; Marko, I. E. *Angew. Chem., Int. Ed.* **2009**, *48*, 3161.

24. Rivada-Wheelaghan, O.; Ortuno, M. A.; Diez, J.; Garcia-Garrido, S. E.; Maya, C.; Lledos, A.; Conejero, S. *J. Am. Chem. Soc.* **2012**, *134*, 15261.

25. Rivada-Wheelaghan, O.; Ortuno, M. A.; Diez, J.; Lledos, A.; Conejero, S. *Angew. Chem., Int. Ed.* **2012**, *51*, 3936.

26. Takagi, N.; Sakaki, S. *J. Am. Chem. Soc.* **2012**, *134*, 11749.

27. Urtel, H.; Meier, C.; Eisentrager, F.; Rominger, F.; Joschek, J. P.; Hofmann, P. *Angew. Chem., Int. Ed.* **2001**, *40*, 781.

28. Yamashita, M.; Hartwig, J. F. *J. Am. Chem. Soc.* **2004**, *126*, 5344.

29. Xu, W. W.; Rosini, G. P.; Gupta, M.; Jensen, C. M.; Kaska, W. C.; KroghJespersen, K.; Goldman, A. S. *Chem. Commun.* **1997**, 2273.

30. Goldman, A. S.; Roy, A. H.; Huang, Z.; Ahuja, R.; Schinski, W.; Brookhart, M. *Science* **2006**, *312*, 257.

31. Arduengo, A. J.; Bertrand, G. *Chem. Rev.* **2009**, *109*, 3209.

32. Arduengo, A. J. *Acc. Chem. Res.* **1999**, *32*, 913.

33. Enders, D.; Niemeier, O.; Henseler, A. *Chem. Rev.* **2007**, *107*, 5606.

34. Hirai, K.; Itoh, T.; Tomioka, H. *Chem. Rev.* **2009**, *109*, 3275.

35. Kamber, N. E.; Jeong, W.; Waymouth, R. M.; Pratt, R. C.; Lohmeijer, B. G. G.; Hedrick, J. L. *Chem. Rev.* **2007**, *107*, 5813.

36. Samojlowicz, C.; Bieniek, M.; Grela, K. *Chem. Rev.* **2009**, *109*, 3708.

37. Kuhl, O. *Chem. Soc. Rev.* **2007**, *36*, 592.

38. Raubenheimer, H. G.; Cronje, S. *Chem. Soc. Rev.* **2008**, *37*, 1998.

39. Wu, T.; Li, M.; Li, D.; Huang, X.-C. *Cryst. Growth Des.* **2008**, *8*, 568.

40. Goreshnik, E. A.; Pavlyuk, A. V.; Schollmeyer, D.; Mys'kiv, M. G. *Russ. J. Coord. Chem.* **1999**, *25*, 653.

41. Hassani, K.; Marsch, M.; Harms, K.; Boche, G. *Z. Kristallogr. - New Cryst. Struct.* **2001**, *216*, 425.

42. Winter, A. M.; Eichele, K.; Mack, H. G.; Potuznik, S.; Mayer, H. A.; Kaska, W. C. *J. Organomet. Chem.* **2003**, *682*, 149.

43. Fryzuk, M. D.; Macneil, P. A.; Rettig, S. J. *Organometallics* **1986**, *5*, 2469.

44. Vasapollo, G.; Giannoccaro, P.; Nobile, C. F.; Sacco, A. *Inorg. Chim. Acta* **1981**, *48*, 125.

45. Chase, P. A.; Stephan, D. W. *Angew. Chem., Int. Ed.* **2008**, *47*, 7433.

46. Nakajima, Y.; Kameo, H.; Suzuki, H. *Angew. Chem., Int. Ed.* **2006**, *45*, 950.

47. Koelliker, R.; Milstein, D. *Angew. Chem., Int. Ed.* **1991**, *30*, 707.

48. Casalnuovo, A. L.; Calabrese, J. C.; Milstein, D. *Inorg. Chem.* **1987**, *26*, 971.

49. Hillhouse, G. L.; Bercaw, J. E. *J. Am. Chem. Soc.* **1984**, *106*, 5472.

50. Jana, A.; Schulzke, C.; Roesky, H. W. *J. Am. Chem. Soc.* **2009**, *131*, 4600.

51. Peng, Y.; Ellis, B. D.; Wang, X. P.; Power, P. P. *J. Am. Chem. Soc.* **2008**, *130*, 12268.

52. Jana, A.; Roesky, H. W.; Schulzke, C.; Samuel, P. P. *Organometallics* **2009**, *28*, 6574.

53. Frey, G. D.; Lavallo, V.; Donnadieu, B.; Schoeller, W. W.; Bertrand, G. *Science* **2007**, *316*, 439.

54. Fafard, C. M.; Adhikari, D.; Foxman, B. M.; Mindiola, D. J.; Ozerov, O. V. *J. Am. Chem. Soc.* **2007**, *129*, 10318.

55. Zhao, J.; Goldman, A. S.; Hartwig, J. F. *Science* **2005**, *307*, 1080.

56. Liang, L. C.; Lin, J. M.; Lee, W. Y. *Chem. Commun.* **2005**, 2462.

57. Liang, L. C.; Lin, J. M.; Hung, C. H. *Organometallics* **2003**, *22*, 3007.

58. Mindiola, D. J. *Acc. Chem. Res.* **2006**, *39*, 813.

59. Adhikari, D.; Mossin, S.; Basuli, F.; Dible, B. R.; Chipara, M.; Fan, H.; Huffman, J. C.; Meyer, K.; Mindiola, D. J. *Inorg. Chem.* **2008**, *47*, 10479.

60. Adhikari, D.; Mossin, S.; Basuli, F.; Huffman, J. C.; Szilagyi, R. K.; Meyer, K.; Mindiola, D. J. *J. Am. Chem. Soc.* **2008**, *130*, 3676.

61. Whited, M. T.; Zhu, Y. J.; Timpa, S. D.; Chen, C. H.; Foxman, B. M.; Ozerov, O. V.; Grubbs, R. H. *Organometallics* **2009**, *28*, 4560.

62. Timpa, S. D.; Fafard, C. M.; Herbert, D. E.; Ozerov, O. V. *Dalton Trans.* **2011**, *40*, 5426.

63. Fafard, C. M.; Chen, C.-H.; Foxman, B. M.; Ozerov, O. V. *Chem. Commun.* **2007**, 4465.

64. Weng, W.; Guo, C. Y.; Celenligil-Cetin, R.; Foxman, B. M.; Ozerov, O. V. *Chem. Commun.* **2006**, 197.

65. DeMott, J. C.; Bhuvanesh, N.; Ozerov, O. V. *Chem. Sci.* **2013**, *4*, 642.

66. Gregor, L. C.; Chen, C.-H.; Fafard, C. M.; Fan, L.; Guo, C.; Foxman, B. M.; Gusev, D. G.; Ozerov, O. V. *Dalton Trans.* **2010**, *39*, 3195.

67. Zhu, Y.; Chen, C.-H.; Fafard, C. M.; Foxman, B. M.; Ozerov, O. V. *Inorg. Chem.* **2011**, *50*, 7980.

68. Fan, L.; Parkin, S.; Ozerov, O. V. *J. Am. Chem. Soc.* **2005**, *127*, 16772.

69. Huacuja, R.; Graham, D. J.; Fafard, C. M.; Chen, C. H.; Foxman, B. M.; Herbert, D. E.; Alliger, G.; Thomas, C. M.; Ozerov, O. V. *J. Am. Chem. Soc.* **2011**, *133*, 3820.

70. Fan, L.; Foxman, B. M.; Ozerov, O. V. *Organometallics* **2004**, *23*, 326.

71. Frisch, M. J.; Trucks, G. W.; Schlegel, H. B.; Scuseria, G. E.; Robb, M. A.; Cheeseman, J. R.; Montgomery, J. A.; Vreven, T.; Kudin, K. N.; Burant, J. C.; Millam, J. M.; Iyengar, S. S.; Tomasi, J.; Barone, V.; Mennucci, B.; Cossi, M.; Scalmani, G.; Rega, N.; Petersson, G. A.; Nakatsuji, H.; Hada, M.; Ehara, M.; Toyota, K.; Fukuda, R.; Hasegawa, J.; Ishida, M.; Nakajima, T.; Honda, Y.; Kitao, O.; Nakai, H.; Klene, M.; Li, X.; Knox, J. E.; Hratchian, H. P.; Cross, J. B.; Adamo, C.; Jaramillo, J.; Gomperts, R.; Stratmann, R. E.; Yazyev, O.; Austin, A. J.; Cammi, R.; Pomelli, C.; Ochterski, J. W.; Ayala, P. Y.; Morokuma, K.; Voth, G. A.; Salvador, P.; Dannenberg, J. J.; Zakrzewski, V. G.; Dapprich, S.; Daniels, A. D.; Strain, M. C.; Farkas, O.; Malick, D. K.; Rabuck, A. D.; Raghavachari, K.; Foresman, J. B.; Ortiz, J. V.; Cui, Q.; Baboul, A. G.; Clifford, S.; Cioslowski, J.; Stefanov, B. B.; Liu, G.; Liashenko, A.; Piskorz, P.; Komaromi, I.; Martin, R. L.; Fox, D. J.; Keith, T.; Al-Laham, M. A.; Peng, C. Y.; Nanayakkara, A.; Challacombe, M.; Gill, P. M. W.; Johnson, B.; Chen, W.; Wong, M. W.; Gonzalez, C.; Pople, J. A. GAUSSIAN (revision A.1), Gaussian, Inc., Wallingford, CT, 2004.

72. Gatard, S.; Chen, C.-H.; Foxman, B. M.; Ozerov, O. V. *Organometallics* **2008**, *27*, 6257.

73. Gatard, S.; Guo, C.; Foxman, B. M.; Ozerov, O. V. *Organometallics* **2007**, *26*, 6066.

74. Weng, W.; Guo, C.; Moura, C.; Yang, L.; Foxman, B. M.; Ozerov, O. V. *Organometallics* **2005**, *24*, 3487.

75. Zhu, Y.; Fan, L.; Chen, C.-H.; Finnell, S. R.; Foxman, B. M.; Ozerov, O. V. *Organometallics* **2007**, *26*, 6701.

76. Brookes, N. J.; Whited, M. T.; Ariafard, A.; Stranger, R.; Grubbs, R. H.; Yates, B. F. *Organometallics* **2010**, *29*, 4239.

77. Radosevich, A. T.; Melnick, J. G.; Stoian, S. A.; Bacciu, D.; Chen, C. H.; Foxman, B. M.; Ozerov, O. V.; Nocera, D. G. *Inorg. Chem.* **2009**, *48*, 9214.

78. Zhu, Y. J.; Smith, D. A.; Herbert, D. E.; Gatard, S.; Ozerov, O. V. *Chem. Commun.* **2012**, *48*, 218.

79. Gatard, S.; Celenligil-Cetin, R.; Guo, C. Y.; Foxman, B. M.; Ozerov, O. V. *J. Am. Chem. Soc.* **2006**, *128*, 2808.

80. Fryzuk, M. D.; Macneil, P. A.; McManus, N. T. *Organometallics* **1987**, *6*, 882.

81. Cohen, R.; Rybtchinski, B.; Gandelman, M.; Rozenberg, H.; Martin, J. M. L.; Milstein, D. *J. Am. Chem. Soc.* **2003**, *125*, 6532.

82. Zhang, X. W.; Emge, T. J.; Ghosh, R.; Goldman, A. S. *J. Am. Chem. Soc.* **2005**, *127*, 8250.

83. Budzelaar, P. H. M.; de Gelder, R.; Gal, A. W. *Organometallics* **1998**, *17*, 4121.

84. Cetinkaya, B.; Lappert, M. F.; Torroni, S. *Chem. Commun.* **1979**, 843.

85. Fryzuk, M. D. *Can. J. Chem.* **1992**, *70*, 2839.

86. Fryzuk, M. D.; Haddad, T. S.; Berg, D. J. *Coord. Chem. Rev.* **1990**, *99*, 137.

87. Fryzuk, M. D.; Montgomery, C. D. *Coord. Chem. Rev.* **1989**, *95*, 1.

88. Holland, P. L.; Cundari, T. R.; Perez, L. L.; Eckert, N. A.; Lachicotte, R. J. *J. Am. Chem. Soc.* **2002**, *124*, 14416.

89. Fout, A. R.; Basuli, F.; Fan, H.; Tomaszewski, J.; Huffman, J. C.; Baik, M.-H.; Mindiola, D. J. *Angew. Chem., Int. Ed.* **2006**, *45*, 3291.

90. Fryzuk, M. D.; Leznoff, D. B.; Thompson, R. C.; Rettig, S. J. *J. Am. Chem. Soc.* **1998**, *120*, 10126.

91. Ingleson, M. J.; Fullmer, B. C.; Buschhorn, D. T.; Fan, H.; Pink, M.; Huffman, J. C.; Caulton, K. G. *Inorg. Chem.* **2008**, *47*, 407.

92. Walensky, J. R.; Fafard, C. M.; Guo, C. Y.; Brammell, C. M.; Foxman, B. M.; Hall, M. B.; Ozerov, O. V. *Inorg. Chem.* **2013**, *52*, 2317.

93. Baratta, W.; Stoccoro, S.; Doppiu, A.; Herdtweck, E.; Zucca, A.; Rigo, P. *Angew. Chem., Int. Ed.* **2003**, *42*, 105.

94. Ingleson, M. J.; Mahon, M. F.; Weller, A. S. *Chem. Commun.* **2004**, 2398.

95. Stambuli, J. P.; Buhl, M.; Hartwig, J. F. *J. Am. Chem. Soc.* **2002**, *124*, 9346.

96. Stambuli, J. P.; Incarvito, C. D.; Buhl, M.; Hartwig, J. F. *J. Am. Chem. Soc.* **2004**, *126*, 1184.

97. Yared, Y. W.; Miles, S. L.; Bau, R.; Reed, C. A. *J. Am. Chem. Soc.* **1977**, *99*, 7076.

98. Walter, M. D.; White, P. S.; Brookhart, M. *New J. Chem.* **2013**, *37*, 1128.

99. HayMotherwell, R.; Wilkinson, G.; Sweet, T. K. N.; Hursthouse, M. B. *Polyhedron* **1996**, *15*, 3163.

100. Walstrom, A.; Pink, M.; Caulton, K. G. *Inorg. Chem.* **2006**, *45*, 5617.

101. Miyaura, N.; Suzuki, A. *Chem. Rev.* **1995**, *95*, 2457.

102. Liu, C.; Zhang, H.; Shi, W.; Lei, A. *Chem. Rev.* **2011**, *111*, 1780.

103. Hartwig, J. F. *Organotransition Metal Chemistry: From Bonding to Catalysis*. University Science Books: Mill Valley, 2010.

104. Roy, A. H.; Hartwig, J. F. *J. Am. Chem. Soc.* **2003**, *125*, 13944.

105. Moncho, S.; Ujaque, G.; Lledos, A.; Espinet, P. *Chem. Eur. J.* **2008**, *14*, 8986.

106. Moncho, S.; Ujaque, G.; Espinet, P.; Maseras, F.; Lledos, A. *Theor. Chem. Acc.* **2009**, *123*, 75.

107. Shilov, A. E.; Shul'pin, G. B. *Chem. Rev.* **1997**, *97*, 2879.

108. Shilov, A. E.; Shteinman, A. A. *Coord. Chem. Rev.* **1977**, *24*, 97.

109. Goldshle, N.; Shteinma, A.; Shilov, A. E.; Eskova, V. V. *Russ. J. Phys. Chem.* **1972**, *46*, 785.

110. Braunschweig, H.; Radacki, K.; Rais, D.; Scheschkewitz, D. *Angew. Chem., Int. Ed.* **2005**, *44*, 5651.

111. Sivignon, G.; Fleurat-Lessard, P.; Onno, J. M.; Volatron, F. *Inorg. Chem.* **2002**, *41*, 6656.

112. Lam, K. C.; Lam, W. H.; Lin, Z. Y.; Marder, T. B.; Norman, N. C. *Inorg. Chem.* **2004**, *43*, 2541.

113. Braunschweig, H.; Green, H.; Radacki, K.; Uttinger, K. *Dalton Trans.* **2008**, 3531.

114. Braunschweig, H.; Radacki, K.; Uttinger, K. *Chem. Eur. J.* **2008**, *14*, 7858.

115. Wurtz, S.; Glorius, F. *Acc. Chem. Res.* **2008**, *41*, 1523.

116. Clavier, H.; Nolan, S. P. *Chem. Commun.* **2010**, *46*, 9260.

117. Masters, S. L.; Grassie, D. A.; Robertson, H. E.; Holbling, M.; Hassler, K. *Chem. Commun.* **2007**, 2618.

118. Ozawa, F.; Kamite, J. *Organometallics* **1998**, *17*, 5630.

119. Chen, W. Z.; Shimada, S.; Tanaka, M. *Science* **2002**, *295*, 308.

120. Crabtree, R. H. *Science* **2002**, *295*, 288.

121. Aullon, G.; Lledos, A.; Alvarez, S. *Angew. Chem., Int. Ed.* **2002**, *41*, 1956.

122. Morales-Morales, D.; Lee, D. W.; Wang, Z. H.; Jensen, C. M. *Organometallics* **2001**, *20*, 1144.

123. Selander, N.; Szabo, K. J. *Chem. Rev.* **2011**, *111*, 2048.

124. Gupta, M.; Hagen, C.; Flesher, R. J.; Kaska, W. C.; Jensen, C. M. *Chem. Commun.* **1996**, 2083.

125. Jensen, C. M. *Chem. Commun.* **1999**, 2443.

126. Gupta, M.; Hagen, C.; Kaska, W. C.; Cramer, R. E.; Jensen, C. M. *J. Am. Chem. Soc.* **1997**, *119*, 840.

127. Liu, F. C.; Pak, E. B.; Singh, B.; Jensen, C. M.; Goldman, A. S. *J. Am. Chem. Soc.* **1999**, *121*, 4086.

128. Lee, D. W.; Kaska, W. C.; Jensen, C. M. *Organometallics* **1998**, *17*, 1.

129. Choi, J.; Wang, D. Y.; Kundu, S.; Choliy, Y.; Emge, T. J.; Krogh-Jespersen, K.; Goldman, A. S. *Science* **2011**, *332*, 1545.

130. Liang, L. C. *Coord. Chem. Rev.* **2006**, *250*, 1152.

131. DeMott, J. C.; Surawatanawong, P.; Barnett, S. M.; Chen, C.-H.; Foxman, B. M.; Ozerov, O. V. *Dalton Trans.* **2011**, *40*, 11562.

132. Herbert, D. E.; Miller, A. D.; Ozerov, O. V. *Chem. Eur. J.* **2012**, *18*, 7696.

133. Fryzuk, M. D.; Macneil, P. A. *J. Am. Chem. Soc.* **1981**, *103*, 3592.

134. Ozerov, O. V.; Watson, L. A.; Pink, M.; Caulton, K. G. *J. Am. Chem. Soc.* **2007**, *129*, 6003.

135. Fan, L.; Yang, L.; Guo, C. Y.; Foxman, B. M.; Ozerov, O. V. *Organometallics* **2004**, *23*, 4778.

136. Davidson, J. J., unpublished results.

137. DeMott, J. C.; Davidson, J. J., unpublished results.

138. Zhu, Y., unpublished results.

139. Vigalok, A. *Chem. Eur. J.* **2008**, *14*, 5102.

140. Murphy, E. F.; Murugavel, R.; Roesky, H. W. *Chem. Rev.* **1997**, *97*, 3425.

141. Grushin, V. V. *Chem. Eur. J.* **2002**, *8*, 1006.

142. Doherty, N. M.; Hoffman, N. W. *Chem. Rev.* **1991**, *91*, 553.

143. Grushin, V. V.; Marshall, W. J. *J. Am. Chem. Soc.* **2009**, *131*, 918.

144. Grushin, V. V.; Marshall, W. J. *Angew. Chem., Int. Ed.* **2002**, *41*, 4476.

145. Grushin, V. V. *Organometallics* **2000**, *19*, 1888.

146. Yahav, A.; Goldberg, I.; Vigalok, A. *J. Am. Chem. Soc.* **2003**, *125*, 13634.

147. Yandulov, D. V.; Tran, N. T. *J. Am. Chem. Soc.* **2007**, *129*, 1342.

148. Grushin, V. V. *Acc. Chem. Res.* **2010**, *43*, 160.

149. Watson, D. A.; Su, M.; Teverovskiy, G.; Zhang, Y.; Garcia-Fortanet, J.; Kinzel, T.; Buchwald, S. L. *Science* **2009**, *325*, 1661.

150. Hull, K. L.; Anani, W. Q.; Sanford, M. S. *J. Am. Chem. Soc.* **2006**, *128*, 7134.

151. Wang, X.; Mei, T.-S.; Yu, J.-Q. *J. Am. Chem. Soc.* **2009**, *131*, 7520.

152. Furuya, T.; Benitez, D.; Tkatchouk, E.; Strom, A. E.; Tang, P.; Goddard, W. A., III; Ritter, T. *J. Am. Chem. Soc.* **2010**, *132*, 3793.

153. Furuya, T.; Ritter, T. *J. Am. Chem. Soc.* **2008**, *130*, 10060.

154. Furuya, T.; Kaiser, H. M.; Ritter, T. *Angew. Chem., Int. Ed.* **2008**, *47*, 5993.

155. Ball, N. D.; Kampf, J. W.; Sanford, M. S. *Dalton Trans.* **2010**, *39*, 632.

156. Huacuja, R.; Herbert, D. E.; Fafard, C. M.; Ozerov, O. V. *J. Fluorine Chem.* **2010**, *131*, 1257.

157. Fafard, C. M.; Ozerov, O. V. *Inorg. Chim. Acta* **2007**, *360*, 286.

158. Ozerov, O. V.; Guo, C. Y.; Papkov, V. A.; Foxman, B. M. *J. Am. Chem. Soc.* **2004**, *126*, 4792.

159. Tolman, C. A. *Chem. Rev.* **1977**, *77*, 313.

160. Bernskoetter, W. H.; Schauer, C. K.; Goldberg, K. I.; Brookhart, M. *Science* **2009**, *326*, 553.

161. Murata, M.; Buchwald, S. L. *Tetrahedron* **2004**, *60*, 7397.

162. Farrugia, L. *J. Appl. Crystallogr.* **1997**, *30*, 565.

163. Yahav, A.; Goldberg, I.; Vigalok, A. *Inorg. Chem.* **2005**, *44*, 1547.

164. Veltheer, J. E.; Burger, P.; Bergman, R. G. *J. Am. Chem. Soc.* **1995**, *117*, 12478.

165. Caskey, S. R.; Stewart, M. H.; Ahn, Y. J.; Johnson, M. J. A.; Rowsell, J. L. C.; Kampf, J. W. *Organometallics* **2007**, *26*, 1912.

166. Brewer, S. A.; Holloway, J. H.; Hope, E. G.; Watson, P. G. *Chem. Commun.* **1992**, 1577.

167. Bourgeois, C. J.; Garratt, S. A.; Hughes, R. P.; Larichev, R. B.; Smith, J. M.; Ward, A. J.; Willemsen, S.; Zhang, D.; DiPasquale, A. G.; Zakharov, L. N.; Rheingold, A. L. *Organometallics* **2006**, *25*, 3474.

168. Agbossou, S. K.; Roger, C.; Igau, A.; Gladysz, J. A. *Inorg. Chem.* **1992**, *31*, 419.

169. Fraser, S. L.; Antipin, M. Y.; Khroustalyov, V. N.; Grushin, V. V. *J. Am. Chem. Soc.* **1997**, *119*, 4769.

170. Dixon, K. R.; McFarlan, J. *Chem. Commun.* **1972**, 1274.

171. Hiyama, T. *J. Organomet. Chem.* **2002**, *653*, 58.

172. Ball, N. D.; Kampf, J. W.; Sanford, M. S. *J. Am. Chem. Soc.* **2010**, *132*, 2878.

173. Fafard, C. M. PhD. Dissertation, Brandeis University, 2009.

174. Gomelya, N. D.; Feshchenko, N. G. *Zh. Obshch. Khim.* **1987**, *57*, 1702.

175. Matthias, B.; Ehrentraut, A.; Hubert, W.; Elisabeth, T.; Fuhrmann, C.; Zapf, A. U.S. Patent 7148176, February 7, 2002.

176. Gusev, D. G.; Madott, M.; Dolgushin, F. M.; Lyssenko, K. A.; Antipin, M. Y. *Organometallics* **2000**, *19*, 1734.

177. Apex2, Version 2 User Manual; M86-E01078, Bruker Analytical X-ray Systems: Madison, WI, June 2006.

178. SADABS, Sheldrick, G.M. “Program for Absorption Correction of Area Detector Frames”, BRUKER AXS Inc., 5465 East Cheryl Parkway, Madison, WI 53711-5373 USA

179. Sheldrick, G. M. *Acta Crystallogr., Sect. A* **2008**, *64*, 112.

180. Spek, A. L. *J. Appl. Crystallogr.* **2003**, *36*, 7.

181. Dolomanov, O. V.; Bourhis, L. J.; Gildea, R. J.; Howard, J. A. K.; Puschmann, H. *J. Appl. Crystallogr.* **2009**, *42*, 339.

182. Cui, W.; Wayland, B. B. *J. Am. Chem. Soc.* **2006**, *128*, 10350.

183. Schweitzer, C.; Schmidt, R. *Chem. Rev.* **2003**, *103*, 1685.

184. Popp, B. V.; Morales, C. M.; Landis, C. R.; Stahl, S. S. *Inorg. Chem.* **2010**, *49*, 8200.

185. Vaska, L. *Acc. Chem. Res.* **1976**, *9*, 175.

186. Lewis, E. A.; Tolman, W. B. *Chem. Rev.* **2004**, *104*, 1047.

187. Momenteau, M.; Reed, C. A. *Chem. Rev.* **1994**, *94*, 659.

188. Miller, S. L.; Townes, C. H. *Phys. Rev.* **1953**, *90*, 537.

189. Chen, P.; Solomon, E. I. *Proc. Natl. Acad. Sci. U. S. A.* **2004**, *101*, 13105.

190. Bakac, A. *Prog. Inorg. Chem.* **1995**, *43*, 267.

191. Talsi, E. P.; Babenko, V. P.; Likholobov, V. A.; Nekipelov, V. M.; Chinakov, V. D. *Chem. Commun.* **1985**, 1768.

192. Liu, Q.; Li, G.; He, J.; Liu, J.; Li, P.; Lei, A. *Angew. Chem., Int. Ed.* **2010**, *49*, 3371.

193. Zhang, Y.-H.; Yu, J.-Q. *J. Am. Chem. Soc.* **2009**, *131*, 14654.

194. Sergeev, A. G.; Neumann, H.; Spannenberg, A.; Beller, M. *Organometallics* **2010**, *29*, 3368.

195. Izawa, Y.; Pun, D.; Stahl, S. S. *Science* **2011**, *333*, 209.

196. Stahl, S. S. *Science* **2005**, *309*, 1824.

197. van Leeuwen, P. W. N. M. *Homogeneous Catalysis: Understanding the Art*. Kluwer Academic Publishers: Dordrecht, The Netherlands, 2004.

198. Dawson, J. H.; Sono, M. *Chem. Rev.* **1987**, *87*, 1255.

199. Cai, X.; Majumdar, S.; Fortman, G. C.; Cazin, C. S. J.; Slawin, A. M. Z.; Lhermitte, C.; Prabhakar, R.; Germain, M. E.; Palluccio, T.; Nolan, S. P.; Rybak-Akimova, E. V.; Temprado, M.; Captain, B.; Hoff, C. D. *J. Am. Chem. Soc.* **2011**, *133*, 1290.

200. Talsi, E. P.; Babenko, V. P.; Shubin, A. A.; Chinakov, V. D.; Nekipelov, V. M.; Zamaraev, K. I. *Inorg. Chem.* **1987**, *26*, 3871.

201. Fiallo, M. M. L.; Garniersuillerot, A. *Inorg. Chem.* **1990**, *29*, 893.

202. Stahl, S. S.; Thorman, J. L.; Nelson, R. C.; Kozee, M. A. *J. Am. Chem. Soc.* **2001**, *123*, 7188.

203. Akita, M.; Miyaji, T.; Hikichi, S.; Moro-oka, Y. *Chem. Commun.* **1998**, 1005.

204. Miyaji, T.; Kujime, M.; Hikichi, S.; Moro-oka, Y.; Akita, M. *Inorg. Chem.* **2002**, *41*, 5286.

205. Ramprasad, D.; Gilicinski, A. G.; Markley, T. J.; Pez, G. P. *Inorg. Chem.* **1994**, *33*, 2841.

206. Jacobson, R. R.; Tyeklar, Z.; Farooq, A.; Karlin, K. D.; Liu, S.; Zubieta, J. *J. Am. Chem. Soc.* **1988**, *110*, 3690.

207. Hayashi, Y.; Obata, M.; Suzuki, M.; Uehara, A. *Chem. Lett.* **1997**, 1255.

208. Hartshorn, R. M.; Telfer, S. G. *Dalton Trans.* **2000**, 2801.

209. Denney, M. C.; Smythe, N. A.; Cetto, K. L.; Kemp, R. A.; Goldberg, K. I. *J. Am. Chem. Soc.* **2006**, *128*, 2508.

210. Wayland, B. B.; Sherry, A. E.; Poszmik, G.; Bunn, A. G. *J. Am. Chem. Soc.* **1992**, *114*, 1673.

211. Maiti, D.; Fry, H. C.; Woertink, J. S.; Vance, M. A.; Solomon, E. I.; Karlin, K. D. *J. Am. Chem. Soc.* **2007**, *129*, 264.

212. Kieber-Emmons, M. T.; Annaraj, J.; Seo, M. S.; Van Heuvelen, K. M.; Tosha, T.; Kitagawa, T.; Brunold, T. C.; Nam, W.; Riordan, C. G. *J. Am. Chem. Soc.* **2006**, *128*, 14230.

213. Dietzel, P. D. C.; Kremer, R. K.; Jansen, M. *J. Am. Chem. Soc.* **2004**, *126*, 4689.

214. Bakac, A.; Guzei, I. A. *Inorg. Chem.* **2000**, *39*, 736.

215. Grushin, V. V. *Organometallics* **2001**, *20*, 3950.

216. Lewis, N. S.; Nocera, D. G. *Proc. Natl. Acad. Sci. U. S. A.* **2006**, *103*, 15729.

217. Betley, T. A.; Wu, Q.; Van Voorhis, T.; Nocera, D. G. *Inorg. Chem.* **2008**, *47*, 1849.

218. Reece, S. Y.; Hamel, J. A.; Sung, K.; Jarvi, T. D.; Esswein, A. J.; Pijpers, J. J. H.; Nocera, D. G. *Science* **2011**, *334*, 645.

219. Kanan, M. W.; Nocera, D. G. *Science* **2008**, *321*, 1072.

220. Blankenship, R. E.; Tiede, D. M.; Barber, J.; Brudvig, G. W.; Fleming, G.; Ghirardi, M.; Gunner, M. R.; Junge, W.; Kramer, D. M.; Melis, A.; Moore, T. A.; Moser, C. C.; Nocera, D. G.; Nozik, A. J.; Ort, D. R.; Parson, W. W.; Prince, R. C.; Sayre, R. T. *Science* **2011**, *332*, 805.

221. Duan, L. L.; Bozoglian, F.; Mandal, S.; Stewart, B.; Privalov, T.; Llobet, A.; Sun, L. C. *Nature Chem.* **2012**, *4*, 418.

222. Khusnutdinova, J. R.; Rath, N. P.; Mirica, L. M. *J. Am. Chem. Soc.* **2010**, *132*, 7303.

223. de Bruin, B.; Hetterscheid, D. G. H. *Eur. J. Inorg. Chem.* **2007**, 211.

224. Hetterscheid, D. G. H.; Kaiser, J.; Reijerse, E.; Peters, T. P. J.; Thewissen, S.; Blok, A. N. J.; Smits, J. M. M.; de Gelder, R.; de Bruin, B. *J. Am. Chem. Soc.* **2005**, *127*, 1895.

225. Hetterscheid, D. G. H.; Mop, M.; Kicken, R.; Smits, J. M. M.; Reijerse, E. J.; de Bruin, B. *Chem. Eur. J.* **2007**, *13*, 3386.

226. Bunn, A. G.; Wayland, B. B. *J. Am. Chem. Soc.* **1992**, *114*, 6917.

227. Altomare, A.; Cascarano, G.; Giacovazzo, C.; Guagliardi, A. *J. Appl. Crystallogr.* **1994**, *27*, 1045.

228. Betteridge, P. W.; Carruthers, J. R.; Cooper, R. I.; Prout, K.; Watkin, D. J. *J. Appl. Crystallogr.* **2003**, *36*, 1487.

229. Becke, A. D. *J. Chem. Phys.* **1993**, *98*, 5648.

230. Lee, C. T.; Yang, W. T.; Parr, R. G. *Phys. Rev. B* **1988**, *37*, 785.

231. Wadt, W. R.; Hay, P. J. *J. Chem. Phys.* **1985**, *82*, 284.

232. Hay, P. J.; Wadt, W. R. *J. Chem. Phys.* **1985**, *82*, 270.

233. Dunning, T. H.; Hay, P. J. In Modern Theoretical Chemistry; Schaefer, H. F., Ed.; Plenum: New York, 1976; Vol. 3, pp 1-28.

234. Dunning, T. H. *J. Chem. Phys.* **1989**, *90*, 1007.

235. Moravskiy, A.; Stille, J. K. *J. Am. Chem. Soc.* **1981**, *103*, 4182.

236. Stambuli, J. R.; Weng, Z.; Incarvito, C. D.; Hartwig, J. F. *Angew. Chem., Int. Ed.* **2007**, *46*, 7674.

237. Ozawa, F.; Ito, T.; Yamamoto, A. *J. Am. Chem. Soc.* **1980**, *102*, 6457.

238. Casares, J. A.; Espinet, P.; Salas, G. *Chem. Eur. J.* **2002**, *8*, 4843.

239. Crabtree, R. H. *The Organometallic Chemistry of the Transition Metals*. 4th ed.; Wiley-Interscience New York, 2005.

240. Stephan, D. W. *Dalton Trans.* **2009**, 3129.

241. Welch, G. C.; Juan, R. R. S.; Masuda, J. D.; Stephan, D. W. *Science* **2006**, *314*, 1124.

242. Grant, D. H. *J. Chem. Educ.* **1995**, *72*, 39.

243. Evans, D. F. *J. Chem. Soc.* **1959**, 2003.

244. Schubert, E. M. *J. Chem. Educ.* **1992**, *69*, 62.

245. Adamo, C.; Barone, V. *J. Chem. Phys.* **1999**, *110*, 6158.

246. Zhao, Y.; Truhlar, D. G. *J. Chem. Phys.* **2006**, *125*.

247. Weigend, F.; Ahlrichs, R. *Phys. Chem. Chem. Phys.* **2005**, *7*, 3297.

248. Beck, W.; Sunkel, K. *Chem. Rev.* **1988**, *88*, 1405.

249. Strauss, S. H. *Chem. Rev.* **1993**, *93*, 927.

250. Reed, C. A. *Chem. Commun.* **2005**, 1669.

251. Davies, J. A.; Hartley, F. R. *Chem. Rev.* **1981**, *81*, 79.

252. Gu, W. X.; Ozerov, O. V. *Inorg. Chem.* **2011**, *50*, 2726.

253. Kobayashi, H.; Sonoda, T.; Iwamoto, H.; Yoshimura, M. *Chem. Lett.* **1981**, 579.

254. Yakelis, N. A.; Bergman, R. G. *Organometallics* **2005**, *24*, 3579.

255. Fujiki, K.; Kashiwagi, M.; Miyamoto, H.; Sonoda, A.; Ichikawa, J.; Kobayashi, H.; Sonoda, T. *J. Fluorine Chem.* **1992**, *57*, 307.

256. Krossing, I.; Raabe, I. *Angew. Chem., Int. Ed.* **2004**, *43*, 2066.

257. Krossing, I. *Chem. Eur. J.* **2001**, *7*, 490.

258. Juhasz, M.; Hoffmann, S.; Stoyanov, E.; Kim, K. C.; Reed, C. A. *Angew. Chem., Int. Ed.* **2004**, *43*, 5352.

259. Stoyanov, E. S.; Hoffmann, S. P.; Juhasz, M.; Reed, C. A. *J. Am. Chem. Soc.* **2006**, *128*, 3160.

260. Romanato, P.; Duttwyler, S.; Linden, A.; Baldridge, K. K.; Siegel, J. S. *J. Am. Chem. Soc.* **2010**, *132*, 7828.

261. Romanato, P.; Duttwyler, S.; Linden, A.; Baldridge, K. K.; Siegel, J. S. *J. Am. Chem. Soc.* **2011**, *133*, 11844.

262. Brookhart, M.; Grant, B.; Volpe, A. F. *Organometallics* **1992**, *11*, 3920.

263. Hoffmann, S. P.; Kato, T.; Tham, F. S.; Reed, C. A. *Chem. Commun.* **2006**, 767.

264. Nishida, H.; Takada, N.; Yoshimura, M.; Sonoda, T.; Kobayashi, H. *Bull. Chem. Soc. Jpn.* **1984**, *57*, 2600.

265. Kim, K. C.; Reed, C. A.; Elliott, D. W.; Mueller, L. J.; Tham, F.; Lin, L. J.; Lambert, J. B. *Science* **2002**, *297*, 825.

266. Walter, M. D.; Moorhouse, R. A.; Urbin, S. A.; White, P. S.; Brookhart, M. *J. Am. Chem. Soc.* **2009**, *131*, 9055.

267. Reinartz, S.; White, P. S.; Brookhart, M.; Templeton, J. L. *J. Am. Chem. Soc.* **2002**, *124*, 7249.

268. Reinartz, S.; White, P. S.; Brookhart, M.; Templeton, J. L. *J. Am. Chem. Soc.* **2001**, *123*, 12724.

269. Muetterties, E. L.; Bleeke, J. R.; Wucherer, E. J.; Albright, T. A. *Chem. Rev.* **1982**, *82*, 499.

270. Johansson, L.; Tilset, M.; Labinger, J. A.; Bercaw, J. E. *J. Am. Chem. Soc.* **2000**, *122*, 10846.

271. Hasegawa, M.; Segawa, Y.; Yamashita, M.; Nozaki, K. *Angew. Chem., Int. Ed.* **2012**, *51*, 6956.

272. Hair, G. S.; Cowley, A. H.; Jones, R. A.; McBurnett, B. G.; Voigt, A. *J. Am. Chem. Soc.* **1999**, *121*, 4922.

273. Guerrero, A.; Martin, E.; Hughes, D. L.; Kaltsoyannis, N.; Bochmann, M. *Organometallics* **2006**, *25*, 3311.

274. Butts, M. D.; Scott, B. L.; Kubas, G. J. *J. Am. Chem. Soc.* **1996**, *118*, 11831.

275. Pangborn, A. B.; Giardello, M. A.; Grubbs, R. H.; Rosen, R. K.; Timmers, F. J. *Organometallics* **1996**, *15*, 1518.

276. Bradley, D.; Williams, G.; Lawton, M. *J. Org. Chem.* **2010**, *75*, 8351.

277. Luck, R.; Morris, R. H. *Inorg. Chem.* **1984**, *23*, 1489.

278. Liston, D. J.; Lee, Y. J.; Scheidt, W. R.; Reed, C. A. *J. Am. Chem. Soc.* **1989**, *111*, 6643.

279. Kauffman, G. B. *Coord. Chem. Rev.* **1973**, *11*, 161.

280. Douvris, C.; Reed, C. A. *Organometallics* **2008**, *27*, 807.

281. Connelly, N. G.; Geiger, W. E. *Chem. Rev.* **1996**, *96*, 877.

282. Sarazin, Y.; Kaltsoyannis, N.; Wright, J. A.; Bochmann, M. *Organometallics* **2007**, *26*, 1811.

283. Sarazin, Y.; Hughes, D. L.; Kaltsoyannis, N.; Wright, J. A.; Bochmann, M. *J. Am. Chem. Soc.* **2007**, *129*, 881.

284. Galvan-Arzate, S.; Santamaria, A. *Toxicol. Lett.* **1998**, *99*, 1.

285. Albietz, P. J.; Cleary, B. P.; Paw, W.; Eisenberg, R. *Inorg. Chem.* **2002**, *41*, 2095.

286. Buschmann, W. E.; Miller, J. S. *Inorg. Synth.* **2002**, *33*, 83.

287. Tellers, D. M.; Yung, C. M.; Arndtsen, B. A.; Adamson, D. R.; Bergman, R. G. *J. Am. Chem. Soc.* **2002**, *124*, 1400.

288. Scott, V. J.; Celenligil-Cetin, R.; Ozerov, O. V. *J. Am. Chem. Soc.* **2005**, *127*, 2852.

289. Aizenberg, M.; Milstein, D. *Chem. Commun.* **1994**, 411.

290. Nava, M.; Reed, C. A. *Organometallics* **2011**, *30*, 4798.

291. McGrady, G. S.; Sirsch, P.; Chatterton, N. P.; Ostermann, A.; Gatti, C.; Altmannshofer, S.; Herz, V.; Eickerling, G.; Scherer, W. *Inorg. Chem.* **2009**, *48*, 1588.

292. Ivanov, S. V.; Rockwell, J. J.; Polyakov, O. G.; Gaudinski, C. M.; Anderson, O. P.; Solntsev, K. A.; Strauss, S. H. *J. Am. Chem. Soc.* **1998**, *120*, 4224.

293. Ramirez-Contreras, R.; Ozerov, O. V. *Dalton Trans.* **2012**, *41*, 7842.

294. Ramirez-Contreras, R., unpublished results.

295. Bahr, S. R.; Boudjouk, P. *J. Org. Chem.* **1992**, *57*, 5545.

296. Pearson, R. G. *J. Chem. Educ.* **1968**, *45*, 581.

297. Xiao, B.; Gong, T. J.; Xu, J.; Liu, Z. J.; Liu, L. *J. Am. Chem. Soc.* **2011**, *133*, 1466.

298. Chernyshova, E. S.; Goddard, R.; Porschke, K. R. *Organometallics* **2007**, *26*, 3236.

299. Yamashita, M.; Takamiya, I.; Jin, K.; Nozaki, K. *Organometallics* **2006**, *25*, 4588.

300. Scharf, A.; Goldberg, I.; Vigalok, A. *J. Am. Chem. Soc.* **2013**, *135*, 967.

301. Casas, J. M.; Falvello, L. R.; Fornies, J.; Martin, A. *Inorg. Chem.* **1996**, *35*, 56.

302. Jones, W. D.; Feher, F. J. *Acc. Chem. Res.* **1989**, *22*, 91.

303. Dong, Y. J.; Jones, R. L.; Wilson, N. H. *Br. J. Pharmacol.* **1986**, *87*, 97.

304. Jones, W. D.; Dong, L. Z. *J. Am. Chem. Soc.* **1989**, *111*, 8722.

305. Sweet, J. R.; Graham, W. A. G. *J. Am. Chem. Soc.* **1983**, *105*, 305.

306. Maslowsky, E. *J. Chem. Educ.* **1993**, *70*, 980.

307. Falvello, L. R.; Fornies, J.; Navarro, R.; Sicilia, V.; Tomas, M. *Angew. Chem., Int. Ed.* **1990**, *29*, 891.

308. Shiba, C. F.; Waddell, W. H. *J. Organomet. Chem.* **1983**, *241*, 119.

309. Fors, B. P.; Watson, D. A.; Biscoe, M. R.; Buchwald, S. L. *J. Am. Chem. Soc.* **2008**, *130*, 13552.

310. Cotton, F. A.; Wilkinson, G. *Advanced Inorganic Chemistry*. 2nd ed.; Wiley-Interscience.: New York, 1966.

311. Pearson, R. G. *J. Chem. Educ.* **1968**, *45*, 643.

312. McCulloch, B., unpublished results.

313. Crabtree, R. H. *J. Organomet. Chem.* **2005**, *690*, 5451.

314. Berlin, K. D.; Butler, G. B. *Chem. Rev.* **1960**, *60*, 243.

315. Albrecht, M. *Chem. Rev.* **2010**, *110*, 576.

316. Shaw, B. L. *J. Am. Chem. Soc.* **1975**, *97*, 3856.

317. Michman, M. *Isr. J. Chem.* **1986**, *27*, 241.

318. Macgregor, S. A. *Chem. Soc. Rev.* **2007**, *36*, 67.

319. Garrou, P. E. *Chem. Rev.* **1985**, *85*, 171.

320. Parkins, A. W. *Coord. Chem. Rev.* **2006**, *250*, 449.

321. Shin, J. H.; Parkin, G. *Chem. Commun.* **1998**, 1273.

322. Lin, W. B.; Wilson, S. R.; Girolami, G. S. *Inorg. Chem.* **1994**, *33*, 2265.

323. Hartwig, J. F.; Bergman, R. G.; Andersen, R. A. *J. Organomet. Chem.* **1990**, *394*, 417.

324. Hirsekorn, K. F.; Veige, A. S.; Wolczanski, P. T. *J. Am. Chem. Soc.* **2006**, *128*, 2192.

325. Xu, H.; Williard, P. G.; Bernskoetter, W. H. *Organometallics* **2013**, *32*, 798.

326. Nakajima, T.; Shimizu, I.; Kobayashi, K.; Koshino, H.; Wakatsuki, Y. *Inorg. Chem.* **1997**, *36*, 6440.

327. Kikukawa, K.; Takagi, M.; Matsuda, T. *Bull. Chem. Soc. Jpn.* **1979**, *52*, 1493.

328. Billig, E.; Jamerson, J. D.; Pruett, R. L. *J. Organomet. Chem.* **1980**, *192*, C49.

329. van Leeuwen, P. W. N. M. *Appl. Catal., A* **2001**, *212*, 61.

330. Nolte, M. J.; Gafner, G.; Haines, L. M. *Chem. Commun.* **1969**, 1406.

331. Bennett, M. A.; Smith, A. K.; Robertson, G. B. *J. Organomet. Chem.* **1972**, *43*, C41.

332. Jun, C. H. *Chem. Soc. Rev.* **2004**, *33*, 610.